



HAL
open science

Weathering of metallurgical slags : a comprehensive study on the importance of chemical and biological contributions

Nang Htay Yin

► **To cite this version:**

Nang Htay Yin. Weathering of metallurgical slags : a comprehensive study on the importance of chemical and biological contributions. Agricultural sciences. Université Paris-Est; Erasmus Mundus ETeCoS3, 2014. English. NNT : 2014PEST1125 . tel-01154324

HAL Id: tel-01154324

<https://theses.hal.science/tel-01154324>

Submitted on 21 May 2015

HAL is a multi-disciplinary open access archive for the deposit and dissemination of scientific research documents, whether they are published or not. The documents may come from teaching and research institutions in France or abroad, or from public or private research centers.

L'archive ouverte pluridisciplinaire **HAL**, est destinée au dépôt et à la diffusion de documents scientifiques de niveau recherche, publiés ou non, émanant des établissements d'enseignement et de recherche français ou étrangers, des laboratoires publics ou privés.

Joint PhD degree in Environmental Technology

UNIVERSITÉ
— PARIS-EST

Docteur de l'Université Paris-Est
Spécialité : Science et Technique de l'Environnement



Dottore di Ricerca in Tecnologie Ambientali

UNESCO-IHE
Institute for Water Education



Degree of Doctor in Environmental Technology

Thèse – Tesi di Dottorato – PhD thesis

Nang Htay YIN

**Weathering of metallurgical slags: A comprehensive study on the importance of
chemical and biological contributions**

Defended on December 2nd, 2014

In front of the PhD committee

Prof. Cécile QUANTIN	Reviewer
Dr. Vojtech ETTLER	Reviewer
Prof. Marc BENEDETTI	Examiner
Prof. François GUYOT	Examiner
Dr. Hab. Eric van HULLEBUSCH	Promotor
Dr. Yann SIVRY	Co-promotor
Prof. Dr. Ir. Piet LENS	Co-promotor
Prof. Giovanni ESPOSITO	Co-promotor



Erasmus Joint doctorate programme in Environmental Technology for Contaminated Solids, Soils and Sediments (ETeCoS³)

Acknowledgement

I would like to express my sincere gratitude to Dr. Hab. Eric VANHULLEBUSCH, my promoter for his valuable suggestions, guidance, and encouragement throughout my thesis work.

I would like to extend my gratitude further to my co-promoters; Dr Yann SIVRY, Prof. Piet LENS, Dr. Hab. Giovanni ESPOSITO for their massive scientific contribution to my research, to examiners; Prof. Marc BENEDETTI and Prof. François GUYOT for scientific advices, and reviewers; Prof. Cécile QUANTIN and Dr. Vojtech ETTLER for their valuable time to read and evaluate my research.

I am truly grateful to my scholarship donor for providing financial support through the Erasmus Mundus Joint Doctorate Programme ETeCoS³ (Environmental Technologies for Contaminated Solids, Soils and Sediments, grant agreement FPA n°2010-0009).

I would like to thank Dr Nicolas Seigneux and Dr Arnaud Gauthier for providing metallurgical slag samples. I would like to thank again Prof. Marc Benedetti for allowing me to conduct my research at Institut de Physique du Globe de Paris (IPGP), Prof. François Guyot for helping me through with SEM and TEM analysis, Prof. Piet Lens for his guidance and suggestion during my mobility in the Netherlands.

My sincere thanks also go to Prof. Pascale Louvat for the fruitful, scientific discussion, to Julien Moureau for his valuable training on MC-ICP-MS, to Laure Cordier for her assistance on ICP-OES, to Prof Remi Losno and Mickael Tharaud for their assistance on Single-ICP-MS.

Finally, I would like to thank my fellow colleagues, friends and my family for being with me through thick and thin and for their emotional support throughout my research work.

Abstract

Primary smelting slags, known as Lead Blast Furnace (LBF) and Imperial Smelting Furnace (ISF), were generated by the former pyrometallurgical industries located in Noyelles-Godault, Northern France. Following its closure in 2003, 4 million tons of primary slags have been landfilled as a heap in the vicinity of the Deûle River, near the industrial basin of Nord-Pas-de-Calais. These slag materials are often enriched in particular metals (Pb, Zn) that can be released into the environment through alteration processes and leaching. Many biological and chemical processes might take place within these tailings and thus affect significantly the slag weathering. Predicting the environmental impact of these wastes requires an understanding of the mineral-water interactions as well as the influence of the biological activities (the involvement of microorganisms). Thus, this research is designed to simulate the natural weathering of slag by simulating different weathering conditions with or without the involvement of the microorganisms as well as by varying several chemical parameters.

Chemical weathering of both LBF and ISF slags was studied by as a function of pHs (4, 5.5, 7, 8.5 and 10) as well as under two atmospheres (open air and nitrogen). Significant amounts of Ca, Fe and Zn were released under acidic conditions (pH 4) with a decrease towards the neutral to alkaline conditions (pH 7 and 10) for both slags. The concentrations of all elements increased gradually after 216 h compared to initial 24 h of leaching period. The presence of oxygen under open-air atmosphere not only enhanced oxidative weathering but also encouraged formation of secondary oxide and carbonate phases compared to nitrogen atmosphere experiments. In addition, Zn dissolution was related to extremes zinc isotopic signatures in the leachate; heavier $\delta^{66}\text{Zn}$ values at low pH than at high pH for both slags under open-air atmosphere.

On the other hand, bioweathering of both slags was studied in the presence of a pure heterotrophic bacterial strain (*Pseudomonas aeruginosa*) in a bioreactor operated in batch condition as well as in a semi-flow through reactor with intermittent leachate renewal conditions. *P. aeruginosa* is shown to play a significant role in slags weathering by enhancing the leaching and solubility of Zn and Pb. In addition, the cumulative bulk release of dissolved Fe, Si, Ca and Mg doubled in the presence of bacteria, probably due to the release of soluble complexing organic molecules (e.g. siderophores). Also, bacterial biomass served as the bioadsorbent for Pb, Fe and Zn as 70-80% of Pb and Fe, 40-60% of Zn released are attached to and immobilized by the bacterial biomass.

Oxides, hydroxides and carbonates were predicted as secondary phases during chemical weathering of slags whereas carbonates and phosphates were dominant phases during bioweathering. These predictions were in agreement with the observations by Scanning Electron Microscopy (SEM) with Energy Dispersive X-Ray Analysis (EDS), and Transmission Electron Microscopy (TEM) analysis.

Keywords: Slag, chemical, biological weathering, leaching, pH dependent, atmospheres, Zn isotopes, fractionation, secondary precipitates

Résumé

Les scories de fonderie primaires, connus sous le nom *Lead Blast Furnace* (LBF) et *Imperial Smelting Furnace* (ISF), ont été générés par les anciennes industries de pyrométallurgie situées à Noyelles-Godault dans le Nord de la France. Après sa fermeture en 2003, 4 millions de tonnes de scories primaires ont été mis en décharge, entassés dans le voisinage de la Deûle, près du bassin industriel du Nord-Pas-de-Calais. Ces scories sont souvent enrichies en métaux (Pb, Zn), qui peuvent être disséminés dans l'environnement par le biais des processus d'altération et de lessivage. De nombreux processus biologiques et chimiques peuvent avoir lieu au sein de ces résidus et ainsi affecter de manière significative l'érosion du laitier. Evaluer l'impact environnemental de ces déchets nécessite de comprendre les interactions eau/minéral ainsi que l'influence de l'activité biologique (la participation des micro-organismes). Ainsi, ces travaux ont pour but de simuler le vieillissement naturel des scories en reproduisant différentes conditions de vieillissement, avec ou sans la participation des micro-organismes, en contrôlant différents paramètres physico-chimiques.

L'altération chimique des scories LBF et ISF a été étudiée en fonction du pH (4, 5.5, 7, 8.5 et 10) ainsi que sous atmosphères contrôlées (ouverte et sous azote). D'importantes quantités de Ca, Fe et Zn sont libérées en conditions acides (pH 4) et des quantités plus faibles en milieux neutres et alcalins (pH 7 et 10) pour les deux types de scorie. Les concentrations de tous les éléments augmentent progressivement entre 24 et 216h de lixiviation. La présence d'oxygène en atmosphère ouverte génère non seulement l'amélioration de l'altération oxydative mais encourage aussi la formation d'oxydes secondaires et de phases carbonatées. En outre, la dissolution de Zn est reliée à des signatures isotopiques dans la solution de lixiviation extrêmement contrastées par rapport à celles des scories initiales : des valeurs de $\delta^{66}\text{Zn}$ plus lourdes à faible pH qu'à pH élevé, pour les deux scories, sous atmosphère ouverte.

D'autre part, l'altération biologique des deux types de scories a été étudiée en présence d'une souche bactérienne hétérotrophe pure (*Pseudomonas aeruginosa*), dans un bioréacteur fonctionnant en système fermé puis en semi-flux (renouvellements intermittents du lixiviat). *P. aeruginosa* s'est révélée jouer un rôle important dans l'altération des laitiers, par l'augmentation de leur lixiviation et en particulier de la solubilité de Pb et Zn. En outre, la quantité cumulée de Fe, Si, Ca et Mg dissous est doublée en présence de bactéries, probablement sous l'effet des complexants solubles libérés par *P. aeruginosa* (molécules organiques de type sidérophores). La biomasse bactérienne sert de bioadsorbent pour Pb, Fe et Zn : 70-80% de Pb et Fe et 40-60% de Zn libérés sont fixés par la biomasse bactérienne.

Les phases secondaires formées lors de l'altération chimique des scories sont les oxydes, les hydroxydes et les carbonates, tandis que les carbonates et les phosphates sont les phases dominantes pendant l'altération biologique. Chacune de ces phases ont été prédites par les calculs thermodynamiques et observées en microscopie électronique à balayage (MEB-EDS), microscopie électronique à transmission (MET), et spectroscopie de photoélectrons X (XPS).

Mots-clés: laitiers, scories, isotopes de Zn, phases secondaires, altération chimique et biologique, lessivage, pH, *Pseudomonas aeruginosa*.

Samenvatting

Hoogovenslak komend van lood hoogovens (Lead blast furnace LBF) en zink hoogovens (Imperial smelting furnace (ISF), zijn ontstaan dankzij pyrometallurgische industrieën dichtbij Noyelles-Godault in Noord Frankrijk. Als gevolg van de sluiting in 2003 van deze industrieën is 4 miljoen ton primaire slakken gedumpt op een grote hoop dichtbij de rivier de Deule vlakbij het industriegebied van Nord-Pas-de Calais. Dit slak materiaal is vaak verrijkt. Vaak gebeurd dit met specifieke metalen zoals Pb en Zn. Deze kunnen dan weer in het milieu terecht komen door uitloging en veranderende processen. Veel biologische en chemische processen vinden plaats rond dit afval en hebben een significant effect op de slak verwerking. Voor het voorspellen van de milieu impact van dit afval is het belangrijk om de mineraalwater interacties en de invloeden van biologische activiteiten (the impact van micro-organismen) te begrijpen. Dit onderzoek is ontworpen om de natuurlijke verwerking van slakken te simuleren door verschillende verweringscondities te simuleren met en zonder micro-organismen en daarnaast ook nog het variëren van enkele chemische parameters.

Chemische verwerking van zowel LBF als ISF slakken is bestudeerd op pH (4, 5.5, 7, 8.5 en 10), atmosfeer (open lucht en stikstof). Grote hoeveelheden Ca, Fe en Zn zijn vrijgelaten onder zure condities (pH 4). Bij alkalische condities (pH7 en 10) verminderen deze waarden voor beide slakken. De concentraties van alle elementen nemen geleidelijk toe na 216 uur vergeleken met de oorspronkelijke 24 uur uitloging periode. De aanwezigheid van zuurstof onder de open lucht condities verbeterde niet alleen de oxidatieve verwerking, maar verbeterde ook de vorming van secundaire oxides en carbonaten fases. Bovendien is de Zn ontbinding te linken aan extreme Zn isotoop herkenning in het extract. Zwaardere $\delta^{66}\text{Zn}$ waarden bij lage pH dan bij hogere pH voor beide slakken in de open lucht condities.

Aan de andere kant is ook de bioverwerking bestudeerd op beide slakken in het bijzijn van een pure heterotrofe bacterie (*Pseudomonas aeruginosa*) in een bioreactor. Dit gebeurde zowel onder batch condities als wel semi-flow through reactor met onderbroken extract vernieuwing condities. *P. Aeruginosa* blijkt een belangrijke rol te spelen in de slak verwerking door het verbeteren van het extract en de oplosbaarheid van Zn en Pb. Bovendien verdubbelde de uitscheiding van opgeloste Fe, Si, Ca en Mg in de ophopende massa door de aanwezigheid van bacterie. Dit wordt waarschijnlijk veroorzaakt door het vrijkomen van oplosbare complexe organische moleculen (zoals siderofoor). De bacteriële biomassa werkte als een bio-absorbent voor Pb, Fe en Zn. Wel 70-80% van het Pb en Fe en 40-60% van het Zn die zijn vrijgekomen zitten vast aan en zijn geïmmobiliseerd door bacteriële biomassa.

Oxides, hydroxides en carbonaten waren voorspeld een minder belangrijke rol te hebben tijdens chemische verwerking van slakken terwijl carbonaten en fosfaten dominant waren tijdens de bioverwerking. Deze voorspellingen zijn in overeenkomst met de gevonden resultaten van de Scanning Electron Microscop (SEM) met Energy Dispersive X-Ray analyses (EDS), Transmission Electron Microscopy (TEM) analyses en X-ray Photoelectron Spectroscopy (XPS) analyses.

Trefwoorden: Slakken, chemische, biologische verwerking, uitspoeling, pH-afhankelijk, atmosferen, Zn isotopen, fractionering, secundaire neerslagen

Sommario

Le scorie di fusione primaria, chiamate anche Lead Blast Furnace (LBF) e Imperial Smelting Furnace (ISF), sono state prodotte dalle ex industrie pirometallurgiche presso Noyelles-Godault, nella Francia del nord. Dopo la chiusura delle industrie nel 2003, 4 milioni di tonnellate di scorie primarie sono state interrare in un cumulo nelle vicinanze di Deûle River, vicino al bacino industriale di Nord-Passo di Calais. Queste scorie sono spesso ricche di specifici metalli (Pb, Zn) che possono essere rilasciati nell'ambiente attraverso processi di alterazione e lisciviazione. Molti processi biologici e chimici possono avvenire in questi scarti e quindi influenzare significativamente la degradazione meteorica delle scorie. Per prevenire l'impatto ambientale di questi rifiuti bisogna capire le interazioni tra il minerale e l'acqua, ma anche in che modo influiscono i processi biologici (il coinvolgimento di microrganismi nel processo). Per questo motivo, questa ricerca è stata finalizzata allo studio della meteorizzazione delle scorie, simulando diverse condizioni atmosferiche, con o senza il coinvolgimento di microrganismi, e anche variando diversi parametri chimici.

La disgregazione chimica di entrambe le scorie LBF e ISF è stata studiata in funzione di diversi pH (4, 5.5, 7, 8.5, 10), ma anche in due diverse atmosfere (all'aria aperta e in azoto). Per entrambe le scorie, quantità significative di Ca, Fe e Zn sono state rilasciate in condizioni di acidità (pH 4), che invece si sono ridotte fortemente in condizioni di neutralità o in condizioni alcaline (pH 7 and 10). La concentrazione di tutti gli elementi è aumentata gradualmente dopo 216 ore rispetto alle 24 ore iniziali del periodo di lisciviazione. La presenza di ossigeno in aria aperta, non solo ha intensificato la disgregazione ossidativa ma ha anche istigato la formazione di ossido secondario e carbonati. Inoltre, la dissoluzione dello zinco è collegata all'estrema composizione isotopica dello zinco; valori di $\delta^{66}\text{Zn}$ più pesanti sono stati registrati a pH più bassi per entrambe le scorie mantenute all'aria aperta.

D'altra parte, la meteorizzazione biologica di entrambe le scorie è stata studiata in presenza di un ceppo batterico eterotrofico puro (*Pseudomonas aeruginosa*) in un bioreattore operato in batch, ma anche in un reattore a semi-flusso continuo con rinnovo intermittente del percolato. È stato dimostrato che *P. aeruginosa* ha un ruolo importante nella meteorizzazione delle scorie, dal momento che aumenta la lisciviazione e la solubilità di Zn e Pb. Inoltre, il rilascio cumulativo di Fe, Si, Ca e Mg disciolti è raddoppiato in presenza di batteri, probabilmente a causa del rilascio di complesse molecole organiche solubili (per esempio siderofore). La biomassa batterica serve come bioadsorbente per Pb, Fe e Zn, dato che il 70-80% di Pb e Fe, e il 40-60% di Zn che è stato rilasciato, viene attaccato e immobilizzato dalla biomassa batterica.

Ossidi, idrossidi e carbonati sono stati previsti come fasi secondarie durante la disgregazione chimica delle scorie, mentre carbonati e fosfati come fasi dominanti durante la meteorizzazione biologica. Queste previsioni sono in accordo con le osservazioni effettuate tramite microscopia elettronica a scansione (SEM) con spettroscopia EDS (Energy Dispersive X-Ray Analysis), microscopia elettronica a trasmissione (TEM), e spettroscopia fotoelettronica a raggi X (XPS).

Parole chiave: Scorie, chimico, meteorizzazione biologica, lisciviazione, pH dipendente, atmosfera, isotopi dello Zn, frazionamento, precipitati secondari

Table of Contents

Acknowledgement

Abstract

Résumé

Samenvatting

Sommario

CHAPTER 1:INTRODUCTION	14
1.1. BACKGROUND.....	14
1.2. PROBLEMS OF STATEMENT	14
1.3. OBJECTIVES	15
1.4. SCOPE OF THE STUDY.....	15
1.5. STRUCTURE OF THE THESIS.....	17
1.6. REFERENCES	18
CHAPTER 2:LEAD AND LEAD AND ZINC METALLURGICAL SLAGS MINERALOGY AND WEATHERING: A REVIEW	22
2.1. INTRODUCTION	22
2.1.1. WORLD PRODUCTION OF LEAD AND ZINC.....	22
2.1.2. <i>Pyrometallurgical processes</i>	22
2.1.3. <i>Environmental profile of pyrometallurgical industries.....</i>	23
2.1.4. <i>Environmental pollution due to slags from metallurgical industries</i>	25
2.2. METALLURGICAL SLAGS.....	25
2.2.1. <i>Methods for Mineral Characterization</i>	26
2.2.2. <i>General composition of slags.....</i>	27
2.2.3. <i>Primary mineralogical phases.....</i>	28
2.3. ALTERATION OF METALLURGICAL SLAGS.....	38
2.3.1. <i>Chemically induced alteration.....</i>	38
2.3.1.1. Short-term leaching assessment of slags	38
2.3.1.2. Long-term leaching assessment of slags	39
2.3.1.3. Applicability of both short and long term leaching tests to metallurgical slags	44
2.3.1.4. Alteration mechanisms and rates of slags (glass vs silicate).....	44
2.3.2. <i>Biologically induced alteration.....</i>	45
2.3.2.1. Bio-alteration / bioleaching	45
2.3.2.2. Sorption of metals onto bacterial cells and complexation by their byproducts (EPS, siderophores).....	46
2.3.2.3. Bio-alteration mechanisms.....	46
2.3.3. <i>Mineralogical control on metal mobility.....</i>	47
2.3.4. <i>Secondary precipitates.....</i>	48
2.4. CONCLUSIONS AND OUTLOOK.....	49
2.5. REFERENCES	49
CHAPTER 3: APPLICATION OF ZN ISOTOPES IN ENVIRONMENTAL IMPACT ASSESSMENT OF Zn-Pb METALLURGICAL INDUSTRIES.....	57
3.1. INTRODUCTION	57
3.2. CONTRIBUTION OF ANALYTICAL DEVELOPMENT	57
3.3. ZINC AND LEAD SMELTERS.....	58
3.3.1. <i>Ore signatures.....</i>	58

3.3.2.	<i>Smelting processes</i>	59
3.3.3.	<i>Slags</i>	60
3.3.4.	<i>Air emissions</i>	60
3.3.5.	<i>Fractionation mechanisms during smelting processes</i>	62
3.3.5.1.	Rayleigh fractionation (roasting process).....	62
3.3.5.2.	Electroplating.....	62
3.4.	SMELTER-IMPACTED ENVIRONMENTAL SAMPLES.....	63
3.4.1.	<i>Natural water bodies (groundwater, stream and river water)</i>	63
3.4.2.	<i>Sediments (lake and reservoir)</i>	63
3.4.3.	<i>Soil (peat bog soil, inland soil)</i>	63
3.4.4.	<i>Fractionation induced by geochemical processes (sorption, complexation and precipitation)</i> ..	66
3.5.	SUMMARY AND CONCLUSIONS.....	67
3.6.	PERSPECTIVES.....	69
3.7.	REFERENCES.....	70
3.8.	SUPPLEMENTARY DATA.....	75
CHAPTER 4: MATERIALS AND METHODS		83
4.1.	MATERIALS.....	83
4.1.1.	<i>Slags</i>	83
4.1.2.	<i>Bacteria</i>	84
4.2.	ZN ISOTOPIC TECHNIQUES.....	85
4.2.1.	<i>Experimental</i>	85
4.2.2.	<i>Reagents and isotopic standards</i>	85
4.2.3.	<i>Chromatographic column separation of Zn</i>	86
4.2.3.1.	Choice of column and resin.....	86
4.2.3.2.	Column chemistry.....	86
4.2.3.3.	Separation protocol.....	87
4.2.4.	<i>Mass spectrometry</i>	88
4.2.5.	<i>Isotopic analyses and data presentation</i>	90
4.2.6.	<i>Analytical quality and error evaluation</i>	90
4.2.6.1.	Spectral interferences (isobaric correction).....	90
4.2.6.2.	Non-spectral mass bias correction (exponential law).....	92
4.3.	SOLID PHASE CHARACTERIZATION TECHNIQUES.....	93
4.3.1.	<i>XRF</i>	94
4.3.1.1.	Sample preparation.....	94
4.3.1.2.	XRF measurement.....	94
4.3.2.	<i>XRD</i>	94
4.3.3.	<i>SEM-EDS</i>	94
4.3.3.1.	Sample preparation.....	94
4.3.3.2.	SEM measurement.....	95
4.3.4.	<i>TEM</i>	95
4.3.4.1.	Sample preparation.....	95
4.3.4.2.	TEM measurement.....	95
4.4.	EXPERIMENTAL DESIGNS.....	95
4.4.1.	<i>Leaching potential assessment (under Phase I)</i>	95
4.4.2.	<i>Acid digestion (under Phase I)</i>	96
4.4.3.	<i>Chemical dissolution of slags (under Phase II)</i>	96
4.4.4.	<i>Biological weathering of slags (under Phase III)</i>	98
4.4.4.1.	Bio/weathering of slags under leachate stagnant conditions (Test 1).....	99
4.4.4.2.	Bio/weathering of slags under leachate renewal conditions (Test 2).....	99
4.4.4.3.	Acid digestion of biological samples.....	99

4.5.	THERMODYNAMIC MODELING BY VISUAL MINTEQ.....	100
4.6.	INDUCTIVELY COUPLED PLASMA OPTICAL EMISSION SPECTROMETRY (ICP-OES)	100
4.7.	REFERENCES	100
CHAPTER 5: EVALUATION ON CHEMICAL STABILITY OF LEAD BLAST FURNACE (LBF) AND IMPERIAL SMELTING FURNACE (ISF) SLAGS		103
5.1.	INTRODUCTION	103
5.2.	MATERIAL AND METHODS.....	103
5.2.1.	<i>Lead blast furnace (LBF) and imperial smelting furnace (ISF) slags.....</i>	<i>103</i>
5.2.2.	<i>pH dependent chemical weathering test</i>	<i>105</i>
5.2.3.	<i>Leachate chemistry and geochemical modeling</i>	<i>105</i>
5.2.4.	<i>Calculation of leaching behavior and rates.....</i>	<i>105</i>
5.2.5.	<i>Solid phase characterization</i>	<i>106</i>
5.3.	RESULTS	106
5.3.1.	<i>Leaching behavior of LBF and ISF as a function of pH under open air atmosphere</i>	<i>106</i>
5.3.2.	<i>Initial leaching rates of LBF and ISF as a function of pH under open air atmosphere.....</i>	<i>110</i>
5.3.3.	<i>Effect of atmospheres on long-term leaching (9 days) of LBF and ISF as a function of pH.....</i>	<i>110</i>
5.3.4.	<i>Thermodynamic modeling</i>	<i>114</i>
5.3.5.	<i>Solid phase characterization of post-weathered LBF and ISF slags</i>	<i>115</i>
5.3.5.1.	<i>Scanning electron microscope (SEM) analysis.....</i>	<i>115</i>
5.3.5.2.	<i>Transmission electron microscopy (TEM) analysis</i>	<i>117</i>
5.4.	DISCUSSION.....	119
5.4.1.	<i>Far-from equilibrium leaching condition.....</i>	<i>119</i>
5.4.1.1.	<i>Dissolution kinetics of both slags</i>	<i>119</i>
5.4.1.2.	<i>Stoichiometric or non-stoichiometric leaching.....</i>	<i>120</i>
5.4.1.3.	<i>Dissolution of primary mineral phases</i>	<i>121</i>
5.4.2.	<i>Near-equilibrium leaching condition.....</i>	<i>122</i>
5.4.2.1.	<i>Newly formed secondary phases.....</i>	<i>123</i>
5.4.2.2.	<i>Bulk release of Pb and Zn during long term leaching of LBF and ISF slags.....</i>	<i>123</i>
5.5.	CONCLUSIONS.....	124
5.5.1.	<i>Effect of pHs.....</i>	<i>124</i>
5.5.2.	<i>Effect of atmospheres.....</i>	<i>124</i>
5.5.3.	<i>Effect of leaching time</i>	<i>125</i>
5.5.4.	<i>Secondary precipitates.....</i>	<i>125</i>
5.6.	REFERENCES	125
CHAPTER 6: Zn ISOTOPIC COMPOSITION DURING LBF AND ISF SLAGS WEATHERING: A COMPREHENSIVE STUDY		129
6.1.	INTRODUCTION	129
6.2.	MATERIALS AND METHODS	130
6.2.1.	<i>Slags.....</i>	<i>130</i>
6.2.2.	<i>Chemical weathering experiment.....</i>	<i>131</i>
6.2.3.	<i>Leachate chemistry and geochemical modeling</i>	<i>132</i>
6.2.4.	<i>Zn isotopes measurement.....</i>	<i>132</i>
6.2.5.	<i>Solid phase characterization</i>	<i>133</i>
6.3.	RESULTS	133
6.3.1.	<i>Oxidative weathering of slags.....</i>	<i>133</i>
6.3.2.	<i>Anoxic weathering of slags</i>	<i>134</i>
6.3.3.	<i>Effect of the atmospheres on Zn isotopes signatures</i>	<i>136</i>
6.3.4.	<i>Thermodynamic modeling</i>	<i>136</i>

6.3.5.	TEM analysis	138
6.4.	DISCUSSION.....	139
6.4.1.	$\delta^{66}\text{Zn}$ variation in primary mineral phases.....	139
6.4.1.1.	$\delta^{66}\text{Zn}$ signature of amorphous glassy phase.....	139
6.4.1.2.	$\delta^{66}\text{Zn}$ signature of crystalline phases.....	141
6.4.2.	$\delta^{66}\text{Zn}$ fractionation induced by geochemical processes.....	141
6.4.2.1.	$\delta^{66}\text{Zn}$ fractionation due to dissolution processes.....	141
6.4.2.2.	$\delta^{66}\text{Zn}$ fractionation due to sorption(s) processes.....	142
6.4.3.	Fractionation factors from slags to leachate.....	145
6.5.	CONCLUSION.....	146
6.6.	REFERENCES.....	147
CHAPTER 7: BIOWEATHERING OF LEAD BLAST FURNACE METALLURGICAL SLAGS BY PSEUDOMONAS		
AERUGINOSA		
151		
7.1.	INTRODUCTION	151
7.2.	MATERIALS AND METHODS	152
7.2.1.	Chemical composition of the slag	152
7.2.2.	Standardized leaching tests procedures	153
7.2.3.	Abiotic and biotic leaching experiments	153
7.2.4.	Thermodynamic modeling	153
7.2.5.	Analytical methods	154
7.3.	RESULTS	154
7.3.1.	Standardized leaching tests	154
7.3.2.	LBF as micro-nutrients substrate for micro-organisms and consequence on pH evolution	155
7.3.3.	Leachate chemistry	156
7.3.4.	Bulk release of the elements	158
7.3.5.	Thermodynamic modeling	158
7.3.6.	Scanning electron microscope (SEM) analysis	162
7.3.6.1.	Surface morphology and physical characteristics of fresh slag	162
7.3.6.2.	Glass alteration and secondary precipitates	162
7.4.	DISCUSSION.....	164
7.4.1.	Environmental stability of LBF slag.....	164
7.4.2.	Influence of abiotic factors on the LBF slags weathering.....	165
7.4.3.	Influence of <i>P. aeruginosa</i> on the LBF slags bioweathering.....	165
7.5.	CONCLUSIONS.....	166
7.6.	REFERENCES.....	166
CHAPTER 8: BIO-ALTERATION OF METALLURGICAL WASTES BY PSEUDOMONAS AERUGINOSA IN SEMI-FLOW		
THROUGH REACTOR.....		
171		
8.1.	INTRODUCTION	171
8.2.	MATERIALS AND METHODS	172
8.2.1.	Lead blast furnace (LBF) slags.....	172
8.2.2.	Bioalteration experiments.....	172
8.2.3.	Sample preparation and analytical methods.....	173
8.2.3.1.	Polished Sections.....	173
8.2.3.2.	Leachate Chemistry.....	174
8.3.	RESULTS	174
8.3.1.	Leachate chemistry and cumulative release of characteristic elements.....	174
8.3.2.	Leachate chemistry and cumulative release of characteristic elements.....	176
8.3.3.	Slags weathering.....	178
8.4.	DISCUSSION.....	180

8.4.1.	<i>Cumulative metal release LBF slags</i>	180
8.4.2.	<i>Leaching rates</i>	182
8.4.3.	<i>Leaching mechanisms</i>	183
8.5.	CONCLUSIONS	185
8.6.	REFERENCES	186
CHAPTER 9: SUMMARY AND CONCLUSIONS		191
9.1.	INTRODUCTION	191
9.2.	CHEMICAL WEATHERING OF SLAGS (CHAPTER 5 AND 6)	191
9.2.1.	<i>Stability of primary mineral phases</i>	191
9.2.2.	<i>Zn isotopes signatures of primary mineral phases</i>	191
9.2.3.	<i>Evolution of leachate chemistry</i>	192
9.2.4.	<i>Secondary precipitates</i>	192
9.2.5.	<i>Zn isotopes fractionation induced by chemical processes</i>	193
9.3.	BIOLOGICAL WEATHERING OF SLAGS (CHAPTER 7 AND 8)	194
9.3.1.	<i>Slags as micro-nutrient substrate</i>	194
9.3.2.	<i>Effect of abiotic factors</i>	194
9.3.3.	<i>Effect of Pseudomonas aeruginosa</i>	195
9.3.4.	<i>Weathering mechanisms</i>	195
9.3.5.	<i>Slag alteration and secondary precipitates</i>	196
9.3.6.	<i>Cumulative metal release (comparison of weathering conditions)</i>	197
9.4.	FUTURE PERSPECTIVES	198

CHAPTER 1

Introduction

Chapter 1

1.1. Background

Metallurgical slags are vitreous by-products derived from the smelting of metallic ores and usually consist of metal silicates and oxides, in some cases, sulfides and native metals (Hudson-Edwards et al., 2011). They are the unwanted metallurgical wastes whose grade is too low for further treatment and of low economic value in spite of being a significant component of waste stream from pyrometallurgical industry.

This research focuses on the primary smelting slags, known as Lead Blast Furnace (LBF) and Imperial Smelting Furnace (ISF), which are generated by the former pyrometallurgical industries located in Noyelles-Godault, Northern France. Following its closure in 2003, 4 million tons of primary slags have been landfilled as a heap in the vicinity of the Deûle River, near the industrial basin of Nord-Pas-de-Calais (Seigneur et al., 2006). These slag materials are often enriched in toxic elements, in particular metals (Cu, Pb, Zn) and in metalloids (As, Sb) that can be released into the environment through alteration processes and leaching (Ettler et al., 2009). The detail composition varies widely depending on the initial ore content and different processing methods applied (Piatak and Seal, 2010).

Metallurgical slags derived from the processing and smelting of Pb/Zn are defined as 'hazardous wastes' according to the European Waste Catalogue (Commission Decision 94/3/EC) and as a 'commercial substance' according to the European Inventory of Existing Commercial Substances (EINECS) adopted by Council Regulation no. 793/93 (Ettler and Johan, 2003b; Ettler et al., 2001). Thus, considerable attention has been given to the characterization and stability of both old and new lead slags in France, the Czech Republic, Germany, South Africa, Belgium, the United Kingdom, Namibia, the United States, and Canada (de Andrade Lima and Bernardez, 2011).

1.2. Problems of statement

Slags containing significant amount of Pb and Zn have been exposed to the open atmosphere and rainfalls, they are susceptible to the weathering which consequently resulted in the metal mobilization. Lead had been detected in the soil of Noyelles-Godault where the concentration varied from 49-500 ppm depending on the different depth (0-82 cm) from the surface. Epidemiological surveys showed that the concentrations of Pb, Zn and Cd were 1.5 to 79 times higher in the agricultural products, 15-66 times higher in vegetables grown on the polluted soil compared to the control soil (Douay et al., 2008; 2009).

Reusing of these slags as a replacement material in the cement composition and road construction has been planned and is being investigated (Morrison et al., 2003; Saikia et al., 2012); however, the main concern and risk is the release of characteristic elements like Pb and Zn. Many studies have been carried out regarding the mechanisms of leaching, alteration of slags which corresponds either to batch system or to open flow experiments by column studies (Ettler et al., 2004; Ettler et al., 2002; Ettler et al., 2003a; Seigneur et al., 2006). Meanwhile, none of the previous published works focus on the role of micro-organisms

present in the natural environment or on the slags disposal sites, and on the impact of the metabolic activity on the slag alteration whereas some micro-organisms are able to alter the chemistry of slags.

1.3. Objectives

This study was mainly conducted using the isotopic techniques in order to identify the slags bio/weathering mechanisms in natural environment, due to the microbial activity of a heterotrophic microorganism (*Pseudomonas aeruginosa*). The main issue was to decipher between the biological and chemical processes (dissolution, precipitation, complexation and adsorption) affecting the elements behavior and mobilization.

The main objectives can be outlined as the followings:

1. To determine the solid phase characterization of the slags as the baseline information;
2. To decipher the chemical dissolution and microbial influenced dissolution of slags;
3. To study the fate of the characteristic elements (dissolution, precipitation, complexation and adsorption);
4. To identify the changes in the morphology of slags pre and post-weathering;
5. To determine isotopic composition and fractionation of Zn during the chemical and microbial-mediated dissolution, and to further comprehend the weathering mechanisms of both slags.

1.4. Scope of the study

The overall research was planned into three main phases; Phase I: Characterization of slags, Phase II: Chemical dissolution of slags, and Phase III: Bio/weathering of slags as given in Figure 1.1. The main objective of the Phase I was to provide background information on physical, chemical and isotopic characteristics of the slags, thereby achieving the first objective of the research and yet, to serve as the main foundation of the whole research before stepping into further phases.

Providing all the background information and results obtained from Phase I, the research activities under Phase II: chemical dissolution and Phase III: bio-weathering by *Pseudomonas aeruginosa* was initiated. These two phases were oriented in a way that the outcomes and findings can be employed to decipher the chemical dissolution and microbial influenced dissolution of slags, therefore achieving the second objective of overall research plan.

The main research highlight in Phase II and Phase III was to investigate the dissolution of elements of interest (Ca, Fe, Mg, Mn, Al, Si, Zn & Pb), the secondary phases or mineral precipitation, the adsorption of these metals on the secondary precipitates, on the surface of bacteria or slags, and the complexation of metals with the siderophores or extracellular polymeric substance (EPS). In such a way, the third objective of the research which is to study the fate of the characteristic elements (dissolution, precipitation, complexation and adsorption) can be achieved successfully.

Furthermore, the isotopic measurement was incorporated into both Phase II and Phase III where the isotopic composition and fractionation of Zn can be integrated to get a better insight into weathering mechanisms of slags. Hence, the fourth and fifth objectives of the research which are to determine isotopic composition and fractionation of Pb and Zn in chemical and microbial-mediated dissolution, and to further comprehend the weathering mechanisms of both slags can be accomplished.

Ultimately, the research was designed in a way to identify the slags bio/weathering mechanisms in natural environment, due to the microbial activity of a heterotrophic microorganism (*Pseudomonas aeruginosa*). Yet, thanks to the evolution of isotopic techniques and advancement, it was possible to decipher between the biological and chemical processes (dissolution, precipitation, complexation and adsorption) affecting the elements behavior.

In general, the research and experimental work related to the first three phases of the research was mainly conducted in France (between Université Paris-Est and Université Paris-Diderot) while there was 6 months mobility to the Netherlands (UNESCO-IHE).

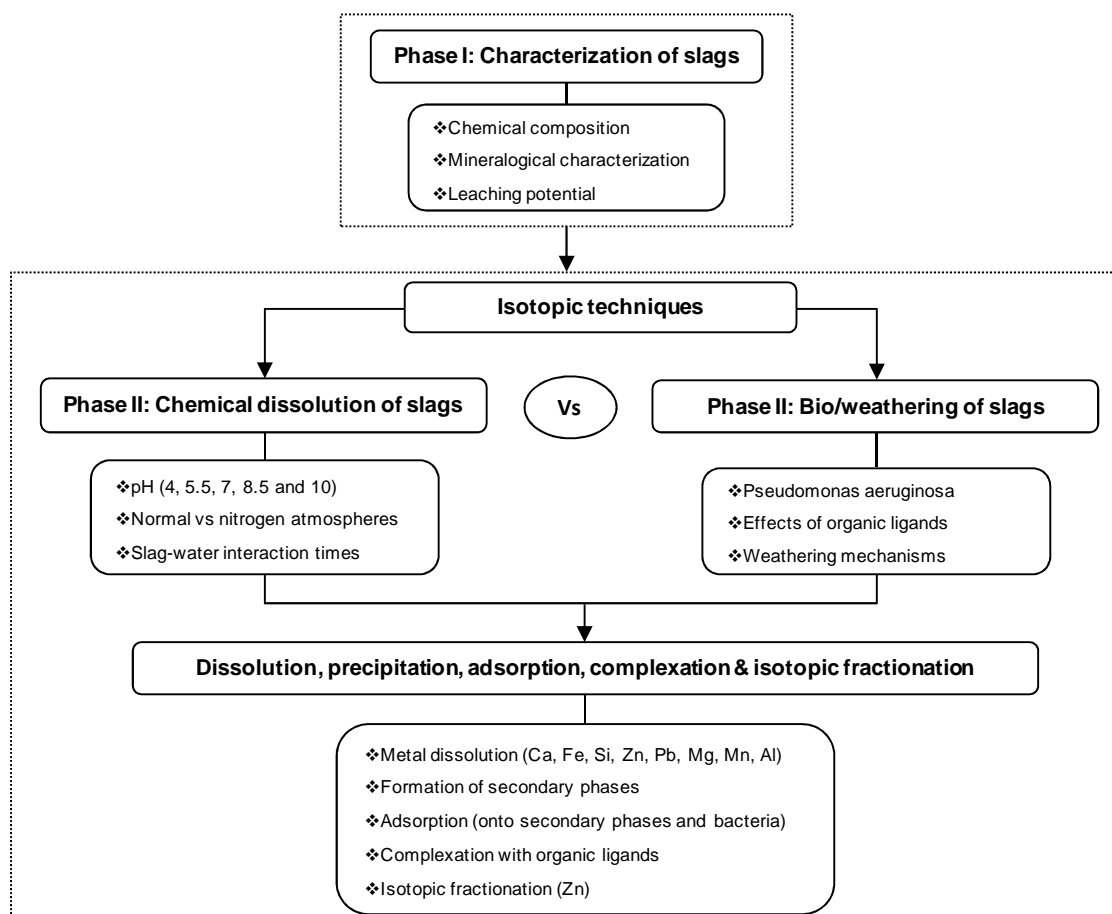


Figure 1.1. Research framework.

1.5. Structure of the thesis

This dissertation is composed of seven chapters as given in Figure (1.2):

Chapter 1: Introduction. It gives an overview of the research such as background information, problem of statement, research objectives and the structure of this thesis.

Chapter 2: Literature review on slags. This review focuses on the microscopic scale characterization of slags, compiles many previous studies of chemical and biological weathering studies, addresses the associated weathering rates and mechanisms, and relates the heavy metal mobilization with environmental pollution.

Chapter 3: Literature review on zinc isotopes. This review outlines the current state of knowledge on Zn isotopic fractionation during the high-temperature roasting process in Zn refineries; $\delta^{66}\text{Zn}$ values variations in air emissions, slags and effluent from the smelters in comparison to geogenic Zn isotopic signature of ores formation and weathering.

Chapter 4: Materials and Research methodology. This chapter gives the detailed information on slags: chemical and mineralogical information; the solid phase characterization techniques: XRD, XRF, SEM and TEM; as well as the isotopic techniques: Zn isotopes.

Chapter 5: Chemical stability of slags. This chapter investigates the leaching behavior of slags as a function of pHs under two different atmospheres (normal atmosphere vs. nitrogen atmosphere) at different slag-water interaction times (1 day vs. 9 days).

Chapter 6: Fractionation of Zn isotopes during chemical weathering of slags. This chapter outlines the active participation of Zn in low-temperature inorganic chemical reactions where the variation in Zn isotopes signature is used as a tool to trace Zn dissolution, formation of Zn secondary phases and Zn adsorption on other secondary precipitates during chemical weathering of slags.

Chapter 7: Bio/weathering of slags under leachate stagnant conditions. This chapter identifies the effect of heterotrophic bacterium (*Pseudomonas aeruginosa*) on the long-term weathering of slags and the bio/weathering mechanisms by simulating natural bio/weathering condition without leachate renewal.

Chapter 8: Bio/weathering of slags under leachate renewal conditions. This chapter further clarifies the role of micro-organisms, and bio/weathering mechanisms during long-term weathering of slags by simulating natural bio/weathering condition in semi flow-through reactors.

Chapter 9: Summary and conclusions: This chapter gives not only summary and conclusions of this study but also recommendations for further development and future research directions.

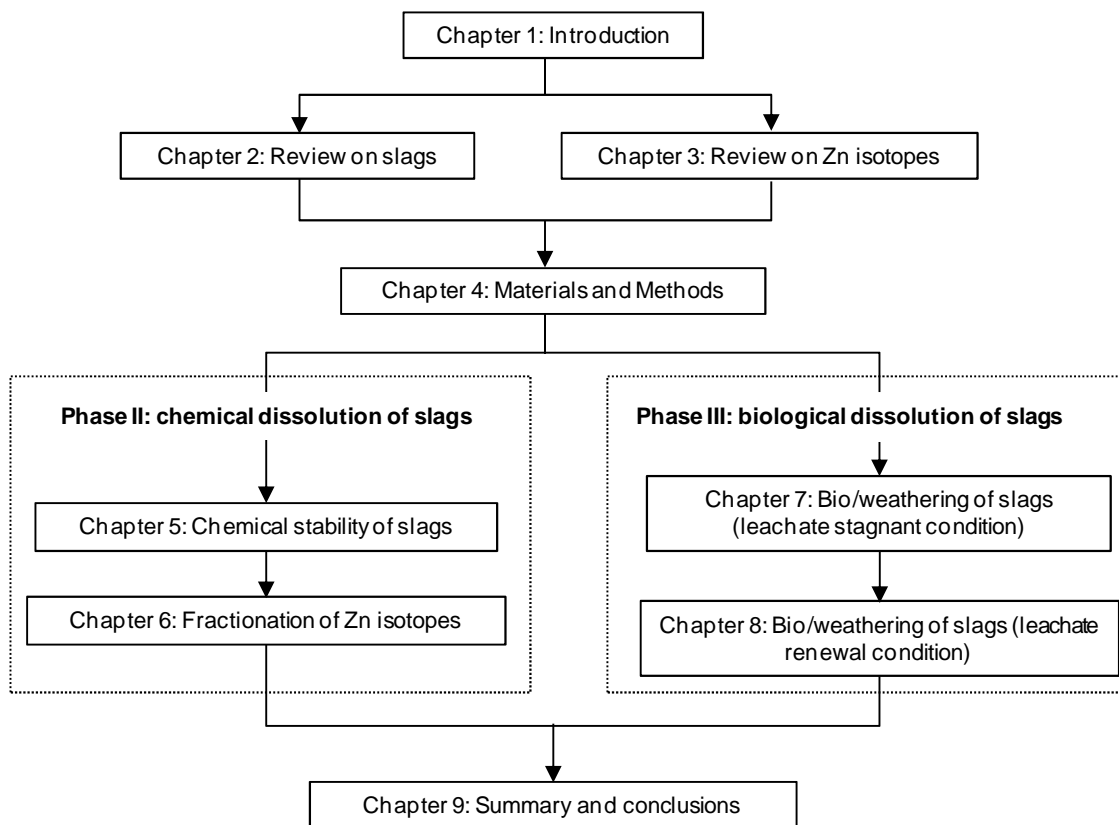


Figure 1.2. Structure of the Thesis.

1.6. References

- De Andrade Lima, L.R.P., Bernardez, L.A., 2011. Characterization of the lead smelter slag in Santo Amaro, Bahia, Brazil. *J Hazard Mater*, 189: 692-9.
- Douay, F., Roussel, H., Pruvot, C., Loriette, A., Fourier, H., 2008. Assessment of a remediation technique using the replacement of contaminated soils in kitchen gardens nearby a former lead smelter in Northern France. *Sci Total Environ*, 401: 29-38.
- Douay, F., Pruvot, C., Waterlot, C., Fritsch, C., Fourier, H., Loriette, A., Bidar, G., Grand, C., de Vaufléury, A., Scheifler, R., 2009. Contamination of woody habitat soils around a former lead smelter in the North of France. *Sci Total Environ*, 407: 5564-77.
- Ettler, V., Legendre, O., Bodéan, F., Touray, J.C., 2001. Primary Phases and Natural Weathering of Old Lead-Zinc Pyrometallurgical Slag from PRÍbram, Czech Republic. *Can Mineral*, 39: 873-888.
- Ettler, V., Mihaljevic, M., Touray, J.C., Piantone, P., 2002. Leaching of polished sections: an integrated approach for studying the liberation of heavy metals from lead-zinc metallurgical slags. *Bulletin de la Société géologique de France*, 173: 161-169.
- Ettler, V., Piantone, P., Touray, J.C., 2003a. Mineralogical control on inorganic contaminant mobility in leachate from lead-zinc metallurgical slag: experimental approach and long-term assessment. *Mineral Mag*, 67: 1269-1283.

- Ettler, V., Johan, Z., 2003b. Mineralogy of metallic phases in sulphide mattes from primary lead smelting. *Comptes Rendus Geosci*, 335: 1005-1012.
- Ettler, V., Komarkova, M., Jehlicka, J., Coufal, P., Hradil, D., Machovic, V., Delorme, F., 2004. Leaching of lead metallurgical slag in citric solutions-implications for disposal and weathering in soil environments. *Chemosphere*, 57: 567-77.
- Ettler, V., Johan, Z., Křibek, B., Šebek, O., Mihaljevič, M., 2009. Mineralogy and environmental stability of slags from the Tsumeb smelter, Namibia. *Appl Geochem*, 24: 1-15.
- Hudson-Edwards, K.A., Jamieson, H.E., Lottermoser, B.G., 2011. Mine Wastes: Past, Present, Future. *Elements*, 7: 375-380.
- Morrison, C., Hooper, R., Lardner, K., 2003. The use of ferro-silicate slag from ISF zinc production as a sand replacement in concrete. *Cem Concr Res*, 33: 2085-2089.
- Piatak, N.M., Seal, R.R., 2010. Mineralogy and the release of trace elements from slag from the Hegeler Zinc smelter, Illinois (USA). *Appl Geochem*, 25: 302-320.
- Saikia, N., Cornelis, G., Cizer, O., Vandecasteele, C., Gemert, D., Van Balen, K., Van Gerven, T., 2012. Use of Pb blast furnace slag as a partial substitute for fine aggregate in cement mortar. *J Mat Cycles Waste Manage*, 14: 102-112.
- Seigneur, N., Bulteel, D., Damidot, D., Gauthier, A., Potdevin, J.L., 2006. Weathering of metallurgical slag heaps: multi-experimental approach of the chemical behaviours of lead and zinc. *Waste Manage Environ III*, 1: 31-40.

CHAPTER 2

**Lead and zinc metallurgical slags
mineralogy and weathering: a review**

Chapter 2

2.1. Introduction

2.1.1. World production of lead and zinc

The mining and industrial production of lead and zinc usually follow the changes and trends in their consumption, and global economic growth. Demand for lead is heavily reliant on the lead-acid battery industry and the automotive sector (Guberman, 2012). The major use for zinc is galvanizing, in which a zinc coating is applied to steel to prevent corrosion. Other uses of zinc include the production of brass and bronze, zinc-base alloys for die-casting, and chemicals (Tolcin, 2012). In 2010, global mining industries produced 4,140,000 metric tons of lead and 12,000,000 metric tons of zinc, corresponding to a 12% and 14% increase compared to the figures of 2006 (Table 2.1). Likewise, primary lead refinery increased the production by 12% and zinc smelting increased by 15% in 2010 compared to 2006.

Table 2.1. World production of lead and zinc (Guberman, 2012; Tolcin, 2012).

Production (metric tons)		2006	2007	2008	2009	2010
Lead	Mine	3,630,000	3,720,000	3,880,000	3,900,000	4,140,000
	Primary refinery	3,690,000	3,660,000	3,980,000	3,860,000	4,200,000
	Secondary refinery	4,200,000	4,420,000	4,600,000	4,860,000	5,090,000
Zinc	Mine	10,300,000	11,000,000	11,700,000	11,400,000	12,000,000
	Smelter	10,800,000	11,400,000	11,700,000	11,300,000	12,700,000

2.1.2. Pyrometallurgical processes

Both lead and zinc are mainly found naturally as a sulfide ore containing small amounts of copper, iron, and other trace elements. The ore, typically after being concentrated at or near the mine, is further processed at the primary refinery. The typical primary lead refinery is done by means of the lead blast furnace technology (LBF) in a counter-current reactor where a charge (mainly sinter, coke and fluxes) moves through a vertical shaft in counter-current to the ascending gas flow. The descending charge successively passes through the preheating zone (at 200°C), the reaction or reduction zone (at 900°C), the melting zone (at 1150°C), and finally the combustion zone (at 2200°C) (Verguts, 2005).

Production of zinc includes the use of high-temperature roasters or smelters using imperial smelting technology (ISF), including multiple-hearth, suspension bed, or fluidized bed roasters. Zinc ore concentrate is introduced into a multiple-hearth roaster (at about 690°C) where the hot gases are passed through the hearths that are oxidized to produce calcine. The concentrates are blown into a suspension roaster or fluidized-bed roaster (at about 980°C)

where the desulfurization and oxidation reactions occur (USEPA, 1986; USEPA, 1995). Thus, the production of lead and zinc are done at very high temperatures and the schematic diagram for primary production of lead and zinc are given in Figure 2.1.

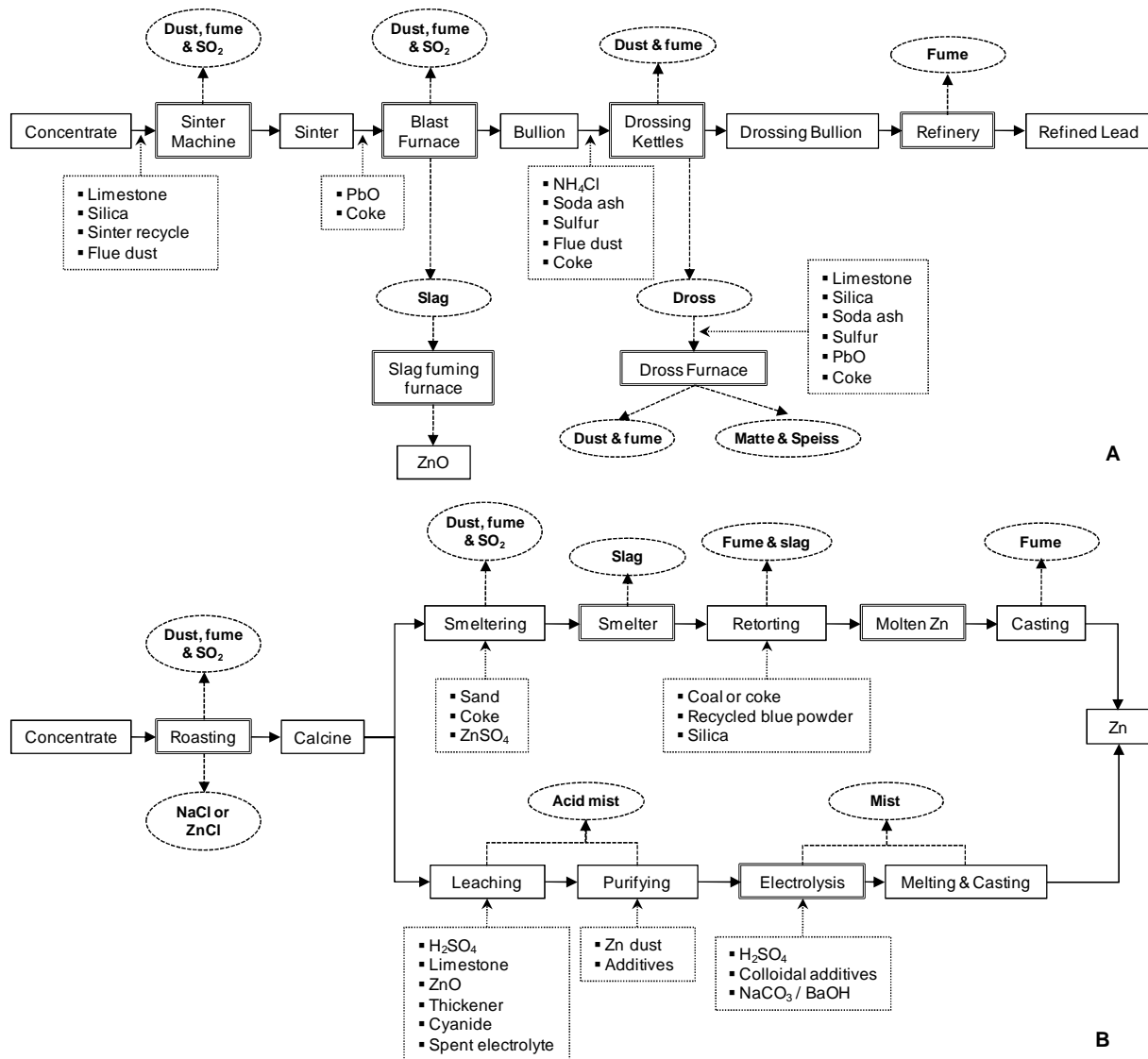


Figure 2.1. Primary production process of lead (A) and zinc (B) redrawn from (USEPA, 1986; USEPA, 1995).

2.1.3. Environmental profile of pyrometallurgical industries

Primary lead refineries generate air emissions, process waste and wastewater, and different types of solid wastes (Table 2.2). Nearly 85% of the sulfur present in the lead ore concentrate is eliminated in the smelting process, where the offgas (>5% of SO₂) is sent to a sulfuric acid plant, while the weak stream (<0.5% of SO₂) is vented to the atmosphere after removal of particulates. Particulate emissions from blast furnaces contain many different kinds of materials, including a range of lead oxides, quartz, limestone, iron pyrites, iron-limestone-silicate slag, arsenic, and other metallic compounds associated with lead ores. The blast furnace slag is composed primarily of iron and silicon oxides, as well as metals, semi-metals

or metalloids such as aluminum, calcium, antimony, arsenic, beryllium, cadmium, chromium, cobalt, copper, lead, manganese, mercury, molybdenum, silver, and zinc. This blast furnace slag is either recycled back into the process or disposed of in piles on site. About 50-60 % of the furnace output is slag and residual lead that are both returned to the blast furnace. Moreover, it also produces wastewaters and slurries, including acid plant blow-down, slag granulation water, and plant wash-down water.

Similar to lead smelters, primary zinc smelters generate air emissions, process wastes, and different solid wastes (Table 2.3). Approximately 93-97% of S from the ore is emitted as SO₂. Thus, all SO₂ from the roasting process at zinc smelters is recovered at on-site sulfuric acid plants. Much of the particulate matter emitted from primary zinc facilities is also attributable to smelters where the composition of particulates varies with operating parameters; the particulates are likely to contain zinc and lead. Wastewaters are generated during the leaching, purification, and electro-winning stages of primary zinc processing when electrolyte and acid solutions become too contaminated to be reused again. Solid wastes, mainly molten slags, are generated at various stages in primary zinc processing.

Table 2.2: Process material inputs and pollution outputs from primary and secondary lead production (USEPA, 1995).

Process	Material Input	Air Emissions	Process Wastes	Other Wastes
Lead Sintering	Lead ore, iron, silica, limestone flux, coke, soda ash, pyrite, zinc, caustic, and bag house dust	Sulfur dioxide, particulate matter containing cadmium and lead	n/a	n/a
Lead Smelting	Lead sinter, coke	Sulfur dioxide, particulate matter containing cadmium and lead	Wastewater, slag granulation water	Slag containing impurities such as zinc, iron, silica, and lime, surface impoundment solids
Lead Drossing	Lead bullion, soda ash, sulfur, bag house dust, coke	n/a	n/a	Slag containing such impurities as copper, surface impoundment solids
Lead Refining	Lead drossing bullion	n/a	n/a	
Lead-acid Battery	Lead-acid batteries	n/a	n/a	Polypropylene case fragments, dilute sulfuric acid
Secondary Lead Smelting	Battery scrap, rerun slag, drosses, oxides, iron, limestone, and coke	Sulfur dioxide, particulate matter containing cadmium and lead	n/a	Slag, emission control dust

Table 2.3: Process material inputs and pollution outputs from primary zinc production (USEPA, 1995).

Process	Material Input	Air Emissions	Process Wastes	Other Wastes
Zinc Calcining	Zinc ore, coke	Sulfur dioxide, particulate matter containing zinc and lead	n/a	Acid plant blowdown slurry
Zinc Leaching	Zinc calcine, sulfuric acid, limestone, spent electrolyte	n/a	Wastewaters containing sulfuric acid	n/a
Zinc Purification	Zinc-acid solution, zinc dust	n/a	Wastewaters containing sulfuric acid, iron	Copper cake, cadmium
Zinc Electro-winning	Zinc in a sulfuric acid/aqueous solution, lead-silver alloy anodes, aluminum cathodes, barium carbonate, or strontium, colloidal additives	n/a	Dilute sulfuric acid	Electrolytic cell slimes/sludges
Zinc Smelting	Zinc scrap, electric arc furnace dust, drosses, diecastings, fluxes	Particulates	n/a	Slags containing copper, aluminum, iron, lead, and other impurities
Secondary Zinc Reduction Distillation	Medium-grade zinc drosses, oxidic dust, acids, alkalines, or ammoniacal solutions	Zinc oxide fumes	n/a	Slags containing copper, aluminum, iron, lead, and other impurities

2.1.4. Environmental pollution due to slags from metallurgical industries

Lead and zinc metallurgical activities are large contributors of anthropogenic Zn and Pb pollution in many environmental compartments: atmospheric heavy metal emissions and deposition (van Alphen, 1999), surface and ground water (Parsons et al., 2001), kitchen garden soil (Douay et al., 2008), woody habitat soil (Douay et al., 2009), agricultural topsoil (Pelfrene et al., 2011), river bank soil (Sivry et al., 2010), river sediment (Audry et al., 2004; Vdovic et al., 2006), stream sediment (Yang et al., 2010), seepage at slag dumps (Navarro et al., 2008) with high potential to groundwater contamination, and evidence of high bio-accessibility of Pb and Zn in the human body (Bosso and Enzweiler, 2008; Ettler et al., 2012).

2.2. Metallurgical slags

Slags are predominantly vitreous by-products derived from smelting of metallic ores and usually consist of metal silicates and oxides, in some cases also sulfides and native metals (Hudson-Edwards et al., 2011). They are the unwanted metallurgical wastes whose grade is too low for further treatment and of low economic value in spite of being a significant component of the waste stream from the mining industry. They are either dumped in the vicinity of the mining site and accumulated for long periods of time or reused as fill, ballast,

abrasive and aggregate in concrete and cement production, and in road construction (Ettler and Johan, 2003b; Lottermoser, 2002). Whereas slags generated from ferrous industry are widely used for construction purposes (Saikia et al., 2012), the use of slags generated from non-ferrous metal (Pb, Zn, Cu, Ni, Cr) industries has so far been limited (Barna et al., 2004).

Zn and Pb slags are produced during pyrometallurgical treatment of sulfide ores and have been used as aggregates in road construction and in concrete (Morrison et al., 2003; Saikia et al., 2012). Metallurgical slags derived from the processing and smelting of Pb/Zn is defined as ‘hazardous waste’ according to the European Waste Catalogue (Commission Decision 94/3/EC), but also as a ‘commercial substance’ according to the European Inventory of Existing Commercial Substances (EINECS) adopted by Council Regulation no. 793/93 (Ettler et al., 2001; Ettler et al., 2003a).

2.2.1. Methods for Mineral Characterization

Several techniques have been applied for the characterization of mineral phases: particle size, surface morphology, degree of crystallinity, detailed chemical composition of each mineral phase, trace metal concentration, etc. Some common techniques applied in recent studies are given in Table 2.4. The availability of powerful X-ray beams generated at synchrotron facilities has produced a new family of techniques that are very useful for characterizing mine waste minerals (Jamieson, 2011). Synchrotron-based X-ray absorption spectroscopy (XAS) can be used to identify the minerals hosting potentially toxic elements such as Pb or Zn. Depending on the part of the absorption spectrum used; the techniques are further extended as X-ray absorption near edge spectroscopy (XANES) or extended X-ray absorption fine structure (EXAFS). If a micro-focused synchrotron beam is used, near-simultaneous analysis using micro-XAS, micro-XRF (which uses the X-ray fluorescence signal to provide information on elemental composition) and micro-XRD (X-ray diffraction) can be accomplished (Jamieson, 2011).

Table 2.4: Analytical techniques applied in the characterization and mineralogical studies of slags.

Analytical techniques	Application	References
Energy-dispersive X-ray fluorescence spectroscopy (XRF)	Elemental concentration of powdered mineral or slag samples	(Scheinert et al., 2009)
X-ray diffraction (XRD)	Mineral identification based on crystal structure	(Piatak and Seal, 2010)
Micro-X-ray diffraction using conventional or synchrotron sources (micro-XRD)	Grain-scale mineral identification based on crystal structure, application to poorly crystalline materials	(Jamieson, 2011)
Scanning Electron Microscopy (SEM) with Energy Dispersive analysis (EDS)	Imaging, element mapping, surface morphology and qualitative spot chemical analysis	(Bosso and Enzweiler, 2008)

Transmission Electron Microscopy (TEM) with energy dispersive analysis (EDS) and selected area electron diffraction (SAED)	Mineral identification of the individual particles, including imaging, qualitative chemical analysis	(Vítková et al., 2013)
Electron microscope (MPA) with a X-ray dispersion energy spectrometry system (EDS)	Quantitative spot chemical analysis of a tiny mineral spot, and the texture of the particles of the slag	(de Andrade Lima and Bernardez, 2013)
Synchrotron-based micro-X-ray radiation fluorescence (μ SXRF), Polarized X-ray absorption fine structure (P-EXAFS) and (μ EXAFS), X-ray absorption near edge structure (XANES)	Oxidation state, speciation of a particular element present in a mineral phase at molecular level analysis	(Manceau et al., 2000)
X-ray photoelectron spectroscopy (XPS) analyses	Analysis of mineral surface chemistry, quantitative analysis of chemical composition, and imaging	(Biesinger et al., 2007)

2.2.2. General composition of slags

Slags are very heterogeneous materials where the composition depends on the smelting history, the chemical composition of the ore, the fluxes (limestone, iron stone, ferrous silicate, silica) and fuel (coke, coal, firewood, charcoal) used (Lottermoser, 2002). The chemical composition of Lead Blast Furnace (LBF) and Imperial Smelting Furnace (ISF) slags from different countries is given in Table 2.5.

The slags originating from different countries are highly enriched in Ca, Fe and Si, where the difference in detailed composition reflects the variation in furnace charges, smelting conditions and technologies used over time. The enrichment of Al, but impoverishment in Ca of the Czech slags indicate the age of the slags (Table 2.6) generated around 1907 to 1943 in the Czech Republic (Ettler et al., 2000) and the origin of the primary ores; mainly carbonate and oxides rich ores rather than sulfides (Ettler et al., 2009). The lesser or higher presence of Zn and Pb, and the relict ores in the slags indicate the efficiencies of the processing technologies used at the time. The S concentrations ranging from 0.7 to 3.85 wt% indicate that metals dissolved in slag melt are present not only in the silicate matrix and pure metallic phases, but can also be associated with S in the form of sulfides (PbS, ZnS, CuS). Moreover, the presence of TiO₂, MnO, CaO, MgO, Na₂O, K₂O and P₂O₅ can be observed in both LBF and ISF. The heterogeneous LBF and ISF can be further compared to the historical slags and secondary processing plant slags (Table 2.6).

Historical slags originating from France and Sweden (generated around the 3-4th and 16th century, respectively) show the highest content of Si and Ca, with relative deficiency in Fe content and the absence of Pb and Zn (Table 2.6). Slags produced during the Middle Ages in the Czech Republic are deficient in Ca compared to other slags, which is due to the lack of usage of CaCO₃ additives. On the other hand, the slags from secondary car batteries processing units and those from Australia (generated early 20th century or modern slags) have a similar chemical composition of Si, Ca, and Fe, with relatively little amounts of Pb and Zn present. Thus, all historical slags produced before the 19th century have a similar chemical

composition regardless of their native countries. The same goes for modern slags generated after the 19th century regardless of their native countries, as well as primary or secondary production sources.

2.2.3. Primary mineralogical phases

Metallurgical slags vary widely in terms of chemical composition, mineralogy and structures, as a result of the initial ore content, additives used, different processing methods, and the age of the slags (Mahé-Le Carlier et al., 2000). The mineralogy of slags originated from Pb and Zn smelters has been summarized in Tables 2.7 to 2.11. Primary mineral phases and the chemical composition of each phase in LBF slags originating from different countries are given in Tables 2.7 and 2.8. Likewise, primary mineral phases and their related chemical composition of ISF slags are given in Tables 2.9, 2.10a and 2.10b. Finally, the chemical composition of each mineral phase present in historical smelting slags versus slags from secondary processing of car batteries are given in Table 2.11.

LBF originated from France is mainly composed of non-silicate minerals such as the spinel groups (spinel, magnesiochromite, franklinite, wüstite, and magnetite) and other oxides (mixture of Zn and Fe oxides) as they contain only one silicate mineral: melilite. In contrast, LBF slags from Brazil and Czech Republic show the presence of more silicate minerals: the olivine group (fayalite, kirschsteinite, olivine), pyroxene group (hedenbergite), and melilite group (unidentified phase and willemite). Non-silicates have not been observed in the slags from the Czech Republic but they contain only substantial amounts of relict ores (galena, sphalerite, würtzite, pyrrhotite) (Table 2.7). The microprobe analysis of detailed chemical compositions of these phases is given in Table 2.8.

ISF slag generated from France includes only one silicate mineral (hardystonite), non-silicates group of spinel (wüstite), other oxides (mixture of Fe, Zn and Al), and traces of relict ores (wurzite and sphalerite). ISF from USA contains the olivine group (fayalite, olivine), pyroxene group (clinoferrosilite, hedenbergite), feldspars (K-feldspar, hyalophane, labradorite), melilite group (hardystonite) and alumino silicate group (willemite, mullite, quartz, sillimanite). ISF slag from Poland contains olivine group (kirschsteinite, olivine), pyroxene group (wollastonite), feldspars (K-feldspar, hyalophane, leucite), melilite group (melilite) and alumino silicate group (willemite). More diversity of silicates and oxides has been observed in slags from the USA and Poland (Table 2.9). Tables 2.10a & 2.10b give the microprobe analysis of detailed chemical compositions of these phases.

For both LBF and ISF slags, Zn and Pb are redistributed among several crystalline phases (silicates, oxides, sulfide or metallic phases) and residual glass. Zinc, being dissolved in the silicate melt, is partially incorporated into the structures of oxides (spinel), silicates (clinopyroxene, melilite, olivine), sulfides (sphalerite or würtzite) and glass. In contrast, Pb behaves as an “incompatible element” and is concentrated in residual glass and in Pb-rich sulfide or metallic inclusions trapped in the glass (Ettler et al., 2000; Ettler et al., 2001).

The composition of the mineral phases bears a direct relationship with the bulk composition of the melt and with the cooling regime, which control the crystallization sequence in the slag. For example, the assemblage I, II and III are from the coarse-grain and outer cast of slag dumped where the presence of the pyroxene group indicates the relatively slow cooling regime of the slag. Assemblage IV is located in the central part of the slag dump where the absence of pyroxene indicates the rapid cooling, quenching effect of the slag (Ettler et al., 2001).

Assemblage I: olivine → clinopyroxene → glass

Assemblage II: spinel → olivine → clinopyroxene → glass

Assemblage III: spinel → melilite → clinopyroxene → olivine → glass

Assemblage IV: spinel → melilite → olivine → glass

Spinel groups are the first mineral phases formed from the high-temperature silicates melts, where silicates nucleating simultaneously with the oxides usually enclose small crystals of spinel. They can be found either in trace or in abundant amount and generally as cubic or octahedral crystals several micrometers across the slag sample. The melilite group is found abundantly in the slag, either as irregular prism with star shape, as dendrites or as phenocrysts from ten to hundreds of micrometers in size. Likewise, olivine is the most abundant crystalline phase in the slags which crystallized either early or as the last silicate filling spaces between the earlier-crystallized silicates. They are present in different shapes such as in a herring-bone pattern, in a thin-narrow-long strip laths pattern of several hundred of micrometers in length or as very fine dendrites from several micrometers to tens of micrometers in size. Feldspars are enriched in Al and silicate, however, the crystallization of Ca-Pb feldspars indicates that the slag melt was poor in alkalis. In addition, feldspar formation completely removed silica from the melt and prevented the formation of residual glass.

The chemical composition of each mineral phase present in historical smelting slags versus slags from secondary processing of car batteries are given in Table 2.11. Historical slags are abundant in silicate minerals: olivine group (fayalite, kirschsteinite, olivine), pyroxene group (wollastonite, hedenbergite), melilite group (melilite) and spinel group (magnetite). Meanwhile, less silicate minerals phases are found from secondary processing slags where Na-bearing phases are due to the use of sodium compounds in the Harris refining technological process from 1941 to 1997. The presence of these mineral phases, either in low or high abundance, is significantly contributing to the behavior of heavy metals during the weathering process. Mineralogy and mineral chemistry are important in understanding the partitioning of metals within primary solid phases when slags are being susceptible to weathering (Piatak and Seal, 2010).

Table 2.5: Major and minor chemical composition of Lead Blast Furnace (LBF) and Imperial Smelting Furnace (ISF) slags from different countries.

Type of slags	LBF				ISF			
Origin of slags	France	Brazil	Czech republic	Belgium	France	USA	Poland	UK
Unit	% (wt)							
SiO ₂	23.17-26.59	21.39	34.92	25.7	21.9-25.82	32.1-57.1	12.43-41.27	11.3-19.83
CaO	20.00-22.47	23.11	20.5	18.9	18.10-18.77	1.55-15.3	4.97-23.53	3.3-15.66
FeO & Fe ₂ O ₃	31.01-33.7	28.1	24.98	34	30.89-33.7	7.3-21.7	9.86-29.68	30.66-52.9
Al ₂ O ₃	1.89-2.48	3.56	5.07	5.4	9.89-10.4	12.7-21.9	3.38-20.69	5.5-8.25
MgO	2.61-2.8	5.44	2.36	1.4	1.78-1.84	0.61-1.28	3.6-10.68	-
MnO	0.80-0.81	1.44	2.28	0.66	1.02-1.06	0.04-0.35	0.34-1.21	-
Na ₂ O	0.58-0.64	0.27	0.23	0.87	0.55-0.58	0.9-3.93	0-0.27	-
K ₂ O	0.27-0.38	0.26	0.97	0.31	0.68-0.7	1.23-3.91	0.18-0.95	-
TiO ₂	0.19-0.2	0.25	0.59	-	0.48-0.49	0.64-1.14	0.13-0.89	-
P ₂ O ₅	0.22-0.29	-	0.34	-	0.5-0.56	0.1-0.46	0.09-0.35	-
Zn	8.06-11.2	7.61	36300*	4.02	6.54-7.51	11.4-8960*	0.3-38.0	5.57-11.43
Pb	3.38-3.55	3.77	11223*	2.29	0.69-1.56	1.9-711*	0.15-6.20	0.57-6.87
S	0.19-0.7	0.37	1.11	-	1.05-1.58	0.08-2.68	0.41-2.23	1.77-4.11
Unit	ppm	mg/kg	mg/kg	mg/kg	ppm	mg/kg	-	-
Ag	12.1-13	-	-	-	44-45	1.0-10	-	-
As	717-780	541	264	4200	930-1210	1.0-32	-	-
Ba	5919-6500	169	1106	-	2410-2440	215-1170	-	-
Cr	908-965	71	36.8	1001	1460-1510	71-103	-	-
Ni	71-83	82.2	20.4	416	198-267	24.3-107	-	-
Mo	266-280	28.4	-	279	81-83	2.4-37.3	-	-
Cd	3.2-4	-	9.22	5.81	<0.5	0.8-48.1	-	-
Cu	1150-1250	538	969	-	2600-2900	16-6360	-	-
References	A, B, C	D	E	F	A, C	G	H	I

*Zn and Pb in ppm unit. Please note that ppm refers to water weight whereas mg/kg refers to solid weight.

A: (Deneele, 2002), B: (Seigneur et al., 2007), C: (Barna et al., 2004), D: (de Andrade Lima and Bernardez, 2012), E: (Ettler et al., 2004), F: (Saikia et al., 2012; Saikia et al., 2008), G: (Piatak and Seal, 2010), H: (Puziewicz et al., 2007), I: (Morrison et al., 2003)

Table 2.6: Major chemical composition of historical smelting slags and slags from secondary process.

Origin of slags	Historical Smelting Slags				Slags from Secondary processing car batteries	
	France	Australia	Sweden	Czech republic	Old tech	Modern tech
	3-4 th century	1901 to 1943	16 th century	Middle Ages		
Unit	% (wt)					
SiO ₂	56.83	34.8	61.28	39.19	29.32	30.06
CaO	15.69	15.53	24.06	3.23	19.79	21.8
FeO & Fe ₂ O ₃	11.97	32.88	1.46	23.41	32.25	28.62
Al ₂ O ₃	7.17	5.41	3.42	4.46	5.46	11.52
MgO	2.71	0.91	5.72	3.46	2.31	2.88
MnO	1.89	0.39	3.27	3.92	1.31	0.88
Na ₂ O	0.06	0.26	0.33	0.21	0.82	0.32
K ₂ O	3.34	0.6	0.51	1.42	0.21	0.11
TiO ₂	0.43	-	0.02	0.41	0.3	0.48
P ₂ O ₅	0.25	0.27	0	0.61	0.23	0.3
Zn	-	23643*	-	5.41	2.17	0.21
Pb	-	7605*	-	11.81	2.51	0.68
S	-	1.15	-	1.19	0.94	0.36
Reference	(Mahé-Le Carlier et al., 2000)	(Lottermoser, 2002)	(Mahé-Le Carlier et al., 2000)	(Ettler, 2000)	(Ettler, 2000)	(Ettler, 2000)

*Zn and Pb in ppm unit.

Table 2.7: Mineralogy of primary phases found in LBF originated from different countries.

LBF						
Minerals	Primary phases	Composition	France	Brazil	Czech republic	
Silicate	Olivine-group	Fayalite ($\text{Fe}^{2+}_2\text{SiO}_4$)			*	
		Kirschsteinite ($\text{CaFe}^{2+}\text{SiO}_4$)		*	*	
		Olivine [$(\text{Ca},\text{Fe})_2\text{SiO}_4$]			*	
		Willemite (Zn_2SiO_4)	*	*		
	Pyroxene-group	Hedenbergite ($\text{CaFe}^{3+}\text{Si}_2\text{O}_6$)			*	
	Melilite-group	$\text{Ca}_2(\text{Fe},\text{Mg},\text{Zn},\text{Al})(\text{Al},\text{Si})_2\text{O}_7$			*	*
Non-silicate	Spinel-group	Spinel (MgAl_2O_4)		*		
		Magnesiochromite (MgCr_2O_4),	*			
		Franklinite [$(\text{Zn},\text{Mn}^{2+},\text{Fe}^{2+})(\text{Fe}^{3+},\text{Mn}^{3+})_2\text{O}_4$]	*	*		
		Magnetite ($\text{Fe}^{3+}_2\text{Fe}^{2+}\text{O}_4$)	*			
	Other oxides	Zn substituted Wüstite ($\text{Fe}_{(0.85-x)}\text{Zn}_x\text{O}$)	*			
		Wüstite (FeO)	*	*		
		Iron(II) Chromate (FeCrO_4)	*			
		Magnetite (Fe_3O_4)	*			
	Pure metals	Zincite (ZnO)			*	
		Lead (Pb)	*	*	*	
	Sulfides-group	Galena (PbS)			*	
		Wurzite (ZnS)			*	
		Sphalerite ($(\text{Zn},\text{Fe})\text{S}$)			*	
		Pyrrhotite ($\text{Fe}_{(1-x)}\text{S}$)			*	
Reference			(Deneel et al., 2002; Seignez et al., 2007; Seignez et al., 2008)	(de Andra de Lima and Bernar dez, 2012)	(Ettler and Johan, 2003b; Ettler et al., 2001)	

Table 2.8: Chemical composition of each mineral phase present in LBF.

Phases (% wt)	Non-Silicate			Silicate						
	G1 (n=7)	Matrix G1	Surface G1	Olivine-group	Pyroxene-group	Melilite-group	Spinel-group			
				Ol	ClIPy	Me	Sp	MgCr	Fr	Mg
SiO₂	26.4	37.95-39.69	33.11-37.38	29.66-32.89	39.87-43.34	38.62-39.98	0.35-5.52	0.28	0.10	0.05
TiO₂	0.2	0.23-0.52	0.06-0.41	0.00-0.06	0.25-1.03	0.00-0.06	0.64-3.89	0.61	0.09	0.34
Al₂O₃	2.5	7.96-13.40	4.26-5.83	0.01-0.74	4.73-11.2	3.48-5.09	13.18-38.99	15.83	0.62	7.60
Cr₂O₃	0.0	0.00-0.05	0.00-0.05	0.01-0.03	0.00	0.00-0.04	0.00-6.96	44.56	1.66	13.59
FeO	26.5	15.50-21.89	11.40-36.00	27.67-55.57	18.91-26.14	7.51-9.00	18.24-30.86	5.55	7.69	17.29
Fe₂O₃	-	-	-	-	-	-	16.63-48.44	8.95	67.62	45.45
CaO	22.9	9.72-20.12	11.30-33.08	2.77-27.48	20.59-22.62	34.11-37.28	-	0.57	0.68	0.13
MgO	1.9	0.01-0.21	1.08-2.97	0.85-5.33	0.19-2.41	1.82-4.45	0.35-2.84	12.46	4.83	1.99
MnO	0.8	0.53-1.43	0.05-5.43	2.13-5.91	0.62-1.8	0.04-1.06	0.27-0.67	0.79	0.91	0.74
ZnO	11.2	2.59-8.00	3.41-9.8	1.98-6.28	1.23-3.12	4.11-10.51	8.92-19.91	9.90	15.79	12.72
PbO	4.3	0.26-3.72	0.09-0.96	0.02-0.18	0.08-0.20	0.02-0.35	-	-	-	-
Na₂O	0.9	0.19-2.27	0.19-2.05	0.08-0.27	0.03-0.28	0.32-2.36	-	-	-	-
K₂O	0.4	0.00-0.05	0.00-0.05	0.03-0.14	0.01-0.26	0.08-0.69	-	-	-	-
Reference	(Deneele, 2002; Seigneur et al., 2007)	(Ettler et al., 2001)					(Ettler et al., 2001)	(Deneele, 2002)		

Me-Melilite, Ol-Olivine, G1-Glass, ClIPy-Clinopyroxene, Fr-Franklinite, MgCr-Magnesiocromite, Mg-Magnetite

Table 2.9: Mineralogy of primary phases found in ISF originated from different countries.

ISF						
Minerals	Primary phases	Composition	France	USA	Poland	
Silicate	Olivine-group	Fayalite ($\text{Fe}^{2+}_2\text{SiO}_4$)		*		
		Kirschsteinite ($\text{CaFe}^{2+}\text{SiO}_4$)			*	
		Olivine [$(\text{Ca},\text{Fe})_2\text{SiO}_4$]		*	*	
		Willemite (Zn_2SiO_4)		*	*	
	Pyroxene-group	Wollastonite ($\text{Ca}_2\text{Si}_2\text{O}_6$)				*
		Clinoferrosilite ($\text{Fe}_2\text{Si}_2\text{O}_6$)		*		
		Hedenbergite ($\text{CaFe}^{3+}\text{Si}_2\text{O}_6$)		*		
	Feldspars	K-feldspar (KAlSi_3O_8)			*	*
		Hyalophane (K,Ba)[Al(Si,Al)Si ₂ O ₈]			*	*
		Anorthite ($\text{CaAl}_2\text{Si}_2\text{O}_8$)			*	
		Labradorite (Ca,Na)[Al(Al,Si)Si ₂ O ₈]			*	
		Leucite (KAlSi_2O_6)				*
	Melilite-group	Hardystonite ($\text{CaZnSi}_2\text{O}_7$)	*	*		
	Alumino silicates	Mullite ($\text{Al}_6\text{Si}_2\text{O}_{13}$)			*	
		Sillimanite (Al_2SiO_5)			*	
Non-Silicate	Spinel-group	Spinel (MgAl_2O_4)		*	*	
		Wüstite (FeO)	*			
	Other oxides	Zincite (ZnO)			*	*
		Quartz or Tridymite (SiO_2)			*	
		Magnetite (Fe_2O_3)			*	
		Goethite [$\text{FeO}(\text{OH})$]			*	
	Pure metals	Fe, Ni, Pb	*	*	*	
	Sulfides-group	Würtzite (ZnS)	*	*		
		Sphalerite (FeS)	*	*		
		Pyrrhotite ($\text{Fe}_{(1-x)}\text{S}$)				*
Reference		(Deneele, 2002)	(Piatak and Seal, 2010)	(Puziewicz et al., 2007)		

Table 2.10a: Chemical composition of each mineral phase present in ISF.

Minerals	Silicate										
	Non-Silicate	Olivine-group			Pyroxene-group			Feldspars			
	Gl	Kir	Ol	Py & wo (n=6)	He	Clif	Leu (n=9)	K-fel	Hya	Ano	La
Unit	% (wt)										
SiO ₂	25.7	34.81	30.96-37.1	30.25	41.13	40.79	50.81	64.99	59.46	44.01	53.78
TiO ₂	0.6	0.00	0.02-0.08	0.30	3.24	2	0.04	-	0.12	0.25	0.06
Al ₂ O ₃	10.0	0.00	0-0.04	4.99	10.97	9.11	25.56	18.8	21.42	35.12	29.07
FeO & Fe ₂ O ₃	25.0	23.01	25.8-64.46	23.99	15.26	40.4	0.54	0.05	0.86	0.2	0.8
MgO	1.8	1.28	3.09-31.2	1.54	5.41	4.27	0.00	-	-	0.06	0.05
MnO	0.8	12.97	0.63-2.67	6.91	0.19	0.25	0.00	-	-	-	-
CaO	21.4	26.55	0.33-4.35	23.98	22.45	1.59	6.38	0.05	1.79	18.52	12.09
PbO	0.2	0.28	0.02-0.07	0.25	-	-	2.83	-	-	-	-
ZnO	8.3	1.29	0.01-2.82.	4.78	0.09	-	0.10	-	-	-	0.16
Cr ₂ O ₃	0.1	-	-	-	0.06	0.05	-	-	-	-	-
BaO	0.3	-	-	-	-	-	4.04	0.28	5.92	0.17	-
Na ₂ O	0.7	-	-	-	0.08	0.23	0.54	0.88	1	0.5	3.51
K ₂ O	0.9	-	-	-	-	0.8	8.53	13.94	9.23	0.22	0.35
Reference	A	B	B & C	B	C	C	B	C	C	C	C

Ano-Anorthite, Clif-Clinoferrosilite, Kir-Kirschsteinite, He-Hedenbergite, Leu-Leucite, Wo-Wollastonite, Me-Melilite, Mg-Magnetite, Ol-Olivine, Gl-Glass, Py-Pyroxene, K fel-Kfeldspar, Hya-Hyalophane, La-Labradorite

A: (Deneele, 2002), B: (Puziewicz et al., 2007), C: (Piatak and Seal, 2010)

Table 2.10b: Chemical composition of each mineral phase present in ISF (Continued).

Minerals	Silicate								
	Melilite-group		Al-Si-O (other silicates)				Spinel and oxides		
	Me (n=3)	Ha	Wil	Mul	Al ₂ SiO ₅	Pb-Si (n=4)	Sp (n=9)	ZnCr ₂ O ₄	ZnAl ₂ O ₄
Unit	% (wt)								
SiO ₂	34.14	39.63	29.86	22.38	35.06	27.78	0.29	0.03	0.08
TiO ₂	0.05	-	0.00	0.84	0.56	4.51	2.40	0.08	0.25
Al ₂ O ₃	0.80	1.75	0.03	72.89	59.38	10.60	27.14	1.96	50.72
FeO & Fe ₂ O ₃	2.03	0.98	0.18-1.16	2.55	2.4	8.4375*	47.63	14.65	10.52
MgO	3.90	0.34	0.05-0.23	0.04		4.29	4.55	0.97	3.19
MnO	0.17	-	10.77	-	0.17	-	2.39	2.27	0.19
CaO	27.20	33.26	0.00	-	0.25	-	-	-	-
PbO	17.86	-	0.04	-		28.92	0.04	0.24	0.13
ZnO	13.16	22.61	58.32-69.66	-		1.42	15.02	18.14	31.08
Cr ₂ O ₃	-	-	-	-		-	-	61.13	4.03
BaO	-	0.38	-	-		8.96	-	-	-
Na ₂ O	-	-	-	-	0.33	0.20	-	-	-
K ₂ O	-	0.04	-	-	0.68	1.82	-	-	-
Reference	B	C	B & C	C	C	B	B	A	A

Me-Melilite, Ha-Hardystonite, Wil-Willemite, Mul-Mullite, Sp-Spinels, Pb-Si =Pb silicate

A: (Deneele, 2002), B: (Puziewicz et al., 2007), C: (Piatak and Seal, 2010)

Table 2.11: Chemical composition of each mineral phase present in historical smelting slags versus slags from secondary processing of car battery.

Slag	Historical Smelting Slags							Secondary processing			
	Oivine-group			Pyroxene-group		Spinel-group	Melilite-group	Gl (n=8)	Me	Gl	Ol
Mineral phases	Fa (n=66)	Kir (n=66)	Ol	Wo (n=59)	He (n=10)	Mg (n=24)	Me (n=12)				
Unit	% (wt)										
SiO ₂	30.76	31.47	31.13	49.57	43.55	0.95	38.63	38.16	39.5-39.84	30.4-31.99	30.2-31.35
TiO ₂	0.02	0.03	0.04	0.05	0.36	1.8	0.02	0.23-0.48	0-0.08	0.54-1.04	0.1-0.25
Al ₂ O ₃	0.14	0.02	0.36	0.18	5.64	5.43	1.65	5.58-5.74	5.38-7.44	6.25-15.62	0.04-0.89
FeO	54.25	40.25	45.39	4.35	24.01	82.25	10.71	14.5-26.4	8.37-10.84	29.7-30.8	39.2-42.52
MgO	5.02	0.96	4.5	0.27	2.79	0.36	2.55	0.27-0.35	2.31-3.53	0.06-2.97	2.65-4.24
MnO	0.83	2.07	8.22	0.07	0.31	0.46	0.3	0.19-2.45	0.04-0.56	0.66-0.92	1.6-2.72
CaO	4.38	23.27	0.49	44.71	20.92	0.44	36.7	5.12-21.77	34.6-34.67	14.3-20.65	17.5-21.75
Na ₂ O	0.01	0.01	0.11	0.01	0.01	-	-	0.05-0.47	2.06-2.57	0.71-0.81	0.11-0.13
K ₂ O	0.03	0.02	0.17	0.03	0.05	0.02	0.31	0.47-1.43	0.11	0.28-0.43	0.03-0.04
BaO	-	-	0.66	-	-	-	-	0.00-4.56	-	0.81-1.05	0.0-0.16
Cr ₂ O ₃	0.01	0.01	0.12	0.01	0.01	0.06	0.01	0.01	0.0-0.06	-	0.0-0.03
NiO	-	-	0.03	-	-	-	-	-	-	0.0-0.12	0.0-0.18
ZnO	5.09	1.64	7.82	0.13	1.93	3.48	9.53	4.69-6.58	3.2-3.4	1.58-1.63	1.29-1.43
PbO	0.01	0.03	0.35	0.01	0.02	0.04	0.01	0.43-16.43	0.03-0.2	0.06-0.44	0.0-0.08
References	A	A	B	A	A	A	A	A & B	B	B	B

Fa-Fayalite, Kir-Kirschsteinite, He-Hedenbergite, Wo-Wollastonite, Me-Melilite, Mg-Magnetite, Ol-Olivine, Gl-Glass

A: (Lottermoser, 2002), B: (Ettler et al., 2000)

2.3. Alteration of metallurgical slags

Unlike slags resulting from iron and steel production (ferrous slags), those from base-metal smelters typically contain elevated levels of potentially toxic elements (e.g. As, Ba, Cd, Cu, Pb, Zn) and are a possible source of surface and ground water (Parsons et al., 2001). Thus, many studies have already contributed to understanding the stability of slags and their short and long term leaching behavior by simulating either chemically or biologically influenced alteration experiments.

2.3.1. Chemically induced alteration

2.3.1.1. Short-term leaching assessment of slags

Short-term leaching tests have been extensively performed by various researchers to assess the alterability of the slags under different conditions, and the details of each test have been summarized in Table 2.12. A wide variety of smelter and slag related samples such as base-metal (Zn+Pb slag), lead smelter slag (LBF), imperial smelting furnace (ISF) slag, secondary lead slag, Pb+Cu blast furnace slag, Pb slag in cement, Zn slag in cement, smelter fly-ash, air-pollution-control residues, soils and agricultural top-soils impacted by mining and smelters (either Pb, Zn or both) have been tested to assess their short-term leaching potential of metals.

Each protocol test is different based on different environmental simulations: synthetic precipitation leach procedure (SPLP) as developed by the American National Mining Association to simulate the composition of acid rain, standard toxicity characterization leaching procedure (TCLP) test developed by the USEPA to simulate the co-disposal scenario with municipal solid waste, special waste extraction procedure (SWEP) developed by British Columbia intended only for special wastes, such as metallurgical and mineral wastes, sequential extraction method developed by Community Bureau of Reference (BCR) to study the metal speciation (especially for smelter impacted soil samples), EN 12457-2 test developed by the European Union to simulate normal rainfall conditions, diffusion-leaching NEN 7341 and NEN 7345 tests developed in the Netherlands to simulate the successive pH drop from neutral to acidic conditions, standardized pH leaching test CEN/TS 14997 developed in the Czech Republic to study the leaching behavior as a function of pH, single oxide extraction to extract free reactive Fe, Mn and Al oxides, simple bio-accessibility extraction test (SBET) developed in Belgium to study bio-accessibility of ingested heavy-metals inside the human gastrointestinal tract, and standard measurement and testing program (SM&T) which is similar to the BCR sequential extraction method for metal speciation (the differences between these two methods can be seen in Table 2.12).

Lewis and Hugo (2000) pointed out that the application of TCLP to mineral processing and metallurgical wastes has been challenged because of the high Acid Neutralizing Capacity (ANC) of the slags, rendering true assessment of the leaching potential impractical. Each leaching test protocol is different based on the different environmental simulations and purposes, nature of targeted wastes or slags, nature of leachant used, different duration of each test, the origin of the country where it is developed, reflecting its country's regulations and

standards. The application of two or more tests (TCLP + SPLP + SWEP) to one single slag can overcome such controversy and might thus be beneficial for short-term assessment. Short-term assessment is quick, simple to carry out and provides reproducible results and a combination of these tests can even be beneficial in assessing the environmental impact of slags in different weathering conditions.

2.3.1.2. Long-term leaching assessment of slags

Many studies have focused on the long-term assessment of heavy metal mobility from slags which are summarized in Table 2.13. The role of many parameters has been assessed such as pH, liquid to solid ratios, type and concentration of leachant, agitation speed, oxic or anoxic conditions, and contact time.

These studies cover *at laboratory batch scale level*: single extraction tests (Romero et al., 2008), equilibrium leaching tests under saturated conditions (Barna et al., 2004), kinetic leaching test (Ettler et al., 2008), intermittent or continuous leachant renewal conditions (Barna et al., 2004), pH dependent leaching test (de Andrade Lima and Bernardez, 2013; Ganne et al., 2006; Vítková et al., 2013), simulation of weathering in soil environment (Ettler et al., 2005a; Ettler et al., 2004) and remobilization of contaminated sediments (Vdovic et al., 2006); *at laboratory pilot scale level*: column leaching studies of slags (Seigneur et al., 2006; Seigneur et al., 2007; Seigneur et al., 2008), of slags and soils mixture (Navarro et al., 2008), of slags coupled with phytostabilization (Houben et al., 2013; Seigneur et al., 2010); *at field application level*: intermittent or continuous leachant renewal conditions (Barna et al., 2004), outdoor weathering of slag dumps (Seigneur et al., 2006; Seigneur et al., 2007; Seigneur et al., 2008), field leaching tests (Piatak et al., 2004); the relationship between laboratory-based test results and measured water compositions at real site (Parsons et al., 2001).

Some of these researchers have combined the results of dynamic leaching assessment tests with geochemical computer models such as PHREEQC-2 (Ettler et al., 2004; 2005a; 2008; 2009; Navarro et al., 2008), Minteq A2 (Ettler et al., 2005a; Ganne et al., 2006), Minteq A4 (Vítková et al., 2013), the statistical models STATISTICA or XLSTAT 2010.6.01 (Pelfrene et al., 2011; 2012), Statistical analysis one-way analysis of variance, ANOVA (Houben et al., 2013), EQ3/6 version 8.0 (Parsons et al., 2001), as well as more sophisticated geochemical codes such as WHAM (Model VI) or ECOSAT (NICA-Donnan model) for accurate prediction of the metal complexation by dissolved organic matter (Ettler et al., 2005a).

Table 2.12: Short-term leaching assessments of slags (Protocol tests).

Name of protocol tests	Sample	Experimental conditions					References					
		pH	L/S ratio (ml/g)	Leachant types (per l)	Shaking (rpm)	Duration						
Synthetic precipitation leaching procedure (SPLP)	Secondary lead slag	4.2	20	Deionized water + H ₂ SO ₄ + HNO ₃	30	18 hrs	A					
	Base-metal slag dump (Zn+Pb)						B					
	ISF slag						C					
	Lead smelter slag						D					
British Columbia special waste extraction procedure (SWEP)	Lead smelter slag	5	20	Acetic acid	10	24 hrs	D					
Community Bureau of Reference (BCR) sequential extraction method	Slag dump	-	40	Step 1: 0.11 M C ₂ H ₄ O ₂	-	16 hrs	E					
• F1: Exchangeable and weak acid soluble												
• F2: Reducible by Iron and manganese oxyhydroxides								1.5	40	Step 2: 0.5 M NH ₂ OH.HCl containing 25 ml of 2 M HNO ₃ ,	-	16 hrs
• F3: Oxidizable organic matter and sulfides								2-3	-	Step 3: 20 ml of H ₂ O ₂ , followed by 50 ml of 1 M NH ₄ O	-	2 hrs, 16 hrs
• F4: Residual in remaining, nonsilicate bound metals	-	-	Step 4: Digest with HF/HNO ₃ /HClO ₄ mixture	-	-							
Dutch diffusion-leaching test, NEN 7345	Pb slags in cement	4	5 (volume)*	Distilled water acidified with 1M HNO ₃	-	64 days	F					
Dutch diffusion-leaching test, NEN 7341	ISF	7 & 4	50	1 M HNO ₃	-	6 hrs	G					
European norm EN 12457-2 (EN)	Air-pollution-control (APC) and fly ash residues of secondary Pb metallurgy plants	5.75	20	MiliQ + demonized water	10	24 hrs	H					
	Pb–Cu blast furnace slags						I					
	Pb slags in cement						F					
	LBF and ISF slags						Q					

Leaching assessment	ISF slag in cement	9.7	4	Deionized water	-	24 hrs	J
		13.4		Buffer solution			
		11.8		Saturated (CaO) solution			
Standardized pH-static leaching test of CEN/TS 14997	Smelter fly ash	5 to 12	10	HNO ₃ & NaOH	-	48 hrs, 168 hrs	K
Simple Bio accessibility Extraction Test (SBET)	Lead from soil, slag, and mine wastes	1.5, 7	100	Solution 1: 0.4 M glycine, Solution 2: 3.2 g pepsin + 7.0 ml HCl + 2.0 g NaCl + 0.2 M NaHCO ₃ , Solution 3: 1.25 g pepsin +, 0.5 g citric + 0.5 g malic + 0.42 ml lactic + 0.5 ml glacial acetic acids	100	1-2 hrs	L
	Mining and smelters affected soils			M			
	Lead smelter impacted soil			N			
Standard Measurement and Testing Program (SM&T)	LBF and ISF slags and polluted soils	2	10	0.11 M C ₂ H ₄ O ₂ , 0.5 M NH ₂ OH.HCl, 8.8 M H ₂ O ₂ + 1M C ₂ H ₇ NO ₂ , HF (48%)+ HClO ₄ (70%) acids	-	2 hrs	O
	Smelter-contaminated agricultural topsoil						P
Single extractions (to extract free Fe, Mn, and Al oxides)	Smelter-contaminated agricultural topsoil	pH drift (2.5 to 10)	20	0.111 M NaHCO ₃ + 0.27 M Na ₃ C ₆ H ₅ O ₇ + 200 g Na ₂ S ₂ O ₄	-	35 mins	P
Toxicity characteristic leaching procedure (TCLP)	Secondary lead slag	4.93	20	TCLP solution no.1 (5.7 ml acetic acid + 500 ml MiliQ + 64.3 ml of 1M NaOH)	30	18 hrs	A
	Base-metal slag dump						B
	Air-pollution-control (APC) and fly ash residues of secondary Pb metallurgy plants						H
	Pb–Cu blast furnace slags						I
	Lead smelter slag						D
	LBF and ISF slags						Q

A: (Lewis and Hugo, 2000), B: (Parsons et al., 2001), C: (Piatak and Seal, 2010; Piatak et al., 2004), D: (de Andrade Lima and Bernardez, 2011; de Andrade Lima and Bernardez, 2013), E: (Houben et al., 2013), F: (Saikia et al., 2012; Saikia et al., 2008), G: (Ganne et al., 2006), H: (Ettler et al., 2005b), I: (Ettler et al., 2009), J: (Morrison et al., 2003), K: (Vítková et al., 2013), L: (Bosso and Enzweiler, 2008), M: (Ettler et al., 2012), N: (Romero et al., 2008), O: (Douay et al., 2009; Douay et al., 2008), P: (Pelfrene et al., 2011; Pelfrene et al., 2012), Q: (Yin et al., 2014)

Table 2.13: Long-term assessment of heavy metal mobility from slags at different experimental conditions.

Name of the tests (if any)	Objectives	Samples	Experimental conditions					Reference
			pH	L/S ratio (ml/g)	Leachant types (per l)	Shaking (rpm)	Duration	
Single extraction test	Equilibrium water soluble Pb extraction test	Pb smelter-impacted soil	7	20	Deionized water	-	18 hrs	A
Kinetic leaching test	Solubility-controlling mechanisms	Air-pollution-control (APC) residues of secondary Pb metallurgy plants	7	10	Demineralized water	60	720 hrs	B
	Effect of L/S ratios			1, 5, 10, 50, 100, 500, 1000			48 hrs	
Batch equilibrium leaching tests	Acid neutralization capacity and the mobilization as a function of pH	Road materials containing ISF and LBF	2 to 14	10	HNO ₃ and NaOH at varying concentrations		48 hrs	
Saturated leaching tests on monolithic material	Contaminants release rate and mass transfer rate under saturated conditions		13	2 ml/cm ² *	Demineralised and synthetic pore water (1 g Ca(OH) ₂ + 2.2 g NaOH + 1.6 g KOH)	-	5-6 months	C
Lab-scale: intermittent wetting conditions	To simulate cyclic wetting and drying under varied environmental conditions (e.g., humidity, temperature, atmospheric CO ₂)						8-9 months	
Pilot-scale: Intermittent wetting conditions			-	-	Natural rainwater		16 months	
pH _{stat} leaching test	Neutral acidification range	ISF	2, 4, 6, 10	10	(pH 2:2.5 M HNO ₃ ; pH 4:1 M HNO ₃ ; pH 6:0.25 M HNO ₃ ; pH 10:2.5 M NaOH)	no shaking	96 hrs	D
pH dependent leaching test	Leaching behavior of slag & Stability of slag over pH range	Lead smelter slag	1.1-12.2	10	HCl & NaOH	-	24 hrs	E
pH _{stat} leaching test	Leaching behaviour as a function of natural soil pH	Smelter fly ash	5-12	10	HNO ₃ & NaOH	-	48, 168 hrs	F

Weathering in soil environments	Effect of low molecular weight organic acids	Primary Pb smelting slags	2.4	10	20 and 8 mM citric acid solutions	-	30 days	G
	Effect of high molecular weight organic acids		3.68	10	Standard fulvic acid (DOC 50.8 mg/L) & peat water (DOC 47.1 mg/L)	60	112 days	H
Remobilization experiments	(i) Slag particles in river water, (ii) sediment in river water, and (iii) sediment and slag mixture in river water	LBF and ISF slags, and polluted sediments	8.27-8.7 for both oxic & suboxic	-	River water, oxic condition (7.8-9.5 mg/dm ³ of O ₂) and suboxic condition (1.8-3.2 mg/dm ³ of O ₂)	-	2-10 days	I
Column leaching test for slag grains and polished section slags	Local structure and composition at the slag surface on metal mobility	LBF	5.6	10	Pure water (60 ml/h recirculation flow rate)	-	15, 26 days	J
Outdoor weathering test	Natural weathering of slag heap		-					
Column leaching test (Slags + soil mixture)	Soil and groundwater contamination from slag dumps	Base-metal-smelter slags (Pb & Zn)	7	-	Demineralised water (2.4 L/h recirculation flow rate)	-	5 hrs	K
Column leaching test for phytostabilization	Long-term behavior of heavy metals, their mobility and speciation from slag dump	Slag dump	-	-	Deionized water	-	17, 25, 30, 55 days	L
Normalized static leaching procedures of Czech regulations (e.g. AFNOR)	Long-term assessment	Pb-Zn metallurgical slags	2, 5.6	10	Solution 1: MiliQ + DI + HNO ₃ , Solution 2: pure DI	60	12 months	M
A modified version of a Field Leach Test	Mineralogical and geochemical controls on the leaching under natural weathering conditions	Base-metals smelting slags	7	20	Deionized water	-	24 hrs	N

A: (Romero et al., 2008), B: (Ettler et al., 2008), C: (Barna et al., 2004), D: (Ganne et al., 2006), E: (de Andrade Lima and Bernardez, 2013), F: (Vítková et al., 2013), G: (Ettler et al., 2004), H: (Ettler et al., 2005a), I: (Vdovic et al., 2006), J: (Seigneur et al., 2006; Seigneur et al., 2007; Seigneur et al., 2008), K: (Navarro et al., 2008), L: (Houben et al., 2013), M: (Ettler et al., 2003a; Morrison et al., 2003), N: (Piatak et al., 2004)

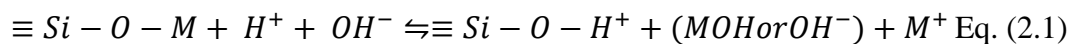
2.3.1.3. Applicability of both short and long term leaching tests to metallurgical slags

The significant differences between both short and long term leaching tests are the contact time, type of leachant, agitation rate, pH, liquid to solid (L/S) ratios, and particle size of the sample. All short term assessment tests are batch tests, quick and simple to carry out with reproducible results. As they are intended for short-term risk assessment and characterization of slags at a glance, a combination of these tests can give an idea of leaching behavior of metals under different leaching scenarios (landfill, acid rain, soil dumping). However, the requirement for particle size reduction of the slags during these tests does not reflect the conditions in which metallurgical slags are generally processed. They are usually rocklike, monolithic structures, where leaching is minimized.

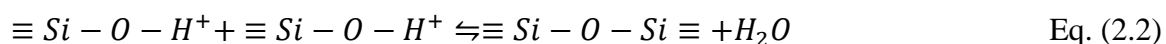
On the other hand, the long term leaching tests cover more criteria. As size reduction is not the requirement, it represents closer to field conditions. It also considers whether or not the acid-base neutralizing capacity of the slag will be depleted over longer period of contact time. In addition, the flow conditions of the water (downward and horizontal flows) along with the simulation of rain-fall (intermittent and cyclic wetting of the slag) are main advantages of long-term leaching tests over short-term ones. The applicability can be challenging if only test is applied and the amount of metals leached out can be either under or over estimated. Thus, the application of both short and long term leaching assessment tests should be considered to fully understand the leaching behavior of the metallurgical slags.

2.3.1.4. Alteration mechanisms and rates of slags (glass vs silicate)

Both Etter et al. (2003b) and Mahé-Le Carlier et al.(2000) observed that the alteration of Pb-Zn slags is initiated by the leaching of network modifier elements like Ca, Mg, Mn and Fe. Curtis (2003) further explained that it is due to the hydrolysis reaction and the nucleophilic property of water on the silicon atom (Eq. 2.1). Conradt (2008) also pointed out the three different equilibria during the slag alteration: (1) an electrochemical equilibrium at the slag surface, (2) a new thermodynamic equilibrium within aqueous solution due to element dissolution, and (3) the equilibrium which involves the solubility formation of stoichiometric hydrates of hydroxide phases due to hydrolysis.



With increasing hydration energy, H–O–H bonds are eventually broken with loss of protons (H⁺ ions) during an exchange with cations (Curtis, 2003). The exchange reaction between H⁺ ions and cations from the slags leads to an increase of the pH creating neutral to moderately basic environment. This accelerates the silica release phenomenon by a probable mechanism of breaking strong links of the residual glass by hydroxyl ions of solution. The condensation reaction between two silanol groups leads to the formation of hydrated silica gel (Eq. 2.2).



The newly formed silica gel or secondary phases serve as the protection layer on the surface of altered slag, thus limiting the contact between the slag and the solution which consequently leads to the pore diffusion control of the aqueous solution through this growing layer (Conradt, 2008). Many silicates and non-silicates phases in the slags are observed to release metals into solution at different rates. The dissolution rates of many silicate and oxide minerals are pH-dependent and the steady-state, far-from-equilibrium dissolution behavior of these minerals produces a U-shaped curve on a log (dissolution rate) vs. pH plot (Brantley, 2008). The overall dissolution rate of the slag can be the sum of the rates of the individual silicate and oxides phases. The newly formed silica gel or secondary phases on the slag surface which is adjacent to the solution can also be the keys to control the sum dissolution rate of the slag, i.e. the solid/ liquid interface affects rates more than the in-depth leached layers (Hamilton et al., 2001).

2.3.2. Biologically induced alteration

In contrast to the extensive studies on chemical alteration of slags, only few studies have focused on the involvement of microbial activity when slags are subjected to alteration. This section will therefore be extended to the dissolution of single glass or silicate phases in the presence of bacteria, and the interaction of bacteria and heavy metals rather than limiting just to the bio-alteration of lead and zinc metallurgical slags.

Microorganisms are well known for their participation during mineral formation and dissolution. Some microorganisms are able to (1) oxidize or reduce a dissolved inorganic species in energy metabolism; (2) detoxify the poisonous inorganic species; (3) actively or passively uptake one or more dissolved inorganic species followed by conversion into a cellular support or protective structure; and (4) enhance their competitiveness in a microbial community. Other microorganisms are able to dissolve a mineral by using it: (1) as a source of energy, (2) as an electron acceptor in respiration, (3) as a trace element requirement, or (4) to enhance competitiveness in a microbial community (Ehrlich, 1996). Several bacterial strains from diverse genera have been reported to have mineral-weathering abilities (Uroz et al., 2009). They can impact mineral stability alone or in association with other microorganisms, forming complex microbial communities that colonize mineral surfaces.

2.3.2.1. Bio-alteration / bioleaching

Bio-alteration due to the heterotrophic microorganisms are focused here due to the high acid-buffering capacity and alkaline nature of metallurgical slags, and the fact that these slags are dumped in soil where organic matter and nutrients are present which heterotrophic microorganisms can utilize. Eleven heterotrophic microorganisms from an alkaline slag dump have been isolated, including nine bacterial strains, one fungus and one yeast isolate (Willscher and Bosecker, 2003). There is even a growing interest in the application of heterotrophic leaching of alkaline slags and filter dusts/oxides from metal processing as most *Thiobacilli* cannot solubilize effectively alkaline wastes with pH values above 5.5 (Gadd, 2000). Hutchens et al. (2003) clearly showed that the K-feldspar dissolution was enhanced in the presence of heterotrophic bacteria, where the degree of dissolution depended on the

different bacterial strains and growth conditions applied: *Serratia marcescens* was very effective in enhancing most feldspar dissolution. The influence of bacteria (*Azotobacter chroococcum*, *Bacillus megaterium* and *Bacillus mucilaginosus*) on Pb and Zn speciation, mobility and bioavailability in soil was reported by (Wu et al., 2006) in a series of single chemical extraction, sequential extraction and in situ soil solution extraction technologies. Heterotrophic microorganisms (*Microbacterium sp.*, *Promicromonospora sp.* and *Pseudomonas cedrina*) improve the solubility of metals primarily released by biooxidation, and enhance the transport of these environmentally relevant metal by excretion of complexing agents (Willscher et al., 2007).

2.3.2.2. Sorption of metals onto bacterial cells and complexation by their byproducts (EPS, siderophores)

During the alteration of basaltic glass and a vitrified bottom ash, the sorption of many dissolved elements (Si, Mg, Fe, Ti, Ba, Co, Zn, Cu, Ni and Cr) was found in the biofilm and adsorbed onto *P. aeruginosa* cells (Aouad et al., 2006). The three conceptual reactive sites: an acidic (carboxyl and/ or phosphodiester), a neutral (phosphomonoester), and a basic (amine and/or hydroxyl) group of three bacteria *Cupriavidus metallidurans CH34*, *Pseudomonas putida ATCC12633*, and *Escherichia coli K12DH5R*, and for Zn sorption were further investigated by (Guine et al., 2006). The increase in Fe concentrations was due to the production of pyoverdine and its chelation capacities (Aouad et al., 2006; Yin et al., 2014). Moreover, the production of chelating compounds (exopolymers, siderophores, pigments) was highlighted by (Hutchens et al., 2003) as possible mechanisms behind enhanced K-feldspar dissolution.

Extracellular polymeric substances (EPS) secreted from bacteria also play an important role in binding with metal-cations due to their anionic properties. Pb has a greater affinity for EPS than Cd where the mineral fraction of the EPS is likely involved to a large extent in the sorption and binding strength between metals and EPS (Guibaud et al., 2006). Similarly, the binding affinity of EPS from fungi (*Pestalotiopsis sp.*) for Pb is higher than for Zn (Moon et al., 2006). In addition, the pH plays an important role in metal sorption onto EPS where no or minimum sorption occurs at acidic pH and the percentage of metal adsorption increases with higher pH (Guibaud et al., 2006).

2.3.2.3. Bio-alteration mechanisms

The possible bio-alteration mechanisms along with different biochemical interactions between the heterotrophic bacterium *Pseudomonas aeruginosa* and LBF slag is illustrated in Figure 2.2. Under the chemical alteration of slag, the solid-liquid reaction first took place where it favored the hydrolysis of Si^{2+} and dissolution of network modifying elements like Ca^{2+} and Mg^{2+} . The matrix neutralization reactions between cations and H^+ from the liquid medium led to the accumulation of OH^- ions which resulted in a pH rise. Under the bio-alteration of slag, Fe dissolution could be significantly enhanced by the siderophores and bacteria bodies served as bio-sorbent due to their higher surface to volume ratio (Konhauser, 2007). Siderophores can be classified into three categories depending on the moiety that donates oxygen ligands

for Fe^{3+} coordination: catecholates or phenolates, hydroxamates or carboxylates, α -hydroxy-carboxylic group or a mixture of these groups (Saha et al., 2013), where complexation occurs not only with Fe, but also with other metals like Cu and Zn.

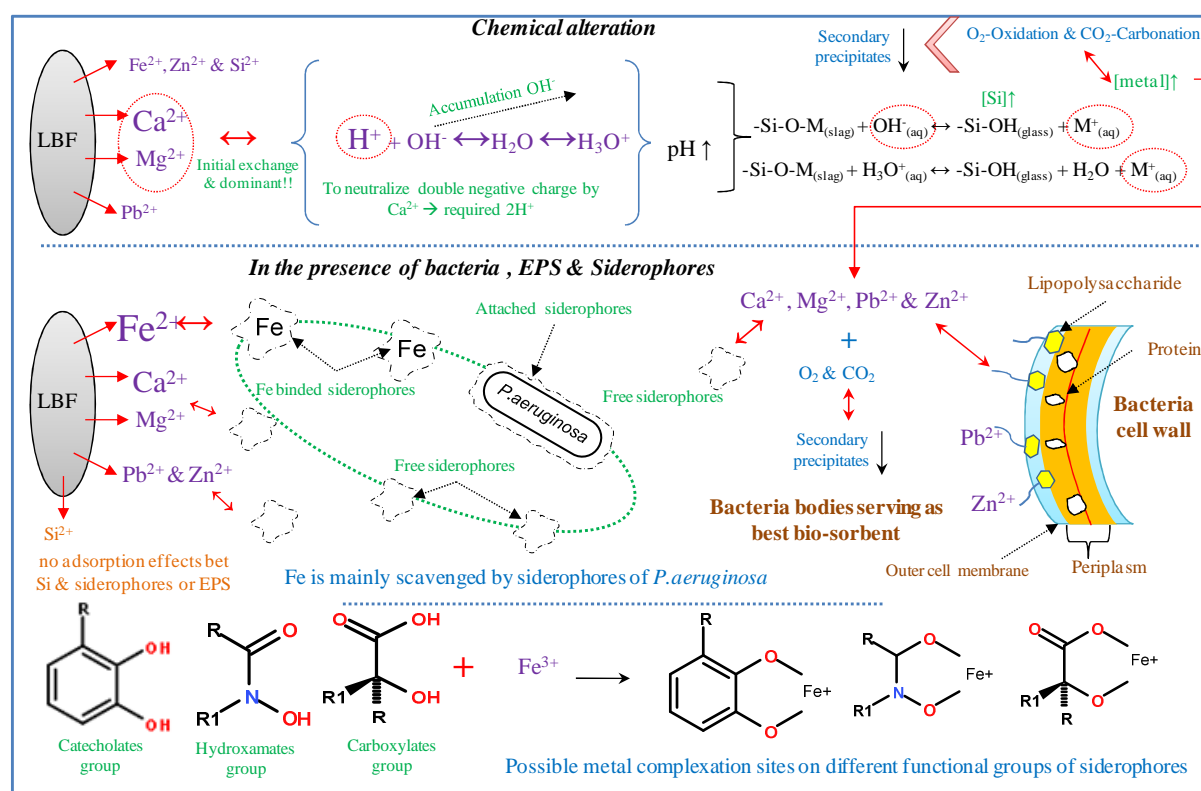


Figure 2.2. Alteration of LBF by the heterotrophic bacterium *Pseudomonas aeruginosa*.(modified from van Hullebusch et al. 2014, in press).

2.3.3. Mineralogical control on metal mobility

The primary mineral phases present in lead and zinc metallurgical slags (Tables 2.6 and 2.8) control the release of metals and metalloids into the environment under weathering conditions. The slags glass phase is more reactive and liberates minor relic sulfide ores, or metallic droplets entrapped in it (Ettler et al., 2003a; Parsons et al., 2001). Zinc is probably leached either from sulfide/metallic droplets such as Fe-rich wurtzite($\text{Fe}+\text{Zn})\text{S}$), or from Zn-bearing silicates (e.g. melilite) and glass. Spinel, main Zn concentrators, as well as willemite (Zn_2SiO_4) are most resistant to weathering and do not significantly contribute to Zn liberation (Ettler et al., 2003a). On the other hand, Zn partitioned volumetrically into minor sulfides is prone to weathering and liberation of Zn (Piatak and Seal, 2010). Other phases such as franklinite are not very reactive and stable up to pH 2 (Ganne et al., 2006). Moreover, the formation of secondary precipitates such as HFO and AlOOH are also controlling the release and mobility of metal and metalloids through sorption and/or co-precipitation (Ettler et al., 2009).

More studies have been done on the bio-accessibility of Pb and Zn, in soils from mining and smelter areas (Ettler et al., 2012), from slags (Bosso and Enzweiler, 2008) and the Pb

mineralogy control on leaching and relative bio-accessibility (Romero et al., 2008). Glass phases are thus very important in controlling heavy metal mobility as well as bio-accessibility when being ingested, while the heavy metals in a silicate matrix are protected against leaching. The presence of heterotrophic bacteria enhances the dissolution of minerals as olivine (clinocllore, lizardite, nimite and willemseite) significantly diminished in quantity (Chiang et al., 2013). Similarly, the presence of *Pseudomonas aeruginosa* dramatically enhances the solubility, and therefore the mobility of metals contained in LBF slags (Yin et al., 2014, van Hullebusch et al., 2014, in press).

2.3.4. Secondary precipitates

Geochemical analyses of leachate was used to model the speciation of dissolved constituents and to evaluate the saturation state of the solutions with various solid phases to investigate potential controls on the water composition (Piatak et al., 2004). The saturation index (SI) of an aqueous solution with respect to a mineral is defined by:

$$SI = \log\left(\frac{Q}{K}\right) \quad \text{Eq. (2.3)}$$

where Q is the ion activity product and K the equilibrium constant for the dissolution reaction. If the SI is zero, the water composition reflects solubility equilibrium, a negative value indicates under-saturation, and a positive value indicates super-saturation, thus indicating the formation of related secondary precipitates (Parsons et al., 2001).

The secondary precipitates formed vary based on the different experimental conditions laid out in Table 12. Under oxidizing conditions, with a supply of atmospheric CO₂ at pH 6-9, formation of cerussite (PbCO₃) and amorphous hydrous ferric oxides (HFO) have been reported reflecting the *long-term leaching assessment conditions* (Ettler et al., 2003a). According to Ettler et al. (2005a), the key factors influencing the precipitation of HFO are (i) the effective dissolution of primary Fe-bearing phases and, to a lesser extent, of primary silicates, oxides and glass accompanied by a release of Fe²⁺ into the solution and (ii) the time necessary for oxidation of dissolved Fe²⁺. In case of *soil weathering environments* with the presence of low or high molecular weight organic acids, the formation of well-developed calcite (CaCO₃) crystals and an amorphous organo-mineral matrix of HFO and amorphous SiO₂ was reported (Ettler et al., 2004). Metals like Pb, Zn, Cu and As present in the leachate were subsequently adsorbed onto newly formed HFO or trapped within the calcite structure. Zn exhibits a more pronounced mobility and is adsorbed on HFO/FO only at pH values higher than 7 (Ettler et al., 2005a). Similar adsorption of Pb onto HFO was also found *at natural alteration* of old metallurgical slag dump sites (Mahé-Le Carlier et al., 2000). In addition to HFO, AlO(OH) as well as phases such as chalcantite (CuSO₄·5H₂O), siderotil (Fe²⁺CuSO₄·5H₂O), jarosite (KFe³⁺₃(OH)₆(SO₄)₂), brochantite (Cu₄SO₄(OH)₆) and gypsum (CaSO₄·2H₂O) were reported at old base-smelter slag dump sites undergoing natural weathering (Piatak et al., 2004). Moreover, brianyoungite [Zn₃(CO₃,SO₄)(OH)₄], and less common phases like bechererite [(Zn,Cu)₆Zn₂(OH)₁₃[(S,Si)(O,OH)₄]₂] were identified as a secondary coating and as fibrous/ bladed crystals filling in cavities of zinc slag on dump sites

(Piatak and Seal, 2010). Alteration of alkaline materials in basicity was accompanied by alteration of mineralogy which undergoes solubilisation–precipitation, as evidenced by the decline of primary phases such as dicalcium-silicate, bredigite and periclase and the augmentation of secondary phases such as merwinite and calcite (Chiang et al., 2013).

2.4. Conclusions and outlook

Comprehensive and extensive studies have already been established concerning chemical alteration of slags under different experimental conditions, and the results of these studies indicate that detailed characterization of slag mineralogy, surface area, and dissolution of slags and mobility of metals is needed, as well as the application of at least two or even three simple leaching tests (TCLP + SPLP + SWEP). This might be beneficial for short-term assessment, as these tests provide reproducible results and their combination can be beneficial in assessing the environmental impact of slags in different weathering conditions. However, most studies have been restricted only to laboratory-based leaching assessments. Thus, many questions are still remaining concerning field weathering conditions and to predict the long-term (i.e. tens to hundreds of years) reactivity of these metallurgical wastes (Ettler and Johan, 2014) or to relate laboratory test results with measured values in the field. In addition, it is still difficult to determine the alteration rates and kinetics of each individual crystalline or glassy phase present in metallurgical slags contributing to the overall alteration of slags even at the laboratory scale.

Compared to chemical alteration studies of metallurgical slags, the focus on involvement of microbial activity on natural alteration of these slags is relatively poor. Thus, further research is required to investigate the microorganisms involved in the leaching of alkaline slag dumps and to pinpoint the physiological processes involved in metal solubilization. With such knowledge, heterotrophic leaching can be an alternative for bio-metal recovery from alkaline slags where improvement in the leaching performance can be achieved by manipulation of the leaching conditions.

2.5. References

- Aouad, G., Crovisier, J.L., Geoffroy, V.A., Meyer, J.M., Stille, P., 2006. Microbially-mediated glass dissolution and sorption of metals by *Pseudomonas aeruginosa* cells and biofilm. *J Hazard Mater*, 136: 889-895.
- Audry, S., Schafer, J., Blanc, G., Jouanneau, J.M., 2004. Fifty-year sedimentary record of heavy metal pollution (Cd, Zn, Cu, Pb) in the Lot River reservoirs (France). *Environ Pollut*, 132: 413-426.
- Barna, R., Moszkowicz, P., Gervais, C., 2004. Leaching assessment of road materials containing primary lead and zinc slags. *Waste Manage*, 24: 945-955.
- Biesinger, M.C., Hart, B.R., Polack, R., Kobe, B.A., Smart, R.S.C., 2007. Analysis of mineral surface chemistry in flotation separation using imaging XPS. *Miner Eng*, 20: 152-162.

- Bosso, S.T., Enzweiler, J., 2008. Bioaccessible lead in soils, slag, and mine wastes from an abandoned mining district in Brazil. *Environ Geochem Health*, 30: 219-229.
- Brantley, S.L., Kubicki, J.D., White, A.F., 2008b. Kinetics of water-rock interaction. *Springer*: 1-843.
- Chiang, Y.W., Santos, R.M., Monballiu, A., Ghyselbrecht, K., Martens, J.A., Mattos, M.L.T., Gerven, T.V., Meesschaert, B., 2013. Effects of bioleaching on the chemical, mineralogical and morphological properties of natural and waste-derived alkaline materials. *Miner Eng*, 48: 116-125.
- Conradt, R., 2008. Chemical Durability of Oxide Glasses in Aqueous Solutions: A Review. *J Am Ceram Soc*, 91(3): 728-735.
- Curtis, C.D., 2003. The aqueous geochemistry of metals in the weathering environment: strengths and weaknesses in our understanding of speciation and process. *Mineral Mag*, 67: 235-246.
- De Andrade Lima, L.R.P., Bernardez, L.A., 2011. Characterization of the lead smelter slag in Santo Amaro, Bahia, Brazil. *J Hazard Mater*, 189: 692-699.
- De Andrade Lima, L.R.P., Bernardez, L.A., 2012. Isotope Source Signatures for a Primary Lead Smelter Located Close to Todos os Santos Bay, Brazil. *Soil Sediment Contam: An Int J*, 20: 672-687.
- De Andrade Lima, L.R.P., Bernardez, L.A., 2013. Evaluation of the chemical stability of a landfilled primary lead smelting slag. *Environ Earth Sci*, 68: 1033-1040.
- Deneele, D., 2002. Caractérisation, simulations expérimentales et thermodynamiques de l'altération de déchets vitreux: les scories de première fusion de plomb et de zinc. *PhD thesis manuscript*, Université Des Sciences et Technologies de Lille I and U.F.R. Des Sciences De La Terre, France, 1-242.
- Douay, F., Roussel, H., Pruvot, C., Loriette, A., Fourier, H., 2008. Assessment of a remediation technique using the replacement of contaminated soils in kitchen gardens nearby a former lead smelter in Northern France. *Sci Total Environ*, 401: 29-38.
- Douay, F., Pruvot, C., Waterlot, C., Fritsch, C., Fourier, H., Loriette, A., Bidar, G., Grand, C., de Vaufléury, A., Scheifler, R., 2009. Contamination of woody habitat soils around a former lead smelter in the North of France. *Sci Total Environ*, 407: 5564-5577.
- Ehrlich, H.L., 1996. How microbes influence mineral growth and dissolution. *Chem Geol*, 132: 5-9.
- Ettler, V., 2000. Etude du potentiel polluant de rejets anciens et actuels de la métallurgie du plomb dans le district de Příbram (République tchèque). *PhD thesis manuscript*, Université D'orleans (France) et Université Charles De Prague (Czech Republic), 1-341 pp.
- Ettler, V., Johan, Z., Touray, J.C., Jelínek, E., 2000. Zinc partitioning between glass and silicate phases in historical and modern lead-zinc metallurgical slags from the

- Prábram district, Czech Republic. *Compt. Rend. Acad. Sci. (Paris), Série II, Sciences de la Terre et des planètes*, 331: 245-250.
- Ettler, V., Legendre, O., Bodéan, F., Touray, J.C., 2001. Primary Phases and Natural Weathering of Old Lead–Zinc Pyrometallurgical Slag from PRábram, Czech Republic. *Can Mineral*, 39: 873-888.
- Ettler, V., Mihaljevic, M., Touray, J.C., Piantone, P., 2002. Leaching of polished sections: an integrated approach for studying the liberation of heavy metals from lead-zinc metallurgical slags. *Bulletin de la Société géologique de France*, 173: 161-169.
- Ettler, V., Piantone, P., Touray, J.C., 2003a. Mineralogical control on inorganic contaminant mobility in leachate from lead-zinc metallurgical slag: experimental approach and long-term assessment. *Mineral Mag*, 67: 1269-1283.
- Ettler, V., Johan, Z., 2003b. Mineralogy of metallic phases in sulphide mattes from primary lead smelting. *Comptes Rendus Geosci*, 335: 1005-1012.
- Ettler, V., Komarkova, M., Jehlicka, J., Coufal, P., Hradil, D., Machovic, V., Delorme, F., 2004. Leaching of lead metallurgical slag in citric solutions-implications for disposal and weathering in soil environments. *Chemosphere*, 57: 567-577.
- Ettler, V., Jehlicika, J., Masiek, V., Hrusika, J., 2005a. The leaching behaviour of lead metallurgical slag in high-molecular-weight (HMW) organic solutions. *Mineral Mag*, 69: 737-747.
- Ettler, V., Mihaljevic, M., Sebek, O., Strnad, L., 2005b. Leaching of APC residues from secondary Pb metallurgy using single extraction tests: the mineralogical and the geochemical approach. *J Hazard Mater*, 121: 149-157.
- Ettler, V., Sebek, O., Grygar, T., Klementova, M., Bezdicika, P., Slavikova, H., 2008. Controls on Metal Leaching from Secondary Pb Smelter Air-Pollution-Control Residues. *Environ Sci Technol*, 42: 7878-7884.
- Ettler, V., Johan, Z., Křibek, B., Šebek, O., Mihaljevič, M., 2009. Mineralogy and environmental stability of slags from the Tsumeb smelter, Namibia. *Appl Geochem*, 24: 1-15.
- Ettler, V., Johan, Z., 2014. 12 years of leaching of contaminants from Pb smelter slags: Geochemical/mineralogical controls and slag recycling potential. *Appl Geochem*, 40: 97-103.
- Ettler, V., Křibek, B., Majer, V., Knésl, I., Mihaljevič, M., 2012. Differences in the bioaccessibility of metals/metalloids in soils from mining and smelting areas (Copperbelt, Zambia). *J Geochem Explor*, 113: 68-75.
- Gadd, G.M., 2000. Bioremedial potential of microbial mechanisms of metal mobilization and immobilization. *Environ biotechnol*, 11: 271-279.
- Ganne, P., Cappuyns, V., Vervoort, A., Buve, L., Swennen, R., 2006. Leachability of heavy metals and arsenic from slags of metal extraction industry at Angleur (Eastern Belgium). *Sci Total Environ*, 356: 69-85.

- Guberman, D.E., 2012. Lead. U.S. *Geological Survey Minerals Yearbook*: 1-18. Retrieved from <http://minerals.usgs.gov/minerals/pubs/commodity/lead/myb1-2010-lead.pdf>
- Guibaud, G., van Hullebusch, E., Bordas, F., 2006. Lead and cadmium biosorption by extracellular polymeric substances (EPS) extracted from activated sludges: pH-sorption edge tests and mathematical equilibrium modelling. *Chemosphere*, 64: 1955-1962.
- Guine, V., Spadini, L., Sarret, G., Muris, M., Delolme, C., Gaudet, J.P., Martins, J.M.F., 2006. Zinc Sorption to Three Gram-Negative Bacteria: Combined Titration, Modeling, and EXAFS Study. *Environ Sci Technol*, 40: 1806-1813.
- Hamilton, J.P., Brantley, S.L., Pantano, C.G., Criscenti, L.J., Kubicki, J.D., 2001. Dissolution of nepheline, jadeite and albite glasses Toward better models for aluminosilicate dissolution. *Geochim Cosmochim Acta*, 65: 3683–3702.
- Houben, D., Couder, E., Sonnet, P., 2013. Leachability of cadmium, lead, and zinc in a long-term spontaneously revegetated slag heap: implications for phytostabilization. *J Soils Sediments*, 13: 543-554.
- Hudson-Edwards, K.A., Jamieson, H.E., Lottermoser, B.G., 2011. Mine Wastes: Past, Present, Future. *Elements*, 7: 375-380.
- Hutchens, E., Valsami-Jones, E., McEldowney, S., Gaze, W., McLean, J., 2003. The role of heterotrophic bacteria in feldspar dissolution - an experimental approach. *Mineral Mag*, 67: 1157-1170.
- Jamieson, H.E., 2011. Geochemistry and Mineralogy of Solid Mine Waste: Essential Knowledge for Predicting Environmental Impact. *Elements*, 7: 381-386.
- Konhauser, K.O., 2007. Introduction to geomicrobiology. *Blackwell Publishing*.
- Lewis, A.E., Hugo, A., 2000. Characterization and batch testing of a secondary lead slag. *J South Afr Inst Min Metall*, 365-370.
- Lottermoser, B.G., 2002. Mobilization of heavy metals from historical smelting slag dumps, north Queensland, Australia. *Mineral Mag*, 66: 475-490.
- Mahé-Le Carlier, C., Le Carlier de Veslud, C., Ploquin, A., Royer, J.J., 2000. Altération des scories de la métallurgie ancienne: un analogue de déchets vitrifiés. *Compt. Rend.Acad. Sci. (Paris), Série II. Sciences de la Terre et des planètes*, 330: 179-184.
- Manceau, A., Lanson, B., Schlegel, M.L., Harge, J.C., Musso, M., Eybert-BeRard, L., Hazemann, J.L., Chateigner, D., Lambelle, G.M., 2000. Quantitative Zn speciation in smelter-contaminated soils by EXAFS spectroscopy. *Am J Sci*, 300: 289-343.
- Moon, S.H., Park, C.-S., Kim, Y.-J., Park, Y.-I., 2006. Biosorption isotherms of Pb (II) and Zn (II) on Pestan, an extracellular polysaccharide, of *Pestalotiopsis sp.* *KCTC 8637P. Process Biochem*, 41: 312-316.
- Morrison, C., Hooper, R., Lardner, K., 2003. The use of ferro-silicate slag from ISF zinc production as a sand replacement in concrete. *Cem Concr Res*, 33: 2085-2089.

- Navarro, A., Cardellach, E., Mendoza, J.L., Corbella, M., Domènech, L.M., 2008. Metal mobilization from base-metal smelting slag dumps in Sierra Almagrera (Almería, Spain). *Appl Geochem*, 23: 895-913.
- Parsons, M.B., Bird, D.K., Einaudi, M.T., Alpers, C.N., 2001. Geochemical and mineralogical controls on trace element release from the Penn Mine base-metal slag dump, California. *Appl Geochem*, 16: 1567–1593.
- Pelfrene, A., Waterlot, C., Mazzuca, M., Nisse, C., Bidar, G., Douay, F., 2011. Assessing Cd, Pb, Zn human bioaccessibility in smelter-contaminated agricultural topsoils (northern France). *Environ Geochem Health*, 33: 477-493.
- Pelfrene, A., Waterlot, C., Mazzuca, M., Nisse, C., Cuny, D., Richard, A., Denys, S., Heyman, C., Roussel, H., Bidar, G., Douay, F., 2012. Bioaccessibility of trace elements as affected by soil parameters in smelter-contaminated agricultural soils: a statistical modeling approach. *Environ Pollut*, 160: 130-138.
- Piatak, N.M., Seal, R.R., Hammarstrom, J.M., 2004. Mineralogical and geochemical controls on the release of trace elements from slag produced by base- and precious-metal smelting at abandoned mine sites. *Appl Geochem*, 19: 1039-1064.
- Piatak, N.M., Seal, R.R., 2010. Mineralogy and the release of trace elements from slag from the Hegeler Zinc smelter, Illinois (USA). *Appl Geochem*, 25: 302-320.
- Piatak, N.M., Parsons, M.B., Seal, R.R., 2014. Characteristics and environmental aspects of slag: A review. *Appl Geochem*, in press.
- Puziewicz, J., Zainoun, K., Bril, H., 2007. Primary phases in pyrometallurgical slags from a zinc-smelting waste dump, swietochlowice, upper silesia, poland. *Can Mineral*, 45: 1189-1200.
- Romero, F.M., Villalobos, M., Aguirre, R., Gutierrez, M.E., 2008. Solid-phase control on lead bioaccessibility in smelter-impacted soils. *Arch Environ Contam Toxicol*, 55: 566-575.
- Saha, R., Saha, N., Donofrio, R.S., Bestervelt, L.L., 2013. Microbial siderophores: a mini review. *J Basic Microbiol*, 53: 303-317.
- Saikia, N., Cornelis, G., Mertens, G., Elsen, J., Van Balen, K., Van Gerven, T., Vandecasteele, C., 2008. Assessment of Pb-slag, MSWI bottom ash and boiler and fly ash for using as a fine aggregate in cement mortar. *J Hazard Mater*, 154: 766-777.
- Saikia, N., Cornelis, G., Cizer, O., Vandecasteele, C., Gemert, D., Van Balen, K., Van Gerven, T., 2012. Use of Pb blast furnace slag as a partial substitute for fine aggregate in cement mortar. *J Mat Cycles Waste Manage*, 14: 102-112.
- Scheinert, M., Kupsch, H., Bletz, B., 2009. Geochemical investigations of slags from the historical smelting in Freiberg, Erzgebirge (Germany). *Chemie der Erde - Geochem*, 69: 81-90.
- Seigneur, N., Bulteel, D., Damidot, D., Gauthier, A., Potdevin, J.L., 2006. Weathering of metallurgical slag heaps: multi-experimental approach of the chemical behaviours of lead and zinc. *Waste Manage Environ III*, 1: 31-40.

- Seigneur, N., Gauthier, A., Bulteel, D., Buatier, M., Recourt, P., Damidot, D., Potdevin, J.L., 2007. Effect of Pb-rich and Fe-rich entities during alteration of a partially vitrified metallurgical waste. *J Hazard Mater*, 149: 418-431.
- Seigneur, N., Gauthier, A., Bulteel, D., Damidot, D., Potdevin, J.L., 2008. Leaching of lead metallurgical slags and pollutant mobility far from equilibrium conditions. *Appl Geochem*, 23: 3699-3711.
- Seigneur, N., Gauthier, A., Mess, F., Brunel, C., Dubois, M., Potdevin, J.L., 2010. Development of Plant Roots Network in Polluted Soils: An X-ray Computed Microtomography Investigation. *Water Air Soil Pollu*, 209: 199-207.
- Sivry, Y., Munoz, M., Sappin-Didier, V., Riotte, J., Denaix, L., de Parseval, P., Destrigneville, C., Dupré, B., 2010. Multimetallic contamination from Zn-ore smelter: solid speciation and potential mobility in riverine floodbank soils of the upper Lot River (SW France). *Eur J Mineral*, 22: 679-691.
- Tolcin, A.C., 2012. Zinc. U.S. *Geological Survey Minerals Yearsbook* (84): 1-11. Retrieved from <http://minerals.usgs.gov/minerals/pubs/commodity/zinc/myb1-2011-zinc.pdf>
- Uroz, S., Calvaruso, C., Turpault, M.P., Frey-Klett, P., 2009. Mineral weathering by bacteria: ecology, actors and mechanisms. *Trends Microbiol*, 17: 378-387.
- USEPA, 1986. Primary Zinc Smelting Background Report for Air Pollution, *US Environmental Protection Agency*, AP-42 (12.7): 1-27. Retrieved from <http://www.epa.gov/ttn/chief/ap42/ch12/bgdocs/b12s07.pdf>
- USEPA, 1995. EPA Office of Compliance Sector Notebook Project Profile of the Nonferrous Metals Industry. Sector Note Project, *US Environmental Protection Agency*: 1-137. Retrieved from <http://www.epa.gov/compliance/resources/publications/assistance/sectors/notebooks/nfmetltn.pdf>
- van Alphen, M., 1999. Atmospheric heavy metal deposition plumes adjacent to a primary lead-zinc smelter. *Sci Total Environ*, 236: 119-134.
- van Hullebusch, E.D., Yin, N.H., Seigneur, N., Labanowski, J., Gauthier, A., Lens, P.N.L., Avril, C., Sivry, Y., in press. Bio-alteration of metallurgical wastes by *Pseudomonas aeruginosa* in a semi flow-through reactor. *J Environ Manage*.
- Vdovic, N., Billon, G., Gabelle, C., Potdevin, J.L., 2006. Remobilization of metals from slag and polluted sediments (case study: the canal of the Deule River, northern France). *Environ Pollut*, 141: 359-369.
- Verguts, P., 2005. Two dimensional mathematical simulation model for a non-ferrous blast furnace. *PhD thesis manuscript*, Katholieke Universiteit Leuven, Belgium: 1-168.
- Vítková, M., Ettler, V., Sebek, O., Mihaljevic, M., Grygar, T., Rohovec, J., 2009. The pH-dependent leaching of inorganic contaminants from secondary lead smelter fly ash. *J Haz Mat*, 167: 427-433.

- Vítková, M., Hyks, J., Ettler, V., Astrup, T., 2013. Stability and leaching of cobalt smelter fly ash. *Appl Geochem*, 29: 117-125.
- Willscher, S., Bosecker, K., 2003. Studies on the leaching behaviour of heterotrophic microorganisms isolated from an alkaline slag dump. *Hydrometallurgy*, 71: 257-264.
- Willscher, S., Pohle, C., Sitte, J., Werner, P., 2007. Solubilization of heavy metals from a fluvial AMD generating tailings sediment by heterotrophic microorganisms. *J Geochem Explor*, 92: 177-185.
- Wu, S.C., Luo, Y.M., Cheung, K.C., Wong, M.H., 2006. Influence of bacteria on Pb and Zn speciation, mobility and bioavailability in soil: A laboratory study. *Environ Pollut*, 144: 765-773.
- Yang, Y., Li, S., Bi, X., Wu, P., Liu, T., Li, F., Liu, C., 2010. Lead, Zn, and Cd in slags, stream sediments, and soils in an abandoned Zn smelting region, southwest of China, and Pb and S isotopes as source tracers. *J Soils Sediments*, 10: 1527-1539.
- Yin, N.H., Sivry, Y., Avril, C., Borensztajn, S., Labanowski, J., Malavergne, V., Lens, P.N.L., Rossano, S., van Hullebusch, E.D., 2014. Bioweathering of lead blast furnace metallurgical slags by *Pseudomonas aeruginosa*, *Int Biodeterior Biodegrad*, 86: 372-381.

CHAPTER 3

Application of Zn isotopes in environmental impact assessment of Zn-Pb metallurgical industries: A Mini Review

This chapter will be submitted to:

Chemosphere

Chapter 3

3.1. Introduction

The global mining industries produced 4,140,000 metric tons of lead (Guberman, 2012) and 12,000,000 metric tons of zinc (Tolcin, 2012) in 2010 where the principal use of lead is heavily reliant on the lead-acid battery industry, and the automotive sector (Guberman, 2012) and the primary demand for zinc is galvanizing, in which a zinc coating is applied to steel to prevent corrosion (Tolcin, 2012). Other uses of zinc include the production of brass and bronze, zinc-base alloys for die-casting, chemicals, and zinc semi-manufactures.

Zn becomes widespread in natural environment due to the major anthropogenic inputs from vehicle emission, sewage sludge and pig slurry spreading, road runoff, industrial emission, and the geogenic input from the weathering of Zn-bearing rocks (John et al., 2007; Juillot et al., 2011). Among all the anthropogenic sources, Zn and Pb smelters are large contributors to Zn and Pb emissions (Shiel et al., 2010). Many studies have highlighted the pollution associated with lead and zinc metallurgical activities in many environmental compartments: atmospheric heavy metal emissions and deposition (van Alphen, 1999), surface and ground water contamination (Parsons et al., 2001), agricultural topsoil (Pelfrene et al., 2011) and river sediment (Vdovic et al., 2006).

Due to active participation of Zn in multiple biological and low temperature inorganic-chemical reactions, isotopic variations of Zn can be used as a tracer of biogeochemical and chemical processes and sources of pollution (Sivry et al., 2008). The variations of Zn isotope compositions from different anthropogenic activities (thermal distillation or electrochemical purification) were reviewed by (John et al., 2007) and in different natural environments (rain, seawater, sediments, etc) by (Cloquet et al., 2008). In this contribution, we endeavor to better understand the Zn isotope fractionation within the content of metallurgical industries and activities. Thus, this mini review is especially dedicated to the Zn isotopes fractionation occurring during Zn-Pb ore formation, smelting processes of these ores, smelters related air emissions, slags (solid wastes), and smelter-impacted environmental compartments (water, air, soil and biological samples).

3.2. Contribution of analytical development

Zinc has five stable isotopes; ^{64}Zn (48.6%), ^{66}Zn (27.9%), ^{67}Zn (4.1%), ^{68}Zn (18.8%), and ^{70}Zn (0.6%) with their relative abundances in nature. Zinc isotopes and their natural abundances were first determined by (Rosman, 1972) due to the limitation in analytical precision, no further work had been done in terrestrial samples. During the late 1990s, the technical development on multi-collector inductively coupled plasma mass spectrometry (MC-ICP-MS) made it possible to measure Zn isotopes simultaneously and accurately (Marechal et al., 1999) in a wide range of samples such as biological materials, sediments, ores and silicate minerals (Maréchal et al., 2000). In the early 2000s, the kinetic and equilibrium mass-dependent fractionation laws was introduced, and their geochemical and cosmo-chemical significance in nature were discussed for O and Mg isotopes (Young et al.,

2002). Later, the analytical challenges of measuring mass-dependent isotopic variations in nature was further addressed in many studies such as the spectral interferences (Mason et al., 2004a) and mass discrimination effect (Mason et al., 2004b) during analysis of Cu and Zn isotopes by plasma source mass spectrometry. The studies have been extended to different non-traditional isotopic systems: Li, Mg, Ca, Cr, Fe, Se, Cl, Mo (Albarède and Beard, 2004). Following the first development in ion-exchange separation techniques for isolation of Cu and Zn isotopes (Marechal and Albarede, 2002), the techniques later evolved for more complex and concentrated solutions like acid mine drainage samples (Borrok et al., 2007), for very dilute aqueous solutions like river waters (Chen et al., 2009). In addition, the matrix effect due to resin-derived contaminants during column separation was evaluated as well (Shiel et al., 2009). Although the extent of Zn isotopes fractionation of environmental samples in nature is quite small ($\delta^{66}\text{Zn} \sim 1.7\text{‰}$) compared to the other transitional metal isotopes ($\delta^{65}\text{Cu} \sim 9\text{‰}$), thanks to MC-ICP-MS, the measured range of $\delta^{66}\text{Zn}$ is approximately 20 times larger than the analytical precision (Wilkinson et al., 2005). The magnitude of Zn stable-isotope fractionation is usually expressed as $^{66}\text{Zn}/^{64}\text{Zn}$, $^{67}\text{Zn}/^{64}\text{Zn}$, $^{68}\text{Zn}/^{64}\text{Zn}$ with normalization to the most abundant form of Zn, ^{64}Zn (48.6% in abundance). It is expressed as the relative deviation with respect to a standard reference: the Johnson Matthey Company (JMC), in either parts per 1000 (δ) or parts per 10,000 (\square) as mentioned in Equation 3.1 (Black et al., 2011).

$$\delta^{66}\text{Zn}_{\text{JMC}} = \{[(^{66}\text{Zn}/^{64}\text{Zn})_{\text{sample}} / (^{66}\text{Zn}/^{64}\text{Zn})_{\text{JMC}}] - 1\} * 1000 (\text{‰}) \quad \text{Eq. (3.1)}$$

3.3. Zinc and lead smelters

3.3.1. Ore signatures

The primary sources of Zn and Pb production are from the minerals sphalerite (ZnS) and galena (PbS) where Zn and Pb are the major constituents of the ores. Variations of Zn isotopes in sulfide-rich ores have been reported by many researchers (Figure 1) where $\delta^{66}\text{Zn}$ values are ranging from -0.17 to 1.33‰ in sphalerite rich samples from Ireland (Wilkinson et al., 2005), from -0.4 to 1.2‰ in ores from Orlovka and Spokoinoe mining site (Dolgopolova et al., 2006), from 0.1 to 0.5‰ in ores from Finland (Weiss et al., 2007), from 0.00 to 1.14‰ in sphalerite rich base metal deposits from Northern Alaska (Kelley et al., 2009), from -0.43 to 0.23‰ in Alexandrinka ore deposit from Russia (Mason et al., 2005), from 0.2 to 0.37 ‰ in ZnS ores from Europe (Sonke et al., 2008), compared to the initial hydrothermal fluid composition of $0.0 \pm 0.1\text{‰}$, respectively. Despite of such variations, the $\delta^{66}\text{Zn}$ signatures of ores used in Pb and Zn smelters have remarkably homogeneous isotopic compositions where the average $\delta^{66}\text{Zn}$ is $0.16 \pm 0.20\text{‰}$ (2SD, n=10 mines, n=61 analyses) considering different mine locations as well as initial ores compositions (Sonke et al., 2008).

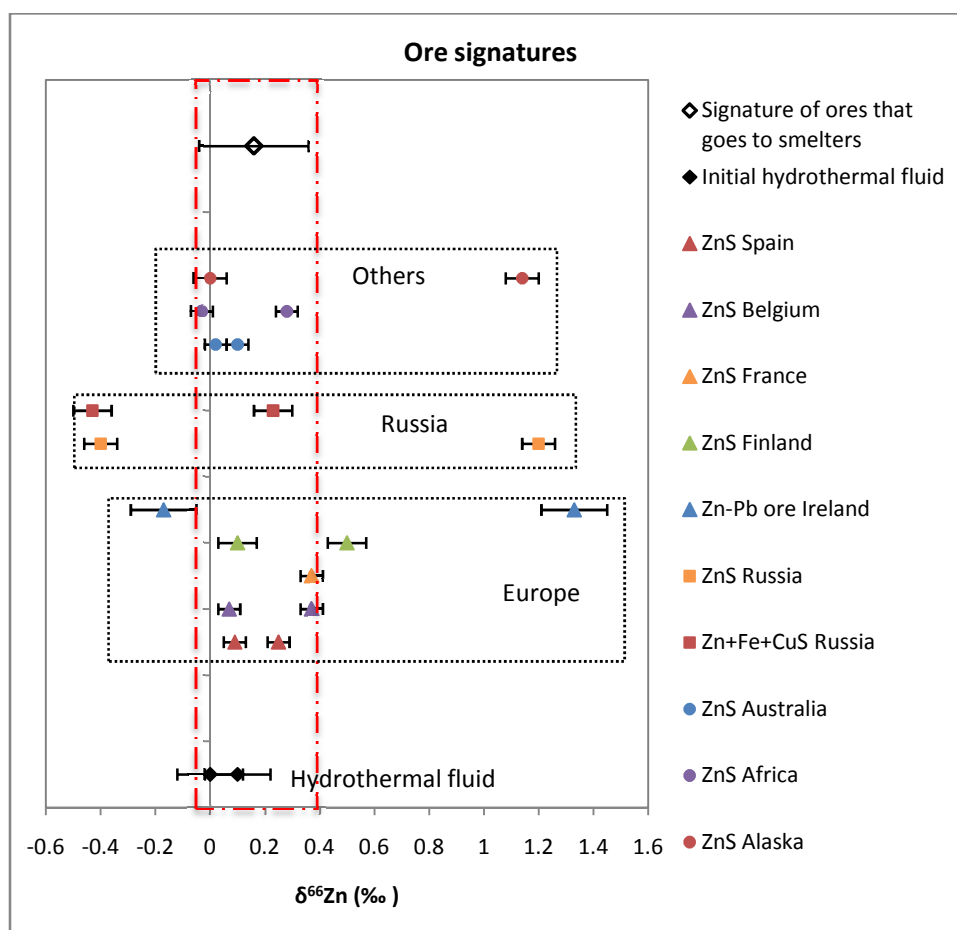


Figure 3.1. Summary of published $\delta^{66}\text{Zn}$ variations in sulfide-derived ores originating from different countries as well as carbonate-derived ores in comparison to $\delta^{66}\text{Zn}$ signature of initial hydrothermal fluid and ore weathering (the detail values are given in Table S1 - Supplementary data).

3.3.2. Smelting processes

The typical primary lead refinery is by means of lead blast furnace technology (LBF) where the roasting of ores, mainly sinter, coke and fluxes moves through a vertical shaft in counter-current to the ascending gas flow. The descending ore concentrates successively passes through the preheating zone (at 200°C), the reaction or reduction zone (at 900°C), the melting zone (at 1150°C), and finally the combustion zone (Verguts, 2005). Production of zinc uses the imperial smelting technology (ISF) which includes the multiple-hearth, suspension, or fluidized bed. Zinc ore concentrate is introduced into a multiple-hearth roaster (at about 690°C) to produce calcine which is later blown into a suspension roaster or fluidized-bed roaster (at about 980°C) (Gordon et al., 2003).

The high-temperature roasting process is closely followed by the electrolytic processes where the calcine is leached with sulfuric acid. The zinc sulfate electrolyte circulated continuously the leach tanks with lead/silver alloy anodes and aluminum cathode where zinc was recovered and stripped from the cathodes, melted, and cast into slabs (Gordon et al., 2003).

The Zn isotopic fractionation induced at different steps of smelting at Pb and Zn smelters are given in Figure 3.2.

The Zn isotopic compositions were evaluated during the smelting activities of zinc and lead ores (Shiel et al., 2010). Zn ore concentrates were normally treated in two parallel processes: roasting (80-85%) and pressure leaching (20-25%), the residue from the Zn leaching plant went to Pb smelters and was fed together with Pb ore concentrate. $\delta^{66}\text{Zn}$ values from Zn smelters ranged from 0.09 to 0.17 ‰ in Zn ore concentrate, 0.17 ± 0.06 ‰ in calcine (~100% recovery from ore to calcine), 0.22 ± 0.06 ‰ in refined Zn (~98% recovery from overall process), and 0.41 to 0.51 ± 0.08 ‰ in smelter effluent. On the other hand, the mixed feed of Zn residues to Pb ore concentrate had $\delta^{66}\text{Zn}$ values of 0.33 ± 0.15 ‰ and ZnO fuming plants (0.43 ± 0.06 ‰). No significant fractionation was observed between ore and refined Zn product despite the significant fractionation in the effluent.

3.3.3. Slags

The Zn isotopes signature related to slag materials at Pb and Zn smelting sites can exhibit a large range of $\delta^{66}\text{Zn}$; 0.81 ± 0.20 ‰ (Juillot et al., 2011), 0.37 to 0.43‰ from Pb-Zn refinery (Couder et al., 2008), 0.85 ± 0.74 ‰ from Belgian Zn refinery (Sonke et al., 2008), 0.18 to 1.49 ± 0.04 ‰ for tailings at a former French Zn refinery site (Sivry et al., 2008), 0.78 ± 0.13 ‰ in Pb slags and 0.13 ± 0.05 ‰ in Zn slags (Yin et al., in preparation). Thus, Zn slags from Zn-Pb refinery displays heavier Zn isotopic signatures ranging from 0.13 ± 0.05 ‰ to 1.49 ± 0.04 ‰.

3.3.4. Air emissions

Unlike the heavy signature of Zn in slags, dust particles from the smelters are enriched in lighter Zn isotopes: -0.07 ± 0.06 ‰ in initial step of Zn grilling, -0.35 to -0.37 ± 0.03 ‰ in final step of imperial smelting furnace, 0.05 to 0.21 ± 0.05 ‰ in initial step of Pb grilling, and -0.66 ± 0.02 ‰ in final step of lead blast furnace (Mattielli et al., 2009).

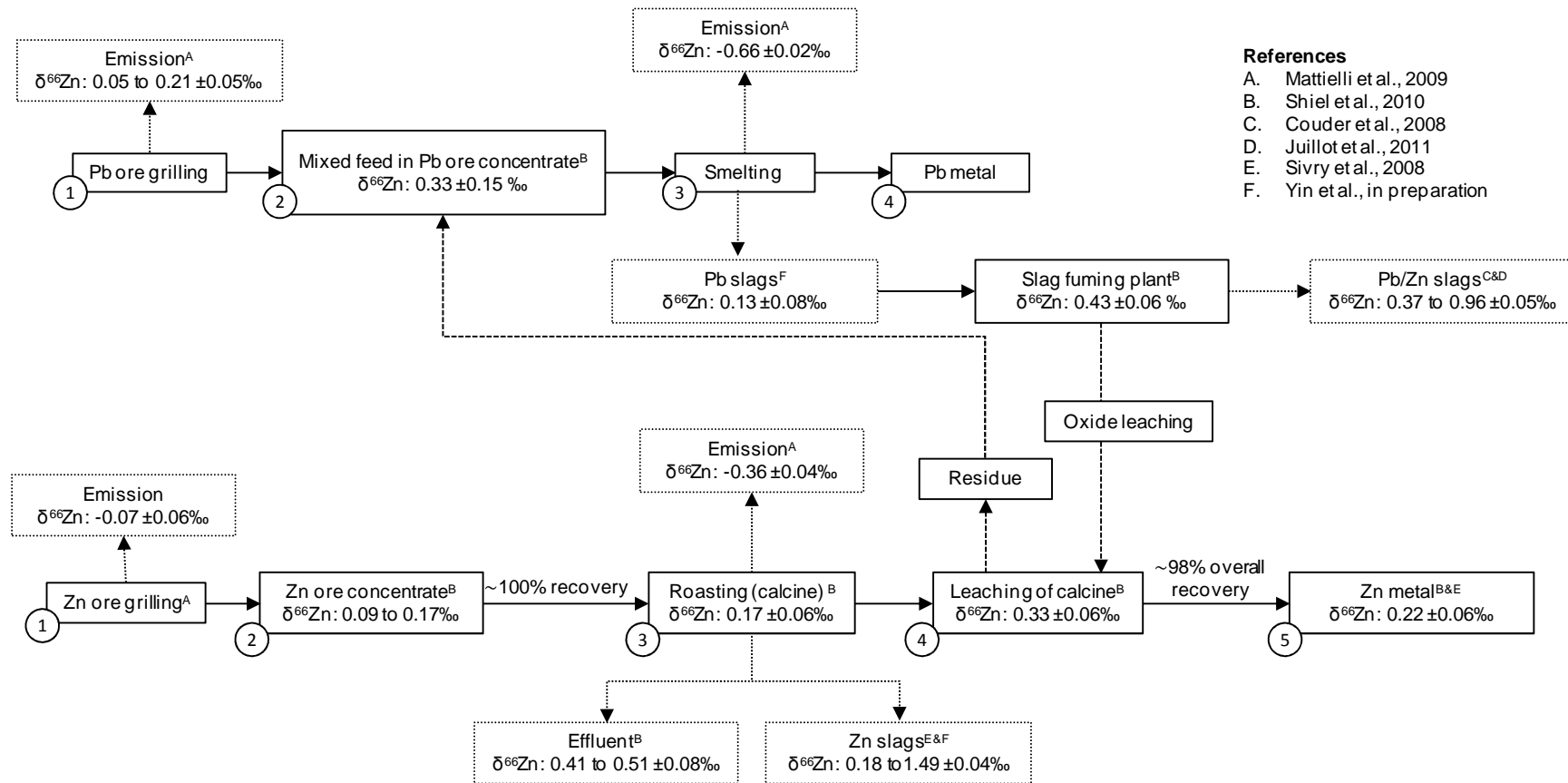


Figure 3.2. Published Zn isotopes variations during different steps of smelting activities at Pb and Zn smelters (The detail values are given in Table S2 - Supplementary data).

3.3.5. Fractionation mechanisms during smelting processes

A significant fractionation of Zn isotopes was induced during high temperature processes involved in roasting steps which followed Rayleigh law, and during electroplating steps where massive transport of Zn ions and solid deposition of Zn onto the electrodes occurred.

3.3.5.1. Rayleigh fractionation (roasting process)

The temperature roasting processes can be as high as up to 1200°C, which favors the Rayleigh fractionation law which depicts the stable isotopic evolution of a homogeneous reservoir from which a phase is continuously extracted and the distinct signature of isotopes between the starting material and the fraction remained providing that it is the closed system.

$$\Delta - \delta_o \sim 10^3 (\alpha - 1) \ln f \quad \text{Eq. (3.2)}$$

where δ and δ_o , respectively, are the stable isotopic compositions of an element in the reservoir to start with and when a fraction f of the original amount of the element is left, α the isotopic fractionation factor between the phase separating out and the reservoir. Zn isotopes fractionation during refining and smelting of sulfide ores clearly reflected this Rayleigh distillation trend; lightest signature in the air emissions ($\delta^{66}\text{Zn}$: -0.66‰) while heaviest signature in slags ($\delta^{66}\text{Zn}$: 1.49‰) compared to the initial ore ($\delta^{66}\text{Zn}$: 0.09 to 0.17‰) and final refined Zn signatures ($\delta^{66}\text{Zn}$: 0.22‰).

3.3.5.2. Electroplating

Only a few studies have focused on the Zn isotopes fractionation during the high-temperature roasting process whereas no study has been done on the fractionation induced due to the electroplating of Zn from the roasted calcine in Zn-Pb smelters. However, some experimental studies highlighted the substantial isotopic fractionation could occur for electroplated Zn and Fe (Rodushkin et al., 2004). John et al. (2007) initially reported the electroplated metallic Zn in coins with $\delta^{66}\text{Zn}$ ranging from -0.56 to -0.2‰. Electroplating induced a significant isotope separation of the electroplated zinc with respect to the starting solution ($\delta^{66}\text{Zn} = 0.00 \pm 0.06\text{‰}$); with lighter Zn isotopes ($\delta^{66}\text{Zn} = -3.5$ to -2.45‰) preferentially deposition (Kavner et al., 2008). Thus, electrochemistry appears to induce larger Zn isotope fractionation than roasting process, future studies focusing on this particular issue might offer a viable explanation for the shift of $\delta^{66}\text{Zn}$ from lighter to heavier values.

Many possible mechanisms contributing to the fractionation during electroplating includes mass transport to the electrode through the solution; electron transfers, aqueous speciation, phase change from aqueous ion to solid metal, nucleation and growth of metal on the electrode. However, the diffusive transport of species to the electrode surface and the stable isotope dependent kinetics of an electron transfer reaction might be the only two processes governing the fractionation (Kavner et al., 2008). Fractionation can be interpreted as a competition between the two kinetic processes: mass-transport-limited kinetics with a large activation energy creating small fractionation, and electrochemical deposition kinetics with a smaller effective activation energy creating large fractionation (Black et al., 2014).

3.4. Smelter-impacted environmental samples

A number of studies have recently focused on the use of Zn isotopes as tracers of pollution related to Pb-Zn refineries in various environments: natural water bodies, sediments and soil in Figures 3.3 and 3.4.

3.4.1. Natural water bodies (groundwater, stream and river water)

Groundwater collected downstream the tailings was strongly enriched in heavier isotopes from 1.18 to 1.4‰ corresponding to the signature slag which confirmed the groundwater contamination from dumpsite seepage (Sivry et al., 2008). The $\delta^{66}\text{Zn}$ varied from 0.02 to 0.46‰ in the stream impacted from historical mining activities (Borrok et al., 2008) which can be further compared to the heavy Zn isotopic signatures of effluent from Zn-Pb refinery i.e., 0.33 to 0.51‰ (Shiel et al., 2010). The isotope signatures in contaminated surface water impacted from former mining sites were remarkably similar: 0.20 to $0.30 \pm 0.09\%$ (Aranda et al., 2012). However, the pore water collected within a nearby metal-impacted wetland area was more variable, ranging from 0.20 to $0.80 \pm 0.09\%$ (Figure 3).

3.4.2. Sediments (lake and reservoir)

The river sediment downstream of the former Zn-ore facility in France carried a $\delta^{66}\text{Zn}$ of $0.91 \pm 0.04\%$ (Figure 3), whereas the reservoir sediment in 40 km downstream of the plant carried a heavier $\delta^{66}\text{Zn}$ of 0.75 to 1.35‰ depending on the depth (0-100 cm) of the sediments (Sivry et al., 2008). The lake sediments taken from 1 km distance of former Zn smelter in Belgium accumulated heavy metals (up to 4.7 wt.% Zn, and 1.1 wt.% Pb), showing variations in $\delta^{66}\text{Zn}$ ranging from 0.07 to 0.39‰ depending on the depth (0 to 40 cm) of the sediments (Sonke et al., 2008). Similarly, isotopic changes in the sediment core in Seattle urban lake were correlated with different periods of smelter operation: $0.39 \pm 0.09\%$ in the pre-smelter period (~1450 to 1900), $0.14 \pm 0.06\%$ during the smelter operation period (~1900 to 1985) and $0.0 \pm 0.1\%$ in the post smelting period after 1985 (Thapalia et al., 2010).

3.4.3. Soil (peat bog soil, inland soil)

The air emissions from Pb-Zn smelters and re-suspension of particles from slags-dump can be considered as major Zn contributors to the soil located at the smelting sites and within 1 to 5 km radius of the smelters. The emissions from grilling and all steps of smelting activities have the $\delta^{66}\text{Zn}$ signatures from -0.66 to 0.21‰ while the particulate matter (PM) collected within 1 to 5 km radius of the smelters from -0.02 to 0.07‰ (Mattielli et al., 2009) (Figure 4). Significant Zn isotope variability (Figure 4) was found in peat bogs sampled adjacent to smelters (0.40 to 1.29‰) where the upper section of the bog was enriched in lighter isotopes and the heavier isotopes enriched in the deeper sections (Weiss et al., 2007). Similarly, the $\delta^{66}\text{Zn}$ of near surface soil and at lowest horizons of soil fell within the same range: 0.22 to 0.76‰ (Juillot et al., 2011).

In contrary, the soils located within 1 to 5 km radius of the smelters showed the light $\delta^{66}\text{Zn}$ signatures where the depth distribution of $\delta^{66}\text{Zn}$ in contaminated soil ranged from -0.47 to -

0.08‰ in 1 km distance, -0.47 to 0.00‰ at 3.8 km distance and -0.53 to -0.06‰ at 5 km distance away from the smelter (Bigalke et al., 2010). The light $\delta^{66}\text{Zn}$ signatures of contaminated soil within 1 to 5 km radius could be related to the lightest signatures of air emissions from the smelters, suggesting that lighter Zn isotopes drifted by the winds away from the smelters and deposited or washed out by the rain afterwards.

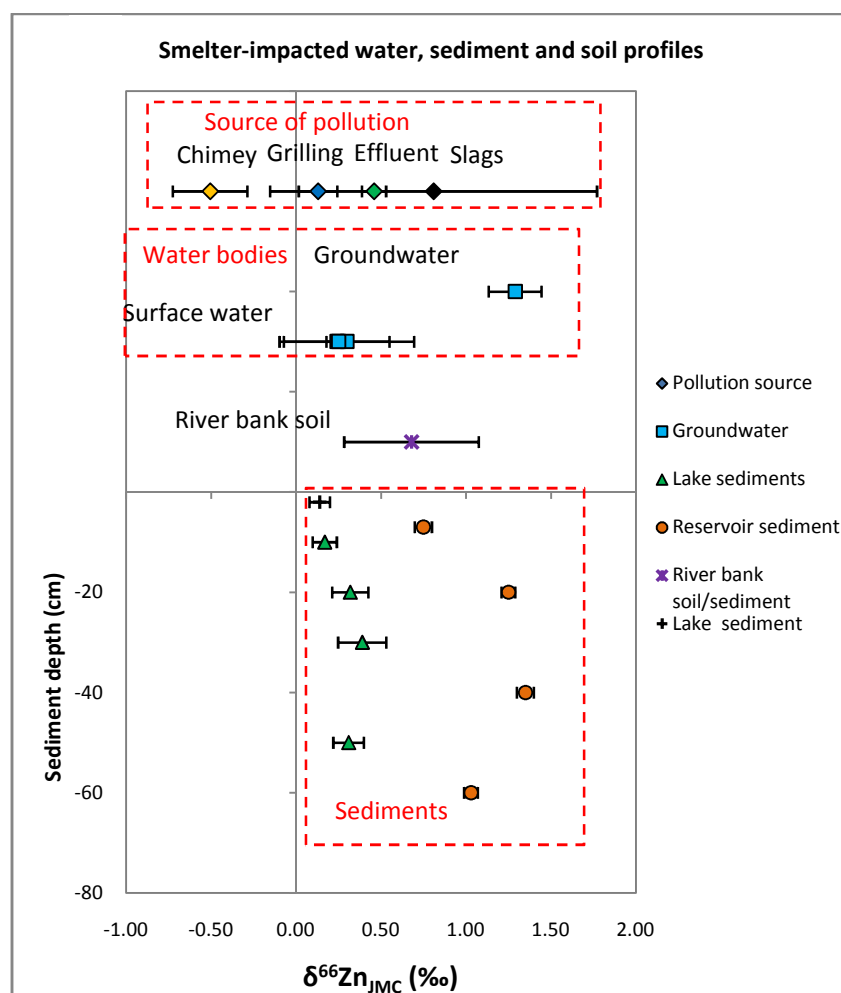


Figure 3.3. Published Zn isotopes variations in smelter-impacted water bodies, sediment, and soil (The detail values are given in Table S3 - Supplementary data).

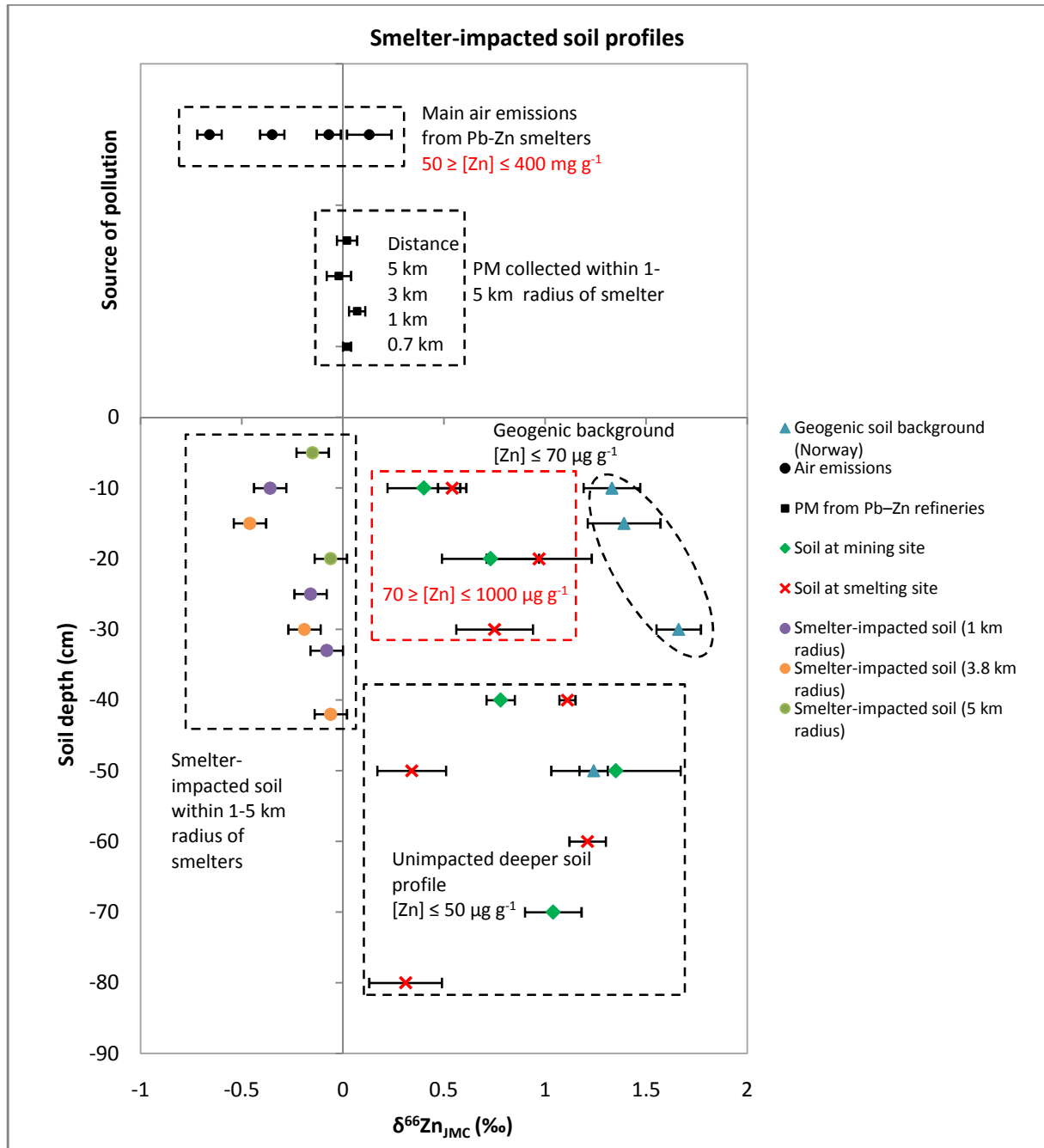


Figure 3.4. Published Zn isotopes variations in smelter-impacted soil (The detail values are given in Table S4 - Supplementary data).

3.4.4. Fractionation induced by geochemical processes (sorption, complexation and precipitation)

The extent of fractionation in the smelter impacted environmental samples can be different following the different geochemical or physiochemical processes such as surface adsorption onto mineral oxide and oxy-hydroxides, complexation with organic acids or different metallic to aqueous species and secondary precipitation of carbonates.

$\delta^{66}\text{Zn}$ values varied significantly during Zn adsorption onto different oxides, hydroxides and oxy-hydroxides minerals as a function of pH (Figure 3.5): 0.11 to 0.64‰ onto Fe_2O_3 (hematite), 0.14 to 0.24‰ onto Al_2O_3 (corundum), 0.15 to 0.18‰ onto $\beta\text{-MnO}_3$ (pyrolusite), 0.12 to 0.20‰ onto $\text{Al}(\text{OH})_3$ (gibbsite), and -0.08 to -0.1‰ onto FeOOH (goethite) where adsorption on most mineral surfaces did not exceed 0.2‰ (Pokrovsky et al., 2005). Similarly, the adsorption of heavy Zn isotopes (0.58‰) onto FeOOH (ferrihydrite) minerals was observed by Cacaly et al. (2004). pH dependent vs. time dependent adsorption of Zn onto goethite and 2-Lines ferrihydrite and its isotopic fractionation were further studied by (Juillot et al., 2008) and (Balistrieri et al., 2008). Thus, lighter Zn isotopes tended to adsorb onto the surface of hematite, corundum and ferrihydrite while heavier isotopes onto the surface of goethite as the pH got higher. However, no significant effect of pH was observed during surface adsorption onto pyrolusite. The adsorption of Zn isotopes onto the mineral surface followed the equilibrium fractionation where the equilibration time can be different based on the types of minerals (Juillot et al., 2008). It was postulated that adsorption reactions of Zn onto oxy(hydr)oxide only contributed to a minor degree to Zn isotope fractionation in natural settings, and that co-precipitation and biological uptake were the main fractionating mechanisms (Pokrovsky et al., 2005).

The magnitudes of Zn isotopes fractionation between aqueous Zn species and metallic Zn displayed $\delta^{66}\text{Zn}$ of 1.75‰ in aqueous $[\text{Zn}(\text{H}_2\text{O})_6]^{2+}$ complex, 2.2 to 2.9‰ in aqueous $[\text{Zn-SO}_4]$ complex, 1.28‰ in aqueous $[\text{ZnCl}_4]^{2-} \cdot 12\text{H}_2\text{O}$ complex, and 2.4‰ in aqueous $[\text{Zn}(\text{H}_2\text{O})_3(\text{C}_3\text{H}_5\text{OH}(\text{COO})_3)]$ complex in equilibrium condition at 25°C (Black et al., 2011). The molecular geometries of Zn complexes (hexaquo Zn, tetrachloro Zn, sulfate Zn, citrate Zn species) in various states of solvation, protonation and coordination changed the degree of Zn partitioning and magnitude of its fractionation (Black et al., 2011). The Zn bound to humic acid (PHA) was heavier than free Zn^{2+} ($0.24 \pm 0.06\text{‰}$) at pH 6 and higher while no measurable Zn isotopic fractionation occurred below pH 6 (Jouvin et al., 2009). The effect of pH on the adsorption of Zn to humic acid (PHA) can be explained by changes in Zn speciation and complexation occurred mostly through binding to high affinity sites (HAS) and low affinity sites (LAS). The higher the pH, the higher in complexation constants and the shorter bond lengths for Zn-PHA complexes compared to the free Zn^{2+} (Jouvin et al., 2009). Unlike any other processes, precipitation of ZnO (zincite) was strongly depleted in heavy isotopes with a $\delta^{66}\text{Zn}$ of $-0.52 \pm 0.08\text{‰}$ as ZnO (Cacaly et al., 2004). A similar enrichment of heavy isotopes during the precipitation of ZnCO_3 can be seen where $\delta^{66}\text{Zn}$ ranged from 0.31 to 0.34‰ in ZnCO_3 (Pichat et al., 2003). The detail values are given in Table 3.5 under supplementary data.

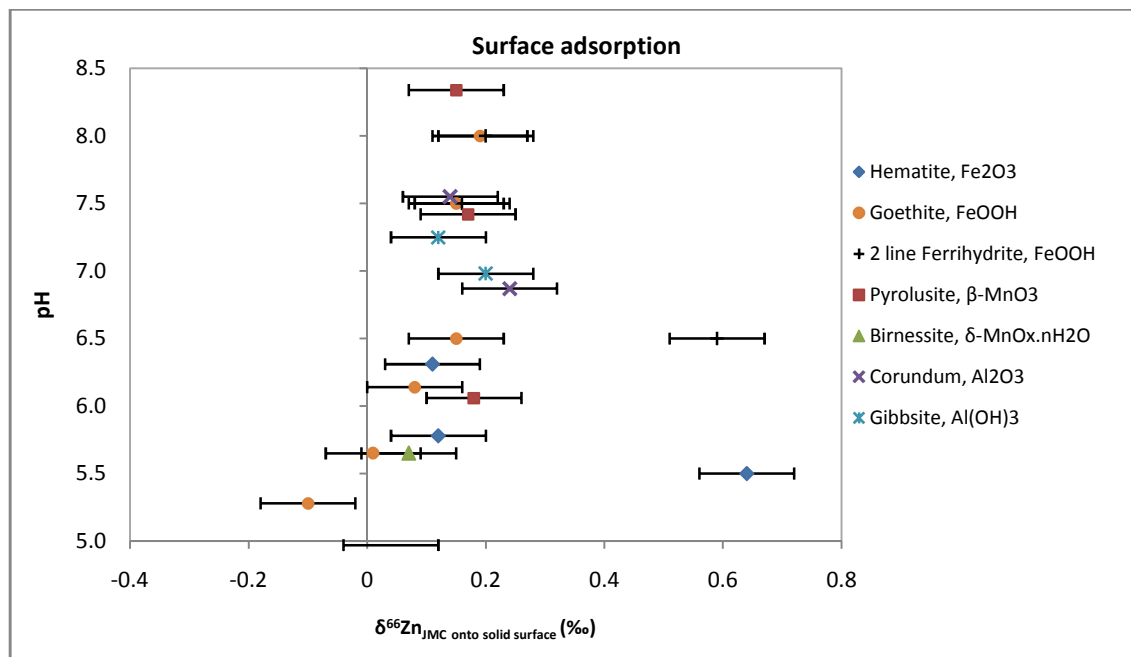


Figure 3.5. Heavy fractionation of Zn isotopes during surface adsorption onto metal oxide and oxy(hydr)oxide phases where the external reproducibility is ± 0.05 to 0.08‰ (The detail values are given in Table S5 - Supplementary data).

3.5. Summary and conclusions

The current state of knowledge on $\delta^{66}\text{Zn}$ variations related to metallurgical activities and the possibility to use these variations to trace the Zn pollution in the different environmental compartments is illustrated in schematic diagram, Figure 3.6. Zn isotopes fractionated significantly from initial ores ($0.16 \pm 0.2\text{‰}$) to final refined Zn metal (0.22‰). The high-temperature process involved during roasting and smelting of ores favors the Rayleigh fractionation law which led to the enrichment of lightest Zn isotopes in air emissions (-0.66 to 0.21‰) whereas enrichment of heaviest isotopes in slags (0.13 to 1.49‰) and in effluent (0.41 to 0.51‰) occur. This distribution of light and heavy isotopes between emissions and slags could also be contributed by the electroplating steps where the ore-concentrate from the smelting steps were further leached and electroplated. However, the extent of Zn isotopes fractionation induced by individual processes (smelting and electroplating) or a combination of both processes is still unclear and undocumented.

The distinct $\delta^{66}\text{Zn}$ signatures of each processing steps of Pb-Zn smelters make it possible to trace the source of Zn pollution in different environmental compartments (air, water, soil, plants) impacted by Zn and Pb metallurgical activities. For instance, the heavy Zn signature in groundwater (1.18 to 1.4‰) could be related to the seepage from the slag dumps (0.13 to 1.49‰), the advective or diffusive transport of pore water from the contaminated soil at smelting site (0.31 to 1.21‰) or the direct discharge of untreated effluent (0.41 to 0.51‰). Similarly, the contaminated surface water (0.02 to 0.58‰) could consequently lead to the contamination of river bank soil (0.40 to 0.96‰) and river sediments (0.91‰). In addition, the signatures of river sediments (0.91‰), reservoir sediments (0.75 to 0.94‰), and lake

sediments (0.07 to 0.39‰) could be further impacted by direct air emission from the smelter's plume (-0.66 to 0.21‰) or re-deposition of particulate matters (-0.02 to 0.07‰) depending on the location of the pollutant receptors.

Significant Zn isotope variations have been observed in the different soil profiles impacted by smelters. The soil within 1 km radius show two distinct signatures; -0.36 to -0.08‰ most likely to be impacted by PM or direct air emission from smelters whereas 0.22 to 0.49‰ impacted by the deposition of particles from the slags with heaviest signatures. Meanwhile, the contaminated soil within >1 to 5 km radius showed the lightest signatures; -0.46 to -0.06‰ suggesting air emission as source of contamination.

Providing the evidences on the water, soil and air contaminated by the Pb-Zn smelters, it is very likely that excessive uptake of Zn by plants (trees, herbs or vegetations) and by aquatic species (plankton, shrimps or fishes) could lead to the contamination in food chain. However, there are no studies related to Zn isotopic signatures in different biological samples impacted by smelters.

Nevertheless, this review provides a framework on $\delta^{66}\text{Zn}$ variations and fractionation within Pb-Zn smelters starting from ore signatures up to final Zn refined products, and in different environmental compartments (air, water, soil) impacted only by Zn and Pb metallurgical activities, as well as fractionation processes (surface adsorption, precipitation, complexation). By compiling the variations, and understanding the processes, Zn isotopes is best-fit as an environmental tracer and to assess the impact of metallurgical industries.

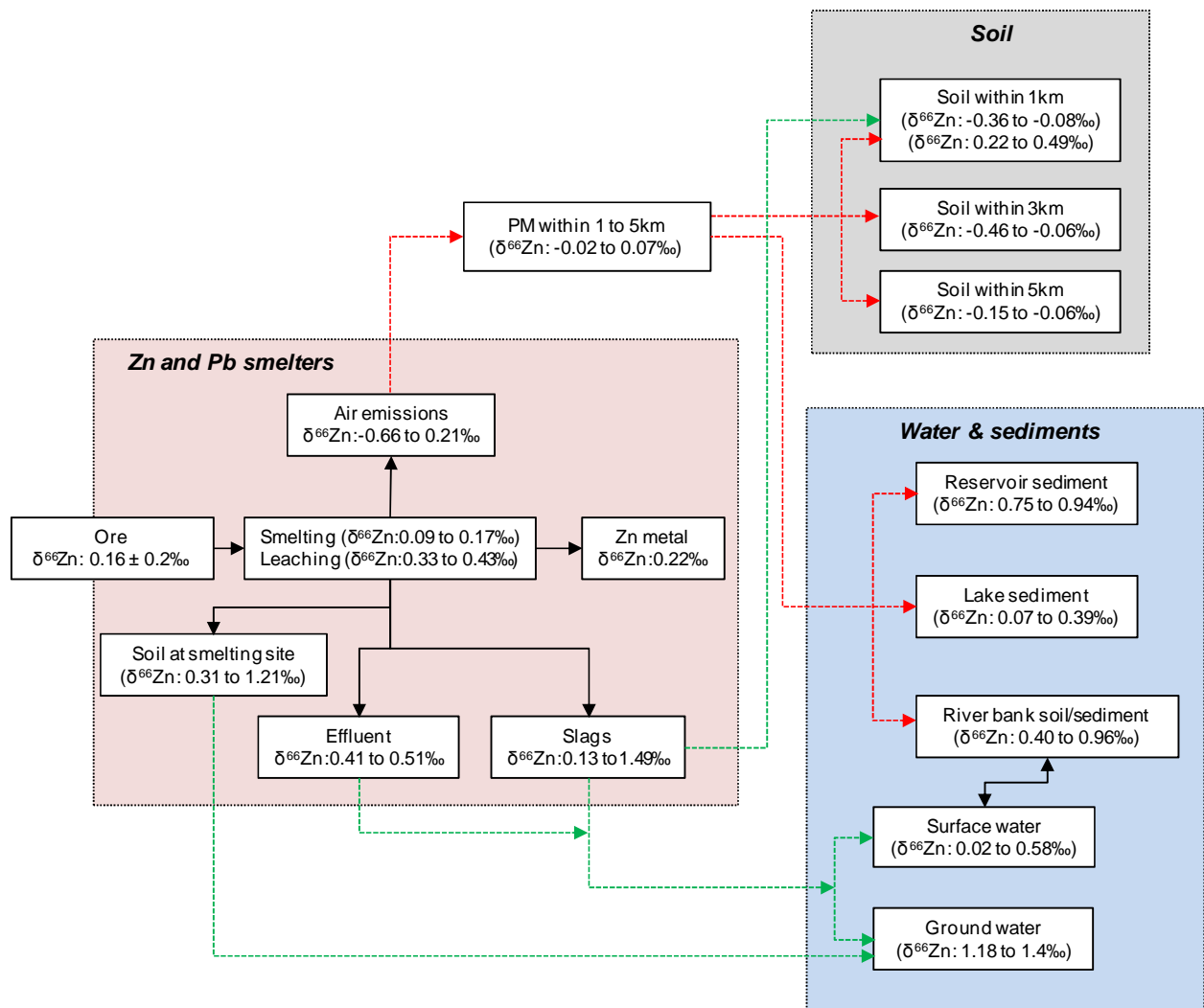


Figure 3.6. Schematic diagram depicting published data on Zn isotopic compositions related to Zn and Pb metallurgical industries.

3.6. Perspectives

While conducting this review, the author came across a few obstacles and limitations which might possibly serve as the bridge for further development in future research directions. The limitation lies within the following context:

- The extent of Zn isotopes fractionation induced by individual process (roasting or electroplating) or by a combination of both processes as shown in Figure 2, thus, it opens more rooms for either field data collection or experimental simulation of such processes;
- Several field studies related to environmental assessment of smelters had massive information on concentration data, whereas, only a few studies focused on isotopic data, thus, the authors would like to encourage to go a step further in collecting more isotopic data;

- Similarly, there are almost no studies related to Zn isotopic signatures in different biological samples impacted by smelters; thus, it clearly has more space for field data collection of both concentration and isotopic data on biological samples. Moreover, the speciation of Zn as well as its bioavailability coupled with concentration and isotopic data will be an advantage as well;
- These adsorption studies onto inorganic mineral phases could be further extended to more mineral phases such as clay; and the application laboratory data on adsorption studies (with oxides and oxy-hydroxides) in real geological setting will be interesting;
- There is no study on Zn isotopic data during its precipitation as ZnCO_3 , ZnO , predominant phases during oxidative environments. Only one study (Jouvin et al., 2009) was documented here regarding Zn complexing with humic acid, thus, it will be an advantage to study deeper into more complexation and precipitation mechanisms; and
- In many geological settings, it is well-known that soil can accommodate different species of micro-organisms and adsorption of Zn onto bacterial cell wall can significantly affect the speciation and mobility of Zn. However, the involvement of micro-organisms on the extent of Zn isotopic fractionation remains unclear and still unknown.

3.7. References

- Albarède, F., Beard, B., 2004. Analytical methods for non-traditional isotopes. *Rev Mineral Geochem*, 55: 113-152.
- Aranda, S., Borrok, D.M., Wanty, R.B., Balistrieri, L.S., 2012. Zinc isotope investigation of surface and pore waters in a mountain watershed impacted by acid rock drainage. *Sci Total Environ*, 420: 202-213.
- Balistrieri, L.S., Borrok, D.M., Wanty, R.B., Ridley, W.I., 2008. Fractionation of Cu and Zn isotopes during adsorption onto amorphous Fe(III) oxyhydroxide: Experimental mixing of acid rock drainage and ambient river water. *Geochim Cosmochim Acta*, 72: 311-328.
- Bigalke, M., Weyer, S., Kobza, J., Wilcke, W., 2010. Stable Cu and Zn isotope ratios as tracers of sources and transport of Cu and Zn in contaminated soil. *Geochim Cosmochim Acta*, 74: 6801-6813.
- Black, J.R., John, S.G., Kavner, A., 2014. Coupled effects of temperature and mass transport on the isotope fractionation of zinc during electroplating. *Geochim Cosmochim Acta*, 124: 272-282.

- Black, J.R., Kavner, A., Schauble, E.A., 2011. Calculation of equilibrium stable isotope partition function ratios for aqueous zinc complexes and metallic zinc. *Geochim Cosmochim Acta*, 75: 769-783.
- Borrok, D., Wanty, R., Ridley, W., Wolf, R., Lamothe, P., Adams, M., 2007. Separation of copper, iron, and zinc from complex aqueous solutions for isotopic measurement. *Chem Geol*, 242: 400-414.
- Borrok, D.M., Nimick, D.A., Wanty, R.B., Ridley, W.I., 2008. Isotopic variations of dissolved copper and zinc in stream waters affected by historical mining. *Geochim Cosmochim Acta*, 72: 329-344.
- Cacaly, S., Maréchal, C., Juillot, F., Guyot, F., Benedetti, M., 2004. Zn isotopes fractionation upon sorption and precipitation. *Geochim Cosmochim Acta*, 68: A366.
- Chen, J.B., Louvat, P., Gaillardet, J., Birck, J.L., 2009. Direct separation of Zn from dilute aqueous solutions for isotope composition determination using multi-collector ICP-MS. *Chem Geol*, 259: 120-130.
- Cloquet, C., Carignan, J., Lehmann, M.F., Vanhaecke, F., 2008. Variation in the isotopic composition of zinc in the natural environment and the use of zinc isotopes in biogeosciences: A review. *Anal Bioanal Chem*, 390: 451-63.
- Couder, E., Delvaux, B., Maerschalk, C., Mattielli, N., 2008. Zinc isotopes in polluted substrates. *Goldschmidt Conference Abstracts*: A184.
- Dolgoplova, A., Weiss, D.J., Seltmann, R., Kober, B., Mason, T.F.D., Coles, B., Stanley, C.J., 2006. Use of isotope ratios to assess sources of Pb and Zn dispersed in the environment during mining and ore processing within the Orlovka–Spokoinoe mining site (Russia). *App Geochem*, 21: 563-579.
- Gordon, R.B., Graedel, T.E., Bertram, M., Fuse, K., Lifset, R., Rechberger, H., Spatari, S., 2003. The characterization of technological zinc cycles. *Resour Conserv Recycl*, 39: 107-135.
- Guberman, D.E., 2012. Lead. U.S. *Geological Survey Minerals Yearsbook*: 1-18. Retrieved from <http://minerals.usgs.gov/minerals/pubs/commodity/lead/myb1-2010-lead.pdf>
- John, S., Genevievepark, J., Zhang, Z., Boyle, E., 2007. The isotopic composition of some common forms of anthropogenic zinc. *Chem Geol*, 245: 61-69.
- Jouvin, D., Louvat, P., Juillot, F., Marechal, C.N., Benedetti, M.F., 2009. Zinc Isotopic Fractionation: Why Organic Matters. *Environ Sci Technol*, 43: 5747-5754.
- Juillot, F., Maréchal, C., Ponthieu, M., Cacaly, S., Morin, G., Benedetti, M., Hazemann, J.L., Proux, O., Guyot, F., 2008. Zn isotopic fractionation caused by sorption on goethite and 2-Lines ferrihydrite. *Geochim Cosmochim Acta*, 72: 4886-4900.

- Juillot, F., Maréchal, C., Morin, G., Jouvin, D., Cacaly, S., Telouk, P., Benedetti, M.F., Ildefonse, P., Sutton, S., Guyot, F., Brown, G.E., 2011. Contrasting isotopic signatures between anthropogenic and geogenic Zn and evidence for post-depositional fractionation processes in smelter-impacted soils from Northern France. *Geochim Cosmochim Acta*, 75: 2295-2308.
- Kavner, A., John, S.G., Sass, S., Boyle, E.A., 2008. Redox-driven stable isotope fractionation in transition metals: Application to Zn electroplating. *Geochim Cosmochim Acta*, 72: 1731-1741.
- Kelley, K.D., Wilkinson, J.J., Chapman, J.B., Crowther, H.L., Weiss, D.J., 2009. Zinc isotopes in sphalerite from base metal deposits in the red dog district, Northern Alaska. *Econ Geol*, 104: 767-773.
- Marechal, C., Telouk, P., Albarede, F., 1999. Precise analysis of copper and zinc isotopic compositions by plasma-source mass spectrometry. *Chem Geol*, 156: 251-273.
- Maréchal, C.N., Nicolas, E., Douchet, C., Albarède, F., 2000. Abundance of zinc isotopes as a marine biogeochemical tracer. *Geochem Geophys Geosyst*, 1: 1-15.
- Marechal, C.N., Albarede, F., 2002. Ion exchange fractionation of copper and zinc isotopes. *Geochim Cosmochim Acta*, 66: 1499-1509.
- Mason, T.F.D., Weiss, D.J., Horstwood, M., Parrish, R.R., Russel, S.S., Mullane, E., Coles, B.J., 2004a. Spectral interferences and their correction. *J Anal At Spectrom*, 19: 209-217.
- Mason, T.F.D., Weiss, D.J., Horstwood, M., Parrish, R.R., Russel, S.S., Mullane, E., Coles, B., 2004b. High-precision Cu and Zn isotope analysis by plasma source mass spectrometry. Part 2. Correcting for mass discrimination effects. *J Anal At Spectrom*, 19: 218-226.
- Mason, T.F.D., Weiss, D.J., Chapman, J.B., Wilkinson, J.J., Tessalina, S.G., Spiro, B., Horstwood, M.S.A., Spratt, J., Coles, B.J., 2005. Zn and Cu isotopic variability in the Alexandrinka volcanic-hosted massive sulphide (VHMS) ore deposit, Urals, Russia. *Chem Geol*, 221: 170-187.
- Mattielli, N., Petit, J.C.J., Deboudt, K., Flament, P., Perdrix, E., Taillez, A., Rimetz-Planchon, J., Weis, D., 2009. Zn isotope study of atmospheric emissions and dry depositions within a 5 km radius of a Pb-Zn refinery. *Atmos Environ*, 43: 1265-1272.
- Parsons, M.B., Bird, D.K., Einaudi, M.T., Alpers, C.N., 2001. Geochemical and mineralogical controls on trace element release from the Penn Mine base-metal slag dump, California. *Appl Geochem*, 16: 1567-1593.

- Pelfrene, A., Waterlot, C., Mazzuca, M., Nisse, C., Bidar, G., Douay, F., 2011. Assessing Cd, Pb, Zn human bioaccessibility in smelter-contaminated agricultural topsoils (northern France). *Environ Geochem Health*, 33: 477-93.
- Pichat, S., Douchet, C., Albarède, F., 2003. Zinc isotope variations in deep-sea carbonates from the eastern equatorial Pacific over the last 175 ka. *Earth Planet Sci Lett*, 210: 167-178.
- Pokrovsky, O.S., Viers, J., Freydier, R., 2005. Zinc stable isotope fractionation during its adsorption on oxides and hydroxides. *J Colloid Interface Sci*, 291: 192-200.
- Rodushkin, I., Stenberg, A., Andrén, H., Malinovsky, D., Baxter, D.C., 2004. Isotopic fractionation during diffusion of transition metal ions in solution. *Anal Chem*, 76: 2148-2151.
- Rosman, K.J.R., 1972. A survey of the isotopic and elemental abundance of zinc. *Geochim Cosmochim Acta*, 36: 801-819.
- Shiel, A.E., Barling, J., Orians, K.J., Weis, D., 2009. Matrix effects on the multi-collector inductively coupled plasma mass spectrometric analysis of high-precision cadmium and zinc isotope ratios. *Anal Chim Acta*, 633: 29-37.
- Shiel, A.E., Weis, D., Orians, K.J., 2010. Evaluation of zinc, cadmium and lead isotope fractionation during smelting and refining. *Sci Total Environ*, 408: 2357-2368.
- Sivry, Y., Riotte, J., Sonke, J., Audry, S., Schafer, J., Viers, J., Blanc, G., Freydier, R., Dupre, B., 2008. Zn isotopes as tracers of anthropogenic pollution from Zn-ore smelters The Riou Mort-Lot River system. *Chem Geol*, 255: 295-304.
- Sonke, J., Sivry, Y., Viers, J., Freydier, R., Dejonghe, L., Andre, L., Aggarwal, J., Fontan, F., Dupre, B., 2008. Historical variations in the isotopic composition of atmospheric zinc deposition from a zinc smelter. *Chem Geol*, 252: 145-157.
- Thapalia, A., Borrok, D., Van Metre, P.C., Musgrove, M., Landa, E.R., 2010. Zn and Cu isotopes as tracers of anthropogenic contamination in a sediment core from an urban lake. *Environ Sci Tech*, 44: 1544-1550.
- Tolcin, A.C., 2012. Zinc. U.S. *Geological Survey Minerals Yearsbook* (84): 1-11. Retrieved from <http://minerals.usgs.gov/minerals/pubs/commodity/zinc/myb1-2011-zinc.pdf>
- Van Alphen, M., 1999. Atmospheric heavy metal deposition plumes adjacent to a primary lead-zinc smelter. *Sci Total Environ*, 236: 119-134.
- Vdovic, N., Billon, G., Gabelle, C., Potdevin, J.L., 2006. Remobilization of metals from slag and polluted sediments (case study: the canal of the Deule River, northern France). *Environ Pollut*, 141: 359-69.

- Verguts, P., 2005. Two dimensional mathematical simulation model for a non-ferrous blast furnace. *PhD thesis manuscript*, Katholieke Universiteit Leuven, Belgium: 1-168.
- Weiss, D.J., Rausch, N., Mason, T.F.D., Coles, B.J., Wilkinson, J.J., Ukonmaanaho, L., Arnold, T., Nieminen, T.M., 2007. Atmospheric deposition and isotope biogeochemistry of zinc in ombrotrophic peat. *Geochim Cosmochim Acta*, 71: 3498-3517.
- Wilkinson, J.J., Weiss, D.J., Mason, T.F.D., Coles, B., 2005. Controls of zinc isotope variability in ore-forming systems preliminary constrains from the Zn-Pb Irish ore fields. *Eco Geol*, 100: 583-590.
- Young, E.D., Galy, A., Nagahara, H., 2002. Kinetic and equilibrium mass-dependent isotope fractionation laws in nature and their geochemical and cosmochemical significance. *Geochim Cosmochim Acta*, 66: 1095-1104.

3.8. SUPPLEMENTARY DATA

Table S1. Zinc isotope variations in ores.

<i>Ore formation</i>	$\delta^{66}\text{Zn}_{\text{JMC}}$ (‰)	2SD	References
Initial hydrothermal fluid	0.0 to +0.1	$\pm 0.12\text{‰}$	Wilkinson et al., 2005
ZnCO ₃ ores (n=77)	-0.31 to +1.34	$\pm 0.07\text{‰}$	Pichat et al., 2003
<u>ZnS ores</u>	-0.43 to +1.33		
<u>Ore from Russia</u>			
Ores from Orlovka and Spokoinoe (n=46)	-0.4 to 1.2	$\pm 0.06\text{‰}$	Dolgoplova et al., 2006
Pure chalcopyrite (Zn+CuFeS ₂)	-0.43	$\pm 0.07\text{‰}$	Mason et al., 2005
Pure sphalerite (Fe+ZnS)	-0.03	$\pm 0.07\text{‰}$	
Sphalerite (Fe+ZnS) with galena, chalcopyrite, and pyrite	+0.23	$\pm 0.07\text{‰}$	
<u>Ore from Europe</u>			
ZnS Spain (n=4)	0.09 to 0.25	$\pm 0.04\text{‰}$	Sonke et al., 2008
ZnS Belgium (n=14)	0.07 to 0.37	$\pm 0.04\text{‰}$	
ZnS France (n=2)	0.37	$\pm 0.04\text{‰}$	
ZnS Finland (n=15)	0.10 to 0.5	$\pm 0.07\text{‰}$	Weiss et al., 2007
Zn-Pb ore Ireland (n=42)	-0.17 to 1.33	$\pm 0.12\text{‰}$	Wilkinson et al., 2005
<u>Ore from other parts of the world</u>			
ZnS Australia (n=6)	0.02 to 0.1	$\pm 0.04\text{‰}$	Sonke et al., 2008
ZnS Africa (n=32)	-0.03 to 0.28	$\pm 0.04\text{‰}$	
ZnS Alaska (n=36)	0.00 to 1.14	$\pm 0.06\text{‰}$	Kelley et al., 2009
PbS Australia (n=6)	0.12 to 0.25	$\pm 0.04\text{‰}$	Sonke et al., 2008
Weathering of sphalerite ores	0.0 to 0.2‰	$\pm 0.07\text{‰}$	Fernandez and Borrok, 2009

Table S2. Zinc isotope variations during smelting activities.

Smelting processes	$\delta^{66}\text{Zn}_{\text{JMC}}$ (‰)	2SD	References
<i>Zn smelters</i>			
Ore concentrate (calcine)	0.09 to 0.17	$\pm 0.07\text{‰}$	Shiel et al., 2010

Refined Zn	0.22	± 0.06‰	
Zn smelter effluent	0.41 to 0.51	± 0.08‰	
<i>Pb smelters</i>			
Pb mix feed	0.33	± 0.15‰	Shiel et al., 2010
Slag fuming plant	0.43	± 0.06‰	
<i>Slags</i>			
Pb-Zn refinery	0.37 to 0.96	± 0.05‰	Couder et al., 2008 and Juillot et al., 2011
Zn slags	0.18 to 1.49	± 0.04‰	Sivry et al., 2008 and Yin et al., in preparation
Pb slags	0.13	± 0.08‰	Yin et al., in preparation
<i>Weathering of slags</i>			
Zn slags at pH 4	0.91	± 0.06‰	Yin et al., 2013
Zn slags at pH 10	-0.19	± 0.06‰	
Pb slags at pH 4	0.1	± 0.06‰	
Pb slags at pH 10	-1.25	± 0.06‰	
<i>Air emissions</i>			
Zn ore grilling emission	-0.07	± 0.06‰	Mattielli et al., 2009
Zn smelting	-0.35 to -0.37	± 0.03‰	
Pb ore grilling emission	0.05 to 0.21	± 0.05‰	
Pb smelting	-0.66	± 0.02‰	

Table S3. Zinc isotope variations in fresh water, sediments and riverbank soil.

<i>Water bodies</i>	$\delta^{66}\text{Zn}_{\text{JMC}}$ (‰)	<i>2SD</i>	<i>References</i>
Groundwater	1.18 to 1.4	± 0.04‰	Sivry et al., 2008
<u>Surface water</u>	0.02 to 0.58		
Stream water	0.02 to 0.46	± 0.07‰	Borrok et al., 2008
River water	0.07 to 0.58	± 0.04‰	Chen et al., 2008 and Aranda et al., 2012
<u>River bank soil samples</u>			Sivry et al., 2008

Riverbank soil upstream and downstream	0.40 to 0.48	$\pm 0.04\text{‰}$	
Riverbank soil downstream after the confluence of two polluted rivers	0.74 to 0.96	$\pm 0.04\text{‰}$	
River sediment (0-3 cm)	0.91	$\pm 0.04\text{‰}$	Sivry et al., 2008
<u>Lake sediments (1 km away from smelters)</u>			
Sediment collected ≤ 10 cm	0.07 to 0.17	$\pm 0.04\text{‰}$	Sonke et al., 2008
Sediment collected 10 to 20 cm	0.17 to 0.32	$\pm 0.04\text{‰}$	
Sediment collected 20 to 40 cm	0.19 to 0.39	$\pm 0.04\text{‰}$	
Sediment collected >50 cm	0.31	$\pm 0.09\text{‰}$	
<u>Reservoir sediment</u>			
Reservoir sediment ≤ 10 cm	0.75	$\pm 0.05\text{‰}$	Sivry et al., 2008
Reservoir sediment 20 cm	1.25	$\pm 0.04\text{‰}$	
Reservoir sediment 40 cm	1.35	$\pm 0.05\text{‰}$	
Reservoir sediment 60 cm	1.03	$\pm 0.04\text{‰}$	
Reservoir sediment 100 cm	0.94	$\pm 0.04\text{‰}$	
<u>Lake sediment</u>			
Pre-smelter period ~1450 to 1900	0.39	$\pm 0.09\text{‰}$	Thapalia et al., 2010
During smelter operation period ~1900 to 1985	0.14	$\pm 0.06\text{‰}$	
Post smelting/stable urban land use period after 1985	0.0	$\pm 0.10\text{‰}$	

Table S4. Zinc isotope variations in smelter impacted soil.

<i>Soil</i>	$\delta^{66}\text{Zn}_{\text{JMC}} (\text{‰})$	Zn conc (mg/kg)	<i>2SD</i>	<i>References</i>
<u>Geogenic soil background (Norway)</u>				Weiss et al., 2007
10 cm	1.33	74	0.14	
15 cm	1.39	56	0.18	
30 cm	1.66	11	0.11	

50 cm	1.24	3	0.07	
<u>PM from Pb–Zn refineries</u>				
0.7 km radius	0.02	n.a	0.02	Mattielli et al., 2009
1 km radius	0.07	n.a	0.04	
3 km radius	-0.02	n.a	0.06	
5 km radius	0.02	n.a	0.05	
<u>Soil at Norway mining site</u>				
10 cm	0.4	87	0.18	Weiss et al., 2007
20 cm	0.73	77	0.24	
40 cm	0.78	46.8	0.07	
50 cm	1.35	11.1	0.32	
70 cm	1.04	10	0.14	
<u>Soil at Norway smelting site</u>				
10 cm	0.54	161.3	0.07	Weiss et al., 2007
20 cm	0.97	74.3	0.26	
40 cm	1.11	5	0.01	
60 cm	1.21	5.3	0.09	
<u>Soil-next to French smelter</u>				
10 cm	0.76	1055	0.19	Juillot et al., 2011
30 cm	0.75	415	0.19	
50 cm	0.34	50	0.17	
80 cm	0.31	45	0.18	
<u>Smelter-impacted soil (1 km radius)</u>				
10 cm	-0.36	2084	0.08	Bigalke et al., 2010
25 cm	-0.16	153	0.08	
33 cm	-0.08	97	0.08	
<u>Soil-away (1 km radius)</u>				
10 cm	0.49	545	0.18	Juillot et al., 2011

25 cm	0.49	568	0.18	Bigalke et al., 2010
60 cm	0.22	50	0.17	
<u>Smelter-impacted soil (3.8 km radius)</u>				
15 cm	-0.46	1324	0.08	
30 cm	-0.19	99	0.08	
42 cm	-0.06	52	0.08	
<u>Smelter-impacted soil (5 km radius)</u>				Bigalke et al., 2010
5 cm	-0.15	666	0.08	
20 cm	-0.06	233	0.08	

Table S5. Zinc isotope fractionation during sorption, complexation and precipitation.

<i>Oxides and oxyhydroxides</i>	$\delta^{66}\text{Zn}_{\text{on solid surface}} (\text{‰})$	<i>2SD</i>	<i>References</i>
<u>Hematite, Fe₂O₃</u>			Pokrovsky et al., 2005
pH 5.5	0.64	± 0.05‰	
pH 5.78	0.12	± 0.05‰	
pH 6.31	0.11	± 0.05‰	
<u>Pyrolusite, β-MnO₂</u>			Pokrovsky et al., 2005
pH 6.06	0.18	± 0.05‰	
pH 7.42	0.17	± 0.05‰	
pH 8.34	0.15	± 0.05‰	
<u>Birnessite, δ-MnO_x.nH₂O</u>			Pokrovsky et al., 2005
pH 4.1	0.04	± 0.05‰	
pH 4.97	0.04	± 0.05‰	
pH 5.65	0.07	± 0.05‰	
<u>Corundum, Al₂O₃</u>			Pokrovsky et al., 2005
pH 6.87	0.24	± 0.05‰	
pH 7.55	0.14	± 0.05‰	
<u>Gibbsite, Al(OH)₃</u>			Pokrovsky et al., 2005

pH 6.98	0.2	± 0.05‰	
pH 7.25	0.12	± 0.05‰	
<u>Goethite, FeOOH</u>			
pH 5.28	-0.1	± 0.05‰	Pokrovsky et al., 2005
pH 5.65	0.01	± 0.05‰	
pH 6.14	0.08	± 0.05‰	
pH 7.5	0.15	± 0.07‰	Juillot et al., 2008
pH 8	0.19	± 0.07‰	
No pH	0.15	± 0.08‰	Cacaly et al., 2004
<u>2 line Ferrihydrite, FeOOH</u>			
pH 6.5	0.59	± 0.07‰	Juillot et al., 2008
pH 7.5	0.16	± 0.07‰	
pH 8.0	0.2	± 0.07‰	
No pH	0.58	± 0.08‰	Cacaly et al., 2004
Complexation	$\delta^{66}\text{Zn}$ in dissolved form (‰)		
<u>Aqueous Zn complexes vs metallic Zn at 25°C</u>			
Aqueous $[\text{Zn}(\text{H}_2\text{O})_6]^{2+}$ complex	1.75		Black et al., 2011
Aqueous $[\text{Zn}-\text{SO}_4]$ complex	2.2 to 2.9		
Aqueous $[\text{ZnCl}_4]^{2-} \cdot 12\text{H}_2\text{O}$ complex	1.28		
Aqueous $[\text{Zn}(\text{H}_2\text{O})_3(\text{C}_3\text{H}_5\text{OH}(\text{COO})_3)]$ complex	2.4		
Humic acid (PHA)	0.24 ± 0.06		Jouvin et al., 2009
Precipitation			
Zincite, ZnO	-0.52 ± 0.08		Cacaly et al., 2004
Zinc carbonate, ZnCO_3	0.31 to 0.34		Pichat et al., 2003

CHAPTER 4

Materials and Methods

Chapter 4

4.1. Materials

4.1.1. Slags

Lead blast furnace (LBF) and imperial smelting furnace (ISF) slags used in this study (Figure 4.1) were obtained from lead and zinc smelters located in the industrial basin of Nord-Pas-de-Calais, northern France. Both slags are granulated waste where the size distribution is log normal with a 500 μm dominant class and the particle size distribution varies from 100 μm to 5 mm (Sobanska et al., 2000). However, the particle size distribution of both LBF and ISF used in this study varies from 100 μm to 2 mm with specific surface area of 0.08-0.09 $\text{m}^2 \text{g}^{-1}$. LBF is mainly composed of amorphous glass with CaO-FeO-SiO_2 as end members (80% in v/v), 19% of crystalline phases and 1% of metallic lead droplets whereas ISF contains higher volume of amorphous glassy part (84% in v/v), 5 % of crystalline phases, 10% of speiss and 1% of Pb droplets (Deneele, 2002). The global chemical compositions as well as the composition of amorphous glassy matrix for both LBF and ISF slags are given in Table 4.1.

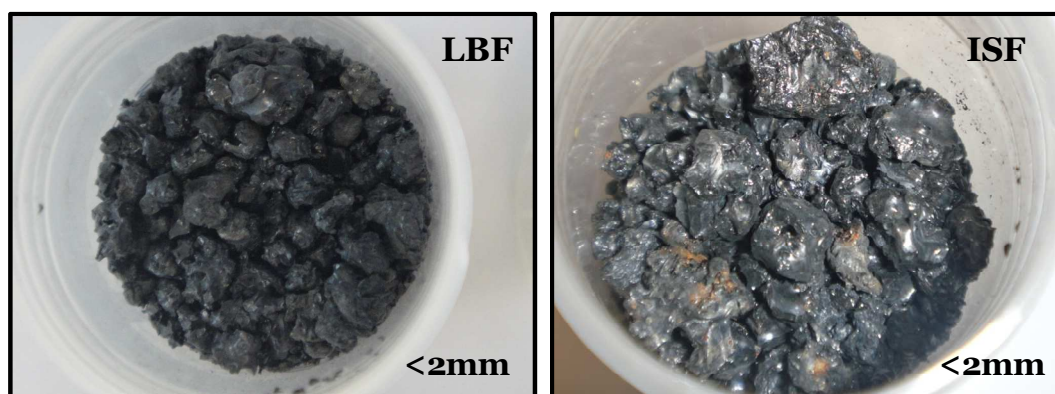


Figure 4.1. Lead blast furnace (LBF) and imperial smelting furnace (ISF) slags

Spinel is the dominant part of crystalline phases which are well embedded and scattered across the glassy matrix of both LBF (19% in v/v) and ISF (5% in v/v). Magnesiochromite (MgCr_2O_4), franklinite (ZnFe_2O_4), magnetite ($\text{Fe}^{2+}\text{Fe}^{3+}_2\text{O}_4$) are dominant spinel phases found in LBF whereas zincochromite (ZnCr_2O_4), and gahnite (ZnAl_2O_4) are the ones found in ISF slags where their respective chemical composition are given in Table 4.2. In addition to spinel phases, some Fe rich speiss are found in ISF as well as some silicate phases such as hardystonite ($\text{Ca}_2\text{ZnSi}_2\text{O}_7$) and willemite (Zn_2SiO_4) are found in both ISF and LBF where detail chemical compositions are given in Table 4.3. Unlike Zn, Pb is mainly present as simple droplet form embedded in the glassy matrix of both slags.

Table 4.1. Chemical composition of global and glassy matrix in LBF and ISF slags.

%wt	Samples	SiO ₂	CaO	Fe ₂ O ₃	FeO	Al ₂ O ₃	MgO	MnO	ZnO	PbO
Global	LBF	24.88	22.14	8.11	23.27	2.46	2.71	0.81	10.77	3.74
	ISF	24.38	18.55	0.39	31.11	10.03	1.81	1.04	8.75	1.66
Glass	LBF	26.38	22.92	-	26.50	2.54	1.91	0.84	11.16	4.30
	ISF	25.68	21.40	-	24.97	9.98	1.80	0.84	8.27	0.22

Note: Global chemical composition obtained by acid digestion (HNO₃-HCl-HF) except for Si by XRF, whereas glassy part obtained by microprobe (Deneele, 2002)

Table 4.2. Chemical composition of primary spinels in LBF and ISF slags.

Samples	Spinel (%wt)	SiO ₂	CaO	Fe ₂ O ₃	FeO	Al ₂ O ₃	MnO	MgO	ZnO	Cr ₂ O ₃
LBF	MgCr ₂ O ₄	0.28	0.57	8.95	5.55	15.83	0.79	12.46	9.90	44.56
	ZnFe ₂ O ₄	0.10	0.68	67.62	7.69	0.62	0.91	4.83	15.79	1.66
	Fe ²⁺ Fe ³⁺ ₂ O ₄	0.05	0.13	45.45	17.29	7.60	0.74	1.99	12.72	13.59
ISF	ZnCr ₂ O ₄	0.03	0.24	3.12	11.52	1.96	2.27	0.97	18.14	61.13
	ZnAl ₂ O ₄	0.08	0.13	3.93	6.59	50.72	0.19	3.19	31.08	4.03

Note: Chemical composition obtained by microprobe (Deneele, 2002)

Table 4.3. Chemical composition of silicates in LBF and ISF slags.

Silicates (% wt)	SiO ₂	CaO	FeO	Al ₂ O ₃	MgO	MnO	ZnO	PbO
Ca ₂ ZnSi ₂ O ₇	38.09	32.96	4.88	2.78	2.63	0.32	12.60	4.56
Zn ₂ SiO ₄	29.86	0.00	1.16	0.03	0.23	10.77	63.99	0.04

Note: Chemical composition obtained by microprobe (Deneele, 2002)

4.1.2. Bacteria

The heterotrophic bacteria, *Pseudomonas aeruginosa* is used as the main bacteria of interest in this research due to its predominant presence in a wide variety of environmental compartments such as air, soil, sediments, sewage etc., its ability to produce the organic ligands known as siderophores, therefore, to simulate soil weathering condition of slags in the presence bacteria and organic ligands and to further comprehend the metal mobility and behavior of slags. The strain number used in this research was CIP 105094, purchased from Institut Pasteur, Paris.

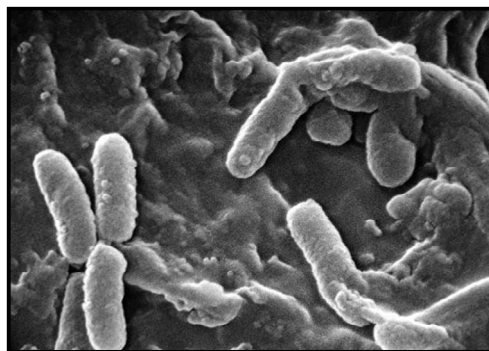


Figure 4.2. *Pseudomonas aeruginosa*(Janice Haney Carr, CDC, USA)

4.2. Zn isotopic techniques

4.2.1. Experimental

The chemical and bio/weathering of slags were conducted in the ISO 8 or class 100,000 labs where the preparation of trace metal and metal analysis were performed under ISO 6 or class 1,000 laminar flow hood. In the meanwhile, preparation of samples for isotopes analysis were carried out under ISO 5 or class 100 the laminar hood inside ISO 6 or class 1,000 cleanrooms (salles blanches) at the Institut de Physique du Globe de Paris (IPGP), Paris, France. The high resolution multi-collector inductively coupled plasma mass spectrometer (MC-ICP-MS) Neptune and Neptune Plus (Thermo Finnigan, Germany) were housed in ISO 6 or class 1,000 labs.

4.2.2. Reagents and isotopic standards

Super pure grade nitric (HNO_3), hydrochloric (HCl) and hydrofluoric (HF) acids purchased from Merck Inc. (Germany) were purified in-house by sub-boiling distillation. Ultra-pure water ($\geq 18.2\text{M}\Omega\text{ cm}$), prepared by de-ionization of reverse osmosis water using a Milli-Q® system (Millipore, USA), was used to prepare all solutions. The entire lab wares were successively cleaned by mildly boiling in either 1% HCl or 5% or 15 N HNO_3 depending on type of lab wares followed by well-rinsing with ultra pure water and drying under laminar flow cabinet.

The in-house IPGP standards were prepared from NIST SRM 3168a for Zn and NIST SRM 3114 for Cu, purchased from SCP Science, Paris, France. In parallel, international reference materials used were JMC Lyon 3-0749L Zn, supplied by F. Albarède (Ecole Normale Supérieure, Lyon, France), IRMM 3702 Zn, and NIST SRM 976 Cu, purchased from respective agencies.

4.2.3. Chromatographic column separation of Zn

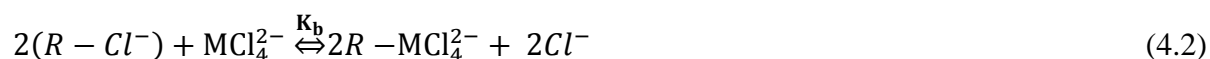
4.2.3.1. Choice of column and resin

The columns used during chromatography were Polypropylene (PP) tubes 4.3 cm in length and 0.7 cm in internal diameter packed with resin, Bio-Rad AG MP-1. Before the first use, the columns were soaked cleaned in ~5% HNO₃ followed by rinsing with MilliQ water. The cleaning process was repeated at least 10 times to prevent the possible trace elements contamination.

The macro-porous form (AG MP-1) of strongly basic anion exchange resins has higher distribution coefficients for Cu(II), Fe(III) and Zn(II) in concentrated HCl than regular AG1. The resin AG MP-1 (100–200 mesh, chloride form) made of chips instead of beads is very fragile and tends to compact with time (Marechal et al., 1999). Before the first use, the resin was settled 10 times in water and the supernatant thrown away in order to eliminate the finest resin particles.

4.2.3.2. Column chemistry

The AG MP-1 resin consists of positively charged, quaternary ammonium groups chemically bound to styrene divinylbenzene copolymers. In HCl acid, the active sites of the resin bind to the anion Cl⁻ that can be reversibly exchanged with other chlorocomplex anions. A solution of Cu and Zn in HCl matrix produces predominantly two chlorocomplex anions (MCl₃⁻ and MCl₄²⁻) where M stands for either Zn(II). Exchanges between these anions and the resin are governed by the following reactions: 4.1 and 4.2.



where K_a and K_b are equilibrium constants, R represents the active sites of the resin matrix.

The chlorocomplex species therefore partition between dissolved and resin-bound forms as a function of a distribution coefficient (4.3). The D value also constrains the reagent volume required for the elution of the element from the column to its maximum concentration (4.4).

$$D = \frac{C_r}{C_s} \quad (4.3)$$

D is distribution coefficient, C_r is the concentration of resin-bound forms per gram of resin ($R-MCl_3^-$ & $2R-MCl_4^{2-}$) and C_s is the concentration of dissolved species per mL of solution (M^{2+} , MCl^+ , MCl_2 , MCl_3^- , and MCl_4^{2-}) where D of Zn(II) is higher than D of Cu(II) ~ 2 to 60

$$v = V(D + 1) \quad (4.4)$$

□ is the reagent volume (mL), V is the fraction of volume not occupied by resin (mL)

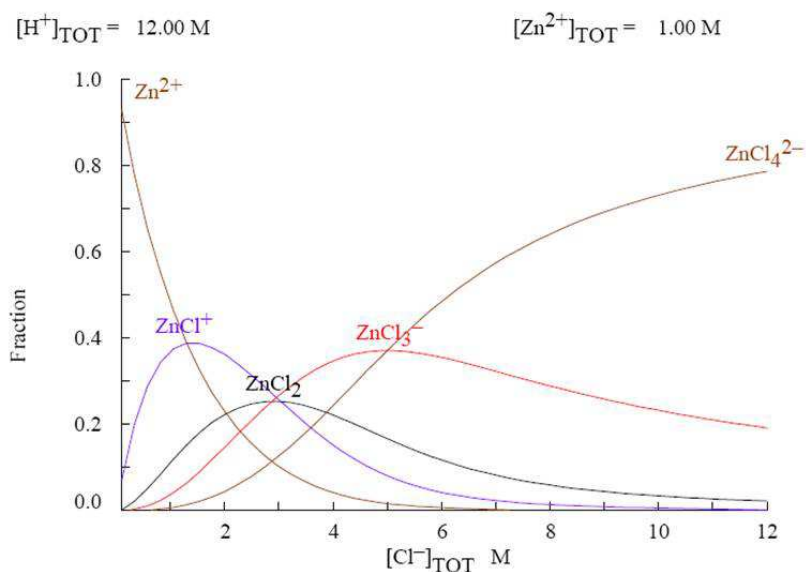
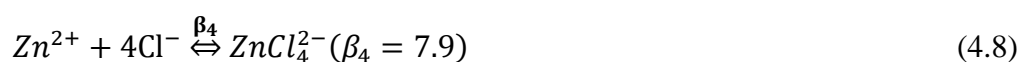
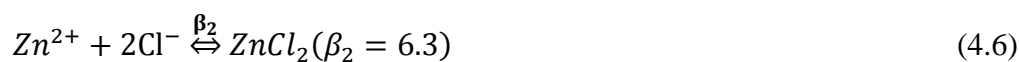


Figure 4.3. Distribution of dissolved species for Zn as a function of different molarities of HCl [Recalculated and redrawn based on Marechal et al. (1999) and Borrok et al. (2007)].

Zn species formed in aqueous solutions of hydrochloric acid are (Zn^{2+} , $ZnCl^+$, $ZnCl_2$, $ZnCl_3^-$, and $ZnCl_4^{2-}$) through a series of reactions (4.5 to 4.8) where stability constants taken from (Marechal and Albarede, 2002).



Cations such as alkali metals and alkaline earth metals do not form chlorocomplexes with Cl^- , therefore, pass through the resin without retardation. In 10 M HCl, Zn is mainly present as $ZnCl_4^{2-}$ (~76%), $ZnCl_3^-$ (~23%), with lesser amount of $ZnCl_2$. In 5 M HCl, Zn is mainly present as $ZnCl_4^{2-}$ (~38%), $ZnCl_3^-$ (~38%), $ZnCl_2$ (~16%) and $ZnCl^+$ (8%). At 1 M HCl, Zn is equally present as Zn^{2+} , $ZnCl_2$ and $ZnCl^-$ with lesser but equal amount of $ZnCl_3^-$, $ZnCl_4^{2-}$. Thus, Zn is well retained even at 1 M HCl but it eluted easily when rinsing with MiliQ water.

4.2.3.3. Separation protocol

Acid digested samples and selected samples from chemical and bio/weathering experiments were prepared for isotopic analysis based on the anion-exchange chromatographic method described in Borrok et al. (2007). The AG MP-1 resin was precleaned using at least 10 washes of HCl (~7 M) followed by several washes of HNO_3 (~5%) and purified water. The resin was regenerated using 10 M HCl before being loaded onto the columns. All samples were

evaporated and re-dissolved in 1 mL of 10 M HCl. The re-dissolved sample was loaded into the column by using an automated pipette. After the last drop of the sample was totally eluted, an additional 4 mL of 10 M HCl was loaded to remove the major cations (Ca, Si, Al, Mg, Mn) present in the sample while retaining Zn inside the resin. Then, 6 mL of 5 M HCl were added to the column to elute the Cu fraction, followed by the addition of 4 mL of 1 M HCl to elute Fe from the column. At last, 4 mL of MilliQ water was added to the column to elute Zn. The final eluted fraction containing Zn was evaporated and redissolved in 2% HNO₃. This step is repeated for at least 3 times to remove residual Cl ions because chlorine is prone to producing molecular species that may interfere with the normal mass spectrum of Cu and Zn (Borrok et al., 2007; Marechal et al., 1999). All additions of acids were made in multiple steps (0.5 or 1 mL increments) in order to prevent re-suspension of resin during column loading. This separation process is summarized in Table 4.4.

Table 4.4. Protocols for Cu, Fe and Zn purification by anion-exchange.

Steps	Acids	Eluents
Pre-washing of resin	7 M HCl	10 washes
	5% HNO ₃	
	MilliQ	
After resin loading	3 mL MilliQ	wash
Conditioning resin	4 mL 10 M HCl	
Sample loading	1 mL 10 M HCl	
Loading & Elution	Acids	Eluents
	4 mL 10 M HCl	Matrix
	6 mL 5 M HCl	Cu, Co
	4 mL 1 M HCl	Fe
	4 mL MilliQ	Zn, Cd

4.2.4. Mass spectrometry

Zn isotopes were measured by using Neptune and Neptune Plus HR-MC-ICP-MS (Thermo Finnigan, Germany) at IPGP, Paris, France. The introduction interface consisted of standard Ni cones, desolvating system, an ESI Teflon micro-nebulizer operating at 100 $\mu\text{L min}^{-1}$, and a CETAC ASX-100 auto sampler. The base-line calibration was performed before every analysis session. ⁶⁴Zn, ⁶⁶Zn, ⁶⁷Zn, ⁶⁸Zn and ⁷⁰Zn were simultaneously measured as well as ⁶²Ni signals were monitored to correct for the potential isobaric ⁶⁴Ni interference on ⁶⁴Zn. The detailed parameters selected for Zn isotopes measurements as well as the configuration of both Neptune and Neptune Plus within one particular analytical session are summarized in Table 4.5.

Table 4.5. Operating conditions and collector configuration used on the Neptune and Neptune Plus.

Parameters	Values	
Skimmer and sampler cones	Ni	
Dry plasma	APEX HF (ESI)	
Heater temperature (°C)	100-140	
Cooler temperature (°C)	-3 to +2	
Flow rate ($\mu\text{L min}^{-1}$)	20 - 400	
Inlet system		
Cool gas (L min^{-1})	15-16	
Auxiliary gas (L min^{-1})	0.8-1.0	
Nebulizer gas (L min^{-1})	0.9-1.0	
Sample uptake ($\mu\text{L min}^{-1}$)	50-100	
Torch positions		
X (mm)	0.14	
Y (mm)	-2.90	
Z (mm)	-0.99	
RF coil power (W)	1200	
Zoom optics		
Focus quad (V)	7.10	
Dispersion (V)	0.50	
Source lenses		
Extraction (V)	-2000	
Focus (V)	-625.0	
X-deflection (V)	4.69	
Y-deflection (V)	-1.24	
Shape (V)	206	
Rot quad (V)	0.50	
Source offset	-3.00	
Mass resolution	Low (300-500)	
Cup configuration		
Cup names	Isotopes	Distance (mm)
L4-F	^{62}Ni	80.0
L3-F	^{63}Cu	59.4
L2-F	^{64}Zn	37.2
L1-F	^{65}Cu	17.8
C-F	^{66}Zn	0.0
H1-F	^{67}Zn	17.2
H2-F	^{68}Zn	35.6
H3-F	^{69}Ga	59.2
H4-F	^{70}Zn	82.6

4.2.5. Isotopic analyses and data presentation

The magnitude of Zn stable-isotope fractionation is usually expressed as $^{66}\text{Zn}/^{64}\text{Zn}$, $^{67}\text{Zn}/^{64}\text{Zn}$, $^{68}\text{Zn}/^{64}\text{Zn}$ with normalization to the most abundant form of Zn, ^{64}Zn (48.6%). All the samples were measured in 0.5 N HNO_3 , spiked with in-house IPGP Cu as internal standard (Zn/Cu ratio 1: 2). Standards such as JMC Lyon Zn and IRMM Zn spiked with in-house IPGP Cu, as well as SRM 976 Cu spiked with in-house IPGP Zn were also measured every 20 samples during one analysis session. An analysis of one sample comprised of 3 blocks of 15*10s integrations.

The individual samples were bracketed by in-house standard (Zn & Cu) and isotopic data were reported in relative to the Johnson Matthey Zinc (JMC) Lyon as shown in Eq. (4.9).

$$\delta^{66}\text{Zn}_{\text{JMC Lyon}} = \{[(^{66}\text{Zn}/^{64}\text{Zn})_{\text{sample}} / (^{66}\text{Zn}/^{64}\text{Zn})_{\text{JMC Lyon}}] - 1\} * 1000 (\text{‰}) \quad (4.9)$$

As the variations of isotopic composition of environmental elements in nature are usually small, it is expressed as the relative deviation with respect to a standard reference, in either parts per 1000 (δ) or parts per 10,000 (\square).

4.2.6. Analytical quality and error evaluation

During the measurement of Cu and Zn isotopes ratios by MC-ICP-MS, there are two major interferences: (1) spectral interferences (Mason et al., 2004a) and (2) non-spectral mass discrimination effects (Mason et al., 2004b). Spectral interferences can be resolved by increasing mass resolution to ($M/\Delta M \sim 3000$), however, increasing mass resolution consequently decreases signal transmission leading to rounding of peak shapes, thus, compromising the high precision isotopic ratio measurements. Because of the very high-precisions required to measure natural mass-dependent isotopic anomalies of Cu and Zn, the mass resolution are usually set at ($M/\Delta M \sim 300$ to 500) and the spectral interferences usually corrected by external mathematical calculations. Likewise, the non-spectral mass bias can be corrected by simple bracketing correction method (Borrok et al., 2007; Thapalia et al., 2010) as well as exponential law (Marechal et al., 1999; Mason et al., 2004a).

4.2.6.1. Spectral interferences (isobaric correction)

Spectral interferences are mostly associated with elemental isobars, major argides, trace oxides and doubly-charged species are common throughout the Cu–Zn mass range (Table 4.6). Spectral interferences are usually associated with either the plasma and nebulizer gas used, matrix components in the solvent and sample, other analyte elements, or entrained oxygen or nitrogen from the surrounding air (Thomas, 2002). The most abundant isotope for Zn is at mass 64 where there is possible interference by ^{64}Ni . Thus, the voltage measured at mass 64 is a total voltage contributed both by ^{64}Ni and ^{64}Zn as shown in Eq. (4.10).

$$\text{Total voltage at mass 64} = \text{Voltage } 64_{\text{Ni}} + \text{Voltage } 64_{\text{Zn}} \quad (4.10)$$

The contribution of ^{64}Ni on ^{64}Zn can be identified by measuring interference-free ^{62}Ni where the correction ratio of $^{64}\text{Ni}/^{62}\text{Ni}$ is applied. The ratio of $^{64}\text{Ni}/^{62}\text{Ni}$ is the ratio of natural abundances of these two isotopes (0.03635/0.00926) and is always constant. Therefore, it gave the following equations (4.11).

$$\text{Voltage } ^{64}\text{Ni} (\text{calculated}) = \text{Voltage } ^{62}\text{Ni} (\text{measured}) * \text{Ratio abundances } \left(\frac{^{64}\text{Ni}}{^{62}\text{Ni}} \right) \quad (4.11)$$

By rewriting Eq. (4.10), the true voltage of ^{64}Zn can be calculated as follows:

$$\text{Voltage } ^{64}\text{Zn} (\text{measured}) = \text{Total voltage at mass 64} - \text{Voltage } ^{64}\text{Ni} (\text{calculated}) \quad (4.12)$$

Likewise, $^{135}\text{Ba}^{2+}$, and $^{138}\text{Ba}^{2+}$ can be determined in order to correct the spectral interferences of $^{130}\text{Ba}^{2+}$, $^{132}\text{Ba}^{2+}$, $^{134}\text{Ba}^{2+}$, and $^{136}\text{Ba}^{2+}$ isotopes (with mass-to-charge ratios ranging from 65 to 68) on ^{65}Cu , ^{66}Zn , ^{67}Zn , and ^{68}Zn . Other potential isobars (mostly molecular species such as $^{24}\text{Mg}^{40}\text{Ar}$ on ^{64}Zn) are mentioned, however, but not corrected (Cloquet et al., 2008; Juillot et al., 2011).

Table 4.6. List of potential interfering species across the mass range ^{62}amu to ^{70}amu .

Mass	Monoisotopic species	Argides	Oxides	Double-charged species	Elemental species
62.0	^{62}Ni (3.59)	Ar^{22}Ne (9.18)	$^{23}\text{Na}^{23}\text{NaO}$ (99.8), ^{46}TiO (7.98)	$^{124}\text{Sn}^{2+}$ (5.79), $^{124}\text{Te}^{2+}$ (4.82), $^{124}\text{Xe}^{2+}$ (0.1)	$^{31}\text{P}^{31}\text{P}$ (100)
63.0	^{63}Cu (69.2)	Ar^{23}Ne (99.6)	$^{31}\text{PO}_2$ (99.5), ^{47}TiO (7.28), $^{47}\text{TiOH}$ (7.98)	$^{126}\text{Te}^{2+}$ (19.0), $^{126}\text{Xe}^{2+}$ (0.09)	
64.0	^{64}Zn (48.6), ^{64}Ni (0.91)	Ar^{24}Mg (78.7), $\text{Ar}^{12}\text{C}^{12}\text{C}$ (97.4)	$^{32}\text{SO}_2$ (94.6), ^{48}CaO (0.19), ^{48}TiO (73.6), $^{47}\text{TiOH}$ (7.98)	$^{128}\text{Te}^{2+}$ (31.69), $^{128}\text{Xe}^{2+}$ (1.91)	$^{32}\text{S}^{32}\text{S}$ (90.3)
65.0	^{65}Cu (30.8)	Ar^{25}Mg (9.96), $\text{Ar}^{12}\text{C}^{13}\text{C}$ (2.17)	$^{32}\text{SO}_2\text{H}$ (94.6), ^{49}TiO (5.49), $^{48}\text{TiOH}$ (73.6)	$^{130}\text{Te}^{2+}$ (33.8), $^{130}\text{Xe}^{2+}$ (4.10), $^{130}\text{Ba}^{2+}$ (0.11)	$^{33}\text{S}^{33}\text{S}$ (1.4)
66.0	^{66}Zn (27.6)	Ar^{26}Mg (11.0)	$^{34}\text{SO}_2$ (4.19), $^{49}\text{TiOH}$ (5.49), ^{50}TiO (5.39), ^{50}CrO (4.34), ^{50}VO (0.24)	$^{132}\text{Xe}^{2+}$ (26.9), $^{132}\text{Ba}^{2+}$ (0.10)	$^{32}\text{S}^{34}\text{S}$ (8.0)
67.0	^{67}Zn (4.10)	Ar^{27}Al (99.6)	$^{35}\text{ClO}_2$ (75.4), $^{34}\text{SO}_2\text{H}$ (4.19), $^{50}\text{TiOH}$ (5.49), $^{50}\text{CrOH}$ (4.34), ^{51}VO (99.5), ^{50}VOH (0.24)	$^{134}\text{Xe}^{2+}$ (10.4), $^{134}\text{Ba}^{2+}$ (2.42)	
68.0	^{68}Zn (18.8)	Ar^{28}Si (91.6), Ar^{12}CO (98.3), $\text{Ar}^{14}\text{N}^{14}\text{N}$ (98.9)	$^{35}\text{ClO}_2\text{H}$ (75.4), ^{52}CrO (83.6), ^{51}VOH (99.5)	$^{136}\text{Xe}^{2+}$ (8.90), $^{136}\text{Ba}^{2+}$ (7.85), $^{136}\text{Ce}^{2+}$ (0.19)	
69.0	^{69}Ga (60.1)	Ar^{29}Si (4.65)	$^{37}\text{ClO}_2$ (24.1), ^{53}CrO (9.48), $^{52}\text{CrOH}$ (83.6)	$^{138}\text{Ba}^{2+}$ (71.7), $^{138}\text{Ce}^{2+}$ (0.25), $^{138}\text{La}^{2+}$ (0.09)	
70.0	^{70}Zn (0.60), ^{70}Ge (20.50)	Ar^{30}Si (3.09), Ar^{14}NO (99.0)	$^{37}\text{ClO}_2\text{H}$ (24.1), ^{54}CrO (2.36), $^{53}\text{CrOH}$ (9.48), ^{54}FeO (5.79)	$^{140}\text{Ce}^{2+}$ (11.1)	$^{35}\text{Cl}^{35}\text{Cl}$ (57.4)

4.2.6.2. Non-spectral mass bias correction (exponential law)

Instrumental mass bias on the Neptune is ~2.0 and 2.8% amu for Zn and Cu respectively (Sonke et al., 2008). During one session of 24 hr, the drift in the mass bias is typically <1%. The instrumental mass bias is corrected with an internal Cu spike, thanks to the linear relationship between the natural logarithm of measured $^{66}\text{Zn}/^{64}\text{Zn}$ versus measured $^{65}\text{Cu}/^{63}\text{Cu}$ for all standards run during an analysis session (John et al., 2007).

According to Marechal et al. (1999) and Mason et al. (2004a), the exponential law assumes that the fractionation of isotopic ratios between real values and measured values of one particular element follows natural logarithm and can be expressed as a function log of mass differences (4.13).

$$\beta = \frac{\ln(r/R)}{\ln(M_2/M_1)} \quad (4.13)$$

Where r is the measured ratio by mass spectrometry, R is the true isotopic ratio of two isotopes of *exact* masses: M_1 and M_2 .

Take Cu, for an example, which is used as the spike during measurement of in-house IPGP standard. The coefficient of fractionation between real and measured values for Cu can be expressed as Eq. (4.14).

$$\beta_{Cu_{spike}} = \frac{\ln(r_{Cu}/R_{Cu})}{\ln(^{65}/^{63})} \quad (4.14)$$

Similar to Eq. (4.14), the fractionation of coefficient of Zn (θ) in the in-house standard can be calculated as follows:

$$\theta_{Zn_{spike}} = \frac{\ln(r_{Zn}/R_{Zn})}{\ln(^{66}/^{64})} \quad (4.15)$$

Based on Eq. (4.14 and 4.15), the slope (\hat{f}) and intercept (y_0) between β and θ can be calculated (Eq. 4.16) in order to identify the fractionation extent between Cu and Zn inside the standard during mass spectrometry measurement.

$$\theta_{Zn_{spike}} = \hat{f} \left(\beta_{Cu_{spike}} \right) + y_0 \quad (4.16)$$

The coefficients of mass fractionation of Cu and Zn inside the standards are already known, thanks to Eq. (4.14 and 4.15). However, only fractionation coefficient of Cu is known inside the samples. By using the values of the slope (\hat{f}) and intercept (y_0) from Eq. (4.16), the fractionation coefficient of Zn inside the samples can be calculated as shown in Eq. (4.17).

$$\theta Z n_{samples} = \int (\beta Cu_{samples}) + y_0 \quad (4.17)$$

Where the values of $\beta Cu_{samples}$ and βCu_{spikes} are the same

Considering all the known fractionation coefficients of Cu and Zn both in the in-house standards and samples, the real ratios of Zn inside the samples can be calculated as Eq. (4.18).

$$R_{Zn\ samples} = \frac{r_{Zn\ samples}}{(66/64)^{\theta_{Zn\ samples}}} \quad (4.18)$$

Further more, the reaction between analyte and spike can be written as follows (4.19 to 4.22),

$$\ln(r/R)_{Cu} = \beta_{Cu} \ln(65/63)_{Cu} \quad (\text{Spike}) \quad (4.19)$$

$$\ln(r/R)_{Zn} = \theta_{Zn} \ln(66/64)_{Zn} \quad (\text{Analyte}) \quad (4.20)$$

By Eq. (4.20) ÷ Eq. (4.19)

$$\frac{\ln(r/R)_{Zn}}{\ln(r/R)_{Cu}} = \frac{\theta_{Zn}}{\beta_{Cu}} * \frac{\ln(66/64)_{Zn}}{\ln(65/63)_{Cu}} \quad (4.21)$$

By simplifying Eq. (9), the following equations can be driven.

$$\ln R_{Zn} = \ln r_{Zn} - \left\{ \ln(r/R)_{Cu} * \frac{\theta_{Zn}}{\beta_{Cu}} * \frac{\ln(66/64)_{Zn}}{\ln(65/63)_{Cu}} \right\} \quad (4.21)$$

$$R_{Zn} = \frac{r_{Zn}}{\{(r/R)_{Cu} * (66/64)_{Zn} * (63/65)_{Cu}\} \exp^{\beta_{Cu}/\theta_{Zn}}} \quad (4.22)$$

Similar calculations can be applied for other pair of Zn isotopes such as $^{67}\text{Zn}/^{64}\text{Zn}$, $^{68}\text{Zn}/^{64}\text{Zn}$, $^{70}\text{Zn}/^{64}\text{Zn}$, $^{68}\text{Zn}/^{66}\text{Zn}$, $^{67}\text{Zn}/^{66}\text{Zn}$, etc.

4.3. Solid phase characterization techniques

X-ray Florescence (XRF), X-ray Diffraction (XRD), Scanning Electron Microscopy (SEM) with Energy Dispersive X-Ray Analysis (EDX), and Transmission Electron Microscopy (TEM) analysis were used to characterize fresh and altered slags in order to give insights regarding the mechanisms of alteration, surface morphology of slags and the formation of secondary mineral phases.

4.3.1. XRF

4.3.1.1. Sample preparation

Both LBF and ISF slags (>2mm in size) were grounded into powder (<1 μ m) at 4500 rpm for 3 mins by PANalytical MiniMill 2 where stainless steel grinding bowl and grinding balls were used which are dedicated for grinding hard and metallic samples. In order to prevent cross contamination between LBF and ISF samples, softer materials like soil was used and grinded in the same procedure to desorb the possible attached fine metallic particles on the wall of the grinding bowl as well as the grinding balls. Then, they were washed with soap followed by milliQ water, before the next sample was grinded. The wax powder (C₁₈H₃₆O₂N₂) was added into powder slag samples in order to strengthen the binding force between particles, in 1:4 wax to sample ratios, and further prepared into pellet (5mm \square) by manual laboratory press.

4.3.1.2. XRF measurement

The measurements were carried out at University of Paris-Diderot by using PANalytical-Epsilon 3XL equipped with energy dispersive XRF spectrometers, 15 kW *Silver* tube. 'Omnian' calibration method containing a series of geo-standard samples and synthetic standards along with the recursive calculation was used to estimate the elemental composition of the samples. This calibration method has an advantage to overcome the defect caused by the matrix such as absorption of emission line by other neighbor atoms, emitting secondary rays, thus, giving the nearest approximation during quantification of elemental sample compositions.

4.3.2. XRD

Sample preparation for XRD was done in the same procedures as XRF except the part of adding binding agent, wax. XRD analyses were performed at University of Paris-Diderot by using a Panalytical X'Pert Pro MPD diffractometer equipped with a multichannel X'celerator detector, and using CuK _{α 1,2} radiation from 5° to 80° 2-theta range at a rate of 0.13°2 θ /min.

4.3.3. SEM-EDS

4.3.3.1. Sample preparation

The wet and altered slag samples at the end of chemical and bio/weathering experiments were lyophilized by Christ Alpha 1-4 LD Freeze Dryer at condensing temperature of -55°C and pressure ranging between 0.024-0.035 mbar for 12 hrs. The freeze-dried grain samples were then mounted onto sticky carbon disc (10 mm \square) and stored for SEM measurement.

Polished sections (60 \times 20 mm²) were prepared where slags were only located on the upper face of the sections and occupied 40% (\approx 500 mm²). During the polished section preparation, contact with water was reduced to a minimum to avoid any early alteration of the most reactive phases like the Pb droplets. The different polishing steps consist of a first lapping and successive polishing using essentially diamond paste. An alcohol-based lubricant liquid was

used to avoid contact with water. After each step the sections were immediately dried with alcohol.

4.3.3.2. SEM measurement

SEM-EDS analysis was performed at University of Paris-Diderot using Philips XL 30 equipped with an energy dispersive X-ray spectrometer (EDX-PGT Ge-detector) operating at 20 kV beam voltage and 1.5 μ A beam current.

4.3.4. TEM

4.3.4.1. Sample preparation

The freeze-dried samples were further grinded in PANalytical MiniMill 2, as previously mentioned before. In order to re-suspend the secondary phases deposited on the altered slag surfaces, MilliQ, and absolute ethanol (Sigma-Aldrich) was added to the freeze-dried powder samples as well as grain samples. The samples were then put in the ultrasonic bath, and sonicated at 30-60 kHz for 1 min in order to loosen particles adhering to surfaces. The supernatant was recovered, allocated on the TEM grid, dried under the clean hood at ambient temperature, and stored for analysis.

4.3.4.2. TEM measurement

TEM analysis was performed at University of Pierre et Marie Curie using Jeol 2100F electron microscope operating at 200 kV and equipped with a ultra high-resolution UHR pole piece and a Gatan GIF 200 L imaging filter.

4.4. Experimental designs

The experiment designs related to three main research phases such as Phase I (characterization), Phase II (chemical dissolution), and Phase III (Bio/weathering) as mentioned in Chapter 1 are further detailed here.

4.4.1. Leaching potential assessment (under Phase I)

Standardized leaching protocols known as European norm (EN 12457) and Toxicity Characteristic Leaching Procedure (TCLP) was used to assess the hazardous properties of slags with respect to regulatory levels. The conditions for each test are detailed in Table 4.7.

European norm (EN 12457-2): A mass of 20 g of solid was placed into the reactor and 200 ml of MilliQ + deionized water (original pH 5.75) was added in order to maintain a L/S (liquid/solid) ratio of 10. The leaching test is performed at $22\pm 3^\circ\text{C}$ for 24 h, and the reactors were gently agitated at 10 rpm.

Toxicity Characteristic Leaching Procedure (TCLP): The leaching solution was prepared by addition of 5.7 mL of acetic acid (reagent grade, Merck, Germany) to 500 mL of deionised

water (MilliQ + deionized water), supplementary addition of 64.3 mL of 1M NaOH (reagent grade, Merck, Germany) and dilution to 1 L. The final pH of the leaching solution was 4.90. An amount of 10 g is placed in the reactor and 200 mL of leaching solution is added in order to achieve an L/S ratio of 20. The experiment was conducted for 18 h at $22\pm 3^\circ\text{C}$, and the reactors were agitated at 30 rpm.

Table 4.7. Detail experimental conditions for TCLP and EN-12457.

Test	Toxicity characteristic leaching procedure (TCLP)	European Norm leaching tests (EN 12457)
Leaching reagent	5.7 mL of acetic acid + 64.3 mL of 1M NaOH in 1 L	MilliQ + deionized water
pH	4.9	5.75
L/S	20 (sample of 10 g in 200 mL)	10 (20 g in 200 mL)
Temperature	$22\pm 3^\circ\text{C}$	$22\pm 3^\circ\text{C}$
Agitation	30 rpm	10 rpm
Retention time	18 hr or over night	24 hr
Filtration	0.6-0.8 μm	0.45 μm
Analysis	Supernatant and elemental analysis	

4.4.2. Acid digestion (under Phase I)

Both LBF and ISF slags along with the Geo-standard material were acid-digested for bulk chemical analysis. Two different acid digestion procedures are proposed according to the recommendation of Ettler et al. (2009) in the following; however, there can be modifications to the procedures based on the nature of the sample.

Acid digestion procedure I: A mass of 0.5 g was dissolved in a mixture of 10 mL HF (38%) and 2 mL HClO₄ (70%) and was evaporated to near dryness. This procedure was repeated and the residue will be dissolved in 2% HNO₃ (v/v), diluted to 100 mL and stored in Teflon vial until analysis.

Acid digestion procedure II: 0.2 g of sample with 0.6 g Na₂CO₃ and 0.05 g NaNO₃ overlapped with a thin layer of supplementary Na₂CO₃ in a Pt crucible at $750\text{-}820^\circ\text{C}$ for 3 h. Then it was dissolved in a mixture of 10 mL H₂O and 8 mL HCl (37%) at 90°C . Likewise, the addition of acid was continued, the residue was dissolved in 2% HNO₃ (v/v), diluted to 100 mL and stored in Teflon vial until analysis.

4.4.3. Chemical dissolution of slags (under Phase II)

As the main goal of Phase II was to identify the chemical dissolution of metals, the key parameters such as pH, O₂ for oxidation, CO₂ for the carbonation effects both on metals leaching and carbonate precipitates were considered (Figure 4.4). pH_{stat} with a complete automatic and continuous titration system (Titroline Alpha plus TL 7000) was used to conduct

the kinetic dissolution experiment where the detail experimental conditions are outlined in Table 4.8.

First of all, the liquid to solid ratio (L/S) was set at 20 and the temperature at $22\pm 2^\circ\text{C}$ for throughout all experiments. Both LBF and ISF slags were sterilized to ensure that the metal dissolution was mainly due to chemical parameters not by the influence of other microorganisms. The pH values were predefined at 4, 5.5, 7, 8.5 and 10 where the set values were based on the preliminary test with bacteria and slags where the values range from 4 to 10. Electrolyte was used in the same ionic strength of the bacteria growth medium to be used in Phase III. All kinetic dissolution tests at different pH and leaching media were carried out at two different atmospheres; in normal atmosphere with the presence of oxygen and carbon dioxide and in nitrogen control atmosphere to identify the oxidation and carbonation effects.

Furthermore, sampling was done at 0, 6, 12, 24, 48, 72, 96, 120, 144, 168, 192, 216 hr for a total length of 9 days of operation time. The leachate of 8 mL in volume was sampled periodically, and replaced by electrolyte. Sampling was done by means of a syringe attached to a flexible tube without interrupting shaking to avoid discontinuity of experimental conditions. Then it was filtered through $0.20\ \mu\text{m}$ (Millipore®), acidified by 2% HNO_3 and stored for further analysis. The inductively coupled plasma optical emission spectrometry (ICP-OES) was used to determine the elements of interest such as Ca, Fe, Mn, Al, Si, Zn, Pb and Mg in the leachate. Likewise, the solid residues was freeze-dried and stored to study the secondary precipitates or surface morphology with XRD and SEM-EDS.

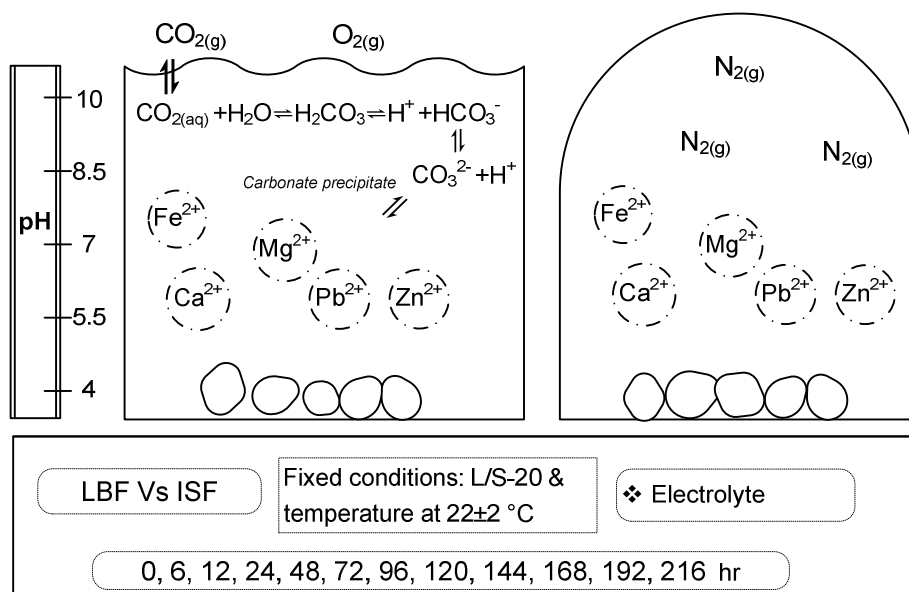


Figure 4.4. Chemical dissolution of slags correlating to pH and carbonation.

Table 4.8. Experimental conditions for chemical dissolution.

pH					LBF	ISF	Atmosphere		Leaching medium	Sampling frequency
4	5.5	7	8.5	10	<2 mm		O ₂ & CO ₂	N ₂	Electrolyte	0, 6, 12, 24, 48, 72, 96, 120, 144, 168, 192, 216 hr
5 sets					2 sets		2 conditions		1 medium	12 sampling frequency in 1 set (9 days)
Fixed conditions: L/S-20 and temperature at 22±3 °C										
20 sets of Experiment										
Sample volume 8 mL (not more than 10% of total volume)										

4.4.4. Biological weathering of slags (under Phase III)

The main goal of Phase III was to simulate the bio-weathering conditions of slags with the presence of heterotrophic bacteria, *Pseudomonas aeruginosa* and to study the impact of metabolic activity on the alteration of slags where the bacteria deprive the essential nutrients within the slags such as iron, calcium and magnesium during the metabolic growth. The overall research idea was depicted in Figure 4.5 and the detailed experimental conditions were given in Table 4.9.

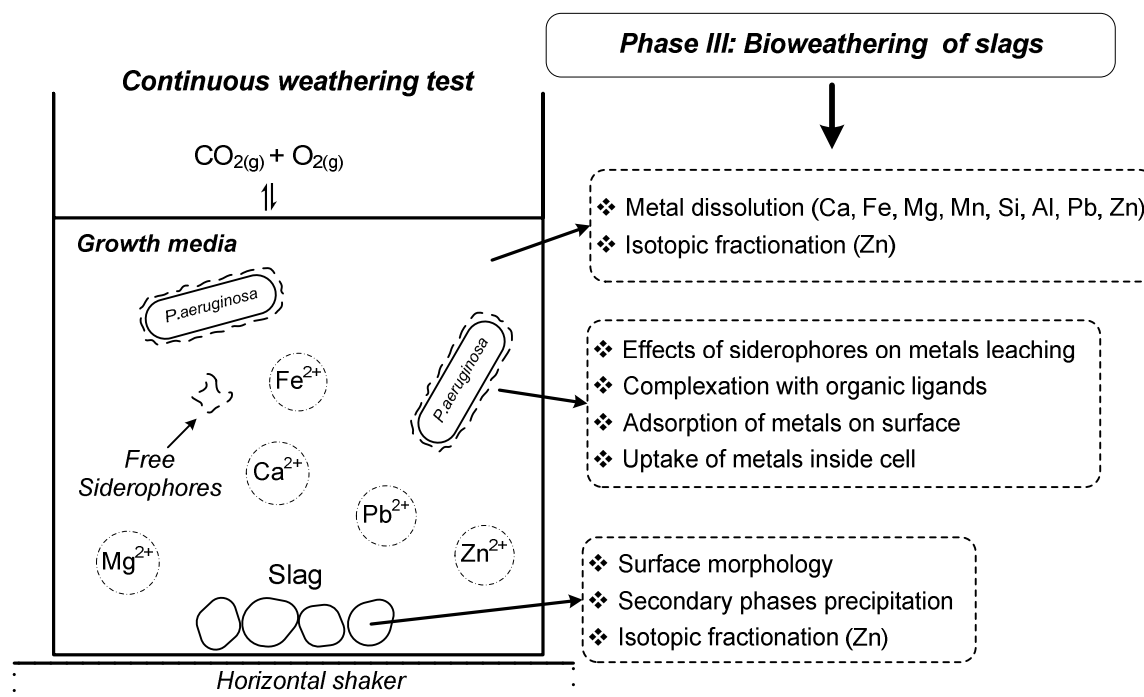


Figure 4.5. Ideal conceptual framework for bio-weathering of slags.

4.4.4.1. Bio/weathering of slags under leachate stagnant conditions (Test 1)

Three different experimental conditions were investigated: ultrapure water (UPW), sterile growth media (GM) and growth media with bacteria (GM+B). The standard succinate medium was used because it was known to permit the synthesis of greater amounts of siderophores for *Pseudomonas* species (Rachid and Ahmed, 2005), but also allows to quantitatively determine the amounts of major elements solubilized during alteration studies (Aouad et al., 2005). One liter of growth medium modified from Aouad et al., (2008) contained 1) 4 g of succinic acid- $C_4H_6O_4$ 2) 1 g of Ammonium sulfate- $(NH_4)_2SO_4$ 3) 0.2 g of Sodium phosphate dibasic- Na_2HPO_4 4) 6 g of TRIS buffer- $C_4H_{11}NO_3$. Finally, the medium was adjusted to pH 7.8 using NaOH. In parallel to biotic experiments, abiotic experiments were performed in both UPW and sterile GM. The experiments were duplicated and were conducted in acid-washed polycarbonate bottles for a time horizon of 4 to 8 months. 2.5 g of crushed slag sample (about 2 mm diameter size) were placed in 75 mL of each leaching solution to obtain a L/S ratio of 30. Reactors were placed at room temperature ($22\pm 2^\circ C$) on horizontal shakers (at 100 rpm). 5 mL of leachate were periodically sampled, and replaced by an equivalent quantity of corresponding leaching medium to maintain the L/S ratio constant.

4.4.4.2. Bio/weathering of slags under leachate renewal conditions (Test 2)

Three parallel weathering experiments were carried out, in duplicate, for 140 days at $23\pm 2^\circ C$: i) in ultrapure water (UPW), ii) in a sterile medium (abiotic) and iii) in the presence of *Pseudomonas aeruginosa* (biotic). The growth media composition was the same as that under Test 1 as mentioned above. The experiment was designed in a way that allowed the successive cycles of bacterial growth with the formation of a biofilm and a possible alteration layer at the surface of the materials (Aouad et al., 2006; Aouad et al., 2005). 2.5 g of slag grains (2 mm diameter size) were placed in a 150 mL polycarbonate flask filled with 75 mL of the three different media and were agitated at 100 rpm. Every 7 days, the reactor was transferred into a new flask containing 75 mL of new medium, thus starting a new cycle. The solid samples were collected at the end of each cycle and were stored for further analysis.

4.4.4.3. Acid digestion of biological samples

The samples from all the biological experiments were acid digested by addition of 2 mL HNO_3 (68%), followed by 2 mL HCl (38%), then by 4 mL of H_2O_2 (30%), 1 mL $HClO_4$ (70%) and finally by 1 mL of HF (38%). The additions of nitric and hydrochloric acids were to digest organic part of the samples (bacteria cells, siderophores, etc) without aggressive degassing during the initial digestion step, where the additions of hydrogen peroxide and perchloric acids were to achieve the complete removal of organic part. The addition of fluoric acid was to eliminate Si from the sample matrix, thus, preventing solidification of samples by Si-gel formation. When the digestion was completed, the samples were evaporated to dryness and re-dissolved in 2% HNO_3 (v/v) where the equivalent acid to initial sample volumes was added. The samples were then stored at $4^\circ C$ for further analysis.

Table 4.9. Experimental conditions for biological dissolution.

Bio/weathering tests	Test 1	Test 2
Materials	<i>P. aeruginosa</i> + slags	<i>P. aeruginosa</i> + slags
Shaking speed (rpm)	100	100
Temperature (°C)	23±2	23±2
Duration (days)	240	140
Growth media compositions	4 g of succinic acid-C ₄ H ₆ O ₄	4 g of succinic acid-C ₄ H ₆ O ₄
	1 g of Ammonium sulfate-(NH ₄) ₂ SO ₄	1 g of Ammonium sulfate-(NH ₄) ₂ SO ₄
	1 g of Sodium phosphate dibasic-Na ₂ HPO ₄	1 g of Sodium phosphate dibasic-Na ₂ HPO ₄
	6 g of TRIS buffer-C ₄ H ₁₁ NO ₃	6 g of TRIS buffer-C ₄ H ₁₁ NO ₃
Experimental conditions	Ultra pure water (UPW) + slags	Ultra pure water (UPW) + slags
	Sterilized growth medium + slags	Sterilized growth medium + slags
	Growth medium + <i>P. aeruginosa</i> + slags	Growth medium + <i>P. aeruginosa</i> + slags
Sampling intervals	Daily (1st week), Per 3 days (1st month), then Per 2 weeks	Per week

4.5. Thermodynamic modeling by Visual Minteq

The chemical equilibrium code Visual MINTEQ v3.0 was used to calculate the saturation indexes and to identify the possible phases controlling solubility. The elemental concentrations measured from the different leaching media were input into the model. Besides, the temperature was kept constant at 25°C, the oversaturated solids were not allowed to precipitate, and the CO₂ partial pressure fixed at 396 ppmv. The model outputs from UPW and GM were used to study the influence of carbonation and the effect of the growth medium composition. Likewise, the model outputs from GM and GM+B media were used to study the effect of bacteria on the metal speciation.

4.6. Inductively coupled plasma optical emission spectrometry (ICP-OES)

Total concentrations of major elements (Ca, Fe, Si, Zn, Pb and Mg), as well as minor elements (As, Ba, Cd, Cr, Cu, Mo, Na, Ni) were measured in the leachate by Inductively Coupled Plasma Optical Emission Spectrometry (ICP-OES, Perkin Elmer Optima 6300). The detection limit was typically 5-10 ppb for most elements and the external precision of ±5%. Quality assurance and quality control (QA/QC) samples, laboratory blanks, calibration check, and sample duplicates were performed to ensure the data quality and validity.

4.7. References

Borrok, D., Wanty, R., Ridley, W., Wolf, R., Lamothe, P., Adams, M., 2007. Separation of copper, iron, and zinc from complex aqueous solutions for isotopic measurement. *Chem Geol*, 242: 400-414.

- Cloquet, C., Carignan, J., Lehmann, M.F., Vanhaecke, F., 2008. Variation in the isotopic composition of zinc in the natural environment and the use of zinc isotopes in biogeosciences: A review. *Anal Bioanal Chem*, 390: 451-63.
- Deneele, D., 2002. Caractérisation, simulations expérimentales et thermodynamiques de l'altération de déchets vitreux: les scories de première fusion de plomb et de zinc. *PhD thesis manuscript*, Université Des Sciences et Technologies de Lille I and U.F.R. Des Sciences De La Terre, France, 1-242.
- John, S., Genevievepark, J., Zhang, Z., Boyle, E., 2007. The isotopic composition of some common forms of anthropogenic zinc. *Chem Geol*, 245: 61-69.
- Juillot, F., Maréchal, C., Morin, G., Jouvin, D., Cacaly, S., Telouk, P., Benedetti, M.F., Ildefonse, P., Sutton, S., Guyot, F., Brown, G.E., 2011. Contrasting isotopic signatures between anthropogenic and geogenic Zn and evidence for post-depositional fractionation processes in smelter-impacted soils from Northern France. *Geochim Cosmochim Acta*, 75: 2295-2308.
- Marechal, C., Telouk, P., Albarede, F., 1999. Precise analysis of copper and zinc isotopic compositions by plasma-source mass spectrometry. *Chem Geol*, 156: 251-273.
- Marechal, C.N., Albarede, F., 2002. Ion exchange fractionation of copper and zinc isotopes. *Geochim Cosmochim Acta*, 66: 1499-1509.
- Mason, T.F.D., Weiss, D.J., Horstwood, M., Parrish, R.R., Russel, S.S., Mullane, E., Coles, B.J., 2004a. Spectral interferences and their correction. *J Anal At Spectrom*, 19: 209-217.
- Mason, T.F.D., Weiss, D.J., Horstwood, M., Parrish, R.R., Russel, S.S., Mullane, E., Coles, B., 2004b. High-precision Cu and Zn isotope analysis by plasma source mass spectrometry. Part 2. Correcting for mass discrimination effects. *J Anal At Spectrom*, 19: 218-226.
- Sobanska, S., Ledésert, B., Deneele, D., Laboudigue, A., 2000. Alteration in soils of slag particles resulting from lead smelting. *Earth Planet Sci*, 331: 271-278.
- Sonke, J., Sivry, Y., Viers, J., Freydier, R., Dejonghe, L., Andre, L., Aggarwal, J., Fontan, F., Dupre, B., 2008. Historical variations in the isotopic composition of atmospheric zinc deposition from a zinc smelter. *Chem Geol*, 252: 145-157.
- Thapalia, A., Borrok, D., Van Metre, P.C., Musgrove, M., Landa, E.R., 2010. Zn and Cu isotopes as tracers of anthropogenic contamination in a sediment core from an urban lake. *Environ Sci Tech*, 44: 1544-1550.

CHAPTER 5

Evaluation on chemical stability of lead blast furnace (LBF) and imperial smelting furnace (ISF) slags

This chapter will be submitted to:

Applied geochemistry

Chapter 5

5.1. Introduction

Metallurgical slags were considered to be chemically inert in the 1980s because metals are associated with glass and silicate; however, many recent studies have pointed out that the leaching from slag dumping sites have deleterious effects on the environment and led to the contamination of soils, sediments, and streams (Douay et al., 2009; Ettler et al., 2005a; Seignez et al., 2008). Several literature reports have been focused on quantifying pollutant mobility resulting from the leaching of metallurgical slags either in batch (Ettler et al., 2002; Ettler et al., 2003a; van Hullebusch et al., in press; Yin et al., 2014) or in open flow experiments (Seignez et al., 2006), in order to approximate their fate under landfill conditions (Mahé-Le Carlier et al., 2000) and in soils or soil-like environments (Ettler et al., 2004; Sobanska et al., 2000).

When slags are subjected to weathering and leaching, the release of major elements and metals is controlled by mineralogical phases present in the slags (Piatak et al., 2014; Piatak et al., 2004), and affected by changes in the pH associated with dissolution/precipitation of a number of solid phases (Vítková et al., 2013). The pH-stat leaching tests have been widely applied for the evaluation of fly ash from municipal solid waste incinerator (Quina et al., 2009), contaminated soils and sediments (Cappuyns and Swennen, 2008), in many environmental samples (Rigol et al., 2009), and secondary lead smelter fly ash (Vitkova et al., 2009). However, only a few studies have applied pH-stat leaching tests on metallurgical slags such as arsenic metallurgical slags (Ganne et al., 2006) and primary lead smelting slags (de Andrade Lima and Bernardez, 2013).

Thus, this paper focused on the pH-stat leaching of lead blast furnace (LBF) and imperial smelting furnace (ISF) slags and further addressed the chemical stability and leaching behaviors of these slags as a function of liquid bulk pH. The objectives of this study were (i) to investigate the leaching behavior of both slags as a function of pH (from 4 to 10), (ii) to evaluate the effect of short term leaching (1 day) as far-from equilibrium condition, (iii) to evaluate the effect of long term leaching (9 days) as near-equilibrium condition, (iv) to couple with the geochemical model to identify possible speciation-solubility controlling phases and (v) to study the newly formed secondary phases as well as changes in slag surface morphology when subjected to weathering.

5.2. Material and Methods

5.2.1. Lead blast furnace (LBF) and imperial smelting furnace (ISF) slags

Lead blast furnace (LBF) and imperial smelting furnace (ISF) slags used in this study were obtained from lead and zinc smelters located in the industrial basin of Nord-Pas-de-Calais, northern France. Both slags are granulated wastes where the size distribution is log normal with a 500 μm dominant class and the particle size distribution varies from 100 μm to 5 mm

(Sobanska et al., 2000). However, the particle size distribution of both LBF and ISF used in this study varies from 100 μm to 2 mm with specific surface area of 0.08-0.09 $\text{m}^2 \text{g}^{-1}$. LBF is mainly composed of amorphous glass with CaO-FeO-SiO₂ as end members (80% in v/v), 19% of crystalline phases and 1% of metallic lead droplets whereas ISF contains higher volume of amorphous glassy part (84% in v/v), 5 % of crystalline phases, 10% of speiss and 1% of Pb droplets (Deneele, 2002). The global chemical compositions as well as the composition of amorphous glassy matrix for both LBF and ISF slags are given in Table 5.1.

Table 5.1. Chemical composition of global and glassy matrix in LBF and ISF slags.

%wt	Samples	SiO ₂	CaO	Fe ₂ O ₃	FeO	Al ₂ O ₃	MgO	MnO	ZnO	PbO
Global	LBF	24.88	22.14	8.11	23.27	2.46	2.71	0.81	10.77	3.74
	ISF	24.38	18.55	0.39	31.11	10.03	1.81	1.04	8.75	1.66
Glass	LBF	26.38	22.92	-	26.50	2.54	1.91	0.84	11.16	4.30
	ISF	25.68	21.40	-	24.97	9.98	1.80	0.84	8.27	0.22

Note: Global chemical composition obtained by acid digestion (HNO₃-HCl-HF) except for Si by XRF, whereas glassy part obtained by microprobe (Deneele, 2002)

Spinel is dominant part of crystalline phases which are well embedded and scattered across the glassy matrix of both LBF (19% in v/v) and ISF (5% in v/v). Magnesiochromite (MgCr₂O₄), franklinite (ZnFe₂O₄), magnetite (Fe²⁺Fe³⁺₂O₄) are dominant spinel phases found in LBF whereas zincochromite (ZnCr₂O₄), and gahnite (ZnAl₂O₄) are the ones found in ISF slags where their respective chemical composition are given in Table 5.2.

Table 5.2. Chemical composition of primary spinels in LBF and ISF slags.

Samples	Spinel (%wt)	SiO ₂	CaO	Fe ₂ O ₃	FeO	Al ₂ O ₃	MnO	MgO	ZnO	Cr ₂ O ₃
LBF	MgCr₂O₄	0.28	0.57	8.95	5.55	15.83	0.79	12.46	9.90	44.56
	ZnFe₂O₄	0.10	0.68	67.62	7.69	0.62	0.91	4.83	15.79	1.66
	Fe²⁺Fe³⁺₂O₄	0.05	0.13	45.45	17.29	7.60	0.74	1.99	12.72	13.59
ISF	ZnCr₂O₄	0.03	0.24	3.12	11.52	1.96	2.27	0.97	18.14	61.13
	ZnAl₂O₄	0.08	0.13	3.93	6.59	50.72	0.19	3.19	31.08	4.03

Note: Chemical composition obtained by microprobe analysis (Deneele, 2002)

In addition to spinel phases, some Fe rich speiss are found in ISF as well as some silicate phases such as hardystonite (Ca₂ZnSi₂O₇) and willemite (Zn₂SiO₄) are found in both ISF and LBF where detail chemical compositions are given in Table 5.3. Unlike Zn, Pb is mainly present as simple droplet form embedded in the glassy matrix of both slags.

Table 5.3. Chemical composition of silicates in LBF and ISF slags.

Silicates (% wt)	SiO ₂	CaO	FeO	Al ₂ O ₃	MgO	MnO	ZnO	PbO
Ca ₂ ZnSi ₂ O ₇	38.09	32.96	4.88	2.78	2.63	0.32	12.60	4.56
Zn ₂ SiO ₄	29.86	0.00	1.16	0.03	0.23	10.77	63.99	0.04

Note: Chemical composition obtained by microprobe analysis (Deneele, 2002)

5.2.2. pH dependent chemical weathering test

The chemical weathering of LBF and ISF slags as a function of pH was conducted according to CEN/TS 14997 (2006) with slight modifications. Two set of experiments under open air and nitrogen atmospheres were performed in duplicate at fixed pH values (4, 5.5, 7, 8.5 and 10) with different equilibration times (1 day and 9 days) in order to identify the effect of pHs, short and long equilibration times, as well as the effect of atmospheres. The experiments were performed in 0.1 M NaNO₃ electrolyte where the liquid to solid ratio (L/S) was maintained at 20, the temperature and mixing speed were set to 23 ± 2°C and 100 rpm, respectively. The pH was controlled by adding either HNO₃ or NaOH via a computer guided titration system (TitroLine® 6000). The leachate was periodically sampled, filtered through 0.20 µm polypropylene filters and prepared for further analysis. The short-term leaching under both atmospheres allowed to assess the far-from equilibrium leaching condition where dissolution kinetics are the main driven force behind the release of metals from the slag. On the other hand, the long-term leaching under both atmospheres allowed assessing the near-equilibrium leaching condition where precipitation of secondary phases occurs.

5.2.3. Leachate chemistry and geochemical modeling

The leachates were periodically sampled, filtered through 0.20 µm polypropylene filters and prepared for further analysis. The inductively coupled plasma optical emission spectrometry ICP-OES) (iCAP™ 6000 series) was used to determine the concentration of the following elements; Ca, Fe, Si, Zn and Pb. In parallel, thermodynamic model Visual MINTEQ v3.0 was used to assess the species distribution of all elements, to calculate the saturation indices of possible secondary precipitates and to give insight regarding the possible phases controlling the solubility of each element. The temperature was kept constant at 25°C, the oversaturated solids were not allowed to precipitate, and the CO₂ partial pressure was fixed at 396 ppmv.

5.2.4. Calculation of leaching behavior and rates

Q_{Ele} was calculated by normalizing to the specific area as well as initial amount of that element present in bulk slags, shown in Eq. (5.1).

$$Q_{Ele} = \left[\left\{ \frac{[Ele]}{AW} \right\} * \left(\frac{V}{W} \right) * \left(\frac{1}{SA} \right) \right]_{Leachate} / \left[\left\{ \frac{[Ele]}{AWM} \right\} * \left(\frac{1}{SA} \right) \right]_{Bulk\ slag} \quad \text{Eq. (5.1)}$$

Where Q_{Ele} is the normalized leaching concentration of element in $\text{mol}\cdot\text{m}^{-2}$, where $[Ele]$ is the leachate concentration in ppm or mg L^{-1} , AW is the standard atomic weight of the element, V is the total liquid volume of the reactor in 10^{-3} L (mL equivalent) whereas W is the solid weight of the bulk samples in g, SA is the specific surface area in $\text{m}^2\cdot\text{g}^{-1}$. By considering the effect of time, T in days, the leaching rate, $\log R_{Zn}$ can be calculated as follow:

$$\log R_{Ele} = \log \left[\left\{ \frac{[Ele]}{AW} \right\} * \left(\frac{V}{W} \right) * \left(\frac{1}{SA*T} \right) \right]_{Leachate} \quad \text{Eq. (5.2)}$$

The stoichiometry of the leachate can be calculated as follows:

$$Stoi_{Ele/Si} = Q_{norm\ Ele} / Q_{norm\ Si\ (leachate)} \quad \text{Eq. (5.3)}$$

Where $Stoi_{Ele/Si}$ is the stoichiometry ratio of normalized the element concentration to normalized Si concentration, where $Q_{norm\ Ele\ or\ Si}$ can be calculated by Eq. (5.1).

5.2.5. Solid phase characterization

X-ray Diffraction (XRD), Scanning Electron Microscopy (SEM) with Energy Dispersive X-Ray Analysis (EDS), and Transmission Electron Microscopy (TEM) analysis were used to characterize fresh and altered slags in order to give insights regarding the mechanisms of alteration, surface morphology of slags and the formation of secondary mineral phases. XRD analyses were performed at University of Paris-Diderot by using a Panalytical X'Pert Pro MPD diffractometer equipped with a multichannel X'celerator detector, and using $\text{CuK}_{\alpha 1.2}$ radiation from 5° to 80° 2-theta range at a rate of $0.13^\circ 2\theta/\text{min}$. SEM-EDS analysis was performed at University of Paris-Diderot using Philips XL 30 equipped with an energy dispersive X-ray spectrometer (EDX-PGT Ge-detector) operating at 20 kV beam voltage and $1.5\ \mu\text{A}$ beam current. Finally, TEM analysis was performed at University of Pierre et Marie Curie using Jeol 2100F electron microscope operating at 200 kV and equipped with a high-resolution UHR pole piece and a Gatan GIF 200 L imaging filter.

5.3. Results

5.3.1. Leaching behavior of LBF and ISF as a function of pH under open air atmosphere

Leaching of major elements (Ca, Fe, Si, Zn and Pb) from LBF and ISF slags can be observed as a function of pH as well as leaching time: short-term leaching (1 day) and long-term leaching (9 days). Figure 5.1 illustrates the different leaching patterns of major elements during pH-dependent leaching of LBF slag. All elements (Ca, Fe, Zn, Mg except Si and Pb) were found to be relatively dependent on the pH where highest concentrations can be found at pH 4 and a sharp decrease or lowest concentrations at higher pH values.

During short-term leaching, the highest concentrations observed at pH 4 were 7.5×10^{-3} M of Ca, 2.7×10^{-3} M of Fe, 4.9×10^{-4} M of Mg, 4.2×10^{-3} M of Si, 1.2×10^{-3} M of Pb, and 2.1×10^{-3} M of Zn whereas, the lowest concentrations observed at pH 10 were 1.1×10^{-4} M of Ca, 3.2×10^{-6} M of Mg, 7.1×10^{-5} M of Si, 2.5×10^{-6} M of Pb, and 5.9×10^{-7} M of Zn, per liter of

leachate respectively. During long-term leaching, the concentrations observed at pH 4 were 1.0×10^{-2} M of Ca, 4.0×10^{-3} M of Fe, 6.9×10^{-3} M of Mg, 3.4×10^{-3} M of Si, 4.4×10^{-4} M of Pb, and 3.0×10^{-3} M of Zn as well as those at pH 10 were 6.2×10^{-5} M of Ca, 7.7×10^{-6} M of Mg, 4.9×10^{-4} M of Si, 8.5×10^{-7} M of Pb, and 1.2×10^{-6} M of Zn per liter of leachate. The concentrations of all elements were higher after 9 days of leaching time compared to initial 1 day of leaching time except for Si at pH 4, whereas the concentration of all elements are lower after 9 days at pH 10.

Figure 5.2 shows the different leaching patterns of major elements during pH-dependent leaching of ISF slag. The highest concentrations were found at pH 4 for all elements whereas the leaching patterns were different for all elements at higher pH values. During short-term leaching, the highest concentrations observed at pH 4 were 2.8×10^{-3} M of Ca, 2.5×10^{-3} M of Fe, 1.8×10^{-4} M of Mg, 2.2×10^{-3} M of Si, 4.7×10^{-5} M of Pb, and 7.1×10^{-4} M of Zn whereas the lowest concentrations observed at pH 10 were 3.6×10^{-5} M of Ca, 1.1×10^{-6} M of Mg, 6.3×10^{-5} M of Si, 1.1×10^{-6} M of Pb and 2.0×10^{-7} M of Zn respectively. During long-term leaching, the concentrations observed at pH 4 were 9.0×10^{-3} M of Ca, 9.3×10^{-3} M of Fe, 6.2×10^{-4} M of Mg, 4.9×10^{-3} M of Si, 2.8×10^{-4} M of Pb, and 2.5×10^{-3} M of Zn as well as those at pH 10 were 4.5×10^{-5} M of Ca, 1.8×10^{-6} M of Mg, 5.4×10^{-4} M of Si, 1.5×10^{-5} M of Pb, and 9.1×10^{-7} M of Zn. The concentrations of all elements (Ca, Fe, Si, Zn and Pb) increased in double after 9 days compared to 1 day of leaching time both at pH 4 and 10.

Fe was not detected at neutral and alkaline pH (7, 8.5 and 10). The highest concentration of Si can be observed at pH 4 and 10 whereas the lowest at neutral pH 7. Leaching of Pb was pH independent and the concentrations were rather fluctuated from neutral to alkaline pH. In contrary, Zn was found to be relatively dependent of the pH except at pH 8.5 and 10 where the concentrations were within the same range of magnitude.

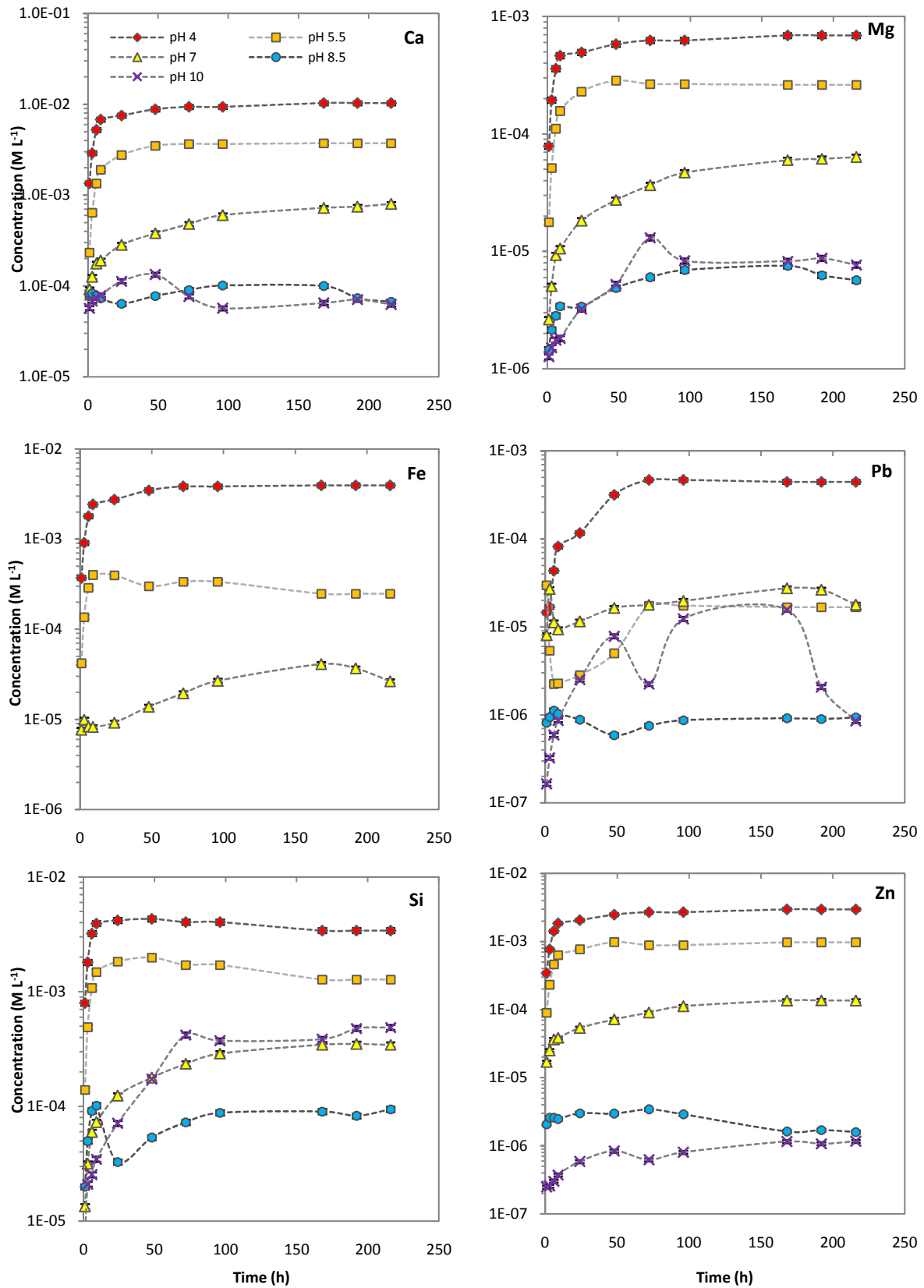


Figure 5.1. Leaching of Ca, Fe, Mg, Si, Pb and Zn as a function of pH under open air atmosphere (LBF).

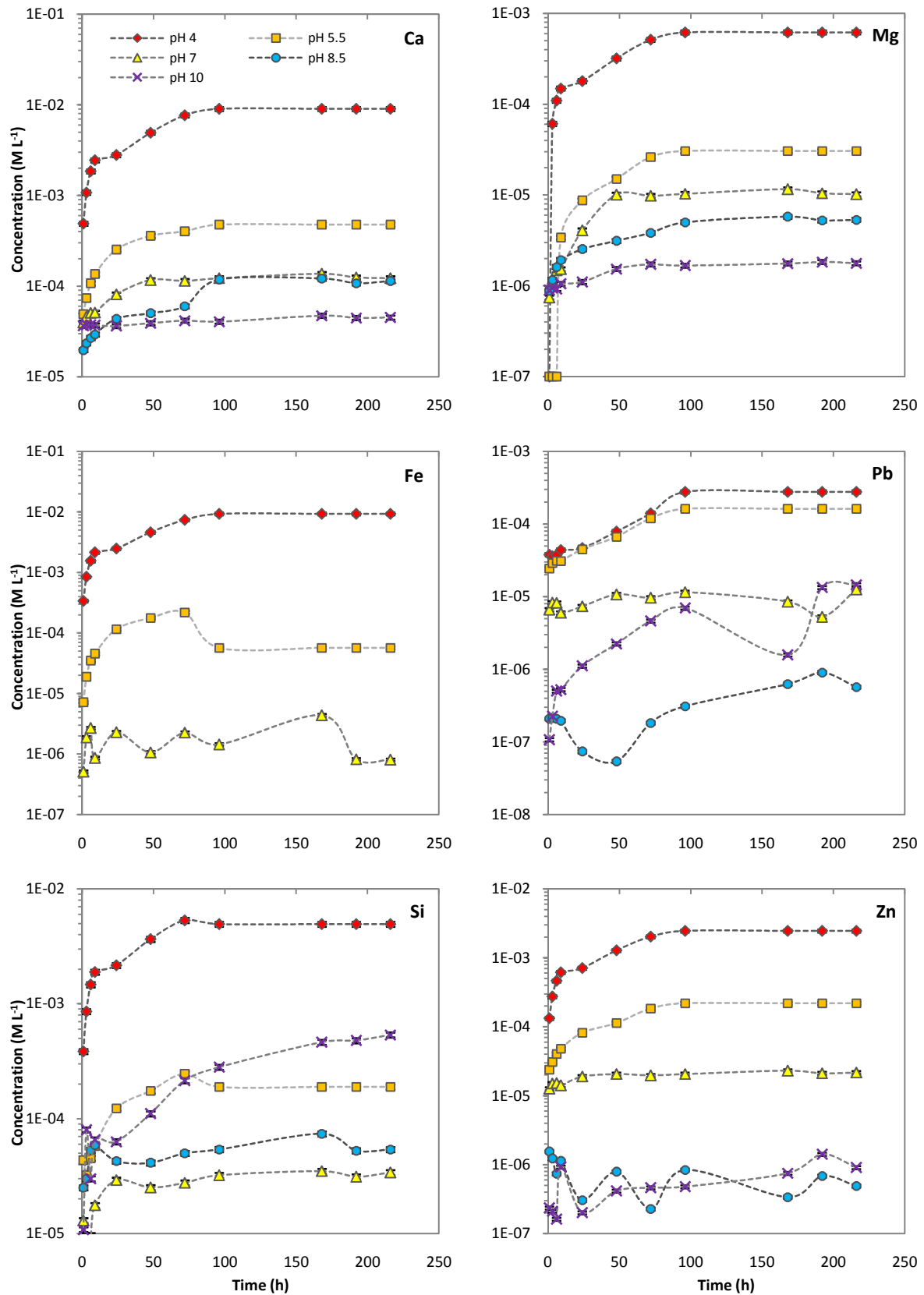


Figure 5.2. Leaching of Ca, Fe, Si, Pb and Zn as a function of pH under open air atmosphere (ISF).

5.3.2. Initial leaching rates of LBF and ISF as a function of pH under open air atmosphere

The initial leaching rates of all elements during the first 24 hrs of leaching from both LBF and ISF slags were given in Table 5.4, where the highest leaching rates were observed at pH 4 and the lowest at pH 10. The highest dissolution rates of Ca, Mg, Pb and Zn can be observed at pH 4, whereas the lowest rates can be seen at pH 10 for both LBF and ISF slags. On the other hand, the dissolution rate of Si is higher at both pH 4 and 10, where the lowest rate can be seen at pH 7. The rates of Fe cannot be calculated at pH 8.5 and 10 as its dissolved concentration is below the detection limit of ICP-OES.

Table 5.4. Log dissolution rates of Ca, Fe, Mg, Si, Pb and Zn from LBF and ISF slags as a function of pH under open air atmosphere.

pH	Log dissolution rate of LBF (mol.m ⁻² s ⁻¹)						Log dissolution rate of ISF (mol.m ⁻² s ⁻¹)					
	Ca	Fe	Mg	Pb	Si	Zn	Ca	Fe	Mg	Pb	Si	Zn
4	-7.66	-8.10	-8.85	-9.47	-7.92	-8.22	-7.90	-7.93	-9.08	-9.69	-8.03	-8.48
5.5	-8.10	-8.94	-9.18	-11.09	-8.28	-8.65	-9.17	-9.51	-10.63	-9.92	-9.48	-9.65
7	-9.09	-10.57	-10.28	-10.48	-9.44	-9.81	-9.68	-11.23	-10.98	-10.72	-10.12	-10.31
8.5	-9.73		-11.01	-11.60	-10.02	-11.06	-9.95		-11.19	-12.72	-9.96	-12.10
10	-9.49		-11.03	-11.14	-9.69	-11.77	-10.03		-11.55	-11.54	-9.79	-12.29

*Specific leaching rate of Fe cannot be calculated as it is below detection limit of ICP-OES.

5.3.3. Effect of atmospheres on long-term leaching (9 days) of LBF and ISF as a function of pH

Figure 5.3 shows the concentration of major elements under open air and nitrogen atmospheres during long-term leaching of LBF slag. The concentration of Ca between two atmospheres showed no significant difference except a slight increase of Ca concentration under nitrogen atmosphere at pH 4. On the other hand, the concentrations of Fe under nitrogen atmosphere were found to be 5 times higher 5.5, and 10 times higher at pH 7. Concentration of Mg under nitrogen atmosphere was slightly higher at pH 4 and 5.5 whereas that under open air atmosphere was higher at pH 8.5 and 10. The oxidation weathering enhanced the leachability of Si at pH 8.5 and 10 where the concentration of Si under open air atmosphere was 5 times higher at pH 8.5 and 10 times higher at pH 10. The concentration of Pb under open air atmosphere was higher at pH 4 and 5.5 whereas that under nitrogen atmospheres was higher at neutral to alkaline pH. Meanwhile, Zn concentration under nitrogen atmosphere is 1.5 times higher at pH 4, 7 and 10.

Figure 5.4 shows the concentration of major elements under open air and nitrogen atmospheres during long-term leaching of ISF slag. Ca concentration under nitrogen atmosphere was 2 to 3 times higher at pH 5.5, 7 where as no significant difference existed at pH 4, 8.5 and 10. Both Fe and Mg concentrations under nitrogen atmosphere were significantly higher at all pH whereas Fe was under the detection limit under open air atmosphere at pH 8.5 and 10. The concentrations of Si under nitrogen atmosphere were higher at pH 4, 5.5, and 7 whereas those under open air atmosphere were higher at pH 8.5 and 10. Unlike other elements, the concentrations of Pb were fluctuating and did not reflect both atmospheres and pH. Similarly, the concentrations of Zn were found to be higher at all pH under nitrogen atmosphere compared to those under open air atmosphere.

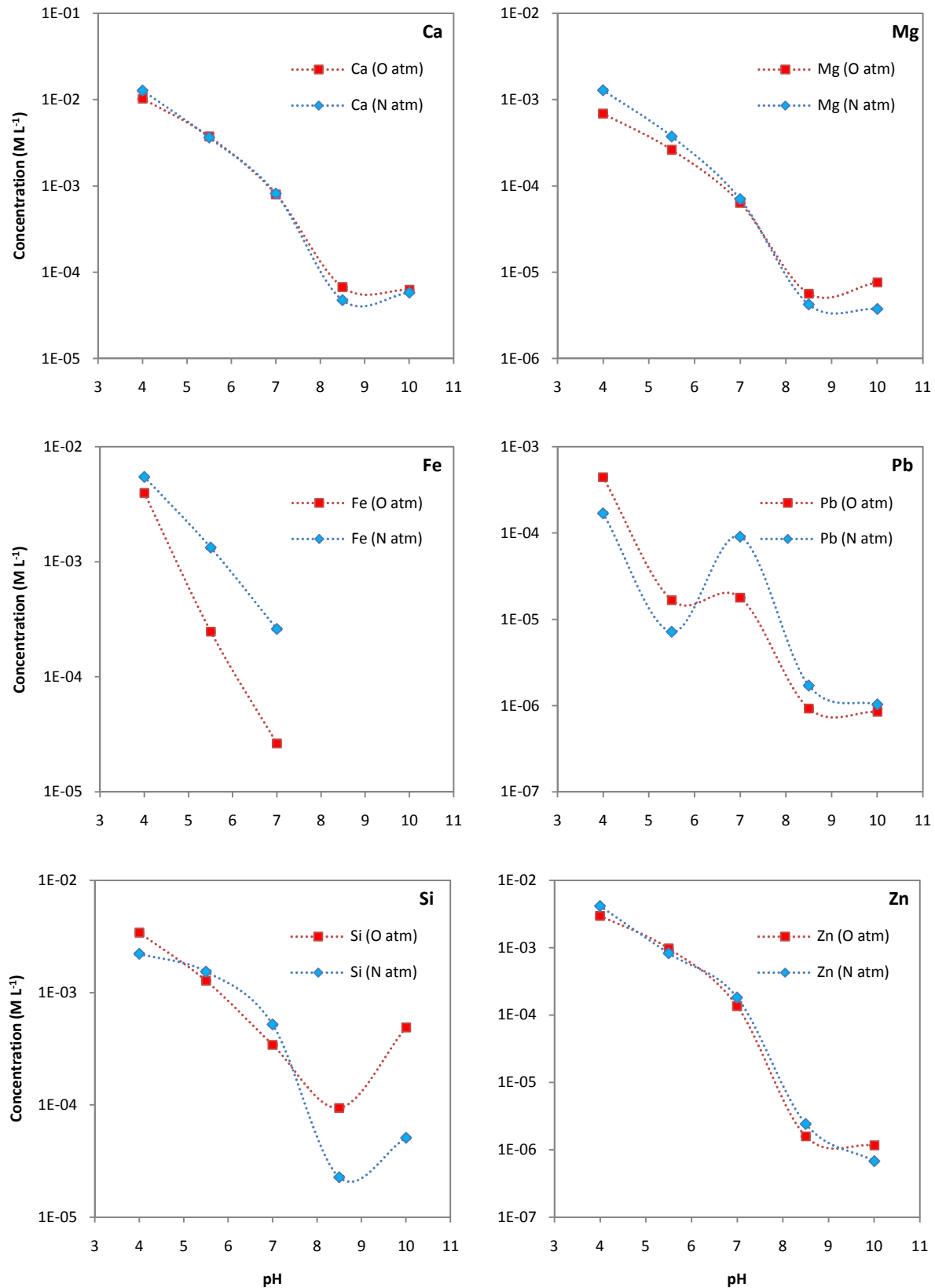


Figure 5.3. Leaching of Ca, Fe, Mg, Si, Pb and Zn from LBF slag as a function of pH under open air and nitrogen atmospheres.

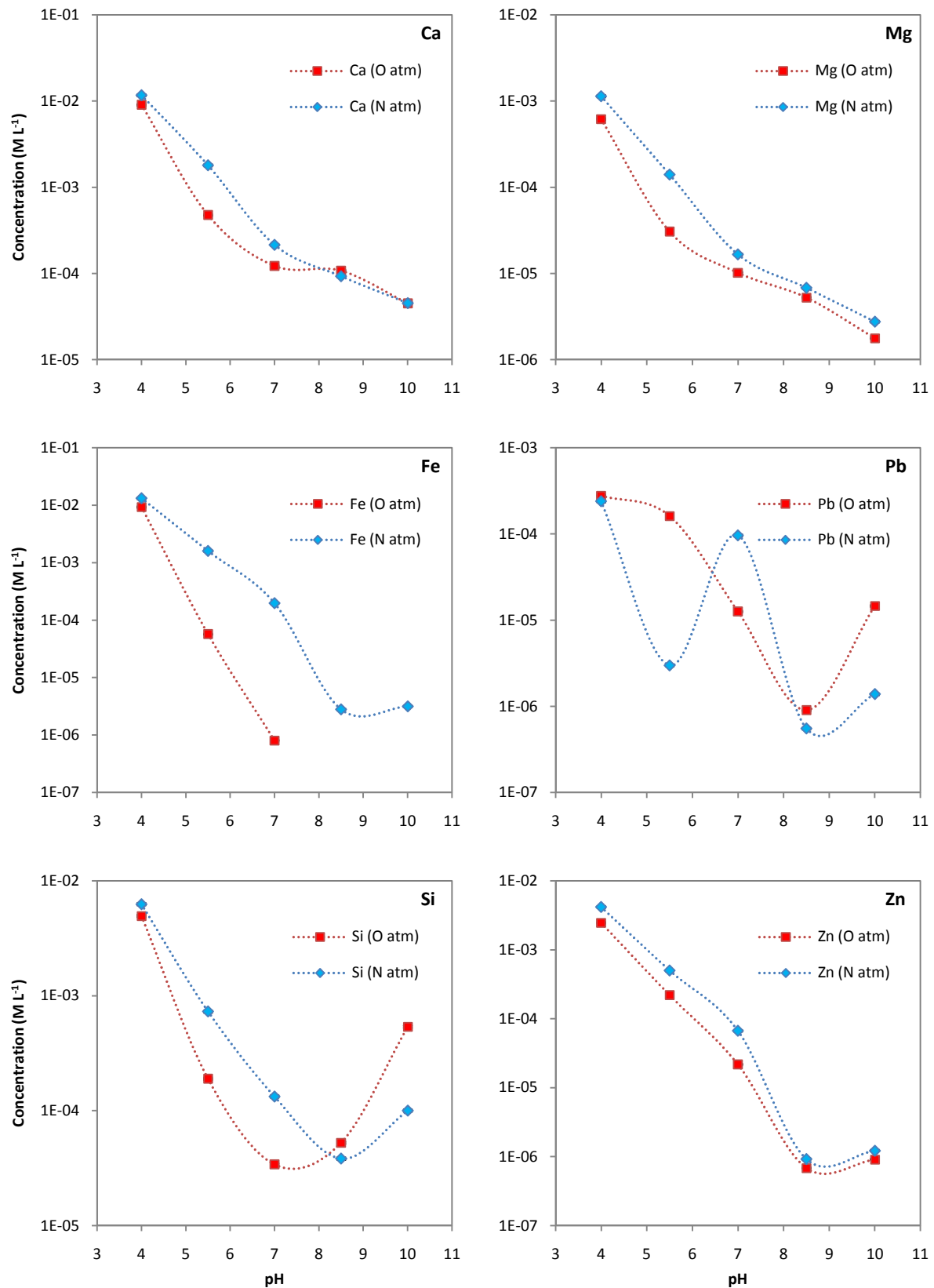


Figure 5.4. Leaching of Ca, Fe, Mg, Si, Pb and Zn from ISF slag as a function of pH under open air and nitrogen atmospheres.

5.3.4. Thermodynamic modeling

Table 5.5 gives the species distribution and the solubility controlling phases of all major elements during LBF weathering under open air atmosphere. High saturation indices at pH 4, 5.5 and 7 showed that ferrihydrite, goethite and hematite are the possible solubility controlling phases of Fe. It was not possible to calculate the SI indices for pH 8.5 and 10 as Fe concentration was under detection limit of ICP-OES. The solubility of Si was controlled by amorphous silica-gel at pH 4, 5.5 and 7 (SI indices: 0.25, -0.18 and -0.74) and by quartz at pH 7, 8.5 and 10 (SI indices: 0.55, -0.04 and 0.23). Meanwhile, Pb solubility was controlled by cerussite at pH 5.5 to 8.5 (SI indices: 0.56, 0.40 and 0.51), and plattnerite at pH 7 and 8.5 (SI indices: 0.36 and 0.46), respectively. In addition, Pb solubility at pH 10 was controlled by cerussite and plattnerite (SI indices: -0.43 and -0.58) where the precipitation of these phases may occur after 7 days. Zn was controlled by zincite at pH 8.5 and 10 (SI indices: -0.81 and -0.56), by layer-double hydroxide at pH 7 (SI index: -0.62), whereas by smithsonite at pH 7 and 8.5 (SI indices: -0.92 and -0.23). Ca was controlled by calcite at pH 8.5 and 10 (SI indices: -0.63 and -0.30).

Table 5.5. Saturation indices (SI) of solubility controlling phases of major elements (LBF slag).

Elements	LBF under O ₂ atm		after 9 days				
	Mineral phases	Formula	pH 4	pH 5.5	pH 7	pH 8.5	pH 10
Fe	Ferrihydrite	FeO(OH)	3.517	4.327	4.867	-	-
	Goethite	FeO(OH)	6.226	7.036	7.576	-	-
	Hematite	Fe ₂ O ₃	7.049	8.668	9.748	-	-
Si	SiO ₂ (am,gel)	SiO ₂	0.252	-0.175	-0.744	-	-
	Quartz		-	-	0.546	-0.041	0.233
Pb	Cerussite	PbCO ₃	-	0.561	0.404	0.506	-0.429*
	Plattnerite	PbO ₂	-	-	0.356	0.459	-0.581*
Zn	Zincite	ZnO	-	-	-	-0.814	-0.562
	Zn-Al LDH(s)		-	-	-0.617	-	-
	Smithsonite	ZnCO ₃	-	-	-0.916	-0.231	-
Ca	Calcite	CaCO ₃	-	-	-	-0.635	-0.301

Note: * refers to SI indices at 7 days, suggesting that the precipitations of such phases can take place earlier than 9 days.

Table 5.6 gives the species distribution and the solubility controlling phases of all major elements during ISF weathering under open air atmosphere. The oversaturation of Fe led to the precipitation of hematite at pH 4 and 5.5 (SI index: 0.0). The solubility of Si was controlled by chalcedony at pH 5.5, 7, 8.5 and 10 (SI indices: -0.45, -0.91, -0.74 and -0.18), whereas by quartz at pH 7, 8.5 and 10 (SI indices: -0.46, -0.94 and -0.38). On the other hand, Pb was equally controlled by three phases: cerussite at pH 7, 8.5 and 10 (SI indices: 0.25, 0.51 and -0.46), hydrocerussite at pH 10 (SI index: -0.67) and plattnerite at pH 7, 8.5 and 10 (SI indices: 0.21, 0.46 and -0.51). Zn was controlled by smithsonite at pH 8.5 (SI index: -0.63). In addition, Zn solubility at pH 8.5 and 10 was controlled by zincite (SI indices: -0.82 and 0.85) where its precipitation may occur after 7 days. Meanwhile, the solubility of Ca was controlled by calcite at pH 8.5 and 10 (SI indices: -0.43 and 0.89).

Table 5.6. Saturation indices (SI) of solubility controlling phases of major elements (ISF slag).

Elements	ISF under O ₂ atm		after 9 days				
	Mineral phases	Formula	pH 4	pH 5.5	pH 7	pH 8.5	pH 10
Fe	Hematite	Fe ₂ O ₃	0	0	-	-	-
Si	Chalcedony	SiO ₂	-	-0.450	-0.908	-0.744	-0.175
	Quartz		0	0	-0.458	-0.944	-0.375
Pb	Cerussite	PbCO ₃	-	-	0.252	0.506	-0.458
	Hydrocerussite	PbCO ₃ .H ₂ O	-	-	-	-	-0.668
	Plattnerite	PbO ₂	-	-	0.205	0.459	-0.506
Zn	Zincite	ZnO	-	-	-	-0.819*	0.849*
	Smithsonite	ZnCO ₃	-	-	-	-0.629	-
Ca	Calcite	CaCO ₃	-	-	-	-0.431	0.891

Note: * refers to SI indices at 7 days, suggesting that the precipitations of such phases can take place earlier than 9 days.

5.3.5. Solid phase characterization of post-weathered LBF and ISF slags

5.3.5.1. Scanning electron microscope (SEM) analysis

The changes in surface morphology as well as the layer of secondary precipitates onto weathered LBF and ISF slags were observed by SEM (Figures 5.5 and 5.6). Many white, thin, long and needle-like structures; several darker grey, big, flat flocs; as well as lighter grey, single fat phases formed during the weathering of LBF slags and precipitated back onto the surface (Figure 5.5A). Many light grey snowflakes-like structures sprawling on the surface were mainly dendritic Zn substituted wüstite which are embedded in the glassy matrix of the

slag (Figure 5.5B). Further EDS analysis showed that the secondary phases mainly consist of oxide and carbonates of Fe, Zn, Ca and Pb (Figure 5.5C). Point #1 corresponds to the one of the darker grey, big, flat floccs observed in Figure 5.5A, where the atomic composition represents oxide and carbonate of Fe (61%) and Zn (10%) with traces of Pb (2%). Point #2 corresponds to white, thin, long and needle-like structures which contain oxide and carbonate of Fe (36%), Ca (23%), Zn (13%) and Pb (4%). Finally, point #3 corresponds to single fat phase which are oxides of Fe (41%), Ca (21%), Zn (13%) and Pb (8%).

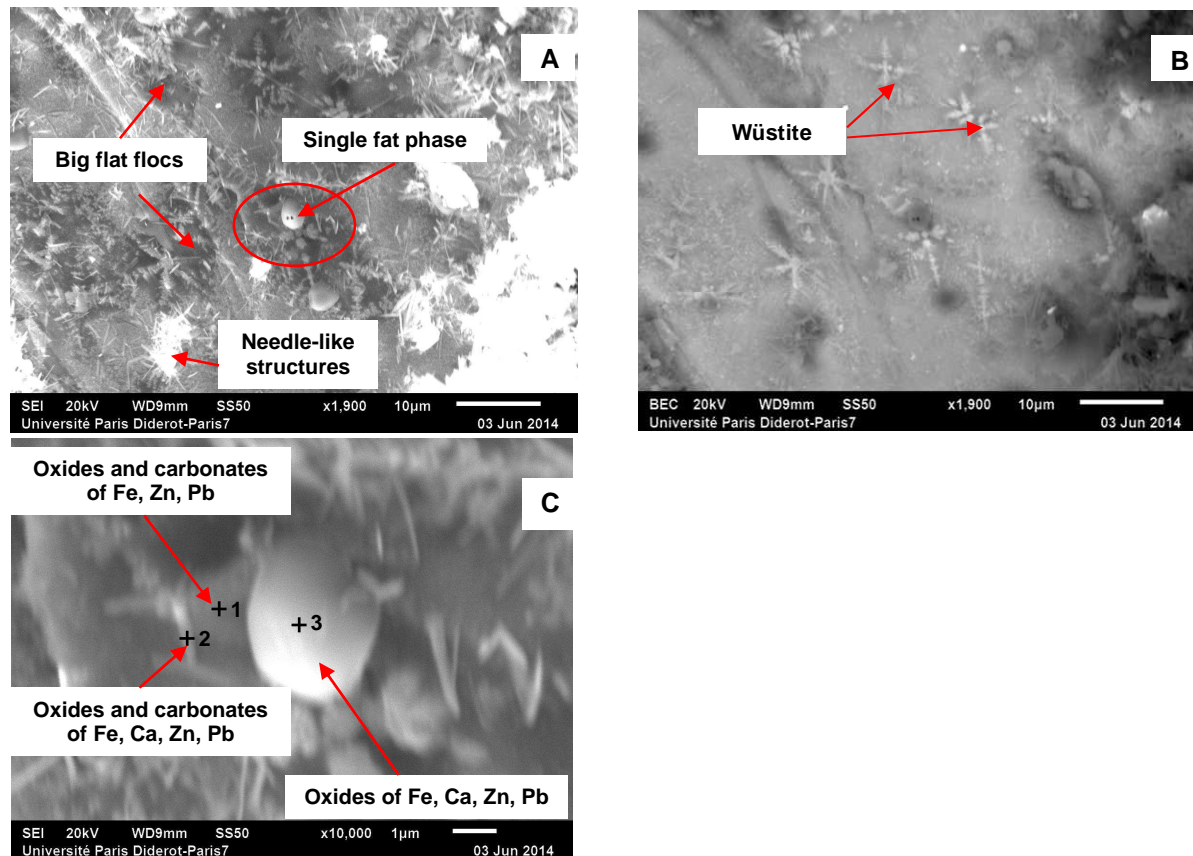


Figure 5.5. Surface morphology and secondary phases onto weathered LBF slags open air (A) secondary electron imaging (SEI) mode on surface morphology, (B) backscattered electron imaging (BEI) mode on surface morphology, and (C) precipitation of secondary phases (oxides and carbonates of Fe, Ca, Zn, and Pb) as observed by SEM.

Several tiny metallic Pb droplets (2-4 nm); many white fluffy floccs; as well as white, thin, long and needle-like structures were observed on the surface of weathered ISF slag (Figure 5.6A). In addition tiny Pb droplets, some huge Pb balls (~5 M) were clearly visible where secondary white fluffy floccs were accommodated (Figure 5.6B). Oxides and carbonates of Fe, Zn, Ca and Pb were the dominant secondary phases formed during weathering of ISF (Figure 6C). Point #1 corresponds to thin layer of Zn carbonates on the Pb metallic droplet whereas point #2 corresponds to white fluffy floccs which contain oxide and carbonate of Fe (44%), Ca (1.7%), Zn (18%) and Pb (4%). Finally, point #3 corresponds to needle-like structures which are oxides and carbonates of Fe (54%), Ca (2.9%), Zn (14%) and Pb (5%) in atom percent.

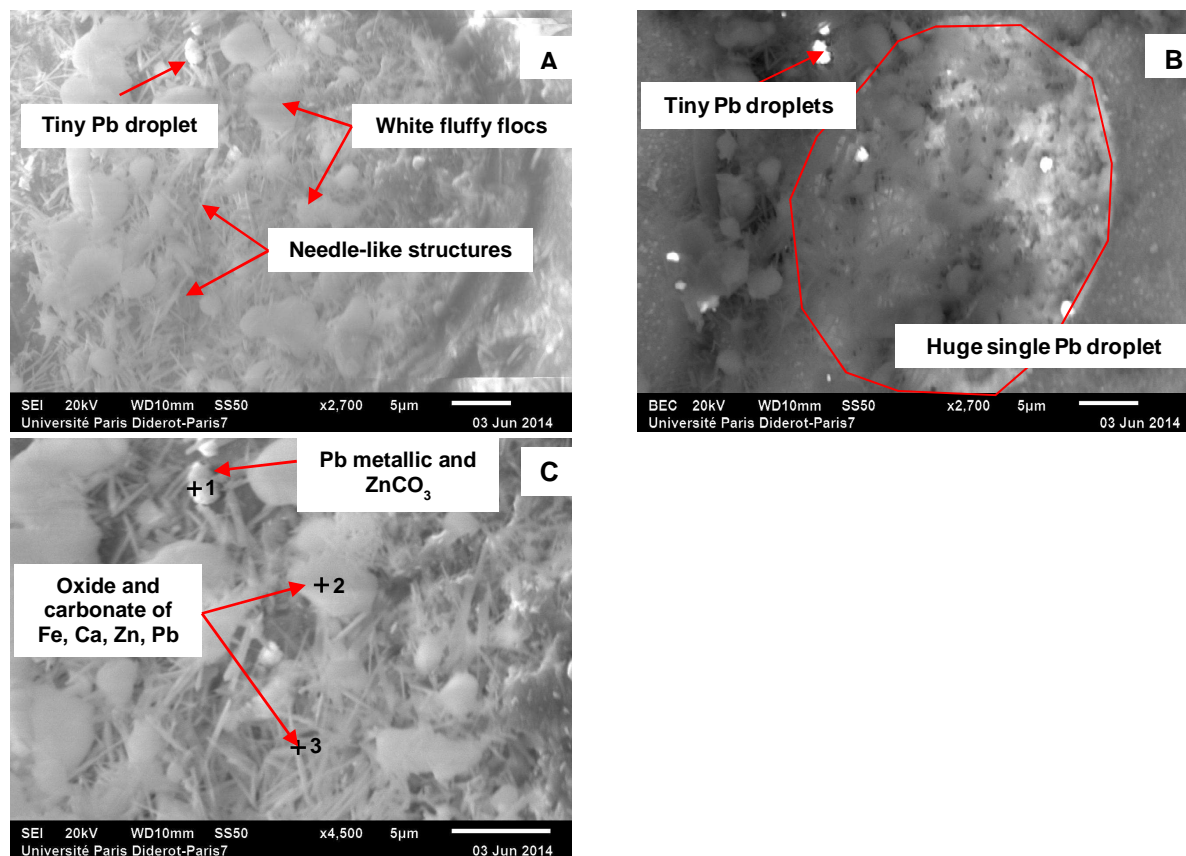


Figure 5.6. Surface morphology and secondary phases onto weathered ISF slags (A) secondary electron imaging (SEI) mode on surface morphology, (B) backscattered electron imaging (BEI) mode on surface morphology, and (C) precipitation of secondary phases (oxides and carbonates of Fe, Zn, and Pb) as observed by SEM.

5.3.5.2. Transmission electron microscopy (TEM) analysis

A mixture of Ca, Pb and Zn carbonates are the major secondary precipitates observed after 9 days of leaching LBF slags (Figures 5.7A, B, C and D). These carbonate phases consist of 73% of Ca, 17% of Pb and 6.7% of Zn (atm %) (Figure 5.7A) and 90% of Ca, 8% of Pb, 1.3% of Fe and 0.8% of Zn (Figure 5.7C). In addition, a Pb metallic ball, ~20 nm in size as well as traces of Si around the carbonates was observed (Figure 5.7A). Not only nearly-well crystallized but also amorphous carbonates were observed (Figure 5.7C) where their sizes range from 10 to 100 nm. The X-ray diffraction analysis of the well-crystallized part of carbonates indicated the calcite as the possible carbonate mineral (Figures 5.7B and D).

On the other hand, not only a mixture of Ca, Pb and Zn carbonates but also some aluminosilicates were observed after 9 days leaching of ISF slags (Figures 5.8A, B, C and D). A thin layer of carbonates mainly enriched in Ca (80-90%) along with the presence of Pb (10-18%) and Zn (1-2%) were deposited on the weathered surface of ISF slags (Figures 5.8A and B). The aluminosilicates phases were rather crystallized, 5 to 25 nm large in size and the X-ray diffraction analysis suggested kaolinite as the possible mineral phase (Figures 5.8C and D).

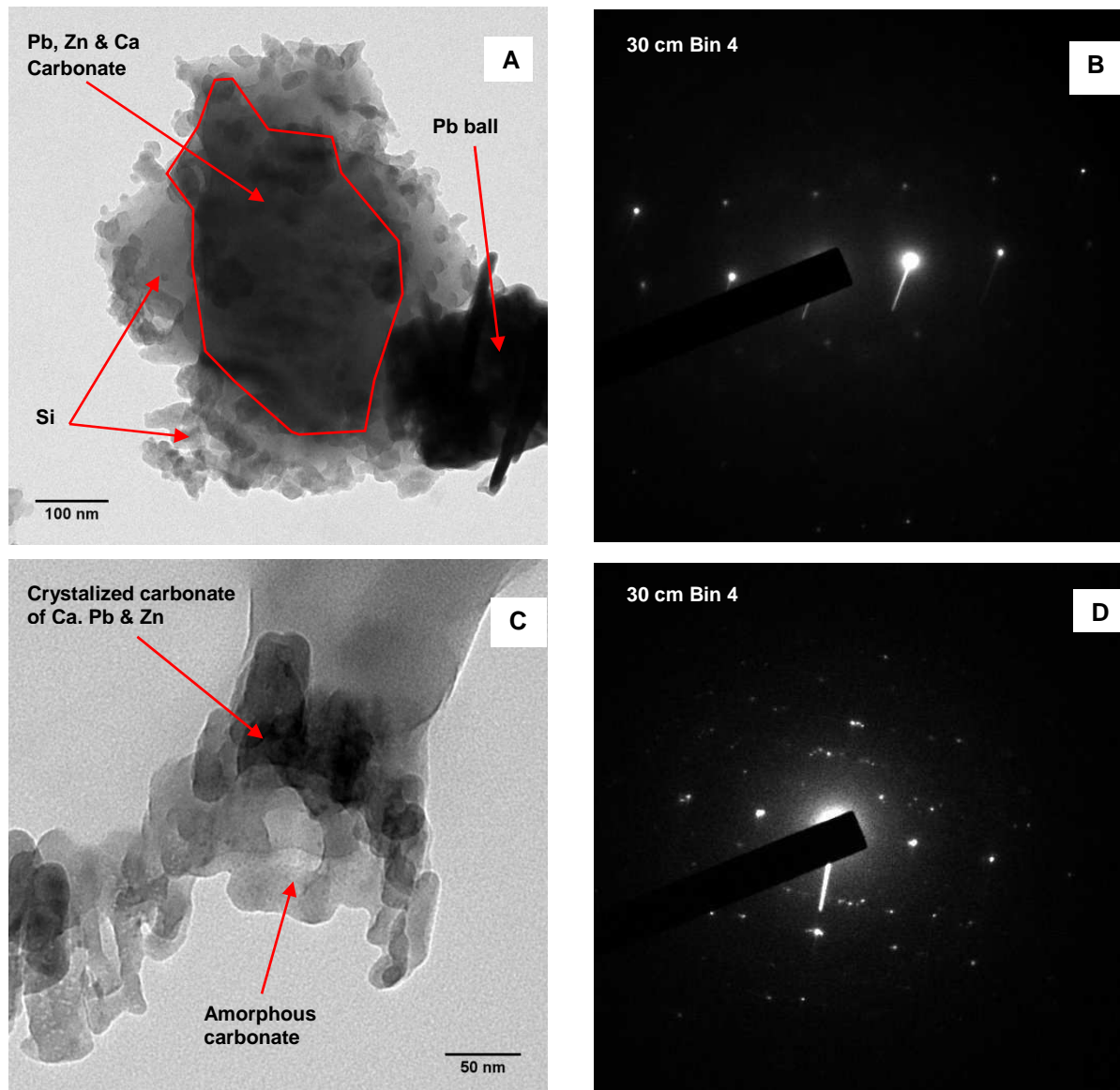


Figure 5.7. Precipitation of secondary phases during weathering of LBF slags open air (A) Ca, Pb and Zn carbonates along with metallic Pb ball and traces of Si and (B) its diffraction pattern of carbonates, (C) more crystallized Ca, Pb and Zn carbonates along with amorphous carbonates and (D) its diffraction pattern on crystallized carbonates (calcite mineral) as observed by TEM.

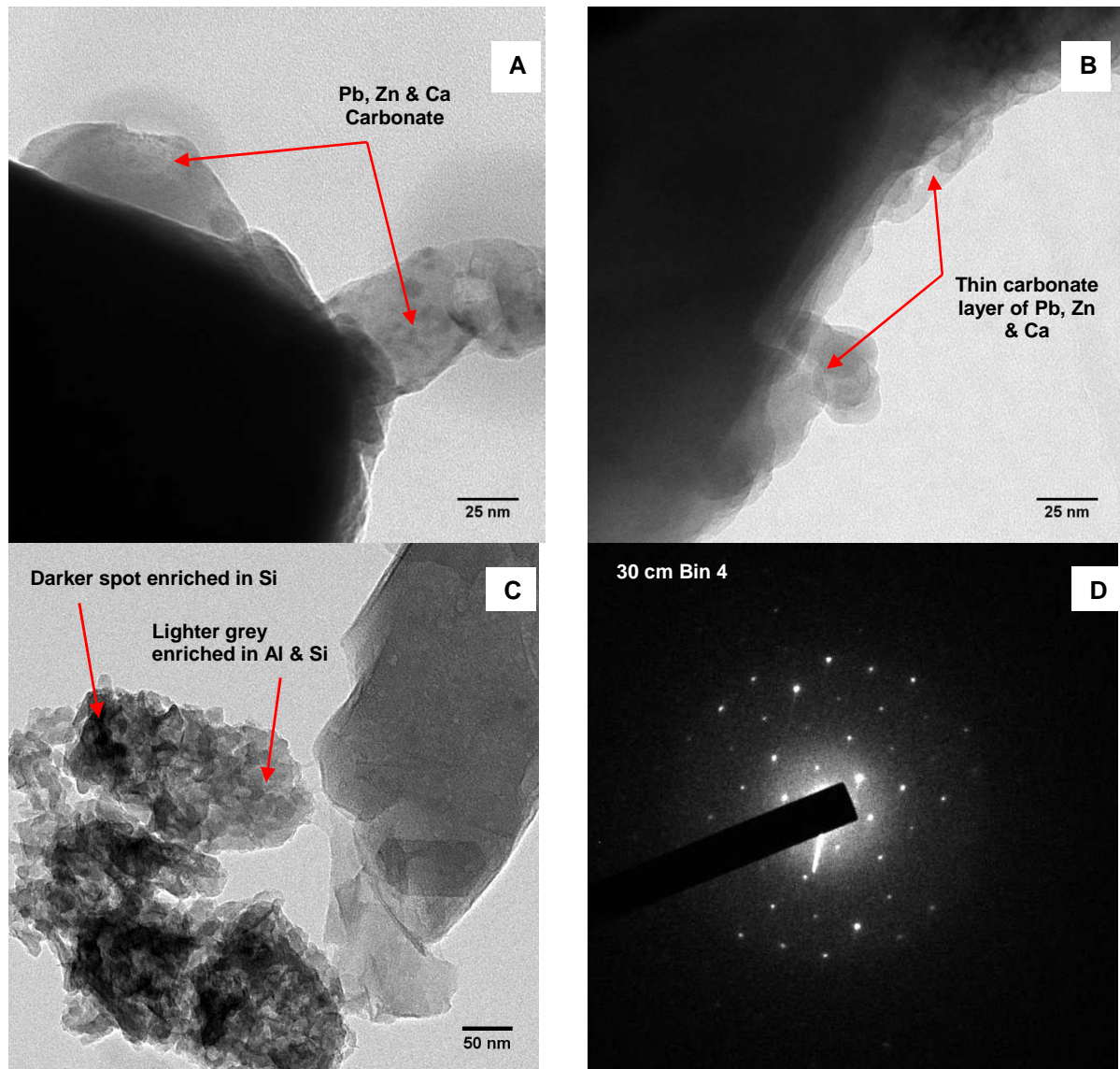


Figure 5.8. Precipitation of secondary phases during weathering of ISF slags open air (A and B) Ca, Pb and Zn carbonates, (C) alumino-silicates phase and (D) its diffraction pattern (kaolinite) as observed by TEM.

5.4. Discussion

5.4.1. Far-from equilibrium leaching condition

5.4.1.1. Dissolution kinetics of both slags

During far-from equilibrium leaching condition under open air atmosphere, the release of elements from both LBF and ISF slags are controlled by dissolution kinetics and the primary mineral phases present in each slag. The leaching rates of Ca, Si and Zn from LBF slags are 2 times faster than those from ISF slags at pH 4, suggesting that LBF slags are prone to weathering under acidic conditions where leaching of two major-matrix elements Ca and Si consequently enhanced the leaching of Zn embedded in the matrix of LBF slags. Similarly,

the leaching rates of Ca, Fe and Si are 2-3 times faster than those of ISF slags which led to the leaching of Zn from LBF slags 2 times faster than that from ISF slags. In contrast, the leaching rates of Si from ISF slags is 2 times faster than that from LBF slags, suggesting that ISF slags are more prone to weathering under alkaline conditions. Unlike Zn, the leaching rates of Pb from LBF is 2.5 time faster at pH 4 and 1.5 times at pH 7 compared to that from ISF slag, whereas it has the same leaching kinetics at pH 10.

5.4.1.2. Stoichiometric or non-stoichiometric leaching

During the leaching of LBF and ISF slags, if the molar ratios of elements in the leachate are equal to those in the un-weathered slags, such kind of leaching can be called as stoichiometric dissolution (Brantley et al., 2008b). The number of molar ratios of major elements in leachate after 24 h of slag-water interaction time was compared to the initial molar ratios of un-weathered slags (Table 5.7). The initial molar ratios of major elements to Si of LBF and ISF slags are 0.85-1.0 for Ca/Si, ~1.1 for Fe/Si, ~ 0.08-0.12 for Mg/Si, ~0.04 for Pb/Si and ~0.3 for Zn/Si, respectively.

During dissolution of LBF slags, preferential leaching of Ca and Mg can be observed at all pHs for both atmospheres. Similarly, preferential leaching of Pb occurs at all pHs except at pH 5.5 under open-air atmosphere and at pH 4 under nitrogen atmosphere. Congruent dissolution between Zn and Si can be expected at pH 5.5 and 7 under open air atmosphere as well as at pH 7 under nitrogen atmosphere where Zn/Si ratios are from 1.09 to 1.20 for LBF slags.

During dissolution of ISF slags, a similar preferential leaching of Ca and Mg can be observed at all pHs for both atmospheres except for Ca at pH 10 under open air atmosphere. Due to the higher contribution of Pb droplets in ISF (68%) compared to that in LBF (24%), the preferential leaching of Pb was enormous at pH 5.5 and 7 under open air atmosphere and at pH 7 and 8.5 under nitrogen atmosphere for ISF slags. In addition, preferential leaching of Zn was observed at acidic to neutral pH for both atmospheres.

Table 5.7. Normalized stoichiometric ratios of leachate and bulk slags as a function of pH and, under different atmospheres

LBF (Open air atm)						LBF (Nitrogen atm)					
Q _{norm}	Ca/Si	Fe/Si	Mg/Si	Pb/Si	Zn/Si	Q _{norm}	Ca/Si	Fe/Si	Mg/Si	Pb/Si	Zn/Si
LBF	0.97	1.12	0.12	0.04	0.36	LBF	0.97	1.12	0.12	0.04	0.36
pH 4	1.84	0.59	0.98	0.67	1.36	pH 4	3.01	0.77	2.96	0.03	1.23
pH 5.5	1.55	0.19	1.04	0.04	1.16	pH 5.5	1.66	0.44	1.21	1.06	1.13
pH 7	2.36	0.07	1.23	2.25	1.20	pH 7	1.38	0.54	0.91	4.80	1.09
pH 8.5	2.01	0.00	0.86	0.65	0.25	pH 8.5	2.71	6.91	0.93	3.10	0.74
pH 10	1.63	0.00	0.38	0.86	0.02	pH 10	5.94	0.01	1.18	2.57	0.20

ISF (Open air atm)						ISF (Nitrogen atm)					
Q _{norm}	Ca/Si	Fe/Si	Mg/Si	Pb/Si	Zn/Si	Q _{norm}	Ca/Si	Fe/Si	Mg/Si	Pb/Si	Zn/Si
ISF	0.85	1.18	0.08	0.02	0.31	ISF	0.85	1.18	0.08	0.02	0.31
pH 4	1.58	1.06	1.03	0.99	1.13	pH 4	1.73	1.39	1.76	0.91	1.53
pH 5.5	2.40	0.80	0.83	16.77	2.16	pH 5.5	2.04	1.21	1.60	1.08	1.35
pH 7	3.24	0.07	1.65	11.56	2.10	pH 7	3.65	1.36	1.59	98.01	3.77
pH 8.5	1.19	0.00	0.70	0.08	0.02	pH 8.5	4.83	0.52	1.93	11.83	1.02
pH 10	0.67	0.00	0.21	0.81	0.01	pH 10	1.54	0.12	0.52	1.10	0.20

5.4.1.3. Dissolution of primary mineral phases

Reflecting the nature of both LBF and ISF slags, the dissolution of primary crystalline phases and glassy phases controlled the major elements leached out from the slags. In general, silicates and spinel phases are well-known for being resistant to weathering whereas amorphous glassy phases are prone to release metals into the solution. In order to extrapolate tracing of the dissolution of primary phases from both slags, the stoichiometric ratios of major elements in the leachate were calculated and compared to those of primary mineral phases. Figure 5.9 shows the stoichiometry of both LBF and ISF calculated from the concentration data after 24 h and under nitrogen atmospheres where there is no formation of secondary precipitates.

The dissolution of spinel such as magnesiochromite and gahnite can be expected at acidic pH of 4 and 5.5 for both slags, whereas spinels phases such as zincochromite, magnetite, and

franklinite can be resistant to weathering even at acidic pH within the given time frame of dissolution periods. Meanwhile, the stoichiometry of the leachate at pH 7 were much closer to that of amorphous glassy part of slags, thus, leachate chemistry at pH 7 can be contributed and controlled by the dissolution of amorphous glassy part of the slags at neutral pH 7 (Figure 5.9). In addition, the stoichiometry of leachate at pH 8.5 for LBF slag were within the range of that of magnetite, thus, the leachate chemistry can be influenced by the partial dissolution of magnetite pH 8.5 for LBF slags.

The dissolution of melilite mineral groups such as hardystonite can be expected at pH 10 for ISF slags as the stoichiometry of leachate fell closer range to that of hardystonite which is in agreement with the study of Kierczak stating that melilite are prone to weathering at alkaline conditions whereas quite resistant to weathering under neutral conditions (Kierczak et al., 2009). In contrast to this study, a significant dissolution of melilite was observed at acidic pH 2 (Kucha et al., 1996). On the other hand, the stoichiometry of leachate for both LBF and ISF slags are far away from that of willemite, suggesting that willemite phases can be rather stable and is not prone to pH changes and weathering.

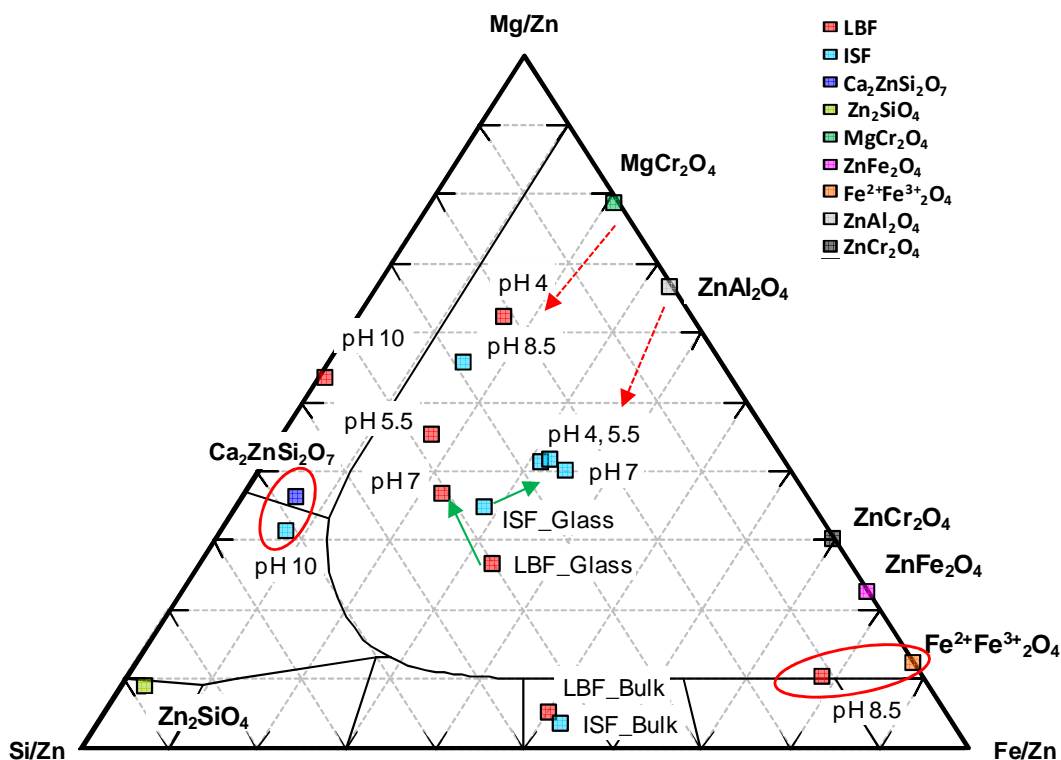


Figure 5.9. Extrapolation of the dissolution of primary phases from slags after weathering of LBF and ISF slags for 24 h under nitrogen atmosphere.

5.4.2. Near-equilibrium leaching condition

During near-equilibrium leaching conditions under open air atmosphere, the release of the elements from both slags are still contributed by the dissolution of primary mineral phases

and glassy matrix, however, the dissolved elements concentrations is further controlled by the new secondary phases formed from prolonged slag-water interaction time. The newly formed secondary phases can control the solubility of the dissolved elements in the leachate. During this stage, incongruent dissolution takes place where the formation of alteration layer with secondary phases consequently controls the fluid diffusion between slag and water, thus, controlling the overall slag dissolution. This phenomenon was extensively studied in the dissolution of medieval glasses and Celia's simple glass (Lombardo et al., 2013; Strachan and Neeway, 2014)

5.4.2.1. Newly formed secondary phases

During LBF weathering, ferrihydrite can be the dominant mineral phase controlling Fe solubility as the transformation rates are 5.7×10^{-9} at acidic pHs and 2×10^{-8} (s^{-1}) at neutral pH 7 at 25°C (Soumya et al., 2011) compared to formation rate constant of goethite is 4×10^{-5} (s^{-1}) at pH 7 (Yee et al., 2006).

Carbonates are the dominant secondary phases during LBF weathering whereas both carbonates and alumino-silicates are formed during ISF weathering. The carbonates formed on weathered LBF slags can be rather large in size (10-100 nm) compared to those formed on weathered ISF slags (1-5 nm) whereas the kaolinite formed ranges 5-25 nm in size. In addition, the chemical composition of carbonate phases observed can be different; 70-90% Ca along with 8 to 18% of Pb, 0.6 to 7% of Zn and 0-1.3% of Fe.

Formation of cerussite phases along with $ZnCO_3$ were also observed during weathering of LBF slag in ultra-pure water medium (Yin et al., 2014). Similarly, precipitation of smithsonite ($ZnCO_3$) and hemimorphite [$Zn_4Si_2O_7(OH)_2$] during of leaching of Zn slags was observed whereas smithsonite was related to the hydration of hardystonite and zincite, and the hemimorphite to the destabilization of willemite (Vanaecker et al., 2014). Apart from the carbonates phases, the formation of amorphous ferric oxides (HFO) was found after leaching of Pb-Zn slags for more than 100 days (Ettler et al., 2005a; Ettler et al., 2003a). This implies that time plays an important role in dissolution of primary Fe-bearing phases, and in the formation of HFO.

5.4.2.2. Bulk release of Pb and Zn during long term leaching of LBF and ISF slags

The total amount of Pb and Zn leached out from LBF and ISF slags after 9 days of leaching are shown in Table 5.8. The total amount of Pb leached out from LBF slag were much higher under open air atmosphere at pH 4 (1842 μ g) and pH 5.5 (69 μ g) whereas that under nitrogen atmosphere were higher at pH 7 (376 μ g) and pH 8.5 (7 μ g). In addition, the amount of Zn from LBF slag were much higher under nitrogen atmosphere at pH 4 (5394 μ g) and pH 7 (238 μ g).

Furthermore, the total amount of Pb (74 μ g) and Zn (176 μ g) at pH 7 under open-air atmosphere were almost as high as the amount leached out during chemical leaching of LBF slag in ultra pure water at pH 7 under leachate renewal condition for 140 days as well as

under leachate stagnant condition for 250 days. During chemical leaching of LBF slag in ultra pure water, the total amount were 20 μ g of Pb and 256 μ g of Zn under leachate renewal condition (van Hullebusch et al., in press), whereas the amount were 747 μ g of Pb and 659 μ g of Zn under leachate stagnant condition (Yin et al., 2014). Thus, the longest slag-water interaction time indeed played a role in bulk release of Pb and Zn from LBF slags.

Meanwhile, the total amount of Pb leached out from ISF slag were much higher under open air atmosphere at pH 4 (1152 μ g), pH 5.5 (668 μ g), pH 8.5 (4 μ g), and pH 10 (61 μ g). Similarly, the amounts of Zn leached out from ISF slag were higher under nitrogen atmosphere at pH 4 (5413 μ g), pH 5.5 (650 μ g), pH 7 (87 μ g), and pH 10 (2 μ g).

Table 5.8. Bulk release of Pb and Zn from LBF and ISF slag after 9 days of leaching.

Bulk release from LBF ($\mu\text{g g}^{-1}$)					Bulk release from ISF ($\mu\text{g g}^{-1}$)				
pH	Pb (O)	Pb (N)	Zn (O)	Zn (N)	pH	Pb (O)	Pb (N)	Zn (O)	Zn (N)
4	1842	702	3874	5394	4	1152	990	3207	5413
5.5	69	30	1261	1072	5.5	668	12	286	650
7	74	376	176	238	7	52	399	28	87
8.5	4	7	2	3	8.5	4	2	1	1
10	4	4	2	1	10	61	6	1	2

5.5. Conclusions

The present study showed that the environmental stability of LBF and ISF slag depends on a wide range of parameters: the changes in pHs, the primary mineral phases present in the slags, the influence of the atmospheres, and slag-water interaction time.

5.5.1. Effect of pHs

The leaching behaviors of each element are different for both slags as a function of pHs. The leachability of Ca and Zn are dependent on pH where the highest concentration at pH 4 and the lowest at pH 10 for both slags whereas the leachability of Si is higher at pH 4 and pH 10 for ISF slags. In addition, the faster leaching rates of Ca, Si and Zn from LBF slag implies that they are prone to weathering under acidic conditions compared to ISF slags. However, the faster leaching rates of Si from ISF slag, suggests that ISF slags are more prone to weathering under alkaline conditions. Unlike other elements, dissolution of Fe is favored at acidic pHs (4 and 5.5) whereas limited at alkaline pHs (7, 8.5 and 10).

5.5.2. Effect of atmospheres

In the context of slags weathering under the open air atmosphere, the presence of oxygen from enhances oxidative weathering whereas the presence of carbon dioxide leads to the

formation of secondary carbonate phases along with other oxide phases. The weathering experiment under Open air atmosphere can be related to the natural weathering scenario when slags are open-dumped whereas the experiment under nitrogen atmosphere can be related to the anoxic weathering scenario when slags are land-filled.

5.5.3. Effect of leaching time

The slag-water interaction time plays an important role in assessing the leachability of elements from both LBF and ISF slags. The dissolution kinetics and the transformation of primary mineral phases and glassy matrix will control the release of the elements from both slags during initial leaching time of 1 day. However, when the prolonged time period of 9 days is employed, the solubility of the elements are furthered controlled by the newly formed phases. In addition, the longer slag-water interaction can lead to the dissolution of some primary phases (spinel for instance) which are against weathering during initial period, the formation of secondary layer which might control the diffusion of water, thus, controlling the dissolution of the slags.

5.5.4. Secondary precipitates

Newly formed secondary phases are (1) the indicators that both LBF and ISF slags are active and (2) the by-products of weathering after slag-water interaction for longer time whereas (3) the stability of these newly formed phases are still left out in most studies. The secondary precipitates observed in this study are mainly oxides, carbonates and clay phases which are predicted by thermodynamic model Visual MINTEQ and further confirmed by SEM and TEM analysis. The newly formed phases observed in this study are related to low-temperature laboratory weathering conditions, whereas a variety of other phases such as ferric oxides and hemimorphite can be expected in natural weathering conditions of Pb-Zn slags.

5.6. References

- Brantley, S.L., Kubicki, J.D., White, A.F., 2008b. Kinetics of water-rock interaction. *Springer*: 1-843.
- Cappuyns, V., Swennen, R., 2008. The application of $\text{pH}_{(\text{stat})}$ leaching tests to assess the pH-dependent release of trace metals from soils, sediments and waste materials. *J Haz Mat*, 158: 185-195.
- De Andrade Lima, L.R.P., Bernardez, L.A., 2013. Evaluation of the chemical stability of a landfilled primary lead smelting slag. *Environ Earth Sci*, 68: 1033-1040.
- Deneele, D., 2002. Caractérisation, simulations expérimentales et thermodynamiques de l'altération de déchets vitreux: les scories de première fusion de plomb et de zinc. *PhD thesis manuscript*, Université Des Sciences et Technologies de Lille I and U.F.R. Des Sciences De La Terre, France, 2002, 1-242.

- Douay, F., Pruvot, C., Waterlot, C., Fritsch, C., Fourier, H., Loriette, A., Bidar, G., Grand, C., de Vaufleury, A., Scheifler, R., 2009. Contamination of woody habitat soils around a former lead smelter in the North of France. *Sci Total Environ*, 407: 5564-5577.
- Ettler, V., Mihaljevic, M., Touray, J.C., Piantone, P., 2002. Leaching of polished sections: an integrated approach for studying the liberation of heavy metals from lead-zinc metallurgical slags. *Bulletin de la Société géologique de France*, 173: 161-169.
- Ettler, V., Piantone, P., Touray, J.C., 2003a. Mineralogical control on inorganic contaminant mobility in leachate from lead-zinc metallurgical slag: experimental approach and long-term assessment. *Mineral Mag*, 67: 1269-1283.
- Ettler, V., Komarkova, M., Jehlicka, J., Coufal, P., Hradil, D., Machovic, V., Delorme, F., 2004. Leaching of lead metallurgical slag in citric solutions-implications for disposal and weathering in soil environments. *Chemosphere*, 57: 567-577.
- Ettler, V., Jehlicika, J., Masiek, V., Hrusika, J., 2005a. The leaching behaviour of lead metallurgical slag in high-molecular-weight (HMW) organic solutions. *Mineral Mag*, 69: 737-747.
- Ganne, P., Cappuyns, V., Vervoort, A., Buve, L., Swennen, R., 2006. Leachability of heavy metals and arsenic from slags of metal extraction industry at Angleur (Eastern Belgium). *Sci Total Environ*, 356: 69-85.
- Kierczak, J., Neel, C., Puziewicz, J., Bril, H., 2009. The mineralogy and weathering of slag produced by the smelting of lateritic Ni ores, Szklary, southwestern Poland. *Can Mineral*, 45 : 557-572.
- Kucha, H., Martens, A., Ottenburgs, R., De Vos, W., Viaene, W., 1996. Primary minerals of Zn-Pb mining and metallurgical dumps and their environmental behavior at Plomberes, Belgium. *Environ Geol*, 27: 1-15.
- Lombardo, T., Gentaz, L., Verney-Carron, A., Chabas, A., Loisel, C., Neff, D., Leroy, E., 2013. Characterisation of complex alteration layers in medieval glasses. *Corros Sci*, 72: 10-19.
- Mahé-Le Carlier, C., Le Carlier de Veslud, C., Ploquin, A., Royer, J.J., 2000. Altération des scories de la métallurgie ancienne: un analogue de déchets vitrifiés. *Compt. Rend.Acad. Sci. (Paris), Série II. Sciences de la Terre et des planètes*, 330: 179-184.
- Piatak, N.M., Seal, R.R., Hammarstrom, J.M., 2004. Mineralogical and geochemical controls on the release of trace elements from slag produced by base- and precious-metal smelting at abandoned mine sites. *Appl Geochem*, 19: 1039-1064.
- Piatak, N.M., Parsons, M.B., Seal, R.R., 2014. Characteristics and environmental aspects of slag: A review. *Appl Geochem*, in press.
- Quina, M.J., Bordado, J.C., Quinta-Ferreira, R.M., 2009. The influence of pH on the leaching behaviour of inorganic components from municipal solid waste APC residues. *Waste Manag*, 29: 2483-2493.

- Rigol, A., Mateu, J., Gonzalez-Nunez, R., Rauret, G., Vidal, M., 2009. $\text{pH}_{(\text{stat})}$ vs. single extraction tests to evaluate heavy metals and arsenic leachability in environmental samples. *Anal chimica acta*, 632: 69-79.
- Seigneur, N., Bulteel, D., Damidot, D., Gauthier, A., Potdevin, J.L., 2006. Weathering of metallurgical slag heaps: multi-experimental approach of the chemical behaviours of lead and zinc. *Waste Manage Environ III*, 1: 31-40.
- Seigneur, N., Gauthier, A., Bulteel, D., Damidot, D., Potdevin, J.L., 2008. Leaching of lead metallurgical slags and pollutant mobility far from equilibrium conditions. *Appl Geochem*, 23: 3699-3711.
- Sobanska, S., Ledésert, B., Deneele, D., Laboudigue, A., 2000. Alteration in soils of slag particles resulting from lead smelting. *Earth Planet Sci*, 331: 271-278.
- Soumya, D., Hendry, M.J., Essilfie-Dughan, J., 2011. Transformation of two line ferrihydrite to goethite and hematite as a function of pH and temperature. *Environ Sci Tech*, 45: 268-275.
- Strachan, D.M., Neeway, J.J., 2014. Effects of alteration product precipitation on glass dissolution. *Appl Geochem*, 45: 144-157.
- van Hullebusch, E.D., Yin, N.H., Seigneur, N., Labanowski, J., Gauthier, A., Lens, P.N.L., Avril, C., Sivry, Y., in press. Bio-alteration of metallurgical wastes by *Pseudomonas aeruginosa* in a semi flow-through reactor. *J Environ Manage*.
- Vanaecker, M., Courtin-Nomade, A., Bril, H., Laureyns, J., Lenain, J.F., 2014. Behavior of Zn-bearing phases in base metal slag from France and Poland: A mineralogical approach for environmental purposes. *J Geochem Explor*, 136: 1-13.
- Vítková, M., Ettler, V., Sebek, O., Mihaljevic, M., Grygar, T., Rohovec, J., 2009. The pH-dependent leaching of inorganic contaminants from secondary lead smelter fly ash. *J Haz Mat*, 167: 427-433.
- Vítková, M., Hyks, J., Ettler, V., Astrup, T., 2013. Stability and leaching of cobalt smelter fly ash. *Appl Geochem*, 29: 117-125.
- Yee, N., Shaw, S., Benning, L.G., Nguyen, T.H., 2006. The rate of ferrihydrite transformation to goethite via the Fe(II) pathway. *Am Mineral*, 91: 92-96.
- Yin, N.H., Sivry, Y., Avril, C., Borensztajn, S., Labanowski, J., Malavergne, V., Lens, P.N.L., Rossano, S., van Hullebusch, E.D., 2014. Bioweathering of lead blast furnace metallurgical slags by *Pseudomonas aeruginosa*, *Int Biodeterior Biodegrad*, 86: 372-381.

CHAPTER 6

Zn Isotopes Fractionation during Chemical Weathering of Slags from Lead Blast Furnace (LBF) and Imperial Smelting Furnace (ISF) Smelters

This chapter will be submitted to:

Environmental Science and Technology

Chapter 6

6.1. Introduction

The development of multi-collector inductively coupled plasma mass spectrometry (MC-ICP-MS) over the past 20 years (Halliday et al., 1995; Rehkämper et al., 2001; Johnson et al., 2004), have induced a great expansion of the knowledge in the field of transition metal isotopes geochemistry such as Zn. Due to the active participation of Zn in multiple biological and low-temperature inorganic-chemical reactions, its isotopic variations may be used as a tracer of biogeochemical and chemical processes. Experiments by Pokrovsky et al. (2005), then Juillot et al. (2008) showed Zn isotopic fractionation ($\Delta^{66}\text{Zn}_{\text{solid-solution}} = \pm 0.20\text{-}0.53\text{‰}$) during Zn adsorption onto oxy(hydr)oxides and anhydrous oxides surfaces under abiotic conditions, whereas Jouvin et al. (2009) highlighted that Zn bound to purified humic acid (PHA) was heavier than free Zn^{2+} ($\Delta^{66}\text{Zn}_{\text{PHA-FreeZn}^{2+}} = 0.24\text{‰}$). Meanwhile, biological processes can also induce fractionation between Zn isotopes: Zhu et al. (2002) have reported Zn fractionation of 1.1‰ for Zn proteins synthesized by yeast, relatively to $\delta^{66}\text{Zn}$ in the nutrient solution and Gélabert et al. (2006) demonstrated that irreversible incorporation of Zn in cultured diatom cells induces an enrichment in heavy isotopes ($\Delta^{66}\text{Zn}_{\text{solid-solution}} = 0.3$ to 0.4‰, compared to the growth media).

While many studies focused on Zn isotopes during natural biogeochemical cycling, other results suggest that Zn isotopes can be used to trace anthropogenic contamination: significant variability of $\delta^{66}\text{Zn}$ was reported in lichens near urban area and mining facilities with Zn isotopic signatures up to 1.40‰ heavier than the local geochemical background (Cloquet et al., 2006a and Dolgoplova et al., 2006). Weiss et al. (2007) managed to estimate probable sources of Zn contamination of peat surface layers affected by atmospheric particles thanks to Zn isotopes, with $\delta^{66}\text{Zn}_{\text{JMC}} = 0.32$ for the mining site and $\delta^{66}\text{Zn}_{\text{JMC}} = 0.66$ for the smelting site. Among anthropic sources, smelting sites and in particular slag tailings were shown to be of major importance in term of inputs of contaminants in the environment (Audry et al., 2004). Indeed, smelting processes were proved to fractionate Zn isotopes (Shiel et al., 2010; Sivry et al., 2008) resulting in heavy isotopes enrichment in the residual solid waste (up to $\delta^{66}\text{Zn}_{\text{JMC}} = 1.50\text{‰}$, Sivry et al., 2008) whereas the dust chimney is enriched in light isotopes (up to $\delta^{66}\text{Zn}_{\text{JMC}} = -0.67\text{‰}$, Mattielli et al., 2009).

Hence, downstream river sediments, lake sediments as well as soils impacted by smelters were proved to contain Zn with isotopic composition directly controlled by the smelting activity itself and many studies have demonstrated the potential of Zn isotopes to trace smelting source contamination (Petit et al., 2008; Mattielli et al., 2009; Sivry et al., 2008; Juillot et al., 2011; Thapalia et al., 2010).

In such pyrometallurgical context, slags are the main waste product (Piatak and Seal, 2010) and they are mineralogically and chemically diverse materials containing variable amount of glass and crystalline phases as well as relict ore and flux minerals (Lottermoser, 2002). Mineralogy of slags has been well characterized especially in relation to origin of ores,

smelting technologies, cooling temperature of slags (Ettler and Johan, 2003b; Ettler et al., 2009; Puziewicz et al., 2007). Slags produced by base-metal smelters contain high concentrations of potentially toxic metals (Piatak et al., 2004). Consequently, risk assessment through the mobilizations of metals from the slags dump have been widely studied in soil or soil-like environment (Ettler et al., 2004; Sobanska et al., 2000), in leaching assessment of road materials containing Pb and Zn slags (Barna et al., 2004), as well as in landfill environment (de Andrade Lima and Bernardez, 2012; Mahé-Le Carliera et al., 2000). Dissolution/precipitation, adsorption/desorption as well as complexation are the main processes controlling the pollutant release from the slag under weathering environment, which were all proven to fractionate Zn isotopes. Thus, assuming that slags are one of the main sources of contamination from Zn-Pb smelter activity, the multiple low-temperature inorganic chemical reactions involving Zn as well as the slag heterogeneity should be carefully considered when using Zn isotopes as tracer of smelting activity contamination.

The overall goal of the present study is to assess the Zn isotope signature resulting from chemical weathering slag considered as source of contamination. For this, specific experiments were designed to leach under controlled physicochemical conditions two different slags from Lead Blast Furnace (LBF) and Imperial Smelting Furnace (ISF) processes. Both liquid solutions and solid phases were chemically and structurally studied, and isotopic compositions were measured in bulk slags and leachate solutions, in order to determine whether $\delta^{66}\text{Zn}$ in the leachate was controlled by Zn bearing phases into the slag (amorphous or crystalline silicate phases) or by the physicochemical processes affecting Zn.

6.2. Materials and Methods

6.2.1. Slags

Pyrometallurgical slags used in this study were originated from former lead blast furnace and imperial smelting furnace smelters (LBF and ISF, resp.) located in the industrial basin of Nord-Pas-de-Calais, northern France. Both LBF and ISF slags are vitreous materials, and particle size distribution varies from 100 μm to 2 mm with specific surface area of 0.08-0.09 $\text{m}^2 \text{g}^{-1}$. LBF contains 80 vol% of amorphous glassy phase with CaO-FeO-SiO₂ as end members, 19 vol% of crystalline phases and 1 vol% of metallic lead droplets whereas ISF contains 84 vol% of glassy phase, 5 vol% of crystalline phases, 10 vol% of speiss and 1 vol% of metallic lead droplets (Deneele, 2002). The chemical composition of global as well as amorphous glassy phase for both LBF and ISF slags are given in Table 6.1. Spinel is the dominant part of crystalline phases which are well embedded and scattered across the glassy matrix of both LBF (19% in v/v) and ISF (5% in v/v). Magnesiochromite (MgCr₂O₄), franklinite (ZnFe₂O₄), magnetite (Fe²⁺Fe³⁺₂O₄) are dominant spinel phases found in LBF whereas zincochromite (ZnCr₂O₄), and gahnite (ZnAl₂O₄) are the ones found in ISF slags where their respective chemical composition are given in Table 6.2. Along with spinel phases, silicate phases such as hardystonite (Ca₂ZnSi₂O₇) and willemite (Zn₂SiO₄) are found in both slags with additional Fe rich speiss found in ISF slags where detail chemical compositions are given in Table 6.3. Unlike Zn, Pb is mainly present as simple droplet form embedded in the glassy matrix of both slags.

Table 6.1. Chemical composition of global and glassy matrix in LBF and ISF slags.

%wt	Samples	SiO ₂	CaO	Fe ₂ O ₃	FeO	Al ₂ O ₃	MgO	MnO	ZnO	PbO
Global	LBF	24.88	22.14	8.11	23.27	2.46	2.71	0.81	10.77	3.74
	ISF	24.38	18.55	0.39	31.11	10.03	1.81	1.04	8.75	1.66
Glass	LBF	26.38	22.92	-	26.50	2.54	1.91	0.84	11.16	4.30
	ISF	25.68	21.40	-	24.97	9.98	1.80	0.84	8.27	0.22

Note: Global chemical composition obtained by acid digestion (HNO₃-HCl-HF) except for Si by XRF, where as glassy part obtained by microprobe (Deneele, 2002).

Table 6.2. Chemical composition of primary spinels in LBF and ISF slags.

Samples	Spinel (%wt)	SiO ₂	CaO	Fe ₂ O ₃	FeO	Al ₂ O ₃	MnO	MgO	ZnO	Cr ₂ O ₃
LBF	MgCr ₂ O ₄	0.28	0.57	8.95	5.55	15.83	0.79	12.46	9.90	44.56
	ZnFe ₂ O ₄	0.10	0.68	67.62	7.69	0.62	0.91	4.83	15.79	1.66
	Fe ²⁺ Fe ³⁺ ₂ O ₄	0.05	0.13	45.45	17.29	7.60	0.74	1.99	12.72	13.59
ISF	ZnCr ₂ O ₄	0.03	0.24	3.12	11.52	1.96	2.27	0.97	18.14	61.13
	ZnAl ₂ O ₄	0.08	0.13	3.93	6.59	50.72	0.19	3.19	31.08	4.03

Note: Chemical composition obtained by microprobe analysis (Deneele, 2002).

Table 6.3. Chemical composition of silicates in LBF and ISF slags.

Silicates (%wt)	SiO ₂	CaO	FeO	Al ₂ O ₃	MgO	MnO	ZnO	PbO
Ca ₂ ZnSi ₂ O ₇	38.09	32.96	4.88	2.78	2.63	0.32	12.60	4.56
Zn ₂ SiO ₄	29.86	0.00	1.16	0.03	0.23	10.77	63.99	0.04

Note: Chemical composition obtained by microprobe analysis (Deneele, 2002).

6.2.2. Chemical weathering experiment

Chemical weathering experiments of LBF and ISF slags were conducted according to standardized leaching test, CEN/TS 14997 (2006) with slight modifications. Two set of experiments were performed at fixed pH values (4, 5.5, 7, 8.5 and 10) under both open-air and nitrogen atmospheres, from 6hours to 9days. The addition of either suprapure grade HNO₃ or NaOH (Merck Inc., Germany) was done via a complete automatic and continuous titration system (Titroline Alpha plus TL 7000). The liquid to solid ratio (L/S) was maintained at 20, the temperature was controlled at 23 ± 2°C, and it was constantly stirred at 100 rpm. 5 mL of leachate were sampled after 6h, 24h and 216 h and replaced by an equivalent quantity of leaching medium to maintain the L/S ratio constant.

6.2.3. Leachate chemistry and geochemical modeling

The leachate from chemical weathering experiments were filtered through 0.20 μM polypropylene filters, and then digested in aqua regia of HCl to HF (4:1). Clear solutions were evaporated to dryness, and finally dissolved in HNO_3 for further analysis on ICP-OES (Thermo Scientific iCAP 6200 Duo), and in HCl for ion chromatography separation. The leachate composition was further processed by thermodynamic model Visual MINTEQ v. 3.0 for determination of solubility controlling phases and for calculation of saturation indices of potential secondary precipitates. The temperature was kept constant at 25°C, the oversaturated solids were not allowed to precipitate, and the CO_2 partial pressure was fixed at 396 ppmv.

6.2.4. Zn isotopes measurement

The anion-exchange chromatographic method dedicated to acid-mine drainage samples was used to separate Zn from the matrix (Borrok et al., 2007). Column yield of each separation was checked prior to the analysis on Neptune MC-ICP-MS (Thermo Finnigan) at IPGP, Paris, France, and found to be $95\pm 5\%$. The introduction interface consisted of standard Ni cones, desolvating system (APEX), an ESI Teflon micro-nebulizer operating at $100 \mu\text{Lmin}^{-1}$, and a CETAC ASX-100 auto sampler. ^{64}Zn , ^{66}Zn , ^{67}Zn , ^{68}Zn and ^{70}Zn were simultaneously measured as well as ^{62}Ni signals, to correct for the potential isobaric ^{64}Ni interference on ^{64}Zn . All the samples were measured in 0.5 N HNO_3 , spiked with in-house IPGP Cu as internal standard (Zn/Cu voltage ratio 1:2). Simultaneously, JMC Lyon Zn and IRMM Zn standards, spiked with in-house IPGP Cu standards, as well as SRM 976 Cu standard spiked with in-house IPGP Zn standard were also measured every 20 samples during one analysis session. An analysis of one sample comprised of 3 blocks of $15\times 10\text{s}$ integrations. The individual samples were bracketed by in-house standard (Zn & Cu) and isotopic data were reported in relative to the Johnson Matthey Zinc (JMC) Lyon as follow (Eq. 6.1):

$$\delta^{66}\text{Zn}_{\text{JMC Lyon}} = \left[\frac{(^{66}\text{Zn}/^{64}\text{Zn})_{\text{sample}}}{(^{66}\text{Zn}/^{64}\text{Zn})_{\text{JMC Lyon}}} - 1 \right] * 1000(\text{‰}) \quad \text{Eq. (6.1)}$$

Both simple bracketing correction method (Borrok et al., 2007; Thapalia et al., 2010) as well as exponential law (Marechal et al., 1999; Mason et al., 2004b; Mason et al., 2004a) were used as alternative mass-bias correction methods. The average $\delta^{66}\text{Zn}$ of in-house IPGP standard in relative to JMC Lyon standard was found to be $-0.04\pm 0.04\text{‰}$ whereas the analytical repeatability of the IRMM 3702 was $0.31\pm 0.04\text{‰}$ (2SD, n=18), that of JMC Lyon was $0.00\pm 0.06\text{‰}$ (2SD, n=18), respectively. External reference material BCR-2 from USGS was analyzed at $0.27\pm 0.06\text{‰}$ (2SD, n=12) during 13 non-consecutive measurement sessions on MC-ICP-MS. This 2SD has been applied to all the Zn isotopic data unless the sample repeatability exceeded 0.06‰ .

6.2.5. Solid phase characterization

Transmission electron microscopy (TEM) analysis has been used in order to give insights regarding the mechanisms of alteration, surface morphology of slags and the formation of secondary mineral phases. Diluted suspensions of the solid phases were deposited on copper grid. TEM analysis was performed at University of Pierre et Marie Curie using JEOL 2100F electron microscope, operating at 200 kV and equipped with a field emission gun, a high-resolution UHR pole piece and a Gatan GIF 200 L imaging filter. To perform chemical analysis, this microscope was coupled with electron-dispersive X-ray spectroscopy (EDXS) using a JEOL detector with an ultrathin window allowing detection of low atomic mass elements. TEM pictures were treated with the software ImageJ 1.43u.

6.3. Results

6.3.1. Oxidative weathering of slags

Zn dissolution. Zn will be the element of interest in this paper, whereas the dissolution chemistry of other elements (Ca, Fe, Mg, Si and Pb) has already been addressed in Chapter 5. Figure 6.1 illustrates the evolution of Si and Zn concentrations as well as Zn isotopes signatures in leachate as a function of time, during open-air atmosphere and pH-dependent leaching of both LBF and ISF slags. The initial Zn contents are 14mM and 12mM in LBF and ISF slags, respectively. Concentration of Zn is found to be dependent on pH for both slags, where the highest concentrations can be found at pH 4 (0.4 to 2.9 mM) whereas the lowest concentrations at pH 10 (0.0002 to 0.0012 mM). In addition, higher Zn concentrations are observed for both slags at all pHs when the slag-water interaction time is prolonged from 6h to 216 h (Figure 6.1 A & B).

Zn isotopes. The Zn isotopic analyses of bulk LBF and ISF displayed $\delta^{66}\text{Zn}$ signatures enriched in heavier isotopes (i.e. $0.13\text{‰} \pm 0.06\text{‰}$, $n=3$ and $0.78\text{‰} \pm 0.13\text{‰}$, $n=3$ for LBF and ISF, respectively). During weathering of LBF slag, $\delta^{66}\text{Zn}$ got heavier as slag-water interaction time was increased from 6h to 216 h: from 0.03‰ to 0.09‰ at pH4, from -0.07‰ to 0.04‰ at pH 5.5, from -2.77‰ to -2.11‰ at pH 8.5. On the other hand, $\delta^{66}\text{Zn}$ got slightly lighter as function of time: from -1.4‰ to -1.65‰ at pH 7 and from -1.25‰ to -1.28‰ at pH 10. Similarly, heavier $\delta^{66}\text{Zn}$ signature as a function of time can be observed during weathering of ISF slag (Figure 6.1 C & D). $\delta^{66}\text{Zn}$ gradually increased from 0.89‰ to 0.91‰ at pH 4, from -0.05‰ to 0.55‰ at pH 5.5, from -0.08‰ to 0.05‰ at pH 7, from -1.17‰ to -0.22‰ at pH 8.5 and from -1.16‰ to -0.27‰ at pH 10. In conclusion, Zn dissolution was related to extremes zinc isotopic signatures in the leachate as a function of pHs and leaching time. Heavier $\delta^{66}\text{Zn}$ values can be observed at low pH than at high pH for both slags; i.e. 0.03‰ and -1.25‰ for LBF, 0.89‰ and -1.16‰ for ISF at pH 4 and 10, respectively after slag-water interaction time of 6h.

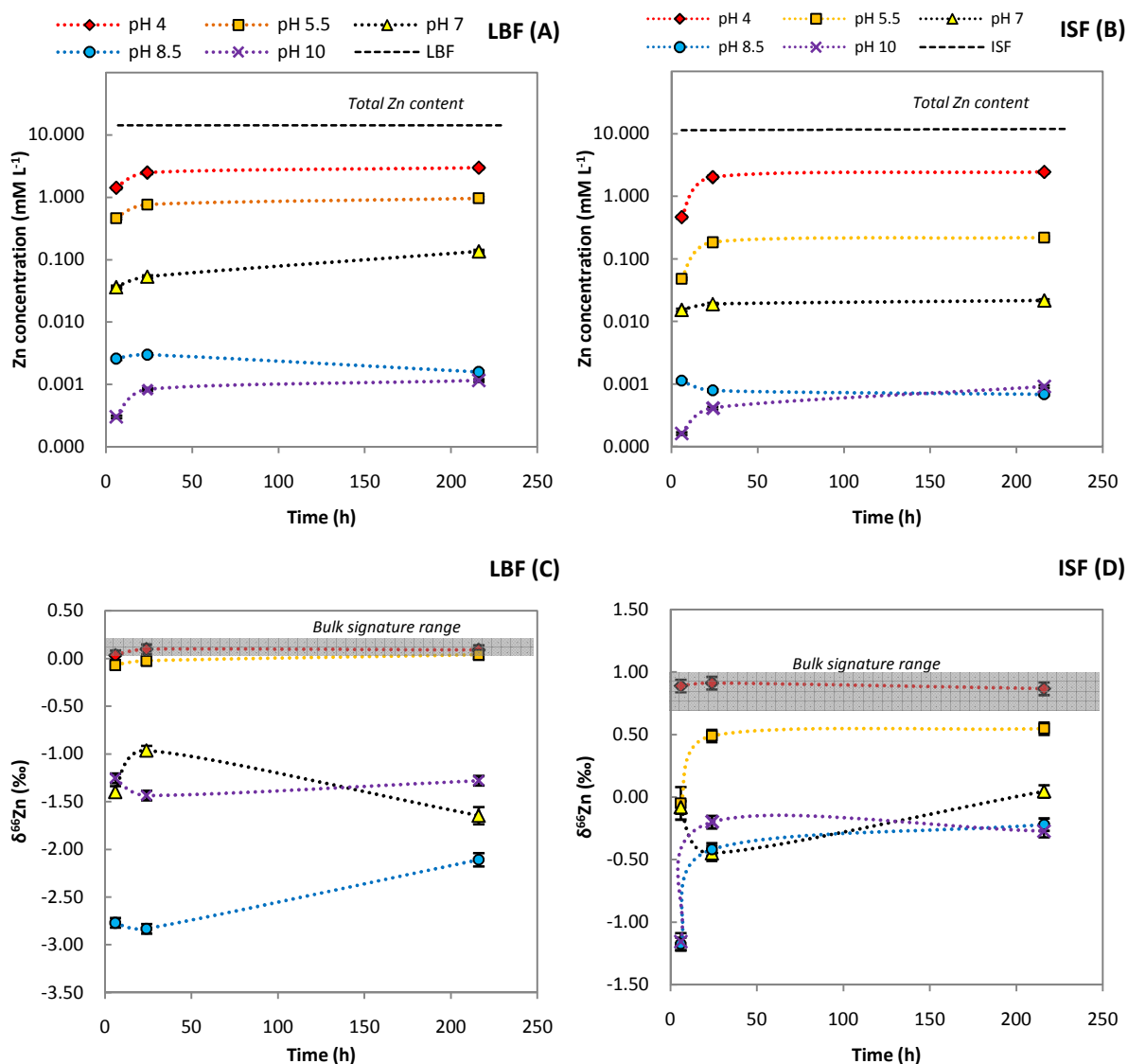


Figure 6.1. Concentration of Zn and its isotopes signatures as a function of pH and time during oxidative weathering of LBF and ISF slags: (A) Zn concentration in leachate from LBF slag, (B) Zn concentration in leachate from ISF slag, (C) Zn isotopic signatures of leachate from LBF slag, and (D) Zn isotopic signatures of leachate from ISF slag.

6.3.2. Anoxic weathering of slags

Zn dissolution. Figure 6.2 illustrates the leaching of Zn and its isotopes signatures during pH dependent leaching of both LBF and ISF slags under nitrogen atmosphere as a function of time. Concentration of Zn is found to be relatively dependent on pH for both slags where the highest concentrations can be found at pH 4 (0.7 to 4.2 mM) whereas the lowest concentrations at pH 10 (0.001 to 0.011 mM). In addition, higher Zn concentrations are observed for both slags at all pHs when the slag-water interaction time is prolonged from 6 h to 216 h (Figure 6.2) except at pH 8.5 for ISF slag.

Zn isotopes. During weathering of LBF slag, the $\delta^{66}\text{Zn}$ got heavier as slag-water interaction time was increased from 6h to 216 h: from -0.14‰ to 0.00‰ at pH4, from -0.70‰ to -0.16‰ at pH 5.5, from -0.42‰ to -0.15‰ at pH 7 and from -0.99‰ to -0.15‰ at pH 10, whereas the signature got lighter from -2.10‰ to -2.35‰ at pH 8.5 (Figure 6.2). During weathering of ISF slag, heavier $\delta^{66}\text{Zn}$ signature can be observed as a function of time for all pHs: from 0.81‰ to 0.78‰ at pH 4, from 0.60‰ to 0.83‰ at pH 5.5, from -0.35‰ to 0.50‰ at pH 7, from -0.51‰ to -0.42‰ at pH 8.5 and from -0.53‰ to 0.85‰ at pH 10. In conclusion, Zn dissolution was related to extremes zinc isotopic signatures in the leachate as a function of pHs and leaching time. Heavier $\delta^{66}\text{Zn}$ values can be observed at low pH than at high pH for both slags; i.e. -0.14‰ and -0.99‰ for LBF, 0.81‰ and -0.53‰ for ISF at pH 4 and 10, respectively after slag-water interaction time of 6h.

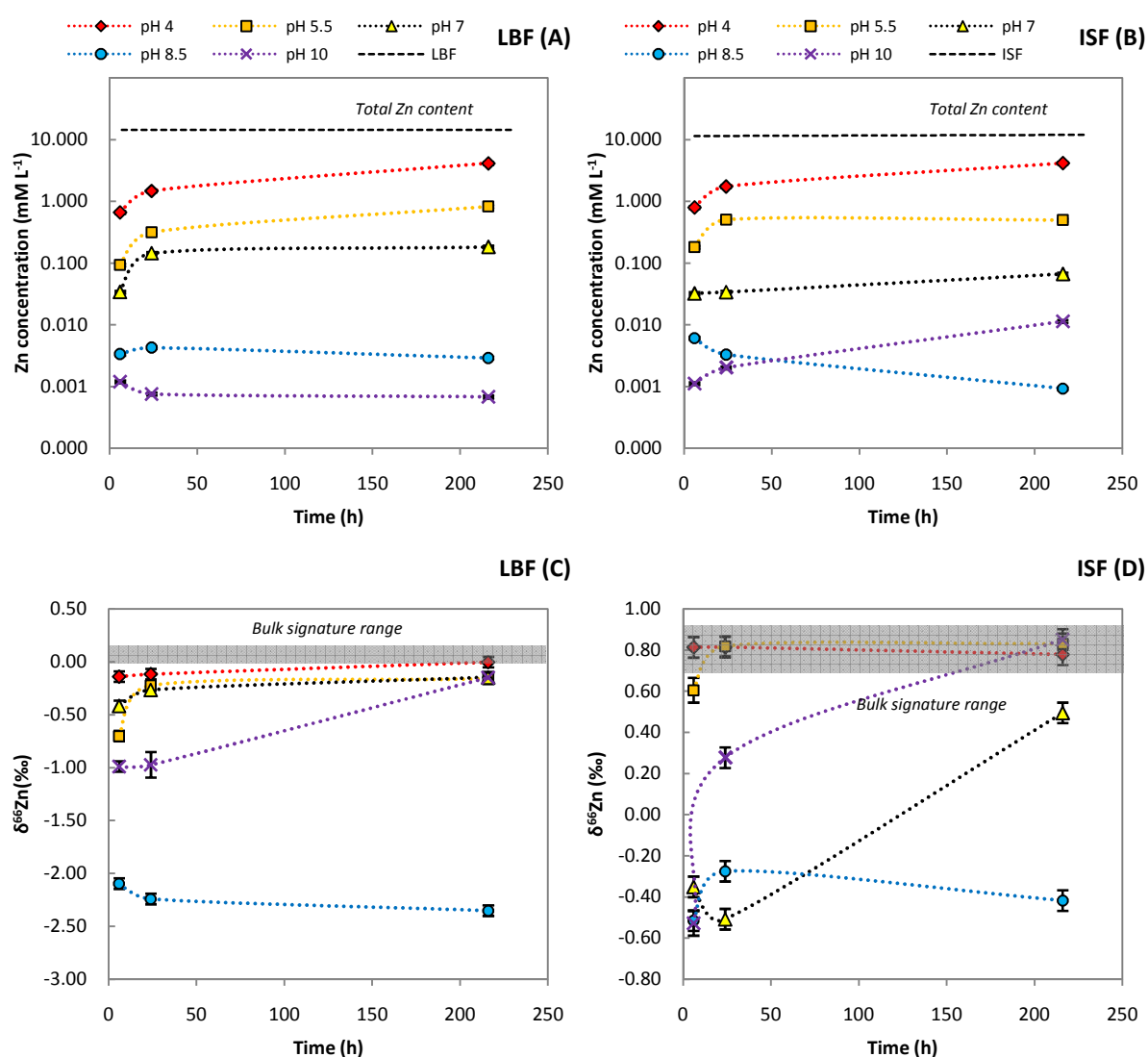


Figure 6.2. Concentration of Zn and its isotopes signatures as a function of pH and time during anoxic weathering of LBF and ISF slags:(A) Zn concentration in leachate from LBF slag, (B) Zn concentration in leachate from ISF slag, (C) Zn isotopic signatures of leachate from LBF slag, and (D) Zn isotopic signatures of leachate from ISF slag.

6.3.3. Effect of the atmospheres on Zn isotopes signatures

Figure 6.3 illustrates the concentration of Zn and its isotopes signatures under both open-air and nitrogen atmospheres after weathering of LBF and ISF slags for 216 h. The concentration of Zn under nitrogen atmosphere is higher than that under open-air atmosphere at acidic pH for LBF slag and at all pHs except pH 8.5 for ISF slag. During weathering of LBF slag, the $\delta^{66}\text{Zn}$ displayed significantly heavier signature under nitrogen atmosphere at pH 7 (-0.16‰) and pH 10 (-0.15‰) compared to signatures under open-air atmosphere at pH 7 (-1.65‰) and pH 10 (-1.28‰). Similarly, the heavier signatures were observed under nitrogen atmosphere during weathering of ISF slags at all pHs: 0.78‰ at pH 4, 0.83‰ at pH 5.5, 0.50‰ at pH 7, -0.42‰ at pH 8.5, 0.85‰ at 10 (Figure 6.3B).

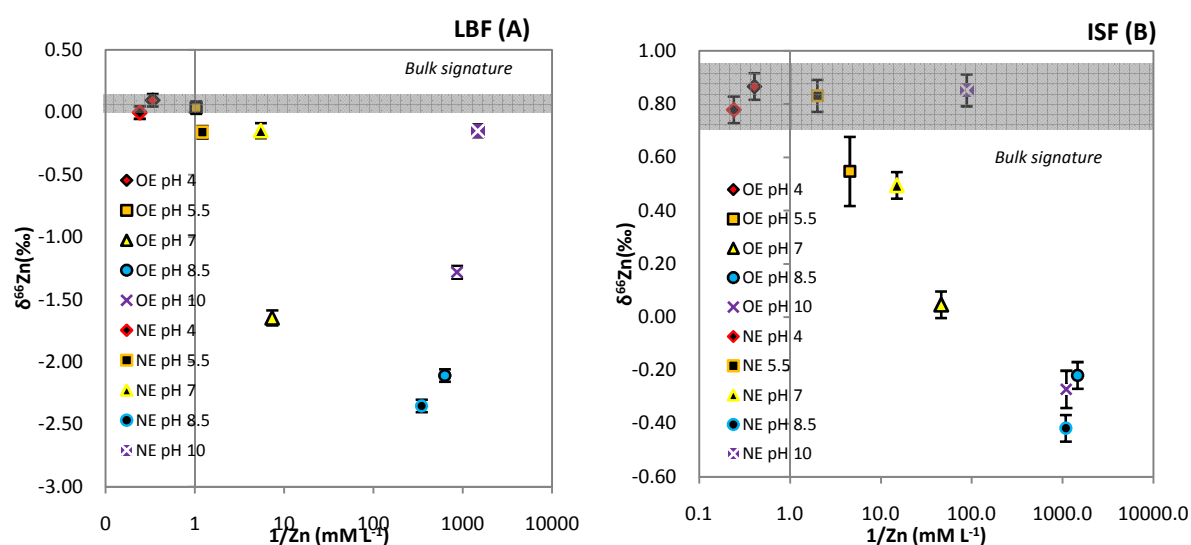


Figure 6.3. Effect of atmospheres on the concentration of Zn and its isotopes signatures as a function of pH after weathering of LBF and ISF slags 216 h: (A) Zn concentration and isotopic signatures of leachate from LBF slag, (B) Zn concentration and isotopic signatures of leachate from ISF slag under open-air and nitrogen atmospheres.

6.3.4. Thermodynamic modeling

Table 6.4 gives the species distribution and the solubility controlling phases of major elements during LBF weathering under both atmospheres. Under open-air atmosphere, ferrihydrite is the only phase controlling Fe solubility at pH 7 whereas it was not possible to calculate the SI indices for pH 8.5 and 10 as Fe concentration was under detection limit. The solubility of Pb was controlled by cerussite at pH 7, 8.5 and 10 (SI: 0.40, 0.50 and -0.43, resp.) whereas that of Ca by calcite at pH 8.5 and 10 (SI: -0.64 and -0.43) after 216 h. Zn was controlled by layer double hydroxides and smithsonite at pH 7 (SI: -0.92 and -0.62), by zincite at pH 8.5 and 10 (SI: -0.39 and -0.56), and by zinc hydroxide at pH 8.5 (SI: 0.08) after 216 h. Meanwhile, hydroxides of Fe, Pb and Zn are dominant solubility controlling phases at pH 7, 8.5 and 10 under nitrogen atmosphere (Table 6.4).

Table 6.4. Saturation indices (SI) of solubility controlling phases of major elements (LBF slag).

LBF under open-air atm			pH 7		pH 8.5		pH 10	
Elements	Mineral phases	Formula	24 h	216 h	24 h	216 h	24 h	216 h
Pb	Cerussite	PbCO ₃	0.214	0.404	0.483	0.506	-0.732	-0.429*
Ca	Calcite	CaCO ₃	-	-	-0.659	-0.635	1.291	1.034
Zn	Smithsonite	ZnCO ₃	-	-0.916	0.07	-0.231		
	Zinc layer double hydroxide	Zn-Al LDH	-	-0.617	-	-	-	-
	Zincite	ZnO	-	-	-0.217	-0.385	-0.465	-0.562
	Zinc hydroxide	Zn(OH) ₂	-	-	0.041	0.08	-	-
LBF under nitrogen atm			pH 7		pH 8.5		pH 10	
Elements	Mineral phases	Formula	24 h	216 h	24 h	216 h	24 h	216 h
Fe	Iron hydroxide	Fe(OH) ₂	-	-	-0.095	-12.91	-0.544	-0.066
Pb	Lead hydroxide	Pb(OH) ₂	1.23	1.328	2.019	1.952	2.810	2.770
Zn	Zinc hydroxide	Zn(OH) ₂	-	-	0.046	0.098	-0.989	-0.769

Note: * refers to SI index at 168 h, suggesting that the precipitations of such phases can take place earlier than 9 days.

Table 6.5 gives the species distribution and the solubility controlling phases of major elements during ISF weathering under both atmospheres. Under open-air atmosphere, amorphous iron hydroxide is the only phase controlling solubility controlling phase of Fe (SI: 1.218) at pH8.5 whereas it was not possible to calculate the SI indices for 7 and 10 as Fe concentration was under detection limit. The solubility of Pb was controlled by cerussite at pH 7 to 10 (SI: 0.25, 0.51 and -0.46) whereas that of Ca by calcite at pH 8.5 and 10 (SI: -0.43 and 0.89) after 216 h. Zn was controlled by smithsonite at pH 8.5 (SI: -0.63), by zincite at pH 8.5 and 10 (SI: -0.82 and -0.85), and by zinc hydroxide at pH 8.5 and 10 (SI: 0.53 and 0.33) after 216 h. Meanwhile, hydroxides of Fe, Pb and Zn are dominant solubility controlling phases at pH 7, 8.5 and 10 under nitrogen atmosphere (Table 6.5).

Table 6.5. Saturation indices (SI) of solubility controlling phases of major elements (ISF slag).

ISF under open-air atm			pH 7		pH 8.5		pH 10	
Elements	Mineral phases	Formula	24 h	216 h	24 h	216 h	24 h	216 h
Fe	Iron hydroxide	Fe(OH) ₂	-	-	0.288	1.218	-	-
Pb	Cerussite	PbCO ₃	0.019	0.252	-0.471	0.506	-1.580	-0.458
Ca	Calcite	CaCO ₃	-	-	-0.822	-0.431	0.798	0.891
Zn	Smithsonite	ZnCO ₃	-	-	-0.930	-0.629	-	-
	Zincite	ZnO	-	-	-0.322	-0.819*	-0.018	0.849*
	Zinc hydroxide	Zn(OH) ₂	-	-	0.395	0.533	-0.574	0.325
ISF under nitrogen atm			pH 7		pH 8.5		pH 10	
Elements	Mineral phases	Formula	24 h	216 h	24 h	216 h	24 h	216 h
Fe	Iron hydroxide	Fe(OH) ₂	-	-	0.334	1.338	0.288	1.218
Pb	Lead hydroxide	Pb(OH) ₂	-1.167	1.355	-0.127	1.174	2.679	3.267
Zn	Zinc hydroxide	Zn(OH) ₂	-	-	0.431	0.306	-1.262	-0.533

Note: * refers to SI index at 7 days, suggesting that the precipitations of such phases can take place earlier than 9 days.

6.3.5. TEM analysis

A mixture of Ca, Pb and Zn carbonates are the major secondary precipitates observed after 9 days of leaching LBF slags and ISF slags at pH 7 and 10 (Figures 6.4 A, B, C and D). These carbonate phases consist of 80-90% of Ca, 8-17% of Pb, 0.8-1.6% of Zn at pH 10 for both slags (Figure 6.4 C & D) whereas it was impossible to do the EDS analysis on the chemical composition of carbonate at pH 7 due to lesser quantity. Not only nearly-well crystallized but also amorphous carbonates were observed at pH 10 (Figure 6.4 C & D) where their sizes range from 10 to 100 nm. The X-ray microdiffraction analysis of the well-crystallized part of carbonates indicated calcite as the possible carbonate mineral.

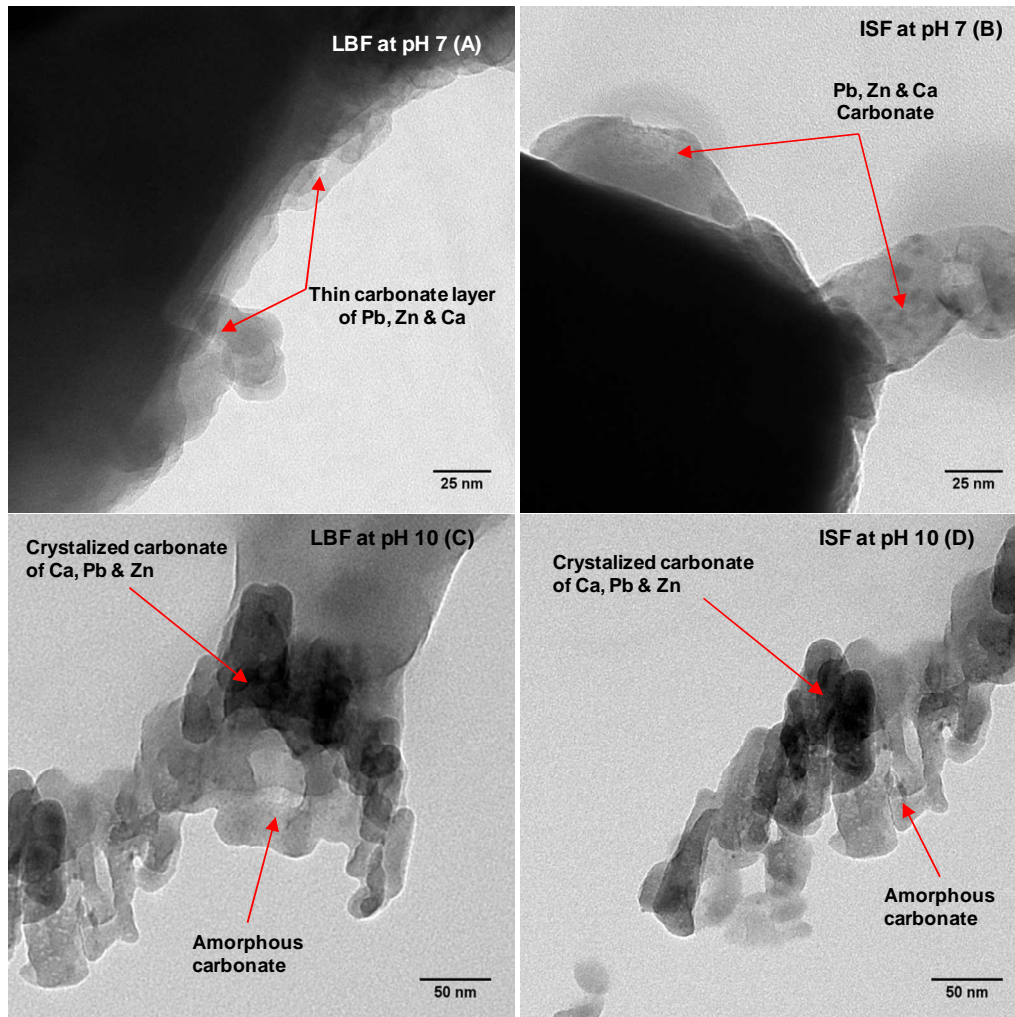


Figure 6.4. Precipitation of carbonate phases under open air atmosphere during weathering of LBF and ISF slags at pH 7 (A and B), and at pH 10 (C and D).

6.4. Discussion

6.4.1. $\delta^{66}\text{Zn}$ variation in primary mineral phases

Zn dissolution and its signature can be related to its primary mineral phases present in each slag (Tables 6.2 and 6.3). Zn included in crystalline phases such as spinels (Table 6.2) and silicates phases (Table 6.3), were more resistant to weathering comparing to amorphous glassy phase of both LBF and ISF slags (Yin et al., 2014). Dissolved Zn concentrations and associated isotopic signatures under nitrogen atmosphere are thus useful to extrapolate the $\delta^{66}\text{Zn}$ value in amorphous glassy and crystalline phases, because the potential fractionation of zinc isotopes induced by newly formed secondary phases (mainly oxides and carbonates, see section 6.3.3 and 6.3.4), is prevented.

6.4.1.1. $\delta^{66}\text{Zn}$ signature of amorphous glassy phase

Both LBF and ISF slags are made of amorphous glassy phase (80% and 84% in v/v, resp.), the dissolution rates of Si (Q_{Si}) from both slags under nitrogen atmosphere are compared to

the theoretical amorphous rates according to pH (Figure 6.5A). At pH 7, these values were found to be particularly consistent, with -9.73 and -10.37 $\text{mol}\cdot\text{m}^{-2}\cdot\text{s}^{-1}$ for LBF and ISF slags, resp. and -10.11 $\text{mol}\cdot\text{m}^{-2}\cdot\text{s}^{-1}$ for the amorphous Si theoretical value (Carroll et al., 2002). Thus, one can assume that the leaching of amorphous glassy phase of both slags were dominant at pH7. In addition, the linear correlation observed between $\log Q_{\text{Zn}}$ to and $\log Q_{\text{Si}}$ (Figure 6.5B & C) indicates that the dissolution of Zn is strongly dependent upon that of Si dissolution, and thus controlled by the dissolution of amorphous glassy phases of LBF and ISF slags at pH 7. Therefore, the $\delta^{66}\text{Zn}$ signatures measured in N_2 leachate at pH 7 can be linked back to the isotopic signature of amorphous glassy phases in both slags: the most probable range lies between -0.42‰ for LBF and between -0.35‰ for ISF (Figure 6.5D). The $\delta^{66}\text{Zn}$ values at the end of the experiment (24 and 216 h) are omitted from the consideration in order to eliminate the effect of fractionation induced by possible hydroxide precipitation.

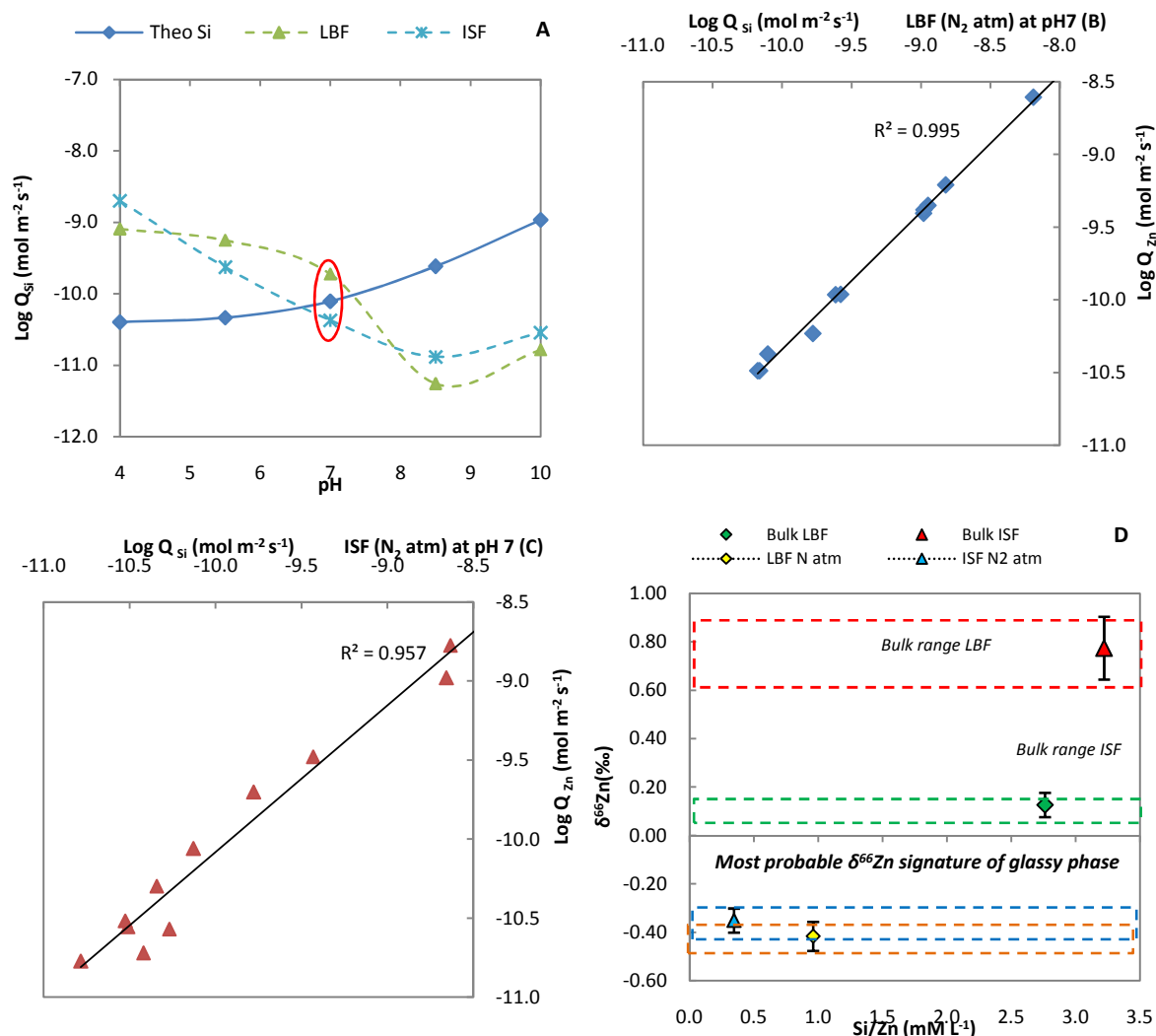


Figure 6.5. (A) Theoretical and experimental log dissolution rates of Si, (B & C) Correlation between log dissolution rates of Zn to Si in LBF and ISF slags, and (D) $\delta^{66}\text{Zn}$ signatures of amorphous glassy part of slags.

6.4.1.2. $\delta^{66}\text{Zn}$ signature of crystalline phases

As LBF and ISF slags contain 80 to 84% of amorphous glassy phases (in v/v) and 4 to 19% of crystalline phases, in which 78 to 82% of total Zn were embedded in amorphous glassy part whereas 18 to 21% of Zn were in the crystalline phase of the slags. Based on the estimated $\delta^{66}\text{Zn}$ signature (section 6.4.1.1) and concentration of Zn in amorphous glassy phases, the corresponding crystalline phases $\delta^{66}\text{Zn}$ values can be calculated by a mass balance following Eq. (6.2):

$$[\text{Zn}]_{\text{Slag}} * \delta^{66}\text{Zn}_{\text{Slag}} = [\text{Zn}]_{\text{Gl}} * \delta^{66}\text{Zn}_{\text{Gl}} + [\text{Zn}]_{\text{Crys}} * \delta^{66}\text{Zn}_{\text{Crys}} \quad \text{Eq. (6.2)}$$

Where $[\text{Zn}]_{\text{Slag}}$ is the concentration of total Zn in LBF and ISF, $[\text{Zn}]_{\text{Gl}}$ is the concentration of Zn in amorphous glassy phase whereas $[\text{Zn}]_{\text{Crys}}$ is that in crystalline phases of slags. $\delta^{66}\text{Zn}_{\text{Slag}}$ is the bulk Zn isotope signatures of slags whereas $\delta^{66}\text{Zn}_{\text{Gl}}$ is the signature of Zn in amorphous glassy part and $\delta^{66}\text{Zn}_{\text{Crys}}$ is the signature of overall crystalline phases present in the slags.

Although LBF and ISF slags contain a wide range of crystalline phases (Tables 6.2 and 6.3) overall signature of overall crystalline phases is calculated and given in Table 6.6. These estimated isotopic signatures lie between 2.12‰ for LBF and 5.74‰ for ISF (Table 6.6). The calculated Zn signatures of crystalline phases can be accounted for spinels: magnesiochromite (MgCr_2O_4), franklinite (ZnFe_2O_4), magnetite ($\text{Fe}^{2+}\text{Fe}^{3+}_2\text{O}_4$) in LBF; zincchromite (ZnCr_2O_4), gahnite (ZnAl_2O_4) in ISF; and for silicates phases; hardystonite ($\text{Ca}_2\text{ZnSi}_2\text{O}_7$) and willemite (Zn_2SiO_4) for both slags.

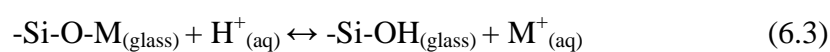
Table 6.6. Chemical composition of silicates in LBF and ISF slags.

	Zn concentration (mM g^{-1})			$\delta^{66}\text{Zn}$ signature (‰)		
	$[\text{Zn}]_{\text{Slag}}$	$[\text{Zn}]_{\text{Gl}}$	$[\text{Zn}]_{\text{Crys}}$	$\delta^{66}\text{Zn}_{\text{Bulk}}$	$\delta^{66}\text{Zn}_{\text{Gl}}$	$\delta^{66}\text{Zn}_{\text{Crys}}$
LBF (6 h N_2 atm)	1.31	1.03	0.28	0.127	-0.42	2.12
ISF (6 h N_2 atm)	1.05	0.86	0.19	0.775	-0.35	5.74

6.4.2. $\delta^{66}\text{Zn}$ fractionation induced by geochemical processes

6.4.2.1. $\delta^{66}\text{Zn}$ fractionation due to dissolution processes

During the early stage of weathering, the modification of the glass network in relation to the leaching of cations take place (van Hullebusch et al., in press; Yin et al., 2014), and ion exchange mechanisms can be depicted as follows:



According to reactions (6.3&6.4), hydrolysis initially take place (6.3) which profoundly modify the silicate network by attacking bridging bonds (Si-O-M) and the subsequent release of the silanol groups (Si-OH) leads to the production of siloxane bonds (Si-O-Si), thus, condensation reaction occurs (6.4). Both hydrolysis and condensation reactions are controlled by the solution's pHs. Hydrolysis of glass network is favored in both acidic and alkaline pHs, however, hydrolysis kinetic is much faster under acidic condition. Similarly, the condensation reaction which can take place before the completion of hydrolysis is favored in both acidic and alkaline pHs, however, condensation kinetic is much faster under alkaline conditions.

Consequently, the competition as a function of pHs between these two processes affected the dissolution of Si as well as Zn, from amorphous glassy matrix of both slags. This may explain why the first drop of leachate displayed highly fractionated Zn isotopes signatures as a function of pHs during early stage of weathering (6 h) as shown in Figure 6.6. If hydrolysis governed leaching conditions (low pHs), thus a high dissolution of Zn with a less fractionated Zn isotopes signatures from slag to leachate is expected. On the other hand, if condensation is the dominant leaching reaction (high pHs), it favors less dissolution of Zn with highly fractionated Zn isotopes signatures.

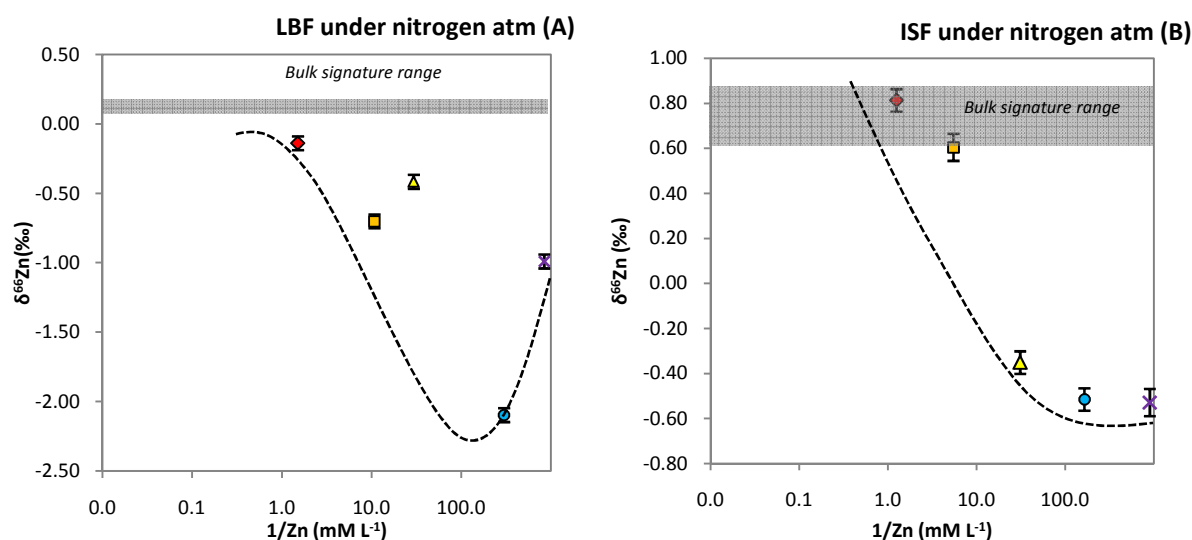


Figure 6.6. Highly fractionated Zn in the leachate during early stage weathering of (A) LBF slags and (B) ISF slags under nitrogen atmosphere.

6.4.2.2. $\delta^{66}\text{Zn}$ fractionation due to sorption(s) processes

Under oxidative weathering conditions, the presence of oxygen and carbon dioxide leads to the formation of secondary phases such as oxides, hydroxides and carbonates, after 9 days of slag-water interaction time. Zn isotopes fractionation can be expected via precipitation processes, either when Zn precipitated itself as ZnO , $\text{Zn}(\text{OH})_2$, ZnCO_3 , when it was co-operated during precipitation of $(\text{Fe}+\text{Ca}+\text{Pb}+\text{Zn})\text{CO}_3$ or, finally, via adsorption process onto the iron oxides. The fractionation of Zn isotopes due to these processes can be identified by

comparing the $\delta^{66}\text{Zn}$ signatures measured during oxic experiments to those measured under anoxic weathering experiment, where no secondary phases were formed and thus no effect of oxide and carbonates on $\delta^{66}\text{Zn}$ is expected.

Fe oxy(hydr)oxides and Zn-Al double layer hydroxides. A significant difference can be observed in the $\delta^{66}\text{Zn}$ signatures between two atmospheres during the chemical weathering of LBF and ISF slags at pH 7 (Figure 6.7). The LBF leachate displayed significantly lighter signature under open-air than under nitrogen atmospheres (-0.96‰ and -0.27‰, resp.), after 24 h of leaching time. The corresponding big delta $\Delta^{66}\text{Zn}_{\text{Nitro-Open.atm}}$ between two atmospheres is 0.70‰ (Figure 6.7A), which could be related to the formation of ferrihydrite (FeOOH), the only secondary phase actually observed at pH7. Indeed, Zn adsorption onto 2-line ferrihydrite at pH 7 was shown to induce $\Delta^{66}\text{Zn}_{\text{sorbed-solution}}$ of $0.53 \pm 0.07\text{‰}$ by Juillot et al. (2008), which is in strong agreement with the big fractionation observed in the present study between two atmospheres. This $\Delta^{66}\text{Zn}_{\text{Nitro-Open.atm}}$ continues increasing with interaction time, up to 1.5‰ after 216 h (Figure 6.7A). At this step of the experiments, PbCO_3 and Zn-Al LDH phases, in addition to FeOOH , were predicted to form by Visual MINTEQ and truly observed by TEM (Figure 6.4A). Thus, the isotopic fractionation observed could be due to the combined effects during formation of double layered Zn-Al hydroxides as well as adsorption of Zn onto FeOOH and partial cooperation of Zn during PbCO_3 precipitation, to reach a final $\delta^{66}\text{Zn}$ value of -1.65‰.

On the other hand, the ISF leachate displayed similar $\delta^{66}\text{Zn}$ values after 24h under both open-air and nitrogen atmospheres (-0.45‰ and -0.51‰, resp.), but significantly heavier after 216 h; from -0.45‰ to 0.05‰ under open-air atmosphere as well as from -0.51‰ to 0.50‰ under nitrogen atmosphere (Figure 6.7B). These heavier signatures could be due to the partial dissolution of crystalline phases (spinel, silicates, or speiss) over the long periods of time regardless of the atmospheres, for which $\delta^{66}\text{Zn}_{\text{Crys}}$ has been estimated to 5.74‰. In addition, this shift toward heavy $\delta^{66}\text{Zn}$ signatures is less pronounced for the open-air atmosphere experiment (from -0.45 to 0.05‰), with a corresponding $\Delta^{66}\text{Zn}_{\text{Nitro-Open.atm}}$ between the two leachate of 0.5‰ after 216 h of interaction (Figure 6.7B). Again, this difference could be due to PbCO_3 precipitation, where partial cooperation of Zn was confirmed by TEM (Figure 6.4B).

Zinc hydroxides precipitation. Significantly light $\delta^{66}\text{Zn}$ signatures were observed during the chemical weathering of LBF and ISF slags at pH 10 for both atmospheres (Figure 6.8). The LBF leachate displayed constantly light signatures (-2.10‰ to -2.35‰) under nitrogen atmosphere, which could be due to the rapid precipitation of $\text{Zn}(\text{OH})_2$ (Figure 6.8A). More than 90% of Zn removal can be expected from total dissolved Zn concentration via precipitation of $\text{Zn}(\text{OH})_2$ within 10 mins of reaction time (Chen et al., 2009). In addition to the $\text{Zn}(\text{OH})_2$, the co-precipitation of Pb and ZnCO_3 , observed under open-air atmosphere after 24h, probably contributed to even lighter signature (-2.83‰). The 24h big delta between the two atmospheres is $\Delta^{66}\text{Zn}_{\text{Nitro-Open.atm}}$: 0.59‰.

On the other hand, the leachate during weathering of ISF slags displayed constantly light signatures; from -0.28‰ to -0.51‰ under nitrogen atmosphere, and -0.22‰ to -0.42‰ under

open-air atmosphere (Figure 6.8B). Even though formation of various carbonates phases as well as hydroxides phases were predicted by Visual MINTEQ, none of the carbonates phases were observed under TEM analysis. Thus, these stable signatures between two atmospheres could be linked to two eligible secondary phases, which were both thermodynamically predicted and observed: $\text{Zn}(\text{OH})_2$ and $\text{Fe}(\text{OH})_2$. The fate of Zn during hydroxides precipitation remains hard to confirm: these phases can either precipitate separately, Fe and Zn can co-precipitate, or Zn can be adsorbed onto $\text{Fe}(\text{OH})_2$. If $\text{Zn}(\text{OH})_2$ precipitate separately, the induced signature of -2.10‰ (Figure 6.8A) in the solution where as adsorption of Zn onto FeOOH induced signature of -1.00‰ (Figure 6.7A), it is more likely that partial Zn co-operation inside during precipitation of $\text{Fe}(\text{OH})_2$.

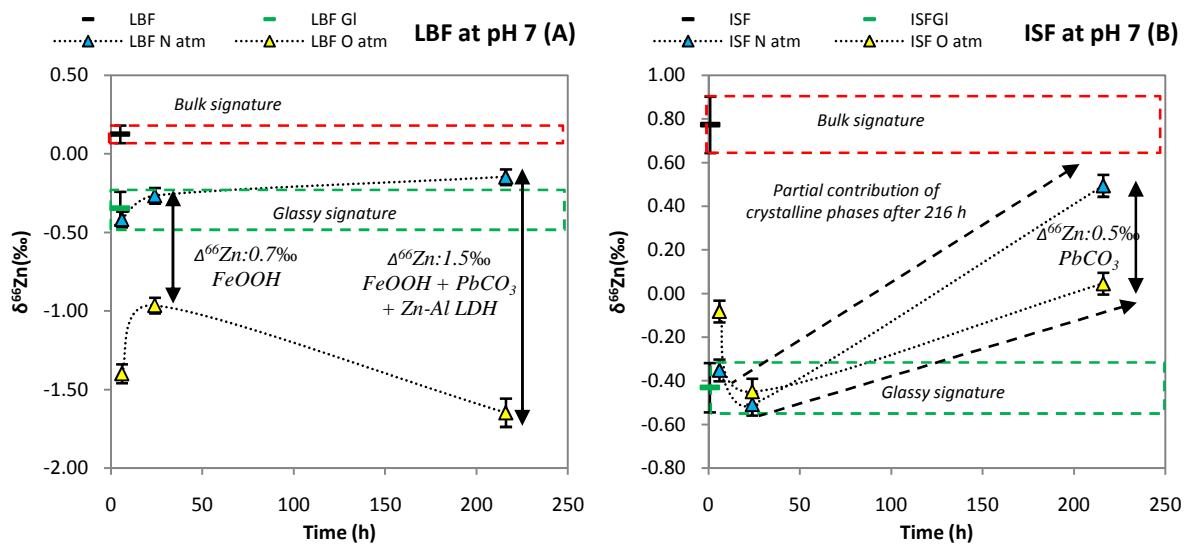


Figure 6.7. (A) Fractionation induced by FeOOH , PbCO_3 and Zn-Al LDH during weathering of LBF, and (B) Fractionation induced by PbCO_3 , during weathering of ISF.

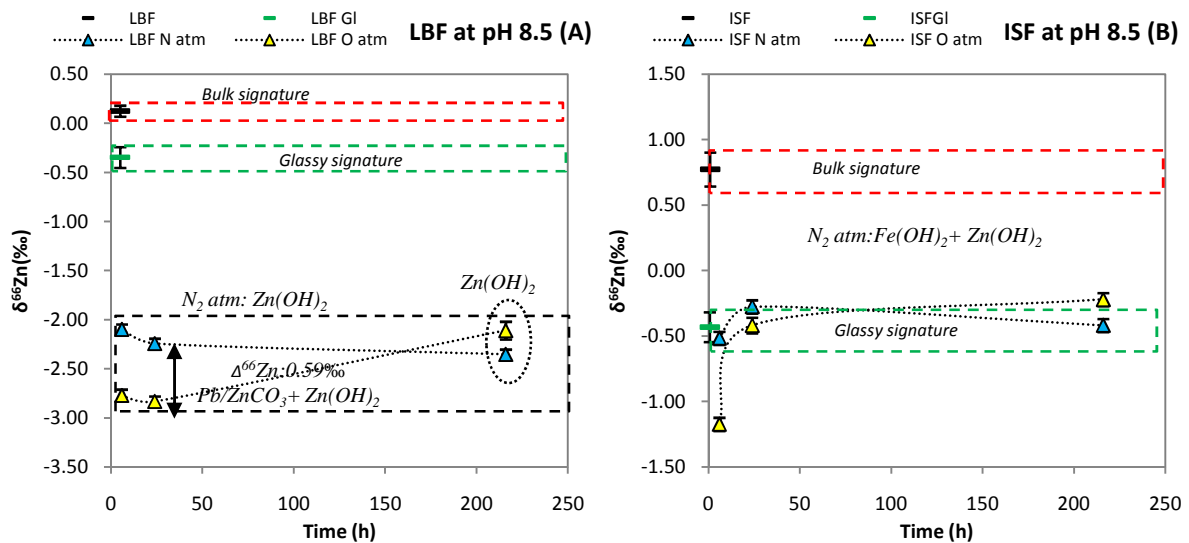


Figure 6.8. (A) Fractionation induced by $\text{Zn}(\text{OH})_2$, Pb/ZnCO_3 during weathering of LBF, and (B) Fractionation induced by $\text{Fe/Zn}(\text{OH})_2$, Pb/ZnCO_3 during weathering of ISF.

Carbonate precipitation. An important difference can be observed in the $\delta^{66}\text{Zn}$ signatures between two atmospheres during the chemical weathering of LBF and ISF slags at pH 10 (Figure 6.9). The LBF leachate displayed significantly lighter signature under open-air atmosphere than under nitrogen atmosphere (-1.28‰ and -0.15‰, resp., Figure 6.9A). A similar trend is observed for ISF leachates, with a lighter signature under open-air atmosphere compared to nitrogen atmosphere (-0.27‰ and 0.85‰, resp., Figure 6.9B). The $\Delta^{66}\text{Zn}_{\text{Nitro-Open.atm}}$ are 1.13‰ and 1.12‰ for LBF and ISF, respectively, after 216h. The potential formation of CaCO_3 , PbCO_3 , ZnO and $\text{Zn}(\text{OH})_2$ are suggested by Visual MINTEQ, however, only co-precipitation of Ca, Zn and PbCO_3 was confirmed by TEM (Figure 6.4C and D). Thus, the fractionation could be induced by co-precipitation of Ca and PbCO_3 with partial cooperation of Zn inside with rather consistent $\Delta^{66}\text{Zn}_{\text{Nitro-Open.atm}}$ values (1.13‰) for both slags.

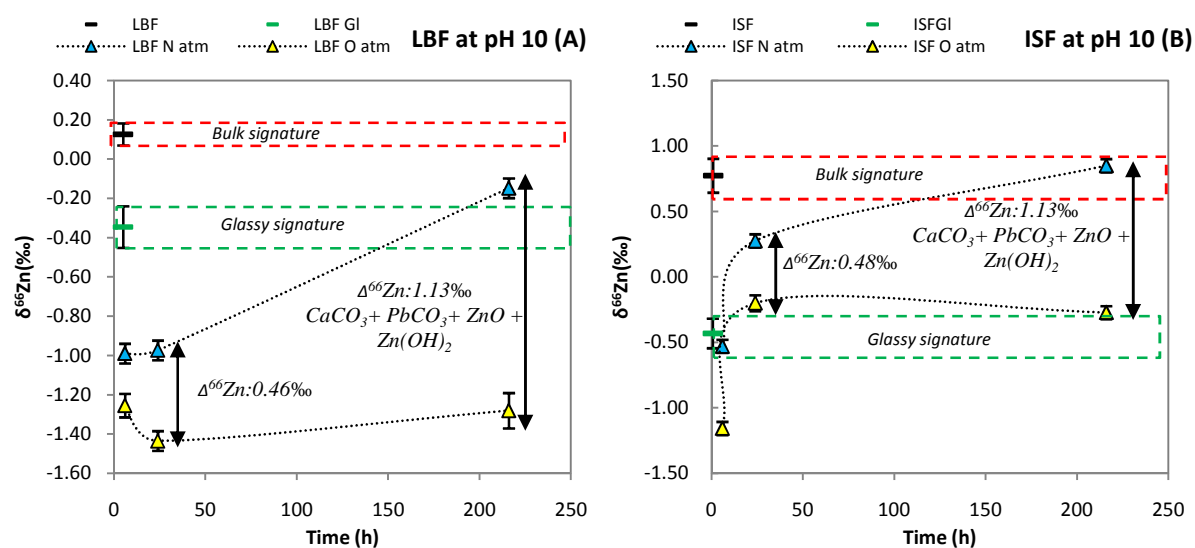


Figure 6.9. Fractionation induced by Zn cooperation inside co-precipitation of CaCO_3 and PbCO_3 during weathering of LBF (A), and that of ISF (B).

6.4.3. Fractionation factors from slags to leachate

Zn isotopes fractionation observed during chemical weathering of LBF and ISF slags were induced by the changes in pH, and the effect of different atmosphere. The corresponding fractionation extent $\Delta^{66}\text{Zn}_{\text{slag-leachate}}$ from slags to leachate is summarized in Table 6.7. During chemical weathering of LBF slags, the highest Zn isotopes fractionations occurred at pH 4 and 5.5 under nitrogen atmosphere, and at pH 7 and 10 under open-air atmosphere. This difference could be reasonably explained by the adsorption of Zn onto FeOOH , partial cooperation of Zn inside PbCO_3 , and formation of Zn-Al LDH at pH 7, as well as (co)precipitation of ZnCO_3 along with Ca and PbCO_3 at pH 10 which induced higher fractionation. On the other hand, the fractionation was consistent at pH 8.5, where $\text{Zn}(\text{OH})_2$ precipitation is dominant, regardless of the effect of atmosphere. During weathering of ISF slag, the fractionation of slag to leachate is slightly higher at pH 7 and 8.5 under open-air atmosphere which could be due to the partial cooperation of Zn inside PbCO_3 at pH 7 and co-

precipitation Fe and Zn(OH)₂ at pH 8.5. In addition, the (co)precipitation of ZnCO₃ with Ca and PbCO₃ induced much higher fractionation under open-air atmosphere at pH 10.

Table 6.7. The fractionation of Zn isotopes from slag to leachate: $\Delta^{66}\text{Zn}_{\text{slag-leachate}}$.

pH	$\Delta^{66}\text{Zn}_{\text{slag-leachate}}$ per mil for LBF slags				$\Delta^{66}\text{Zn}_{\text{slag-leachate}}$ per mil for ISF slags			
	Open-air atm	SD	Nitrogen atm	SD	Open-air atm	SD	Nitrogen atm	SD
4	0.05	0.03	0.21	0.07	-0.11	0.02	-0.03	0.02
5.5	0.14	0.05	0.49	0.30	0.45	0.33	0.02	0.13
7	1.46	0.35	0.40	0.14	0.94	0.26	0.90	0.54
8.5	2.70	0.40	2.36	0.13	1.38	0.50	1.18	0.12
10	1.45	0.10	0.83	0.48	1.32	0.53	0.57	0.69

6.5. Conclusion

Zn isotopes were significantly fractionated during chemical weathering of both LBF and ISF slags. The extent of fractionation was greatly influenced by changes in solution pHs (heavier signatures at low pHs and lighter signature at high pHs); leaching time (lighter signatures during 6 h of leaching compared to heavier signature at 216 h); different atmospheres (fractionation induced by secondary precipitates such as oxide, carbonates and (oxy)hydroxides under open-air atmosphere vs. hydroxides under nitrogen atmosphere). In addition, the signatures of primary phases of slags were extrapolated where the amorphous glassy signature lies -0.42‰ for LBF and -0.35‰ for ISF, whereas the overall crystalline signature lies 2.12‰ for LBF and 5.74‰ for ISF.

6.6. References

- Audry, S., Schafer, J., Blanc, G., Jouanneau, J.M., 2004. Fifty-year sedimentary record of heavy metal pollution (Cd, Zn, Cu, Pb) in the Lot River reservoirs (France). *Environ Pollut*, 132: 413-426.
- Barna, R., Moszkowicz, P., Gervais, C., 2004. Leaching assessment of road materials containing primary lead and zinc slags. *Waste Manage*, 24: 945-955.
- Borrok, D., Wanty, R., Ridley, W., Wolf, R., Lamothe, P., Adams, M., 2007. Separation of copper, iron, and zinc from complex aqueous solutions for isotopic measurement. *Chem Geol*, 242: 400-414.
- Carroll, S.A., Maxwell, R.S., Bourcier, W., Martin, S., 2002. Evaluation of silica-water surface chemistry using NMR spectroscopy. *Geochim Cosmochim Acta*, 66: 913-926.
- Chen, Q., Luo, Z., Hills, C., Xue, G., Tyrer, M., 2009. Precipitation of heavy metals from wastewater using simulated flue gas: sequent additions of fly ash, lime and carbon dioxide. *Water Res*, 43: 2605-2614.
- Cloquet, C., Carignan, J., Lehmann, M.F., Vanhaecke, F., 2008. Variation in the isotopic composition of zinc in the natural environment and the use of zinc isotopes in biogeosciences: A review. *Anal Bioanal Chem*, 390: 451-463.
- De Andrade Lima, L.R.P., Bernardez, L.A., 2012. Isotope Source Signatures for a Primary Lead Smelter Located Close to Todos os Santos Bay, Brazil. *Soil Sediment Contam: An Int J*, 20: 672-687.
- Deneele, D., 2002. Caractérisation, simulations expérimentales et thermodynamiques de l'altération de déchets vitreux: les scories de première fusion de plomb et de zinc. *PhD thesis manuscript*, Université Des Sciences et Technologies de Lille I and U.F.R. Des Sciences De La Terre, France, 1-242.
- Dolgoplova, A., Weiss, D.J., Seltmann, R., Kober, B., Mason, T.F.D., Coles, B., Stanley, C.J., 2006. Use of isotope ratios to assess sources of Pb and Zn dispersed in the environment during mining and ore processing within the Orlovka–Spokoinoe mining site (Russia). *App Geochem*, 21: 563-579.
- Ettler, V., Johan, Z., 2003b. Mineralogy of metallic phases in sulphide mattes from primary lead smelting. *Compt Ren Geosci*, 335: 1005-1012.
- Ettler, V., Komarkova, M., Jehlicka, J., Coufal, P., Hradil, D., Machovic, V., Delorme, F., 2004. Leaching of lead metallurgical slag in citric solutions-implications for disposal and weathering in soil environments. *Chemosphere*, 57: 567-577.
- Ettler, V., Johan, Z., Kříbek, B., Šebek, O., Mihaljevič, M., 2009. Mineralogy and environmental stability of slags from the Tsumeb smelter, Namibia. *Appl Geochem*, 24: 1-15.

- Gélabert, A., Pokrovsky, O.S., Viers, J., Schott, J., Boudou, A., Feurtet-Mazel, A., 2006. Interaction between zinc and freshwater and marine diatom species: surface complexation and Zn isotope fractionation. *Geochim Cosmochim Acta*, 70: 839-857.
- Halliday, A.N., Lee, D.-C., Christensen, J.N., Walder, A. J., Freedman, P.A., Jones, C. E., Hall, C.M., Yi, W., and Teagle, D., 1995. Recent developments in inductively coupled plasma magnetic sector multiple collector mass spectrometry, *Int. J. Mass Spec. Ion Process*, 146: 21-33.
- Johnson, C.M., Beard, B.L., Albarède, F., 2004. Overview and general concepts. *Rev Mineral Geochem*, 55: 1-24.
- Jouvin, D., Louvat, P., Juillot, F., Marechal, C.N., Benedetti, M.F., 2009. Zinc Isotopic Fractionation: Why Organic Matters. *Environ Sci Technol*, 43: 5747-5754.
- Juillot, F., Maréchal, C., Ponthieu, M., Cacaly, S., Morin, G., Benedetti, M., Hazemann, J.L., Proux, O., Guyot, F., 2008. Zn isotopic fractionation caused by sorption on goethite and 2-Lines ferrihydrite. *Geochim Cosmochim Acta*, 72: 4886-4900.
- Juillot, F., Maréchal, C., Morin, G., Jouvin, D., Cacaly, S., Telouk, P., Benedetti, M.F., Ildefonse, P., Sutton, S., Guyot, F., Brown, G.E., 2011. Contrasting isotopic signatures between anthropogenic and geogenic Zn and evidence for post-depositional fractionation processes in smelter-impacted soils from Northern France. *Geochim Cosmochim Acta*, 75: 2295-2308.
- Lottermoser, B.G., 2002. Mobilization of heavy metals from historical smelting slag dumps, north Queensland, Australia. *Mineral Mag*, 66: 475-490.
- Mahé-Le Carlier, C., Le Carlier de Veslud, C., Ploquin, A., Royer, J.J., 2000. Altération des scories de la métallurgie ancienne: un analogue de déchets vitrifiés. *Compt. Rend. Acad. Sci. (Paris), Série II. Sciences de la Terre et des planètes*, 330: 179-184.
- Marechal, C., Telouk, P., Albarede, F., 1999. Precise analysis of copper and zinc isotopic compositions by plasma-source mass spectrometry. *Chem Geol*, 156: 251-273.
- Mason, T.F.D., Weiss, D.J., Horstwood, M., Parrish, R.R., Russel, S.S., Mullane, E., Coles, B.J., 2004a. Spectral interferences and their correction. *J Anal At Spectrom*, 19: 209-217.
- Mason, T.F.D., Weiss, D.J., Horstwood, M., Parrish, R.R., Russel, S.S., Mullane, E., Coles, B., 2004b. High-precision Cu and Zn isotope analysis by plasma source mass spectrometry. Part 2. Correcting for mass discrimination effects. *J Anal At Spectrom*, 19: 218-226.
- Mattielli, N., Petit, J.C.J., Deboudt, K., Flament, P., Perdrix, E., Taillez, A., Rimetz-Planchon, J., Weis, D., 2009. Zn isotope study of atmospheric emissions and dry depositions within a 5 km radius of a Pb-Zn refinery. *Atmos Environ*, 43: 1265-1272.
- Petit, J.C.J., Jong, J.D.J., Chou, L., Mattielli, N., 2008. Development of Cu and Zn isotope MC-ICP-MS measurements: application to suspended particulate matter and sediments from the Scheldt Estuary. *Geostd Geoanal Res*, 32: 149-166.

- Piatak, N.M., Seal, R.R., Hammarstrom, J.M., 2004. Mineralogical and geochemical controls on the release of trace elements from slag produced by base- and precious-metal smelting at abandoned mine sites. *Appl Geochem*, 19: 1039-1064.
- Piatak, N.M., Seal, R.R., 2010. Mineralogy and the release of trace elements from slag from the Hegeler Zinc smelter, Illinois (USA). *Appl Geochem*, 25: 302-320.
- Pokrovsky, O.S., Viers, J., Freydier, R., 2005. Zinc stable isotope fractionation during its adsorption on oxides and hydroxides. *J Colloid Interface Sci*, 291: 192-200.
- Puziewicz, J., Zainoun, K., Bril, H., 2007. Primary phases in pyrometallurgical slags from a zinc-smelting waste dump, swietochlowice, upper silesia, poland. *Can Mineral*, 45: 1189-1200.
- Rehkämper, M., Schönbacher, M., Stirling, C.H., 2001. Multiple collector ICP-MS: introduction to instrumentation, measurement techniques and analytical capabilities. *J Geostd Geoanal*, 25: 23-40.
- Shiel, A.E., Weis, D., Orians, K.J., 2010. Evaluation of zinc, cadmium and lead isotope fractionation during smelting and refining. *Sci Total Environ*, 408: 2357-2368.
- Sivry, Y., Riotte, J., Sonke, J., Audry, S., Schafer, J., Viers, J., Blanc, G., Freydier, R., Dupre, B., 2008. Zn isotopes as tracers of anthropogenic pollution from Zn-ore smelters The Riou Mort-Lot River system. *Chem Geol*, 255: 295-304.
- Sobanska, S., Ledésert, B., Deneele, D., Laboudigue, A., 2000. Alteration in soils of slag particles resulting from lead smelting. *Earth Planet Sci*, 331: 271-278.
- Thapalia, A., Borrok, D., Van Metre, P.C., Musgrove, M., Landa, E.R., 2010. Zn and Cu isotopes as tracers of anthropogenic contamination in a sediment core from an urban lake. *Environ Sci Tech*, 44: 1544-1550.
- van Hullebusch, E.D., Yin, N.H., Seignez, N., Labanowski, J., Gauthier, A., Lens, P.N.L., Avril, C., Sivry, Y., in press. Bio-alteration of metallurgical wastes by *Pseudomonas aeruginosa* in a semi flow-through reactor. *J Environ Manage*.
- Weiss, D.J., Rausch, N., Mason, T.F.D., Coles, B.J., Wilkinson, J.J., Ukonmaanaho, L., Arnold, T., Nieminen, T.M., 2007. Atmospheric deposition and isotope biogeochemistry of zinc in ombrotrophic peat. *Geochim Cosmochim Acta*, 71: 3498-3517.
- Yin, N.H., Sivry, Y., Avril, C., Borensztajn, S., Labanowski, J., Malavergne, V., Lens, P.N.L., Rossano, S., van Hullebusch, E.D., 2014. Bioweathering of lead blast furnace metallurgical slags by *Pseudomonas aeruginosa*, *Int Biodeterior Biodegrad*, 86: 372-381.
- Zhu, X.K., Guo, Y., Williams, R.J.P., O'Nions, R.K., Matthews, A., Belshaw, N.S., Canters, G., Canters, E.C., de Waal, E.C., Weser, U., Burgess, B.K., Salvato, B., 2002. Mass fractionation processes of transition metal isotopes. *Earth Planet Sci Lett*, 200: 47-62.

CHAPTER 7

Bioweathering of lead blast furnace metallurgical slags by *Pseudomonas aeruginosa*

This chapter has been published as:

Yin, N.H., Sivry, Y., Avril, C., Borensztajn, S., Labanowski, J., Malavergne, V., Lens, P.N.L., Rossano, S., van Hullebusch, E.D., 2014. Bioweathering of lead blast furnace metallurgical slags by *Pseudomonas aeruginosa*, *Int Biodeterior Biodegrad*, 86(C): 372-381.DOI: 10.1016/j.ibiod.2013.10.013

Chapter 7

7.1. Introduction

Metallurgy of non-ferrous materials, especially lead blast furnace (LBF), is known to generate huge amounts of primary smelting slags (Verguts, 2005). They are unwanted metallurgical wastes whose grade is too low for further treatment and of low economic value in spite of being a significant component of waste streams from non-ferrous metallurgical industries. As they are usually dumped in the vicinity of the smelting site and accumulated for long periods of time, they are exposed to the open atmosphere and rainfalls, and are thus susceptible to the weathering which consequently could result in the metal leaching (Piatak and Seal, 2010). In northern France, about 4 million tons of these potentially hazardous materials have been landfilled in the industrial basin of Nord-Pas-de-Calais. Several studies have mentioned the risk associated to the release of toxic compounds by these wastes (Barna et al., 2004; Ettler and Johan, 2003b; Lima and Bernardez, 2011; Parsons et al., 2001; Piatak and Seal, 2010; Seignez et al., 2006). LBF slags generated in the industrial basin of Nord-Pas-de-Calais are granulated materials equivalent to a glass-ceramic rich in Zn (10–12 wt%), Pb (0.5–3 wt%) and other elements such as Cr, Cd, and As present in lower amount (Seignez et al., 2006). Crystalline phases (spinel and wüstite) contained in LBF slags are generally stable in batch and open flow experiments. In contrast, fayalite (Fe_2SiO_4), melilite $(\text{Ca,Na})_2(\text{Al,Mg,Fe}^{2+})[(\text{Al,Si})\text{SiO}_7]$, sulfides, glass matrix and metallic Pb droplets are often partially or totally dissolved (Ettler et al., 2002). Generally, the altered layers are relatively enriched in Si, Fe and Al. Exposed to weathering, the iron–silica–lime glass matrix is progressively depleted in alkali and alkaline-earth elements, e.g. Na, K, and Ca. Other elements (e.g. Pb, Zn) can also be noticeably released (Ettler et al., 2001). In oxidizing conditions, Fe (II) ions contained in the glass matrix are usually transformed into Fe(III) and remain in place (Mahé-Le Carlier et al., 2000).

Considering the potential hazards that the slags and dust emitted by the furnace waste residues may represent, a large number of works were interested in their fate in landfill conditions (Mahé-Le Carlier et al., 2000), in soils or soil-like environments (Ettler et al., 2004; Sivry et al., 2010; Sobanska et al., 2000) and in others various open flow (Seignez et al., 2006; Seignez et al., 2008; Sivry et al., 2008) or batch (Ettler and Johan, 2003b; Ettler et al., 2002) experiments. However, few studies have focused on the role of microorganisms in the weathering of these materials (Willscher and Bosecker, 2003). For instance, previous studies have suggested that the microbial activity influences the weathering process and thus the rate of leaching of potentially toxic elements (Cheng et al., 2009; Willscher et al., 2007).

The deterioration of minerals and materials of anthropogenic origin (stained glasses, cements, blast-furnace slags) depends partly on the presence of organic or inorganic compounds and micro-organisms (Uroz et al., 2009). Banerjee and Muehlenbachs (2003) have pointed out that bacteria accelerate the deterioration of marine basaltic glasses due to the observation of “hair channels” that could represent bacterial activity. Another aspect of microbial activity is the potential toxic metals sequestration by the bacteria and the exopolymers they produce

(Guibaud et al., 2012). Apart from some well-defined cases, such as the biodeterioration of stainless steel or concrete cement in sewer pipes by bacterial strains such as *Acidithiobacillus* genus (Herisson et al., 2013; Okabe et al., 2007; Roberts et al., 2002), the exact role of micro-organisms remains to be deciphered. The principal difficulty is to determine whether the degradation observed under the layers rich in living micro-organisms are due to microbial action (acidification, complexation), or is simply explained by the higher water retention of these layers (Uroz et al., 2009). Micro-organisms may only benefit from the availability of water and nutrients produced by pure physicochemical reactions (dissolution, precipitation, sorption reactions) without actively accelerating deterioration processes. LBF slags have been open-dumped in the vicinity of the lead smelters. In addition, these slags have been deposited on soils (Douay et al., 2008) and significant amount of slags have been removed from dredged sediments of the nearby passing river (Vdovic et al., 2006). Thus, the experiments were designed to simulate the weathering conditions where the slag comes into contact with the water and bacteria. As sediments and soils contain a significant amount of biodegradable organic matter, one might expect that heterotrophic bacteria are the predominant active micro-organisms.

The present study aims to investigate the effect of heterotrophic bacteria on the aqueous weathering of LBF slags. *Pseudomonas aeruginosa* has been chosen as a proxy of heterotrophic bacteria as this bacterium is well-known for its affinity towards Fe and iron scavenging by production of siderophores possibly also involved in enhance solubilisation of metals such as zinc and lead (Schalk et al., 2011). The leachate chemistry was studied and the rate of elemental release during bacteria-slugs interactions was determined under laboratory scale conditions. A specific focus was given on major elements involved in the FeO-SiO₂-CaO glass matrix and trace elements (Pb and Zn). Scanning Electron Microscopy (SEM) with Energy Dispersive X-Ray Analysis (EDX) has been used to characterize fresh and altered slags in order to give insights regarding the mechanisms of alteration of the slag mineralogy and the formation of secondary mineral phases. The Visual Minteq software was further used to model the leachate chemistry.

7.2. Materials and Methods

7.2.1. Chemical composition of the slag

The slag contains eight major and minor elements as shown in Table 7.1. It is mainly composed of an iron-calcium and silica matrix: Fe (224 g kg⁻¹), Si (101 g kg⁻¹) and Ca (140 g kg⁻¹) where the matrix is significantly enriched in metals: Zn (85 g kg⁻¹) and Pb (31 g kg⁻¹). Along with the major elements, trace amount of As, Ba, Cd, Cr, Cu, Mo, Na and Ni are present as well.

Table 7.1. Chemical composition of lead blast furnace slag, based on X-ray fluorescence spectrometry (XRF) & acid digestion analysis.

Major elements (g kg ⁻¹)	Al	Ca	Fe	Mg	Mn	Pb	Si	Zn
	11.0	139.5	224.2	10.5	5.4	30.7	100.8	85.0
Trace elements (g kg ⁻¹)	As	Ba	Cd	Cr	Cu	Mo	Na	Ni
	0.05	5.53	0.01	0.55	0.78	0.18	4.15	0.07

7.2.2. Standardized leaching tests procedures

Simple extraction experiments were conducted according to standardized short-term leaching protocols proposed by the EU and US EPA (European norm EN 12457 and Toxicity Characteristic Leaching Procedure ~ TCLP, respectively). Their main objective was to assess the hazardous properties of slags with respect to regulatory limits defined by the European Committee for Standardization (CEN) and by the USEPA for EN 12457 and TCLP, respectively (more information is given in the supporting information). No micro-organisms were inoculated in these experiments.

7.2.3. Abiotic and biotic leaching experiments

Three different experimental conditions were investigated: ultrapure water (UPW), sterile growth media (GM) and growth media with bacteria (GM+B). *Pseudomonas aeruginosa* (strain no. CIP 105094), purchased from the Institut Pasteur (Paris, France) was used in the bioweathering experiments. The standard succinate medium was used because it was known to permit the synthesis of greater amounts of siderophores for *Pseudomonas* species (Rachid and Ahmed, 2005), but also allows to quantitatively determine the amounts of major elements solubilized during alteration studies (Aouad et al., 2005). One liter of growth medium modified from (Aouad et al., 2008) was composed of (i) 4 g of succinic acid-C₄H₆O₄ (ii) 1 g of ammonium sulfate-(NH₄)₂.SO₄ (iii) 1 g of sodium phosphate dibasic-Na₂HPO₄ (iv) 6 g of Tris buffer-C₄H₁₁NO₃. Finally, the medium was adjusted to pH 7.8 using NaOH. In parallel to biotic experiments, abiotic experiments were performed in both UPW and sterile GM. The experiments were duplicated and were conducted in acid-washed polycarbonate bottles for a time horizon of 4 to 8 months. 2.5 g of crushed slag sample (about 2 mm diameter size) were placed in 75 mL of each leaching solution to obtain a L/S ratio of 30. Reactors were placed at room temperature (22±2°C) on horizontal shakers (at 100 rpm). 5 mL of leachate were periodically sampled, and replaced by an equivalent quantity of corresponding leaching medium to maintain the L/S ratio constant.

7.2.4. Thermodynamic modeling

In parallel to the leaching experiments, the chemical equilibrium code Visual MINTEQ v3.0 was used to calculate the saturation indexes and to identify the possible phases controlling solubility. The elemental concentrations measured from the different leaching media were input into the model. Besides, the temperature was kept constant at 25°C, the oversaturated solids were not allowed to precipitate, and the CO₂ partial pressure fixed at 396 ppmv. The

model outputs from UPW and GM were used to study the influence of carbonation and the effect of the growth medium composition. Likewise, the model outputs from GM and GM+B media were used to study the effect of bacteria on the metal speciation.

7.2.5. Analytical methods

Surface morphology of both fresh and weathered LBF samples were examined using SEM (Ultra 55 ZEISS) operating at 15 KeV. Qualitative chemical analyses of the slags were acquired by the acid digestion method and by X-ray fluorescence (XRF) using Panalytical X fluorescence spectrometer equipped with an Energy Dispersive Minipal 4 (Rh X Ray tube-30kV-9W) at a resolution of 150 eV (Mn K α).

Total concentrations of major elements (Ca, Fe, Si, Zn, Pb and Mg), as well as minor elements (As, Ba, Cd, Cr, Cu, Mo, Na, Ni) were measured in the leachates by Inductively Coupled Plasma Optical Emission Spectrometry (ICP-OES, Perkin Elmer Optima 6300). The leachates were acidified with HNO₃ for the UPW and GM experiments and the samples from the GM+B experiments were subjected to an acid digestion step upon HClO₄ addition and gentle heating. Note that all liquid samples were filtered on 0.2 μ m polycarbonate filter membrane prior acid treatments. The detection limit was typically 5-10 ppb for most elements and the external precision of \pm 5%. Quality assurance and quality control (QA/QC) samples, laboratory blanks, calibration check, and sample duplicates were performed to ensure the data quality and validity. In the biotic experiments, an absorbance spectrophotometer was used to monitor bacterial growth by measuring optical density at 600 nm. The pH was monitored using a “WTW pH 340i” pH-meter.

7.3. Results

7.3.1. Standardized leaching tests

The leaching results of As, Ba, Pb and Zn following both EN 12457 and TCLP procedures were compared with the respective regulatory concentration levels of each leaching test (Figure 7.1). Results from the EN 12457 leaching test showed that concentrations of As, Ba and Pb were generally below the limits imposed for both non-hazardous and hazardous wastes (Figure 7.1a). Likewise, the same trend was observed for the TCLP test (Figure 7.1b). There was no regulatory limit set for Zn in both protocol tests in spite of the high concentration leached out. At the end of the leaching experiments, the final pH was around 6.8 (\pm 0.1) and 8.2 (\pm 0.2) in the TCLP and EN tests, respectively.

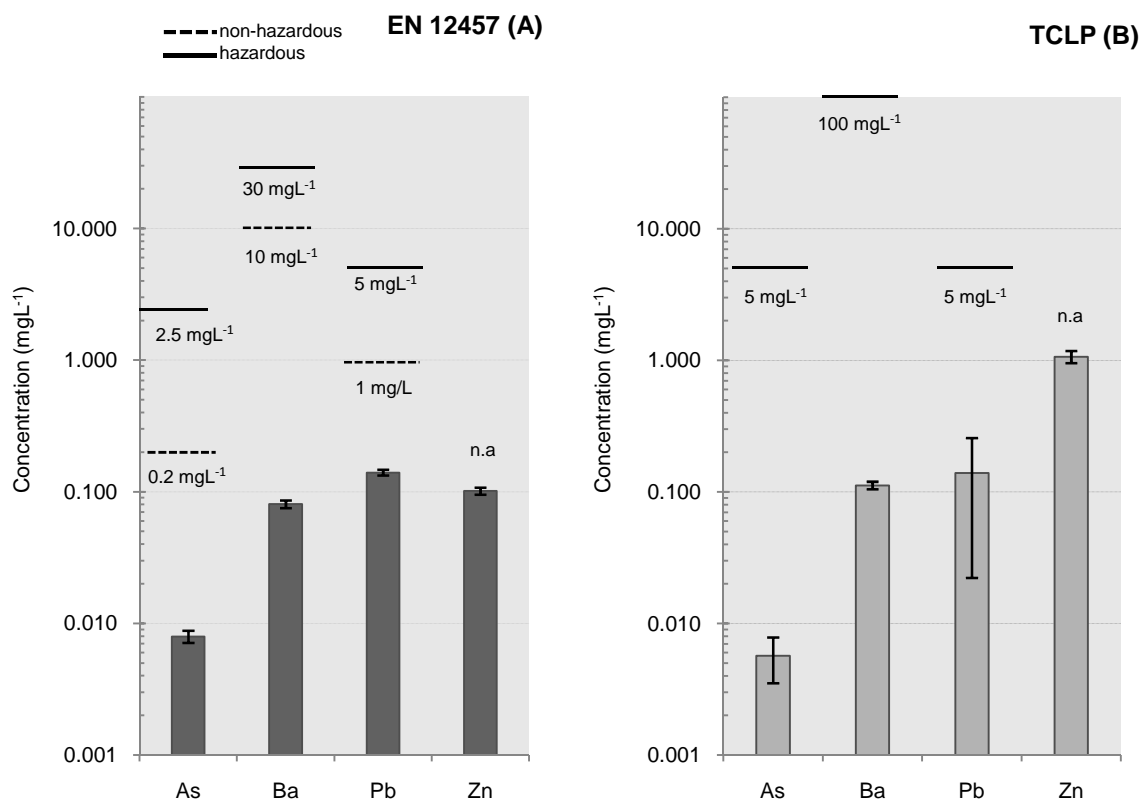


Figure 7.1. Results of protocol leaching test (a) EN 12457, (b) TCLP and comparison with respective regulatory concentration levels.

7.3.2. LBF as micro-nutrients substrate for micro-organisms and consequence on pH evolution

The fastest growth of *Pseudomonas aeruginosa* can be observed in the presence of LBF slags with a maximum absorbance of 1.1 (Figure 7.2a). In contrast, it hardly reached an absorbance value of 0.01 in the absence of slags, showing poor bacterial growth. It can be concluded that the microbial growth was not only possible, but was also enhanced in the presence of slags, these latter serving as (micro)nutrients source for the growth (Aouad et al., 2006). The decrease in absorbance after 1000 hours incubation was likely due to biofilm formation around the LBF slags.

Starting from an initial value of 5.6, the pH of the UPW solution gradually increased to 6.8 in 254 hrs before remaining stable throughout the whole experiment (Figure 7.2b). On the other hand, the initial pH of both the GM and GM+B solution was equal to 7.8, a value exceeding that of the UPW solution due to the presence of TRIS buffer and to the initial pH adjustment with NaOH (Figure 7.2b). The pH of GM remained constant around 7.7-7.9 throughout the experiment, while in presence of *Pseudomonas aeruginosa*, it increased up to 9.1 after 2057 hrs.

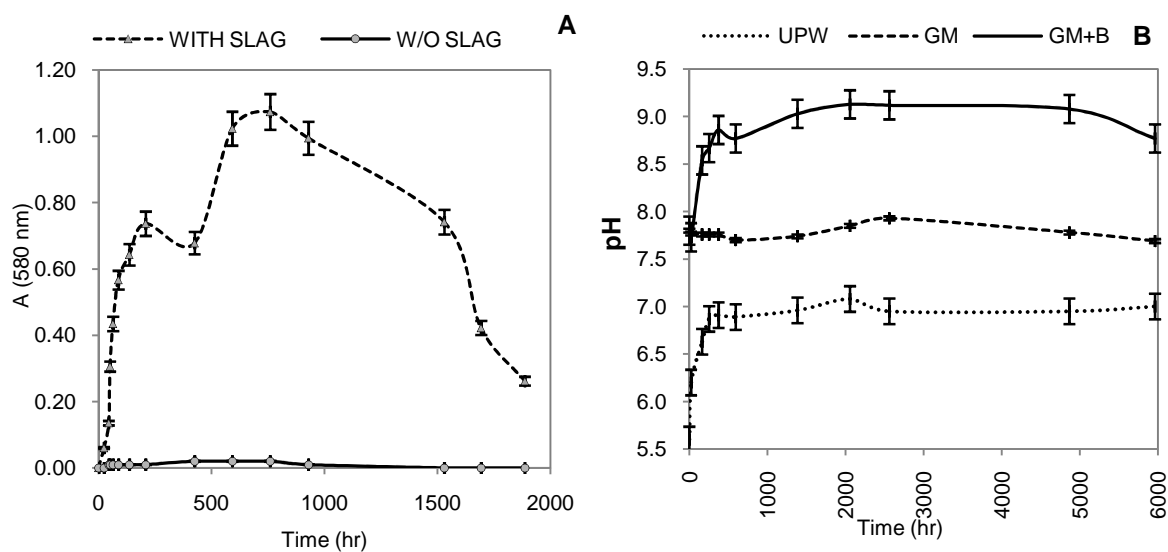


Figure 7.2. (a) Growth evolution of *Pseudomonas aeruginosa* as a function of time with or without slag, and (b) Evolution of pH in different media.

7.3.3. Leachate chemistry

The Ca concentration in GM+B was the highest, 18.4 mg L^{-1} compared to that in UPW and GM, 5.6 to 8.7 mg L^{-1} (Figure 7.3a). The concentration of Mg leached out in UPW was the lowest (i.e. 0.6 mg L^{-1}), whereas it was 2 times higher in GM and GM+B media (i.e. 1.2 mg L^{-1} and 1.3 mg L^{-1} , respectively, Figure 7.3b). The release of Si in all media increased gradually with time as shown in Figure 7.3c. The release of Si in the presence of bacteria reached maximum 6.1 mg L^{-1} whereas the maximum concentrations found in UPW and GM was 2.9 mg L^{-1} and 5 mg L^{-1} respectively. The Fe concentration in UPW and GM was around 0.01 mg L^{-1} (Figure 7.3d). In contrast, the concentration of Fe in the presence of bacteria was much higher and varies between 0.4 - 1.6 mg L^{-1} throughout the experiment. Zn concentration in the presence of bacteria gradually increased from 0.6 to 1.5 mg L^{-1} (Figure 7.3e). A similar range was found in UPW (1.1 - 1.4 mg L^{-1}) whereas GM had the lowest Zn concentration (less than 0.5 mg L^{-1}). A rather stable and gradual increase of Pb concentration, from 0.2 to 1.1 mg L^{-1} , was found in GM+B media as shown in Figure 7.3f. Moreover, the Pb concentration in UPW was higher than in GM (0.2 - 0.5 mg L^{-1} versus 0.1 - 0.4 mg L^{-1} , respectively).

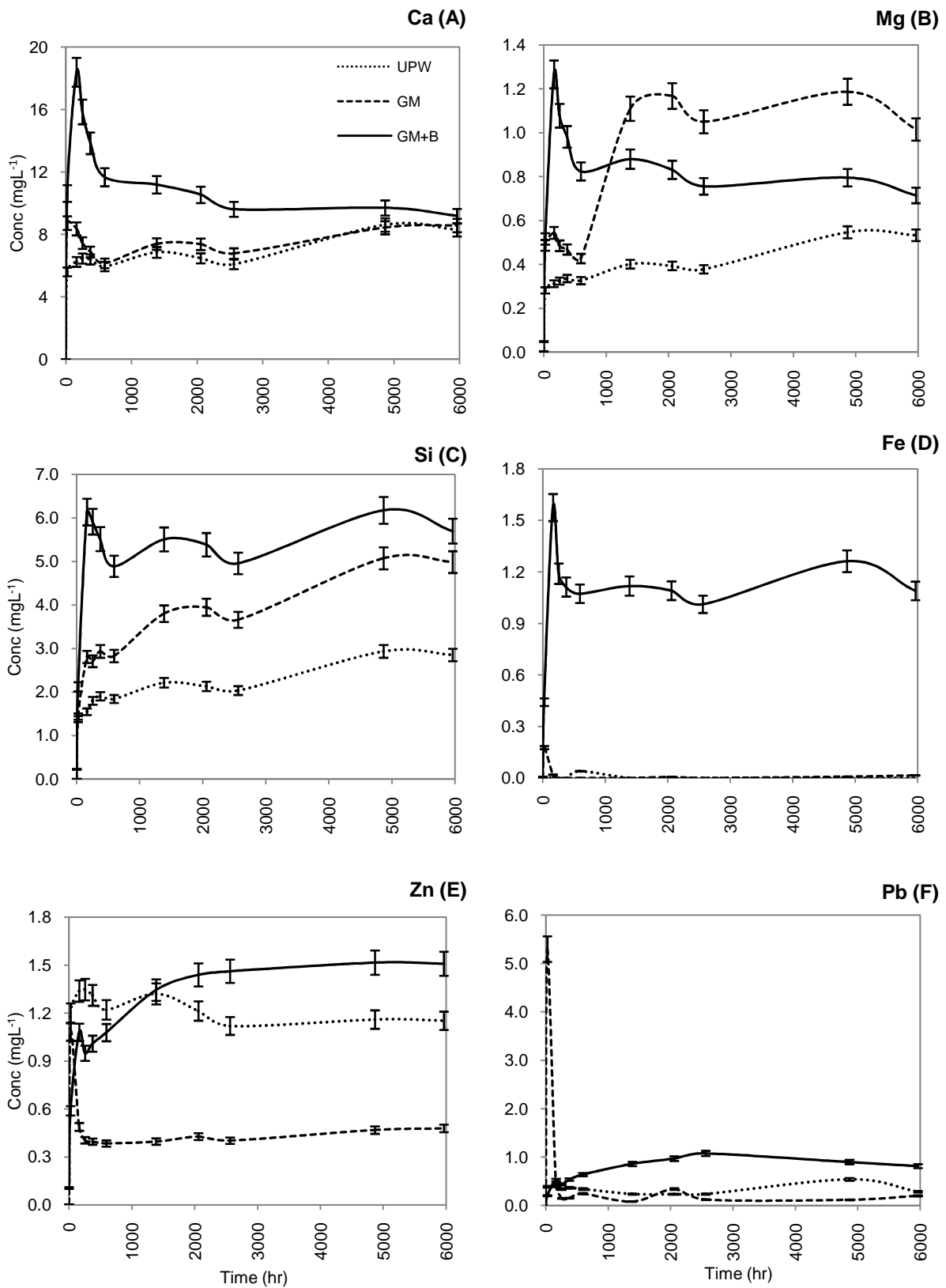


Figure 7.3. Total concentrations in solution of (a) Ca; (b) Mg; (c) Si; (d) Fe; (e) Zn and (f) Pb

7.3.4. Bulk release of the elements

At the end of the experiment, the cumulative amount of major elements leached out was normalized per unit weight of LBF slag (Table 7.2). The bulk release of Ca, Mg, Pb and Si in GM+B was almost two times higher than those in UPW, meaning that the presence of bacteria significantly increased and enhanced matrix dissolution of glassy materials. The bulk Zn release was almost the same in UPW and GM+B, whereas the Fe bulk release was solely due to the presence of bacteria.

Table 7.2. Cumulative bulk release of major elements from slag after 6 months of alteration.

Cumulative leached out (mg g ⁻¹ of LBF)			
Elements	UPW	GM	GM+B
Ca	2.16	2.50	3.83
Mg	0.12	0.25	0.27
Fe	0.00	0.01	0.33
Zn	0.40	0.16	0.37
Pb	0.11	0.24	0.22
Si	0.66	1.05	1.59

UPW: Ultra pure water, GM: Sterile growth media and GM+B: Growth media with bacteria

7.3.5. Thermodynamic modeling

In UPW, Pb solubility was mainly controlled by carbonate and hydroxide phases (Figure 7.4a) and Si was controlled by quartz formation (Figure 7.4b). For other elements including Zn, the concentrations did not reach the saturation, thus, their solubility was not controlled by precipitates formation.

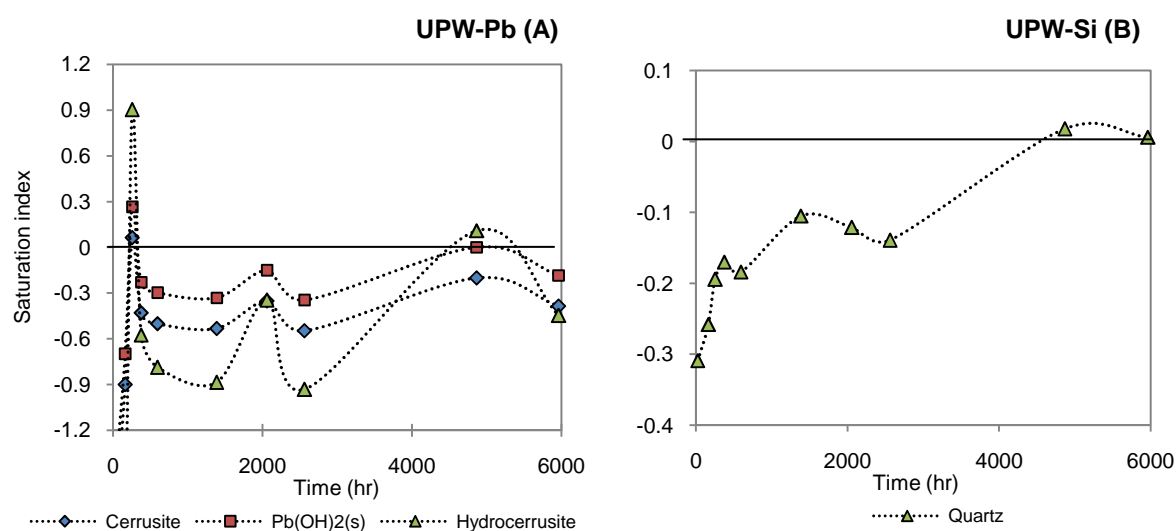


Figure 7.4: Saturation indexes of solubility controlling phases for Pb (a) and Si (b) in UPW medium.

In GM medium, phosphate was the main species controlling the solubility of Ca, Zn and Pb (Figures 7.5a,c,d). Precipitation of these phases was favored as the saturation indexes were ranging from 0.2 to 1.4. Unlike other elements, Si was controlled by the quartz concentration (Figure 7.5b).

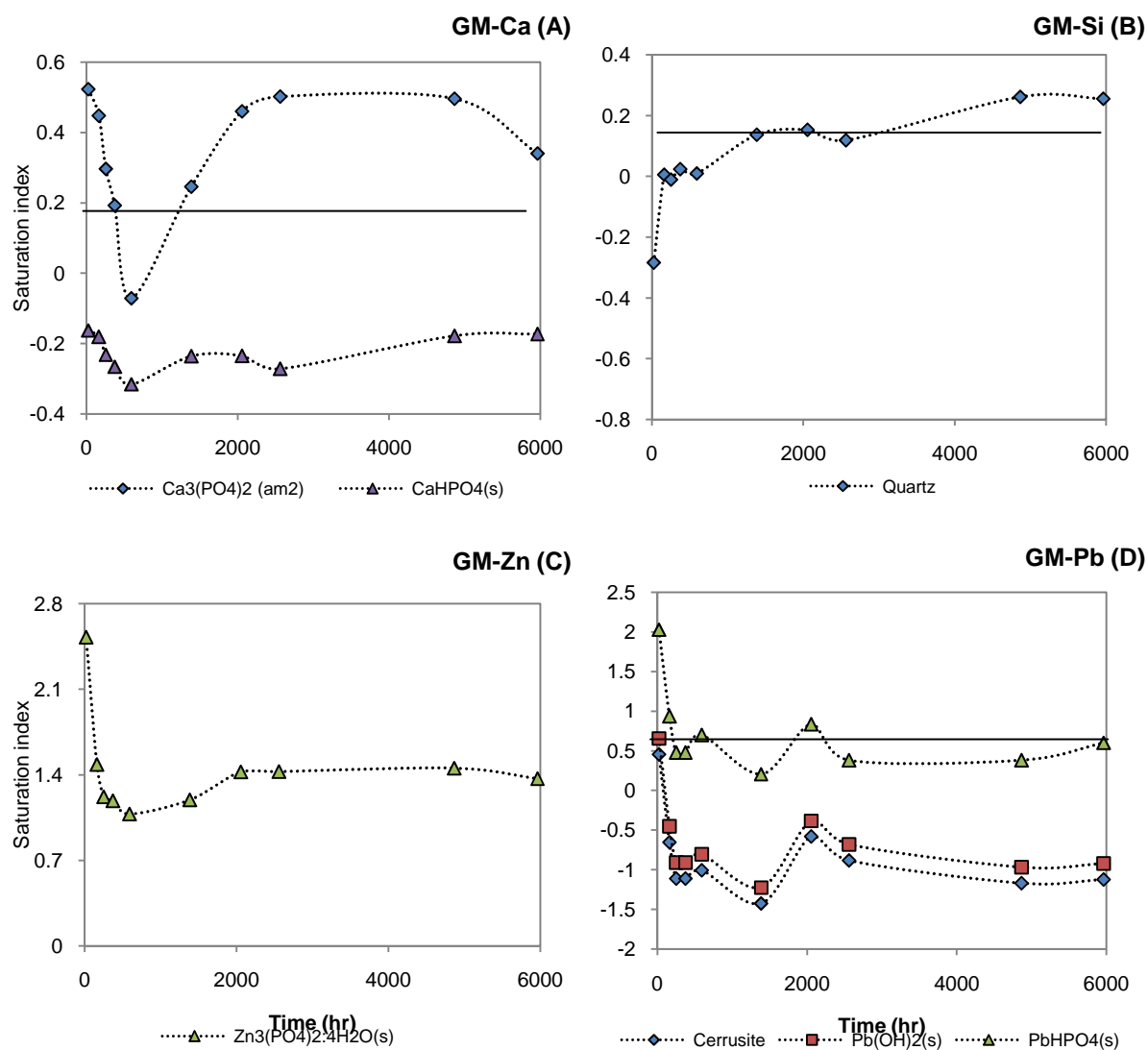


Figure 7.5: Saturation indexes of solubility controlling phases for Ca (a), Si (b), Zn (c) and Pb (d) in GM medium.

In the presence of bacteria, quartz was the main phase controlling Si (Figure 7.6a), whereas Fe oxide related phases displayed high saturation indices (Figure 7.6b), meaning that Fe solubility was not controlled by the precipitation of iron oxides. Ca and Mg solubility was controlled by the formation of carbonate and phosphate species (Figures 7.6c,d). Co-precipitation of Mg and Ca in the form of dolomite (disordered) was possible, where calcite can be the main carbonate species as vaterite was highly unstable and it converted to Calcite at low temperature (Anthony et al., 2005). Zn was widely controlled by 2 species: zincite (ZnO) and zinc carbonate (ZnCO_3) (Figure 7.6e) and Pb was only controlled by lead phosphate (PbHPO_4 (s)) (Figure 7.6f). Thus, species controlling solubility were specific to each

element. For instance, only Pb solubility was controlled by carbonate and hydroxide as $\text{Pb}_3(\text{CO}_3)_2(\text{OH})_2$ and $\text{Pb}(\text{OH})_2$ in UPW, whereas in GM phosphates species were the main phase controlling the solubility of three elements: Ca, Zn and Pb in the form of CaHPO_4 , $\text{Zn}_3(\text{PO}_4)_2 \cdot 4\text{H}_2\text{O}$ and PbHPO_4 . In GM+B medium, carbonate was controlling the solubility of Zn, Ca and Mg in the form of ZnCO_3 , CaCO_3 and $\text{CaMg}(\text{CO}_3)_2$. Phosphate was controlling Pb and Ca solubility as $\text{PbHPO}_{4(s)}$ and $\text{CaHPO}_{4(s)}$. Moreover, oxide was controlling only Zn as ZnO .

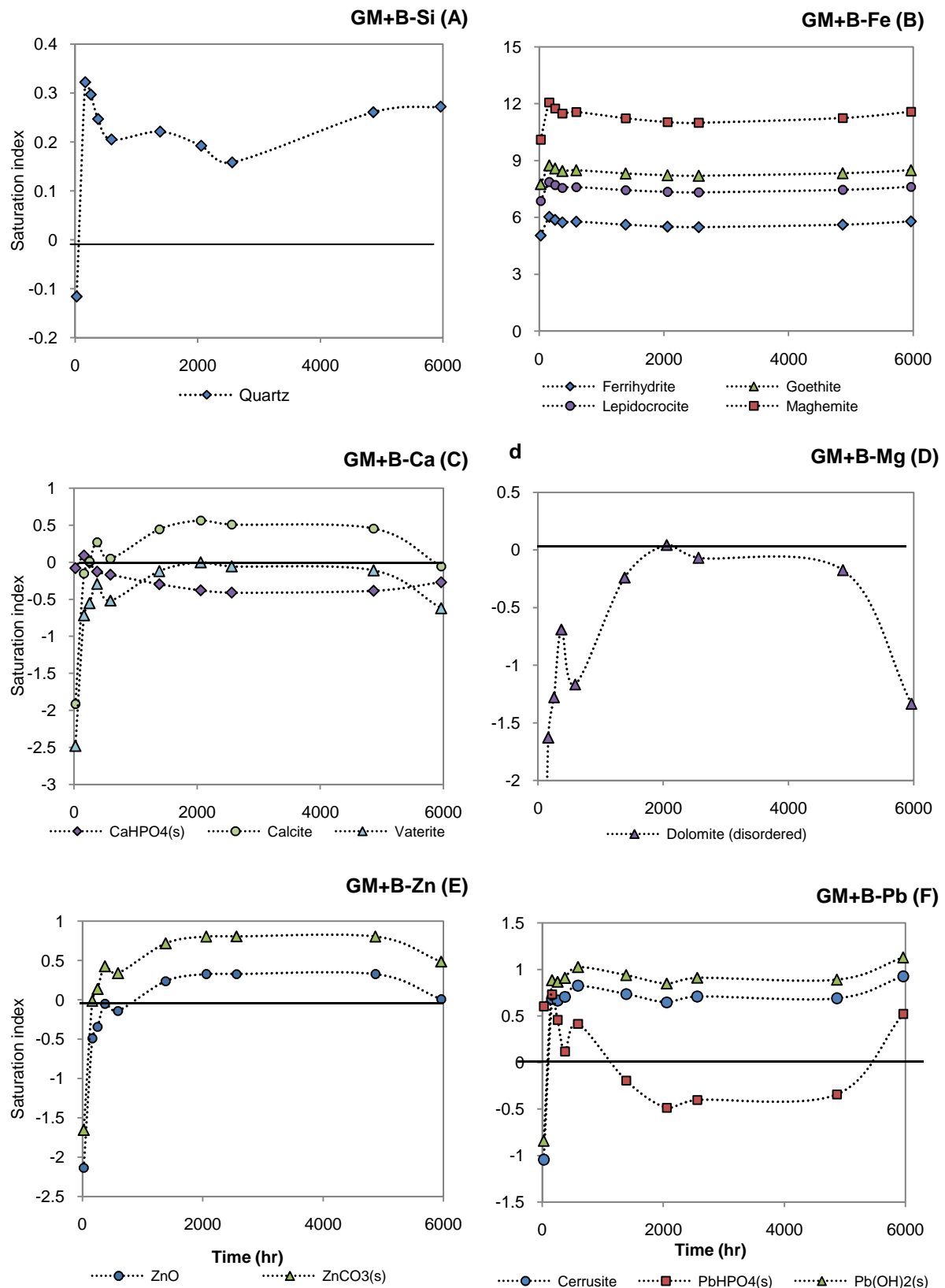


Figure 7.6: Saturation indexes of solubility controlling phases for Si (a), Fe (b), Ca (c), Mg (d), Zn (e) and Pb (f), respectively, in GM+B medium.

7.3.6. Scanning electron microscope (SEM) analysis

7.3.6.1. Surface morphology and physical characteristics of fresh slag

Many white metallic lead droplets were found either on the surface or in sectional views of the slags as shown in Figure 7.7. They consisted of either small or large balls ranging from 2-20 μm in size and sprawling all over the slag grain (Figure 7.7a). The large white metallic droplet (Figure 7.7b) was mainly composed of metallic Pb up to 97.9 wt% along with the presence of trace amounts of Sb always observed on the large Pb droplets. The cubic-cut shape grey phase (Figure 7.7b) was very rich in Fe (44.4 wt%), Cr (31.5 wt%) and Zn (15.8 wt%), where the possible mineral phases can be Fe-Cr rich or Fe-Zn rich spinel series such as chromite, franklinite, gahnite or magnetite (Deneele, 2002). Both lead droplets and spinel phases were borne by iron-silica-lime grey glassy matrix, in which Fe contributed up to 35.9-68.7 wt%.

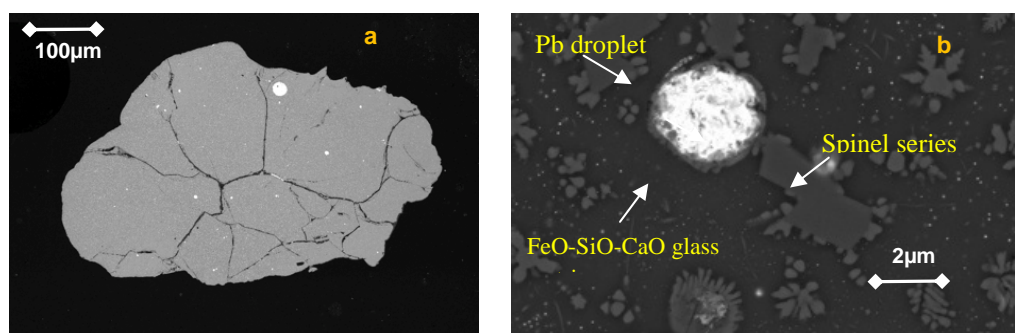


Figure 7.7. Surface investigation of fresh slag by SEM, (a) global view of slags, (b) free lead droplet and mineral phases present.

7.3.6.2. Glass alteration and secondary precipitates

The surface morphology of LBF had significantly changed after a long immersion time in the different media (Figures 7.8a,b,c). The alteration was non-uniform and mostly found at the edge, where there was a contact between the leaching medium and bacteria. The glass surface alteration layer in UPW medium (Figure 7.8a) was more porous compared to other media (Figures 7.8b,c). Close to the edge, some zones were visibly altered in GM medium (Figure 7.8b). Likewise, diffusion on the edge of the matrix and highly fractured glass surface can be observed in GM+B medium (Figure 7.8c). For the overall conditions, the leaching of metals from the matrix led to the creation of micro-canyons on the glass surface as seen in all media (Figures 7.8a,b,c). This complied with the finding of Seignez et al. (2008) showing that dendritic Fe oxides appeared to be very stable phases since they were protuberant objects at the weathered glass surface.

In UPW, the formation of a white thin crust, most likely cerussite or hydrocerussite was observed (Figure 7.9a), although it was difficult to differentiate with SEM-EDS due to their high tendency of breaking down under electron beam which consequently enhanced the amount of Pb in the analysis (Gee et al., 1997). However, the formation of carbonate

precipitates confirmed that carbonation mostly took place where the source of CO_2 could be from the atmosphere in UPW. The formation of white efflorescence and clusters of white grains observed in GM and GM+B (Figures 7.9b and 7.9c, respectively), were highly enriched in Fe, Pb, Ca, Zn and P which led to the secondary phosphate precipitates. In SEM-EDS analysis, the formation of carbonate with Pb was observed in UPW while in GM and GM+B, the formation of phosphate with Fe, Pb, Ca, and Zn was observed (Figures S-1a,b,c). Thus, the weathering conditions and the presence of the bacteria induced the leaching of metals from the matrix, which consequently precipitated in the presence of complexing agents like phosphates confirming thermodynamic simulation results.

Thus, the formation of lead carbonate in UPW (Figure 7.9a) was confirmed by SEM-EDS analysis which was in agreement with the Visual Minteq model (Figure 7.4a). Likewise, the phosphate was confirmed by both the SEM/EDS and Minteq model as the phase most contributing to solubility control of Ca, Pb, Zn in GM and GM+B (Figures 7.9 b and 7.9c and Figures 7.5 and 7.6) except that oxide and hydroxides forms were not observed by SEM-EDS and the precipitation of Fe with phosphates was not predicted by the visual Minteq model.

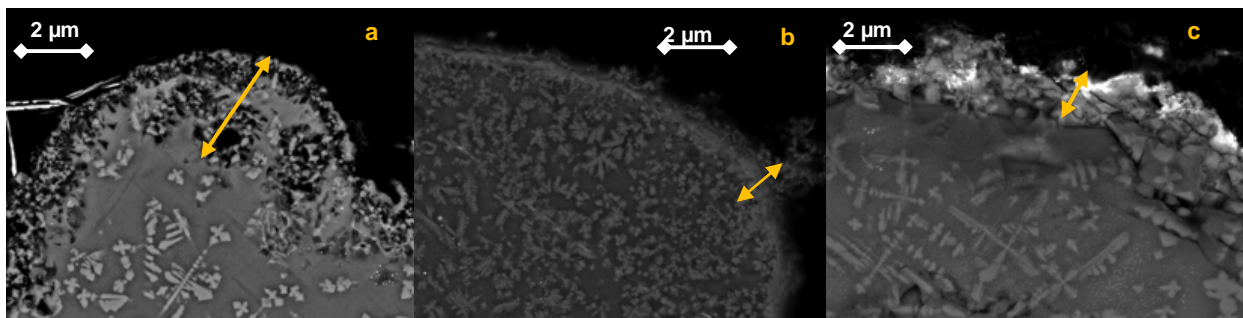


Figure 7.8. Surface investigation of LBF slags weathered in (a) UPW, (b) GM, and (c) GM+B by SEM.

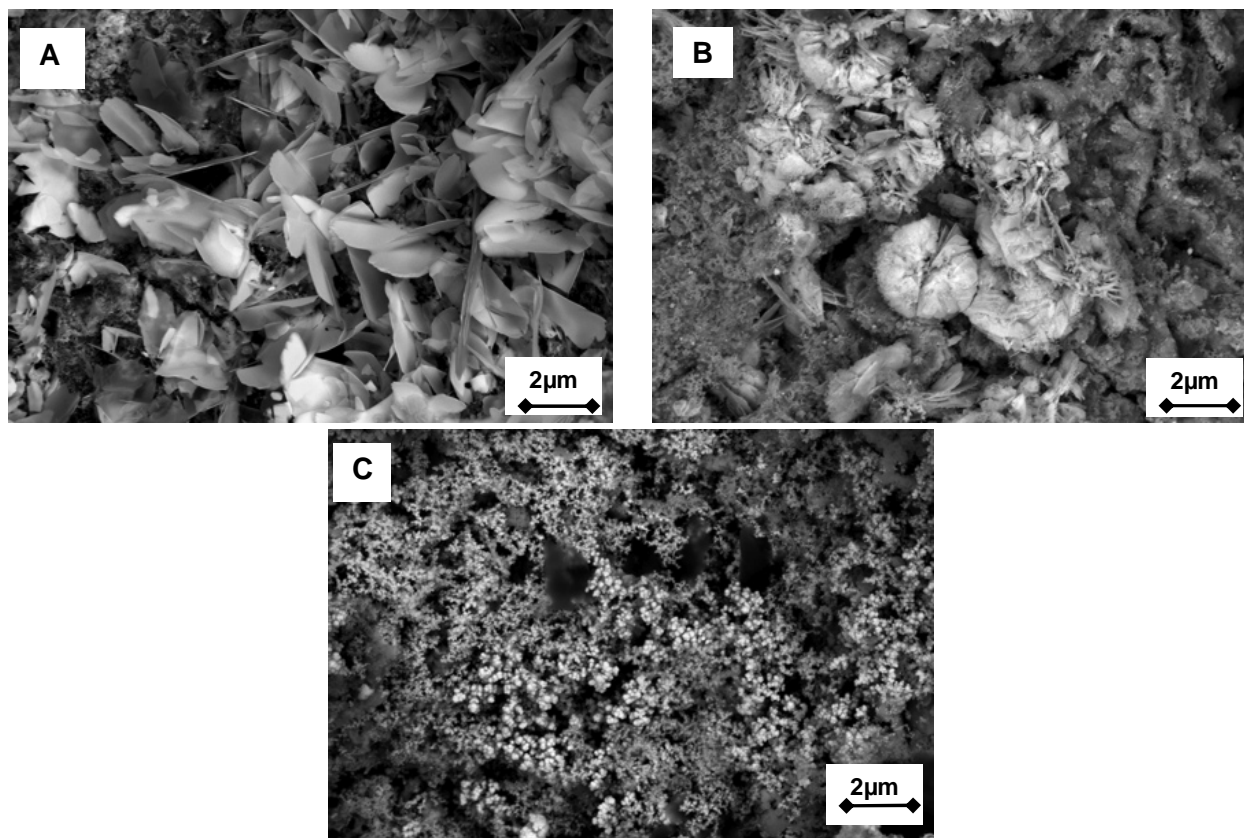


Figure 7.9. Precipitation of secondary phases on LBF slags weathered in (a) UPW, (b) GM, and (c) GM+B observed by SEM

7.4. Discussion

7.4.1. Environmental stability of LBF slag

Standardized tests (EN 12457 and TCLP) revealed that the concentration of As, Ba and Pb were below the regulatory limits, meaning that the LBF slags can be considered as non-hazardous wastes. Likewise, the concentration of As, Ba, Pb and Zn leached with TCLP was higher than the values in EN 12457 which was due to the different leaching media, acetic acid in TCLP and UPW in EN 12457. In spite of the LBF slags stability regarding EN 12457 results, its environmental stability was reduced in the presence of organic complexation agents, as displayed by TCLP results with acetate: the elements were leached out at more elevated concentration with possible potential risk to the environment. Therefore, open air dumping or co-disposal of LBF with normal MSW landfill was not appropriate as the slag might potentially pose a risk to the environment in the presence of organic acids. Weathering of slags present also an effect on pH, which rose in the final solutions from both TCLP and EN tests (See Section 7.312), reflecting the occurrence of H^+ consuming reactions commonly occurring at the solid–water interface. The same phenomena were observed during leaching test procedures of air pollution control residues from secondary Pb metallurgy (Ettler et al., 2005).

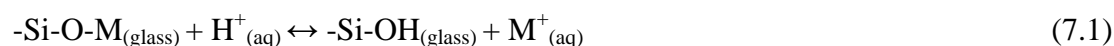
7.4.2. Influence of abiotic factors on the LBF slags weathering

The concentration of Zn and Pb are higher in UPW than in GM (Figures 7.3 e & f), which can be related to solution pH (pH = 6.8 and 7.8 in UPW and GM experiments, respectively), where the enhancement of metal solubility in acidic pH was a well-known process (Stumm and Morgan 1996). The formation of possible secondary precipitates of Zn ($\text{Zn}_3(\text{PO}_4)_2 \cdot 4\text{H}_2\text{O}_{(s)}$) and Pb (PbHPO_4 , $\text{Pb}(\text{CO}_3)$ and $\text{Pb}(\text{OH})_2$) was indicated by thermodynamic modeling and then confirmed by SEM-EDS analysis by co-localization of these elements (Figures S-1a,b,c). Several of these precipitates (except $\text{Pb}(\text{OH})_2$ as PbO) can be directly observed on the altered slag's surface. Thus, leachate information, thermodynamic modeling and SEM observations gave consistent results on the chemistry of Zn and Pb. Mg showed a different behavior as its concentration went even higher in GM than in UPW (Figure 7.3b), which could be due to the presence of complexation agents like phosphates, or sulfate in GM. In contrast, thermodynamic modeling showed that the solubility of Mg was governed neither by phosphates and sulfates.

7.4.3. Influence of *P. aeruginosa* on the LBF slags bioweathering

Pseudomonas sp. needs Fe for its growth and is well-known for producing siderophores which are involved in Fe complexation (Braud et al., 2009) and Fe metabolic acquisition (Cornelis, 2010). The visual observation of fluorescent color also suggested the presence of siderophores during the experiments, but this was not quantified. This was the main reason why the Fe concentration (i.e. solubility) was strongly enhanced in GM+B despite a high pH: 9 (Figure 7.3d). On the other hand, the Fe concentration in UPW and GM was around 0.01 mg L^{-1} ($10 \text{ } \mu\text{g L}^{-1}$), which was very close to the detection limit of Fe ($5 \text{ } \mu\text{g L}^{-1}$). Fe extraction by *P. aeruginosa* had probably weakened the bonding of the $\text{FeO-SiO}_2\text{-CaO}$ glass matrix, which possibly led to the high release of Ca. When major cations such as Ca^{2+} and Fe^{2+} were leached out from the matrix (Figures 7.3a,d), protons were exchanged back from the medium to the solid matrix to maintain the charge equilibrium, resulting in a quick pH rise from 7.8 to 9.1 in the presence of *P. aeruginosa* (Figure 7.2b).

Thus, the early stage of weathering was the modification of the glass network in relation to the leaching of Fe^{2+} , Ca^{2+} and Mg^{2+} ions which were further enhanced by the presence of *Pseudomonas aeruginosa*. This can be depicted in the following ion exchange mechanisms:



Hydrolysis profoundly modified the silicate network by attacking bridging bonds (Si-O-M) which consequently led to the release of elements embedded in silica matrix according to reaction (7.1). The rupture of the four bridging bonds likely to surround a silicon atom in the glass ultimately led to the release of orthosilicic acid, (H_4SiO_4) according to reaction (7.2). This reaction depended on the nucleophilic character of water, and was thus facilitated in basic media (Frugier et al., 2008). This explained why the increase in pH of GM+B has a

strong influence on glass matrix corrosion and increase of solubility of Si. Quartz was the main phase controlling the Si solubility phase instead of amorphous silica, which was not identified during SEM-EDS analysis meaning that this phase was probably formed during bulk liquid sample storage.

Silica network modification (reaction 7.1) had significant effects on the release of Zn and Pb from the LBF slag which were further enhanced by the presence of bacteria. Unlike Zn, Pb was present in the slag as free metallic droplets, highly prone to oxidation and solubilization. Zn and Pb were known adsorb onto bacterial cell walls and biofilms (Guibaud et al., 2006) as well as to form complexes with soluble siderophores (Schalk et al., 2011) or EPS (Guibaud et al., 2012; Guibaud et al., 2006). Sorption might played a role in the extraction of Zn and Pb from the LBF slag, however, complexation with siderophores and EPS can only be accounted for the high dissolved concentration of Zn and Pb as the samples were filtered prior to ICP analysis. In addition, formation of Zn and Pb precipitates was not different with or without the presence of bacteria meaning that this bacterium did not favor biomineralization or bioprecipitation, but rather enhanced Zn and Pb solubilities by sorption onto microbial cell wall and complexation with microbial by-products.

7.5. Conclusions

Despite that LBF slags were not recognized as dangerous solid waste based on EN 12457 and TCLP, long-term alteration was strongly affected by the medium composition and the microbial activity. The presence of phosphate in the growth media was strongly affecting the solubility of Zn, Pb and Ca. The thermodynamic calculations corroborated the results of SEM-EDS characterization (i.e. formation of phosphate precipitates in the bacterial growth media and formation of carbonate precipitates in the ultrapure water media). The microbial activity played a significant role in LBF slags weathering by enhancing the solubility of Zn and Pb and thus contributing to the bulk release of toxic elements from the slags. The solubilization of Fe by the bacteria through the siderophores production increased the total dissolved iron solubility. The leaching of alkaline elements such as calcium and magnesium, possibly due to the uptake and sorption by bacteria, led to a pH rise and, hence, to a more intense release of Si from the slags glass matrix. Consequently, this enhanced the leaching of other metals such as Zn and Pb embedded within the silica matrix. It can be concluded that despite the alkaline nature of LBF slags, the presence of heterotrophic bacteria like *P. aeruginosa* alone was capable to weather these slags and to increase the release of toxic elements into the environment. This research, therefore, highlighted the high possibility of LBF slags weathering phenomenon upon their contact with heterotrophic bacteria.

7.6. References

Anthony, J.W., Bideaux, R.A., Bladh, K.W., Nichols, M.C., 2005. Handbook of Mineralogy, Mineralogical Society of America, Chantilly, VA 20151-1110, USA.

- Aouad, G., Geoffroy, V., Meyer, J.M., Crovisier, J.L., Damidot, D., Stille, P., 2005. Mise au point d'un milieu de culture pour l'étude de l'altération de silicates en présence de *Pseudomonas aeruginosa*. *Comptes Rendus Geoscience*, 337: 1340-1347.
- Aouad, G., Crovisier, J.L., Geoffroy, V.A., Meyer, J.M., Stille, P., 2006. Microbially-mediated glass dissolution and sorption of metals by *Pseudomonas aeruginosa* cells and biofilm. *J Hazard Mater*, 136: 889-95.
- Aouad, G., Crovisier, J.L., Damidot, D., Stille, P., Hutchens, E., Mutterer, J., Meyer, J.M., Geoffroy, V., 2008. Interactions between municipal solid waste incinerator bottom ash and bacteria (*Pseudomonas aeruginosa*). *Sci Total Environ*, 393: 385-93.
- Barna, R., Moszkowicz, P., Gervais, C., 2004. Leaching assessment of road materials containing primary lead and zinc slags. *Waste Manage*, 24: 945-55.
- Banerjee, N.R., Muehlenbachs, K., 2003. Tuff life: Bioalteration in volcanoclastic rocks from the Ontong Java Plateau. *Geochem Geophys Geosys*, 4: 1037-1059.
- Braud, A., Hoegy, F., Jezequel, K., Lebeau, T., Schalk, I.J., 2009. New insights into the metal specificity of the *Pseudomonas aeruginosa* pyoverdine-iron uptake pathway. *Environ Microbiol*, 11: 1079-91.
- Cheng, Y., Guo, Z., Liu, X., Yin, H., Qiu, G., Pan, F., Liu, H., 2009. The bioleaching feasibility for Pb/Zn smelting slag and community characteristics of indigenous moderate-thermophilic bacteria. *Bioresour Technol*, 100: 2737-40.
- Cornelis, P., 2010. Iron uptake and metabolism in *Pseudomonads*. *Appl Microbiol Biotechnol*, 86: 1637-45.
- De Andrade Lima, L.R.P., Bernardez, L.A., 2011. Characterization of the lead smelter slag in Santo Amaro, Bahia, Brazil. *J Hazard Mater*, 189: 692-9.
- Deneele, D., 2002. Caractérisation, simulations expérimentales et thermodynamiques de l'altération de déchets vitreux: les scories de première fusion de plomb et de zinc. *PhD thesis manuscript*, Université Des Sciences et Technologies de Lille I and U.F.R. Des Sciences De La Terre, France, 1-242.
- Ettler, V., Johan, Z., Touray, J.C., Jelínek, E., 2000. Zinc partitioning between glass and silicate phases in historical and modern lead-zinc metallurgical slags from the Prábram district, Czech Republic. *Compt. Rend.Acad. Sci. (Paris), Série II, Sciences de la Terre et des planètes*, 331: 245-250.
- Ettler, V., Legendre, O., Bodéan, F., Touray, J.C., 2001. Primary Phases and Natural Weathering of Old Lead-Zinc Pyrometallurgical Slag from PRábram, Czech Republic. *Can Mineral*, 39: 873-888.
- Ettler, V., Mihaljevic, M., Touray, J.C., Piantone, P., 2002. Leaching of polished sections: an integrated approach for studying the liberation of heavy metals from lead-zinc metallurgical slags. *Bulletin de la Société géologique de France*, 173: 161-169.

- Ettler, V., Piantone, P., Touray, J.C., 2003a. Mineralogical control on inorganic contaminant mobility in leachate from lead-zinc metallurgical slag: experimental approach and long-term assessment. *Mineral Mag*, 67: 1269-1283.
- Ettler, V., Komarkova, M., Jehlicka, J., Coufal, P., Hradil, D., Machovic, V., Delorme, F., 2004. Leaching of lead metallurgical slag in citric solutions-implications for disposal and weathering in soil environments. *Chemosphere*, 57: 567-77.
- Ettler, V., Mihaljevic, M., Sebek, O., Strnad, L., 2005b. Leaching of APC residues from secondary Pb metallurgy using single extraction tests: the mineralogical and the geochemical approach. *J Hazard Mater*, 121: 149-57.
- Ettler, V., Sebek, O., Grygar, T., Klementova, M., Bezdicka, P., Slavikova, H., 2008. Controls on Metal Leaching from Secondary Pb Smelter Air-Pollution-Control Residues. *Environ Sci Technol*, 42: 7878-84.
- Gee, C., Ramsey, M.H., Maskall, J., Thornton, I., 1997. Mineralogy and weathering processes in historical smelting slags and their effect on the mobilisation of lead. *J Geochem Explor*, 58: 249-257.
- Guibaud, G., van Hullebusch, E., Bordas, F., 2006. Lead and cadmium biosorption by extracellular polymeric substances (EPS) extracted from activated sludges: pH-sorption edge tests and mathematical equilibrium modelling. *Chemosphere*, 64: 1955-62.
- Guibaud, G., Bhatia, D., d'Abzac, P., Bourven, I., Bordas, F., van Hullebusch, E.D., Lens, P.N.L., 2012. Cd(II) and Pb(II) sorption by extracellular polymeric substances (EPS) extracted from anaerobic granular biofilms: Evidence of a pH sorption-edge. *J Taiwan Inst Chem Eng*, 43: 444-449.
- Guine, V., Spadini, L., Sarret, G., Muris, M., Delolme, C., Gaudet, J.P., Martins, J.M.F., 2006. Zinc Sorption to Three Gram-Negative Bacteria: Combined Titration, Modeling, and EXAFS Study. *Environ Sci Technol*, 40: 1806-1813.
- Herisson, J., van Hullebusch, E.D., Moletta-Denat, M., Taquet, P., Chaussadent, T., 2013. Toward an accelerated biodeterioration test to understand the behavior of Portland and calcium aluminate cementitious materials in sewer networks. *Int Biodeterior Biodegrad*, 84: 236-243.
- Mahé-Le Carlier, C., Le Carlier de Veslud, C., Ploquin, A., Royer, J.J., 2000. Altération des scories de la métallurgie ancienne: un analogue de déchets vitrifiés. *Compt. Rend.Acad. Sci. (Paris), Série II. Sciences de la Terre et des planètes*, 330: 179-184.
- Okabe, S., Odagiri, M., Ito, T., Satoh, H., 2007. Succession of sulfur-oxidizing bacteria in the microbial community on corroding concrete in sewer systems. *Appl Environ Microbiol*, 73: 971-80.
- Parsons, M.B., Bird, D.K., Einaudi, M.T., Alpers, C.N., 2001. Geochemical and mineralogical controls on trace element release from the Penn Mine base-metal slag dump, California. *Appl Geochem*, 16: 1567-1593.

- Piatak, N.M., Seal, R.R., Hammarstrom, J.M., 2004. Mineralogical and geochemical controls on the release of trace elements from slag produced by base- and precious-metal smelting at abandoned mine sites. *Appl Geochem*, 19: 1039-1064.
- Piatak, N.M., Seal, R.R., 2010. Mineralogy and the release of trace elements from slag from the Hegeler Zinc smelter, Illinois (USA). *Appl Geochem*, 25: 302-320.
- Roberts, D., Nica, D., Zuo, G., Davis, J., 2002. Quantifying microbially induced deterioration of concrete: initial studies. *Int Biodeterior Biodegrad*, 49: 227-234.
- Schalk, I.J., Hannauer, M., Braud, A., 2011. New roles for bacterial siderophores in metal transport and tolerance. *Environ Microbiol*, 13: 2844-54.
- Seigneur, N., Bulteel, D., Damidot, D., Gauthier, A., Potdevin, J.L., 2006. Weathering of metallurgical slag heaps: multi-experimental approach of the chemical behaviours of lead and zinc. *Waste Manage Environ III*, 1: 31-40.
- Seigneur, N., Gauthier, A., Bulteel, D., Damidot, D., Potdevin, J.L., 2008. Leaching of lead metallurgical slags and pollutant mobility far from equilibrium conditions. *Appl Geochem*, 23: 3699-3711.
- Sivry, Y., Riotte, J., Sonke, J., Audry, S., Schafer, J., Viers, J., Blanc, G., Freydier, R., Dupre, B., 2008. Zn isotopes as tracers of anthropogenic pollution from Zn-ore smelters The Riou Mort-Lot River system. *Chem Geol*, 255: 295-304.
- Sivry, Y., Munoz, M., Sappin-Didier, V., Riotte, J., Denaix, L., de Parseval, P., Destigneville, C., Dupré, B., 2010. Multimetallic contamination from Zn-ore smelter: solid speciation and potential mobility in riverine floodbank soils of the upper Lot River (SW France). *Eur J Mineral*, 22: 679-691.
- Sobanska, S., Ledésert, B., Deneele, D., Laboudigue, A., 2000. Alteration in soils of slag particles resulting from lead smelting. *Earth Planet Sci*, 331: 271-278.
- Stumm, W., J.J. Morgan, J.J., 1996. Aquatic chemistry, chemical equilibria and rates in natural waters, 3rd ed. *John Wiley & Sons, Inc.*, New York.
- Uroz, S., Calvaruso, C., Turpault, M.P., Frey-Klett, P., 2009. Mineral weathering by bacteria: ecology, actors and mechanisms. *Trends Microbiol*, 17: 378-87.
- Verguts, P., 2005. Two dimensional mathematical simulation model for a non-ferrous blast furnace. *PhD thesis manuscript*, Katholieke Universiteit Leuven, Belgium: 1-168.
- Willscher, S., Bosecker, K., 2003. Studies on the leaching behaviour of heterotrophic microorganisms isolated from an alkaline slag dump. *Hydrometallurgy*, 71: 257-264.
- Willscher, S., Pohle, C., Sitte, J., Werner, P., 2007. Solubilization of heavy metals from a fluvial AMD generating tailings sediment by heterotrophic microorganisms. *J Geochem Explor*, 92: 177-185.

CHAPTER 8

Bio-alteration of metallurgical wastes by *Pseudomonas aeruginosa* in semi-flow through reactor

This chapter has been published as:

van Hullebusch, E.D., Yin, N.-H., Seignez, N., Labanowski, J., Gauthier, A., Lens, P.N.L., Avril, C., Sivry, Y., (2014). Bio-alteration of metallurgical wastes by *Pseudomonas aeruginosa* in a semi flow-through reactor. *J Environ Manage*, in press. DOI: 10.1016/j.jenvman.2014.09.018.

Chapter 8

8.1. Introduction

Metallurgy of non-ferrous materials, especially associated with lead blast furnace (LBF) processing, is known to generate huge amounts of primary smelting slags (Verguts, 2005). In northern France, for instance, about 4 million tons of these hazardous materials have been landfilled in the industrial basin of Nord-Pas-de-Calais (Sobanska et al., 2000). Several papers have detailed the risks associated with the release of toxic compounds by slags and dust emitted by LBFs (Barna et al., 2004; de Andrade Lima and Bernardez, 2011; de Andrade Lima and Bernardez, 2012).

In light of this, a large number of studies have been conducted either in batch (Ettler et al., 2002; Ettler et al., 2003a) or open flow (Seigneur et al., 2006; Seigneur et al., 2008) experiments to study the fate of LBF waste products in landfill conditions (Mahé-Le Carlier et al., 2000) and in soils or soil-like environments (Ettler et al., 2004; Sobanska et al., 2000). The LBF slags are typically granulated glassy materials enriched in Zn (10-12 wt%), Pb (0.5-3 wt%) and other toxic elements such as Cr, Cd and As (Seigneur et al., 2006). Exposed to weathering, spinels and wuestite contained in LBF slags are generally stable in batch and open flow experiments. Thus, the FeO-SiO₂-CaO glass matrix is progressively depleted in alkali and alkali-earth elements, e.g. Ca, Na; although other elements (e.g. Pb, Zn) can also be noticeably released (Ettler et al., 2001; Yin et al., 2014). In contrast, any fayalite, melilite, sulfides, glass matrix and metallic Pb droplets present in the slags are partially or totally dissolved (Ettler et al., 2002). Under oxidizing conditions, Fe(II) contained in the glass matrix is usually transformed into Fe(III) and remains stable (Mahé-Le Carlier et al., 2000). Generally, altered layers are relatively enriched in Si, Fe and Al (Seigneur et al., 2007).

To date, only few studies have focused on the role of microorganisms in the weathering of LBF slags. This is important, as microbial activity influences the weathering process and thus the rate of leaching of potentially toxic elements (Cheng et al., 2009; Willscher et al., 2007; Yin et al., 2014). Moreover, the deterioration of natural secondary minerals as well as materials of anthropogenic origin (stained glasses, cements and blast-furnace slags) depends partly on the presence of biogenic organic compounds (i.e. inorganic or organic acids and siderophores involved in acidolysis and complexolysis) and micro-organisms involved in oxidation-reduction reactions (Uroz et al., 2009). For instance, bacteria are well known to accelerate the deterioration of natural glass material like marine basalt (Banerjee and Muehlenbachs, 2003). Moreover, Aouad et al. (2006) found that bacterial biofilms were able to retain most of the elements present in the system as they are constituted of polyanionic polymers having a strong affinity for heavy metals.

Although studies have been conducted on the role of bacterial cells during the weathering of solid mineral wastes (Anderson and Pedersen, 2003), there is still a lack of data which quantify the role of bacterial biofilms (i.e. the cell-exopolymer-solution matrix) and the degradation that occurs in abiotic (sterile) systems. Apart from some well-defined cases, such

as the biodeterioration of stainless steel or concrete cement in sewer pipes by bacterial strains such as *Acidithiobacillus* (Herisson et al., 2013; Okabe et al., 2007; Roberts et al., 2002), the exact role of micro-organisms remains unclear.

In order to clarify the role of micro-organisms during the weathering of LBF slags, the present study aims to investigate the effect of heterotrophic bacteria (*Pseudomonas aeruginosa* was chosen as a proxy) under relevant conditions regarding the natural environment (i.e. close to the natural weathering conditions of heap slags; pH 7.8 and 23°C) in semi-flow through reactors. Leachate chemistry is studied under both biotic and abiotic conditions, and the rates of elemental release are determined during bacteria-slag interactions for 140 days at the laboratory scale. Major elements involved in the carbonate–silicate geochemical cycle (e.g., Si and Ca) as well as life-supporting nutrients (e.g., Fe and Mg) and toxic metals (i.e., Pb and Zn) are focused on. Finally, Scanning Electron Microscopy (SEM-EDS) was used to characterize and compare fresh and altered glass in order to link the leachate chemistry and the alteration mechanisms.

8.2. Materials and Methods

8.2.1. Lead blast furnace (LBF) slags

The LBF slags studied were generated at the former lead-zinc smelter of Noyelles-Godault (Northern France). These slags are granulated, with grain sizes typically smaller than 2 mm, having a log-normal size distribution dominated by the 500 µm class (Sobanska et al., 2000) and varying from 100 µm to 5 mm at the most. The averaged elemental composition was determined by Deneele (2002) and is displayed in Table 8.1. “Fresh” LBF slags typically comprise 80% FeO-SiO₂-CaO glass matrix by volume (of which PbO ≈ 4.3 wt.% and ZnO ≈ 11 wt.%) and 19% of crystalline phases. The final ~1% consists of metallic lead droplets, which vary in size between 1 µm and 400 µm (Deneele, 2002; Seignez et al., 2006).

Table 8.1. Bulk chemistry¹ of the LBF slag samples (n = 7) in oxide wt%.

	TiO ₂	SiO ₂	Al ₂ O ₃	FeO	MnO	MgO	CaO	Cr ₂ O ₃	PbO	ZnO
Wt (%)	0.22	26.38	2.54	26.5	0.84	1.91	22.92	0.04	4.3	11.16

8.2.2. Bioalteration experiments

Bioalteration experiments were carried out in a well-defined growth medium, allowing both the growth of bacteria and the precise measurement of the elements solubilized from the slags. Most conventional bacteria growth media contain very high base cation concentrations that could potentially mask the effects of mineral dissolution. Therefore, the modified growth medium used in this study is described by Aouad et al. (2005 and 2006) and contained, per liter : i) 4 g of succinic acid-C₄H₆O₄; ii) 1 g of ammonium sulfate-(NH₄)₂.SO₄; iii) 1 g of

¹ reprint from Deneele, 2002

sodium phosphate dibasic- Na_2HPO_4 ; and iv) 6 g of TRIS buffer- $\text{C}_4\text{H}_{11}\text{NO}_3$. The medium was adjusted to pH 7.8 using NaOH. As this growth medium is lacking iron, calcium and magnesium to allow the growth of bacteria, it was expected that these elements would be provided by the dissolution of the LBF slags, as previously shown by Seignez et al. (2008) when performing leaching experiments in ultrapure water.

Three parallel weathering experiments were carried out, in duplicate, for 140 days at $23 \pm 2^\circ\text{C}$: i) in ultrapure water (UPW), ii) in a sterile medium (abiotic) and iii) in the presence of *Pseudomonas aeruginosa* (biotic). The experiment was designed in a way that allowed the successive cycles of bacterial growth with the formation of a biofilm and a possible alteration layer at the surface of the materials (Aouad et al., 2006; Aouad et al., 2005). Precisely, 2.5 g of slag grains (2 mm diameter size) were placed in a 150 mL polycarbonate flask filled with 75 mL of the three different media, which were agitated at 100 rpm. Every 7 days, the reactor was transferred into a new flask containing 75 mL of new medium, thus starting a new cycle. The solids were collected at the end of each cycle and stored for further analysis.

During each cycle, two liquid samples were taken from the biotic medium: one was filtered through a $0.2 \mu\text{g}$ pore size membrane in order to remove the suspended bacterial cells and any neoformed precipitates; this filtrate was labelled as "biotic dissolved sample". It was then acidified with $50 \mu\text{L}$ of nitric acid. The second sample (5 mL) was digested by adding 0.5 mL H_2O_2 (30%) and heated at 80°C for 30 min. It was labelled as "biotic digested sample".

8.2.3. Sample preparation and analytical methods

8.2.3.1. Polished Sections

Polished sections of slag material ($60 \times 20 \text{ mm}^2$) were placed in semi-continuous batch reactors to observe the mineralogical effects of slag alteration. Slags were only located on the upper face of the sections and therefore occupied $\approx 40\%$ ($\approx 500 \text{ mm}^2$) of each section. During the polished section preparation, contact with water was reduced to a minimum to avoid any early alteration of the most reactive phases, such as the Pb droplets. The different polishing steps consist of a first lapping and successive polishing using diamond paste. An alcohol-based lubricant liquid was used to avoid contact with water. After each step, the sections were immediately dried with alcohol.

Both unaltered and altered slag sections (after undergoing alteration for 60 and 150 days) were studied using an environmental scanning electron microscope (ESEM, FEI Quanta 200). This instrument is equipped with a W electron source at 20 keV and an X-ray energy dispersive system (EDS) probe with a spatial resolution of $1 \mu\text{m}^3$. The polished sections were not carbon-coated and were inserted in the ESEM chamber in low vacuum mode (≤ 0.45 Torr).

8.2.3.2. Leachate Chemistry

The pH was constantly monitored in the solutions obtained from bioalteration experiments by using a “WTW pH 340i” pH-meter. The metal content (Ca, Fe, Mg, Mn, Pb, Si and Zn) was determined by using inductively coupled plasma atomic emission spectroscopy (ICP-AES Thermo iCAP 6000, Ecole des Mines de Douai, France) equipped with an ultra-sonic nebulizer. The external calibration was performed with a minimum of four standards before the analysis, and quality assurance/quality control (QA/QC) samples such as blank, sample spikes, sample duplicates, and calibration check samples were included in the analysis. Detection limits are 10 ppb for most of the elements except Pb and Zn (20 ppb), Si (50 ppb) and Ca (200 ppb).

8.3. Results

8.3.1. Leachate chemistry and cumulative release of characteristic elements

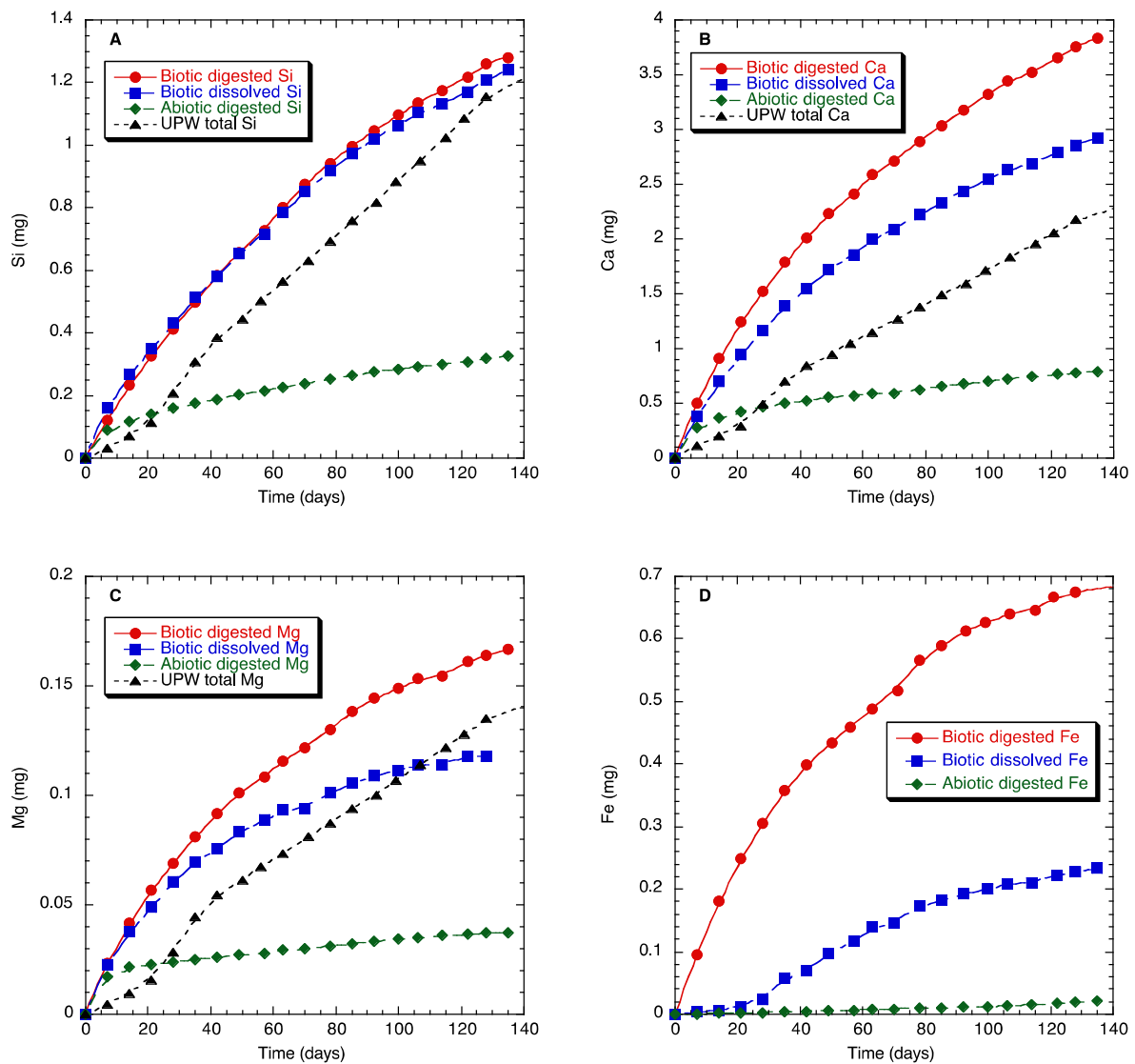
Alteration of LBF slags induced changes in the chemistry of the aqueous medium (Figure 8.1). The initial pH of the biotic medium was 8.2, which gradually increased to 8.5 at the end of the experiment, while the pH of the abiotic medium remained constant at 8.2. The pH of the ultra-pure water (UPW) experiment also increased from an initial value of 5.6 to a final value of 7.5.

The cumulative release of Si, Ca, Mg, Fe, Zn and Pb from the alteration of LBF slags in different media is demonstrated in Figure 8.1. The cumulative amount of Si released in the UPW medium (Figure 8.1a) was only 0.2 mg within the first 30 days, while the same amount was released during the first 10 days in both biotic digested and biotic dissolved media. Moreover, the cumulative Si released in the presence of bacteria was 1.5 times higher than in UPW medium from 30 days to 120 days. The cumulative amount of Si released in the abiotic medium experiment increased steadily but at a much lower rate throughout the experiment, reaching ~0.3 mg after 140 days.

The cumulative amount of leached Ca gradually increased and reached 2.4 mg in UPW, 2.8 mg in the biotic dissolved medium and 3.8 mg in the biotic digested medium after 140 days (Figure 8.1B). Figure 8.1C shows that the amount of Mg released in the biotic digested and biotic dissolved media is almost the same, around 0.07 mg during the first 30 days, which later increased to 0.16 mg and 0.12 mg at the end of the experiment. The bulk release of Ca and Mg was low and steady in the abiotic digested medium (Figures 8.1B & C).

In the biotic digested medium, the amount of Fe released reached 0.3 mg during the first 30 days of alteration and 0.7 mg at the end of the experiment (Figure 8.1D); this is much greater than the UPW medium where almost no Fe was mobilised. Dissolved Fe in the biotic dissolved medium is 3-3.5 times lower compared to the total iron measured in the biotic digested medium, below 0.04 mg during the first 30 days of alteration, rising to 0.24 mg at the end of the experiment. Iron concentrations are below detection limits in the UPW experiment samples.

The amount of Zn released gradually increased as alteration proceeded and reached 0.64 mg, 0.68 mg and 0.36 mg after 140 days in the UPW, biotic digested medium and biotic dissolved medium experiments, respectively (Figure 8.1E). The amount of Zn mobilized by both biotic media and UPW is up to 2.3 times higher than that in abiotic medium. A steep increase of cumulative Pb release in the UPW experiment is observed during the first 40 days of alteration. Thereafter, it stabilized between 0.04 and 0.05 mg (Figure 8.1F). In the biotic digested and dissolved medium the cumulate amount of Pb released increased to a final value of 0.076 mg and 0.02, respectively. Both Pb and Zn released in abiotic digested medium was low and steady, reaching 0.02 mg for Pb and 0.1 mg for Zn at the end of the alteration experiment. After 140 days of alteration, Zn is equally present both in suspended and in dissolved forms (Figure 8.1E), whereas only 20% of total Pb is present in the dissolved form, whilst 80% in suspended form (Figure 8.1F).



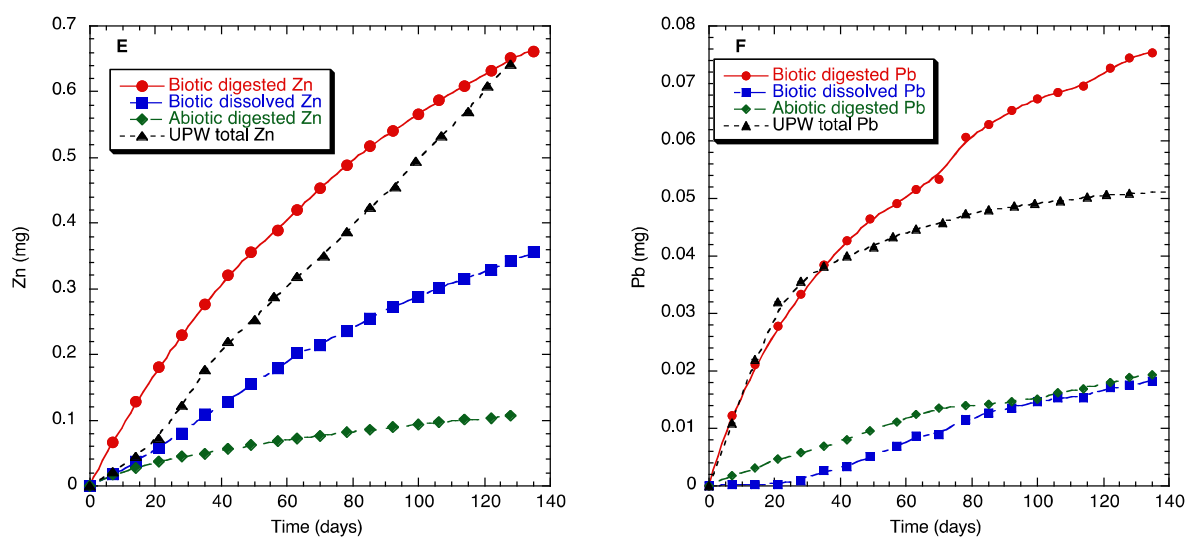


Figure 8.1. Cumulative leaching of Si (A), Ca (B), Mg (C), Fe (D), Zn (E) and Pb (F) from 2.5 g LBF slags during aqueous alteration in UPW, abiotic and biotic solutions at $23\pm 2^\circ\text{C}$.

8.3.2. Leachate chemistry and cumulative release of characteristic elements

The highest leaching rates observed in biotic digested medium were at the beginning of the experiments and started at 0.017 mg d^{-1} for Si; 0.07 mg d^{-1} for Ca; 0.0034 mg d^{-1} for Mg and 0.0095 mg d^{-1} for Zn (Figures 8.2A,B,C,E). The leaching rates in biotic digested medium gradually decreased during the experimental period to 0.006 mg d^{-1} for Si; 0.015 mg d^{-1} for Ca; 0.0005 mg d^{-1} for Mg and 0.003 mg d^{-1} for Zn. In contrast, the leaching rates in UPW show a sharp increase up to day 30, a smaller decrease thereafter to day 45 where upon they remained stable for the duration of the experiment (Figures 8.2A,B,C,E). Zn in UPW shows the highest leaching rate, 0.008 mg d^{-1} after 30 days, after which it decreased to remain stable with an average of 0.006 mg d^{-1} until the end of the experiment.

The initial leaching rates of Fe and Pb in biotic digested medium were 0.014 mg d^{-1} and 0.002 mg d^{-1} , respectively (Figures 8.2D,F). The leaching rates of Fe and Pb continuously decreased till the end of the experiment, as with the other elements. The Fe concentration in the UPW experiment is below the analytical detection limit, thus, the leaching rate of Fe cannot not be reported (Figure 8.2D). The leaching rate of Pb in UPW displays the same value as the one in biotic digested medium during the first 20 days of the experiments after which it decreased to a lower leaching rate (average of $0.00015\text{ mg Pb d}^{-1}$) (Figure 8.2F).

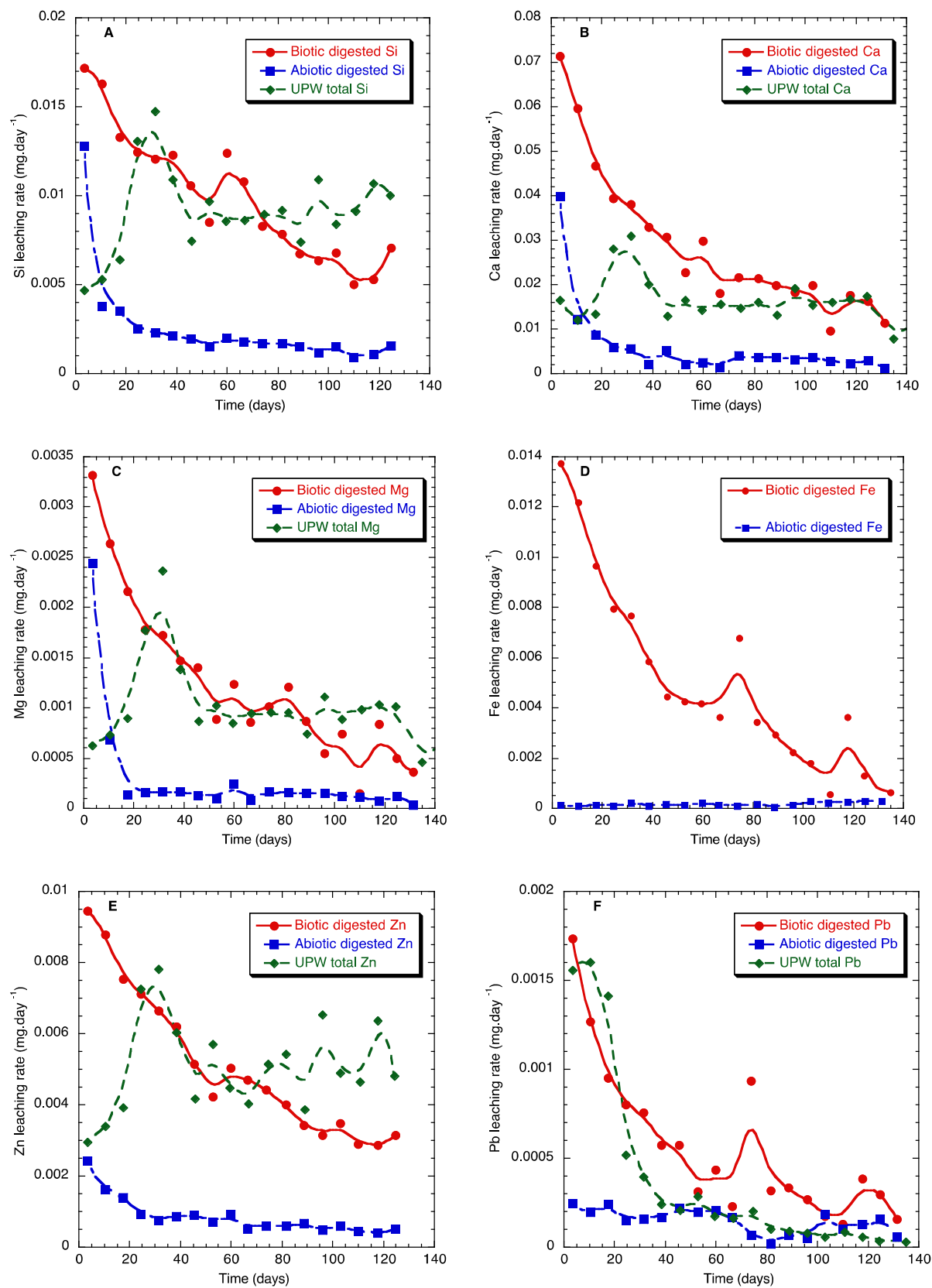


Figure 8.2. Evolution of the leaching rate as a function of time calculated from the elemental concentration of Si (A), Ca (B), Mg (C), Fe (D), Zn (E) and Pb (F) in weekly changed leaching aqueous media.

8.3.3. Slags weathering

A characteristic picture of a LBF slag surface before alteration is given in Figure 8.3. Typically, the SEM backscattered slag micrographs show white metallic lead droplets ranging from 2-20 μm in size, with spinel and dendrite embedded into the glass matrix. The spinel mineralogy has been previously described by Seignez et al. (2007) and varies from magnesiochromite (MgCr_2O_4), franklinite (ZnFe_2O_4) and magnetite ($\text{Fe}^{2+}\text{Fe}_2^{3+}\text{O}_4$) compositions. Along with the Pb droplets and spinels, plurimicrometric dendritic Zn substituted wüstite ($\text{Fe}_{0.85-x}\text{Zn}_x\text{O}$ with $0.085 < x < 0.170$) is observed in the glass matrix.

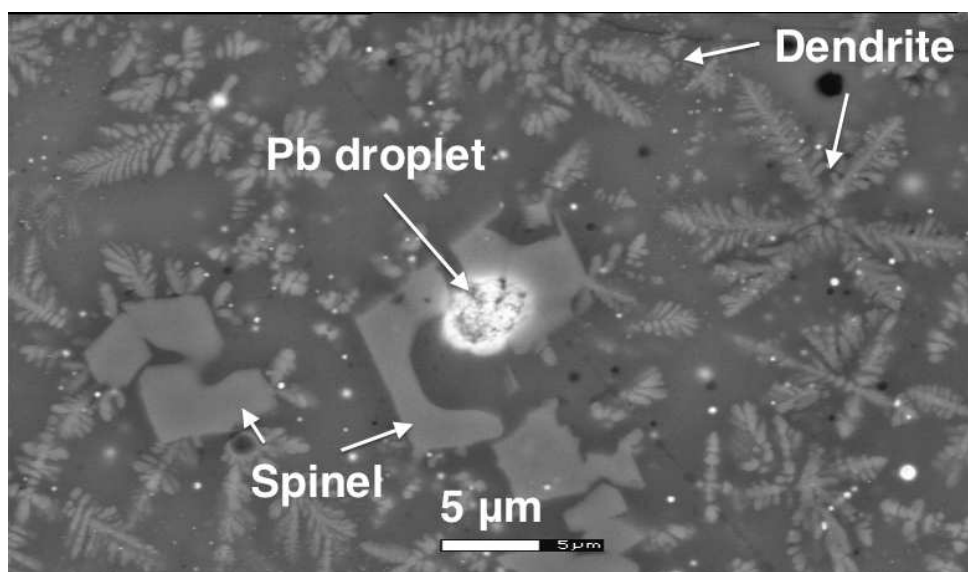


Figure 8.3. Surface investigation of LBF slags before alteration.

The surface of the slags is significantly changed after the alteration experiments in UPW (Figure 8.4), abiotic growth medium (Figure 8.5) and in biotic growth medium (Figure 8.6). The formation of lead carbonate as secondary phase is observed on the surface of slags incubated in UPW (Figure 8.4B). The slag glass matrix shows several micro-canyons (Figures 8.4A & 8.5A), while dendritic Fe-Zn oxides appear very stable since they are protuberant at the surface of the glass (Figure 8.5A). Like dendritic Fe oxides, spinel phases are stable to alteration and remain in place on the glass surface in abiotic medium (Figure 8.5A), while lead droplets are either strongly weathered or completely removed (Figure 8.5B). Figure 8.6A shows the distribution of major elements on the surface of a strongly weathered glass, altered in the biotic growth medium. The bacterial colonization and adhesion as a biofilm to the surface of the slag can also be observed (Figure 8.6B).

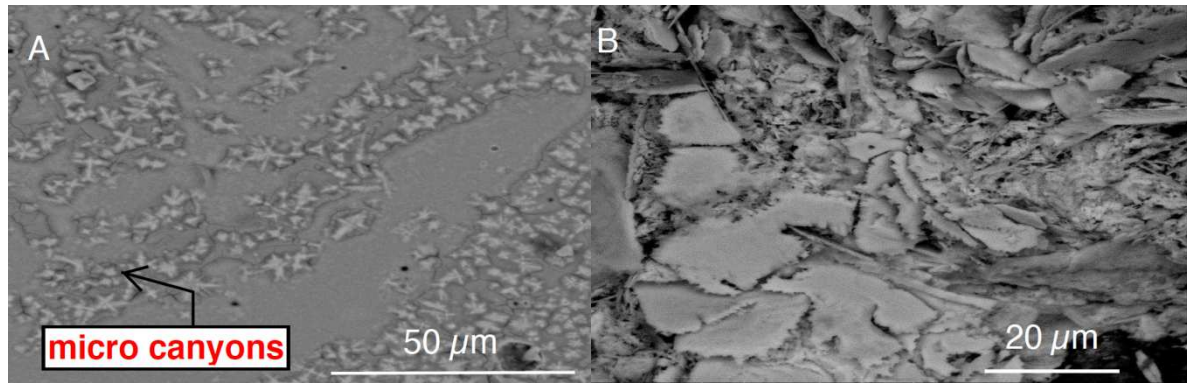


Figure 8.4. Alteration of LBF slags in ultrapure water medium. A: overall slag picture B: focus on a secondary mineral phase made of lead carbonate

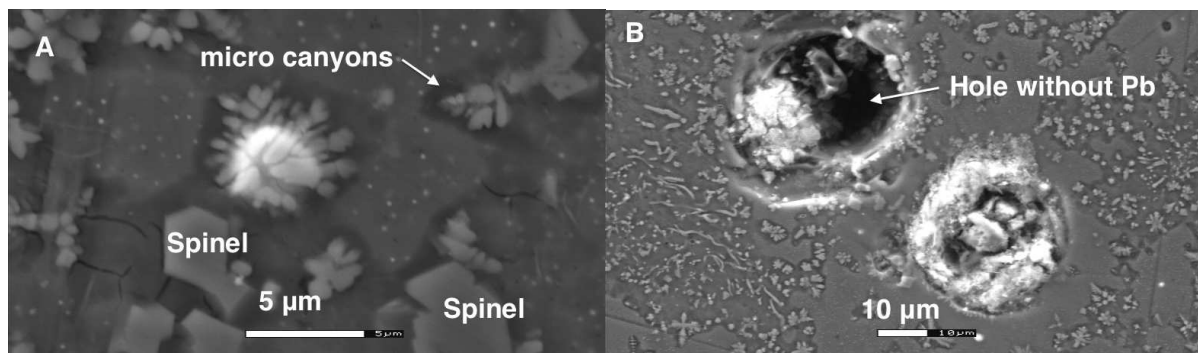


Figure 8.5. Alteration of LBF slags in the abiotic growth medium. A: overall slag picture B: focus on a hole where a Pb droplet was located

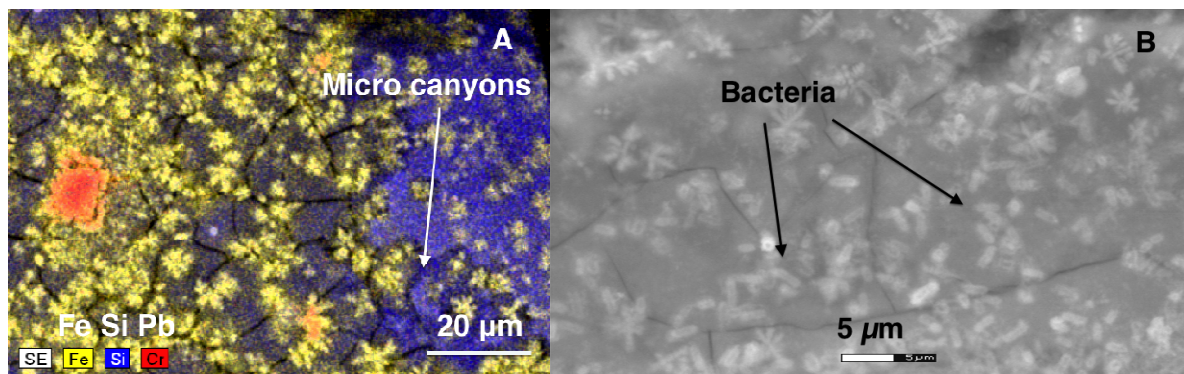


Figure 8.6. Alteration of LBF slags in the biotic growth medium. A: Elemental mapping with Fe in yellow and Si in blue, B: slags surface showing a bacterial layer.

Table 8.2 shows the evolution of the elemental composition of the slag glass matrix when incubated in ultrapure water and biotic growth medium. SEM-EDS analyses of the glass matrix shows that Ca is preferentially leached out compared to the other major elements. After 60 days of alteration, the glass matrix incubated in the biotic growth medium shows a slightly lower content of CaO compared to the glass matrix incubated in the ultrapure water medium. In the biotic growth medium, the glass matrix is progressively enriched in SiO₂ and FeO and displays a decrease in CaO as function of the leaching time (Table 8.2).

Table 8.2. SEM-EDS analyses of fresh and altered glass matrix when LBF slags are in contact with ultrapure water after 150 days, and biotic growth medium after 60 and 150 days.

Mass %	Mean composition of fresh glass matrix ²	Weathered glass matrix (in UPW)			Weathered glass matrix (in biotic growth medium)			
		Contact time (days)			60		150	
SiO ₂	34.35	28.32	29.53	30.62	28.60	32.67	38.80	48.06
FeO	36.72	50.38	47.94	45.57	55.27	46.30	54.97	47.76
CaO	28.92	21.30 ³	22.53	23.80	16.12	21.03	6.23	4.81

8.4. Discussion

8.4.1. Cumulative metal release LBF slags

This study showed that the total bulk release of Fe in the biodigested medium is 270.1 µg g⁻¹, compared to 7.5 µg g⁻¹ in the abiotic medium and below detection limit in UPW (Table 3). This could be due to the fact that Fe is the bio-essential element for *Pseudomonas aeruginosa* and Fe dissolution is enhanced by complexing with low molecular weight iron chelators "siderophores" produced by the bacteria. A similar trend has been found for the bulk release of Fe from shales in the presence of *Azotobacter vinelandii* known to release organic ligands (i.e. hydroxamate siderophore desferrioxamine B) that can make strong complexes with Fe (Liermann et al., 2011).

Comparing the biodigested to the biodissolved Fe content, the Fe release is 91.1 µg g⁻¹ in biodissolved medium (accounting for 28%) while the remaining 72% is associated with bacterial cells. During weathering, therefore, most of the solubilized Fe has been either complexed to the siderophores for further transport to the bacteria or already adhered onto the cell surface of the bacteria for further bio-uptake. This agrees with a recent study by (Julien et al., 2014).

²from Seignez et al., 2006

Concerning the major elements (i.e. Fe, Ca and Mg), the highest release per g of LBF was observed in the biodigested media compared to abiotic and UPW medium. The Si release is approximately the same between biodigested and biodissolved media (504.2 compared to 483.2 $\mu\text{g g}^{-1}$ of LBF) indicating that the bacterial cell surface is not serving as sorbent for Si; this is in contrast to Ca, Mg and Fe. The Si dissolution in UPW is almost as high as in the biotic media (462.7 μg of Si per g of LBF in UPW compared to 504.2 $\mu\text{g g}^{-1}$ in biodigested medium). However, the Si dissolution can be indirectly related to the presence of bacteria, because microbial growth enhances the release of alkali and alkali earth ions which may promote the solubilization of Si from the glassy matrix by allowing a better hydrolysis of the silica network (Frugier et al., 2008).

The cumulative Zn release amounts to 257.0 $\mu\text{g g}^{-1}$ and 260.4 $\mu\text{g g}^{-1}$ in UPW and biodigested medium, respectively (Table 8.3). The significant release of Zn in the UPW experiment may be explained by the lower pH: 7.5 compared to 8.5 in the growth medium. Half of the Zn released in the biotic digested medium has been sorbed onto bacterial surfaces or embedded in the biofilm matrix since only 136.8 μg of Zn was measured per g of LBF in the biotic dissolved medium (Table 8.3). The amount of Pb released in biotic digested medium and in UPW is 29.7 $\mu\text{g g}^{-1}$ and 20.3 $\mu\text{g g}^{-1}$ respectively, while only 7.0 $\mu\text{g g}^{-1}$ was found in the biodissolved medium. According to Wu et al. (2006) and Karimzadeh et al. (2012), the mobility of heavy metals like Pb and Zn during slag bioweathering is not only due to the presence of bacteria, but also to siderophores with the formation of Pb-siderophore and Zn-siderophore complexes (Karimzadeh et al., 2012; Wu et al., 2006).

Table 8.3. Cumulative element release from LBF slag after 128 days of alteration. The calculations have been performed considering the total amount of each element leached in solution and the total mass of slags present in the reactors.

Cumulative release ($\mu\text{g g}^{-1}$ of LBF)	Biodigested	Biodissolved	Abiotic	UPW
Fe	270.1 (± 0.1)	91.1 (± 0.1)	7.5 (± 0.1)	<DL
Ca	1502.6 (± 0.1)	1144.1 (± 0.1)	312.3 (± 0.1)	871.4 (± 0.1)
Mg	65.6 (± 0.1)	47.2 (± 0.1)	14.9 (± 0.1)	54.0 (± 0.1)
Si	504.2 (± 0.1)	483.2 (± 0.1)	127.2 (± 0.2)	462.7 (± 0.1)
Zn	260.4 (± 0.1)	136.8 (± 0.1)	42.6 (± 0.1)	257.0 (± 0.1)
Pb	29.7 (± 0.2)	7.0 (± 0.2)	7.6 (± 0.1)	20.3 (± 0.1)

Figures 8.7A and 8.7B give the percentage of all the elements leached out compared to the initial bulk content. The release of metals in the biodigested medium follows the order (greatest to least): 1.08% of Ca > 0.63% of Mg > 0.5% of Si > 0.31% of Zn > 0.12% of Fe > 0.1% of Pb. The same trend can be seen in the Abiotic medium except Fe was below the detection limit. The presence of bacteria (considering both Biotic digested and Abiotic) clearly

elevated the release of all elements from slag (Figure 8.7A). In addition, the data confirm that bacterial cells are good sorbents for Fe, Pb and Zn as 0.08% out of 0.12% total Fe, 0.07% out of 0.10% of total Pb and 0.15% out of 0.31% total Zn are found as sorbed fraction (here denoted as particulate) (Figure 8.7B).

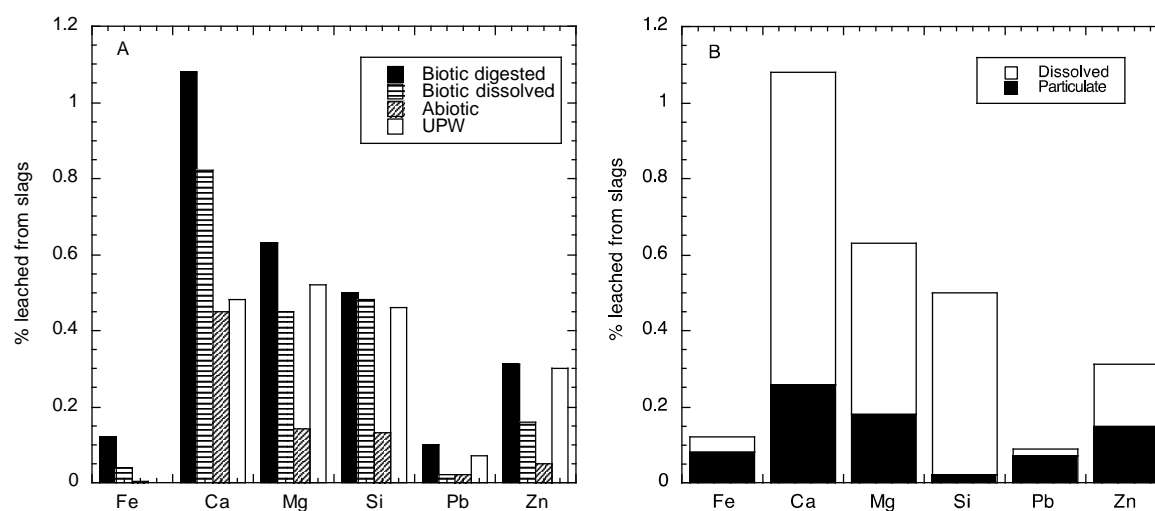


Figure 8.7. A: Percentage of leached elements compared to initial content after 128 days of alteration, B: Leached element partitioning between the dissolved and particulate fractions in the biotic leaching experiments.

8.4.2. Leaching rates

After 60 days of alteration, the leaching rates of Si, Ca and Mg are higher in UPW compared to those in biotic digested medium. Leaching rates of Si, Ca and Mg are notably accelerated by *Pseudomonas aeruginosa* (biotic digested medium) in the early stages of the experiments (<45 days); these rates are later governed by chemical processes (UPW) at a stable and constant pace (Figures 8.2A,B,C). Thus, chemical processes also play an important role in leaching at a constant rate in the long-term. Meanwhile, the leaching rate of Fe is solely governed by the bacteria as the rate in biotic digested medium is significantly faster than that of the other media. Likewise, the Pb leaching rate is mainly controlled and accelerated by the bacteria (biotic digested medium) even though similar initial leaching rates are observed in UPW during the first 40 days of the experiment. This could be due to the higher affinity of extracellular polymeric substances (EPS) for Pb over Zn: as the adsorption capacity and the complexation intensities of EPS is different depending on the metal ions. Moon et al (2006) reported that the adsorption capacity ($\ln K$) and intensity ($1/n$) of EPS are 1.06 and 0.637 for Pb, which are much higher than those for Zn (0.41 and 0.62, respectively).

Assuming that the LBF slags are dumped on site, and the conditions present in our experiments reflect the natural environment of the slag heap, the leaching rate of the metals have been recalculated in Table 8.4. Also shown is the amount of time needed to leach all the metals. These calculations suggest that it will take 114 years to leach all Zn (and 362 years for all Pb) from 1 g of LBF from the slag dump in the presence of bacteria. For this prediction,

the formation of secondary phases on the slags surface acting as the preservative layer against dissolution is neglected.

Table 8.4. Extrapolated time in years required to completely leach 1 g of LBF under the conditions applied in this study.

Elements	Leaching rate ($\mu\text{g g}^{-1} \text{d}^{-1}$ of LBF)		Time required to leach 1 g of LBF completely (Years)	
	Biodigested	UPW	Biodigested	UPW
Fe	2.11	0.00	291.1	n.a
Ca	11.74	6.81	32.6	56.2
Mg	0.51	0.42	56.0	68.0
Pb	0.23	0.16	362.4	530.0
Si	3.94	3.62	70.1	76.4
Zn	2.03	2.01	114.4	116.0

n.a: not applicable

8.4.3. Leaching mechanisms

Cumulative molar concentrations of Ca, Mg and Zn have been normalized to a cumulative Si molar concentration (Figures 8.8 A,B,C), which is considered as the most representative element of glass alteration (Gauthier et al., 2000). It is therefore possible to use these Si concentrations to assess the stoichiometric/non-stoichiometric dissolution of the glass (Chardon et al., 2006). From the bulk composition determined by Deneele (2002) (Table 8.1) the molar ratios are expected to be 1, 0.11 and 0.34 for Ca/Si, Mg/Si and Zn/Si, respectively. The measured Ca/Si and Mg/Si ratios are above the theoretical ratio, meaning that Ca and Mg are more easily leached out compared to Si (Figures 8.8A and 8.8B). The ratios of Ca/Si and Mg/Si are much higher in the biotic digested medium than in the abiotic digested medium and UPW medium, which implies that the microbial activity greatly influences the leachability of Ca and Mg compared to the physico-chemical conditions prevailing in the UPW and the abiotic medium. However, Figure 8.8C shows that the Zn/Si ratio is below the theoretical ratio, which implies that the Zn mobility is far less important than Ca and Mg. As the Zn/Si ratio in UPW exceeds that of biotic digested medium, Zn dissolution appears to be greatly influenced by chemical parameters compared to biological ones.

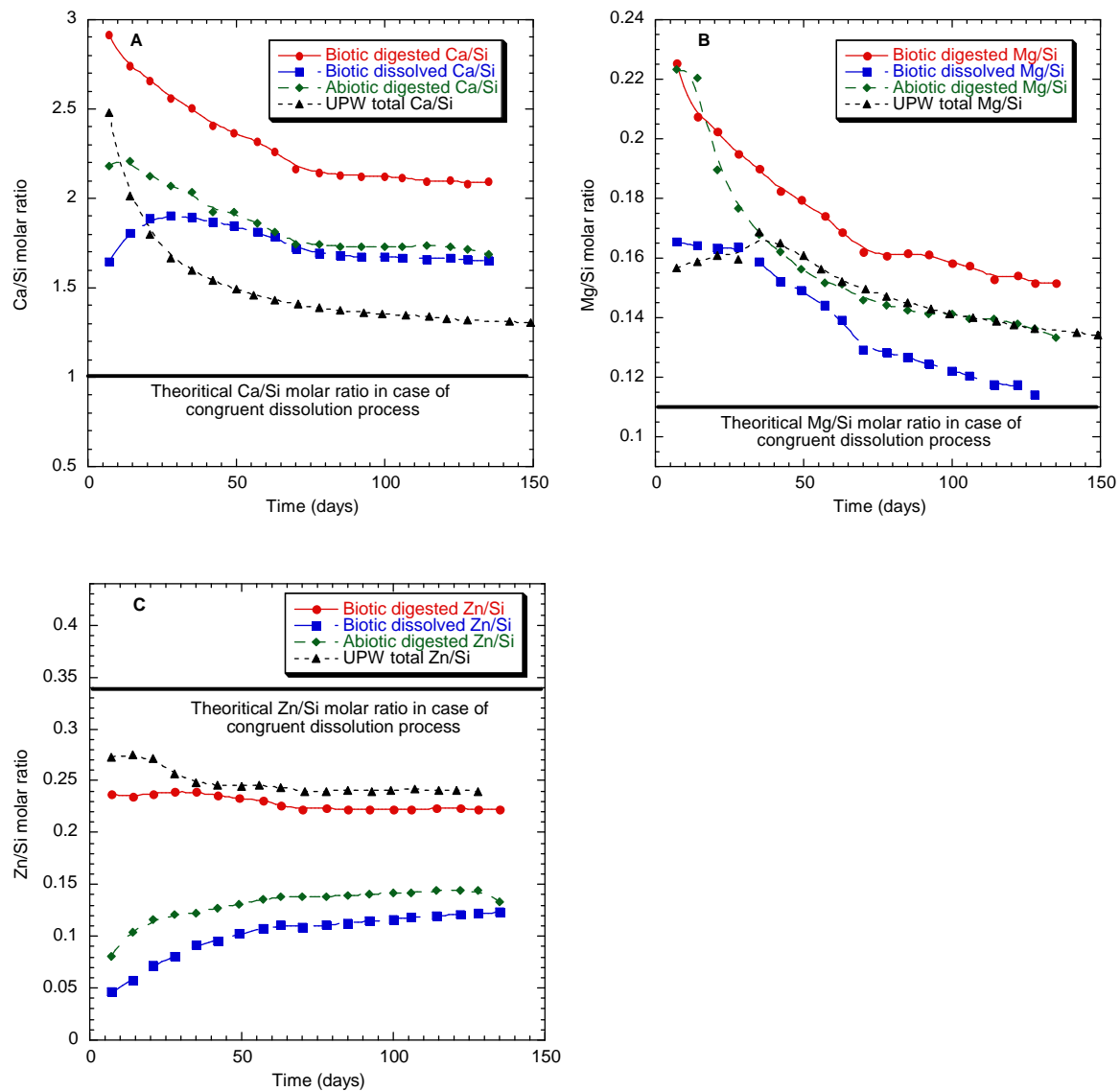


Figure 8.8. Evolution of Ca/Si (A), Mg/Si (B) and Zn/Si (C) cumulative leached molar ratios for the three experimental conditions investigated, compared the theoretical molar ratio in case of a congruent dissolution process.

The possible leaching mechanisms can be schematized as in Figure 8.9. One can assume that pure chemical reactions (i.e. solid-liquid interactions) are initiated first, prior to being enhanced by the presence of bacteria, which act as good cation bio-sorbents. The interaction between LBF slag and UPW (simplest medium as a reference) leads to the dissolution of Ca^{2+} and Mg^{2+} , leaving the slag's surface negatively charged. The negative charge in the silicon network is neutralized by H^+ from H_2O , resulting in a pH increase. At the same time, bacteria, which are known to have the highest surface to volume ratio of any life form (Konhauser, 2007) with plenty of binding sites such as phosphoryl, carboxyl, hydroxyl, and amino groups begin to bind heavy metal ions (Guibaud et al., 2009). The pH increase (7 to 9) related to

enhanced Ca^{2+} and Mg^{2+} dissolution would lead to the deprotonation of the metal binding sites of polysaccharides, resulting in increased cation biosorption (Moon et al., 2006).

In addition, bacteria such as *Pseudomonas* sp. need Fe for their growth and this microorganism is well-known for producing siderophores which are involved in Fe complexation (Braud et al., 2009). This is very likely the main reason why the Fe concentration (i.e. solubility) is strongly enhanced in the Biotic media (this study, Yin et al., 2014). The presence of siderophores may also enhance the dissolution (via a ligand promoted dissolution mechanism) and solubility of zinc and lead (Karimzadeh et al., 2012; Wu et al., 2006). The presence of siderophores as well as the bacterial cells in the bulk solution increases the slag dissolution by complexing the main cations (i.e. Ca, Mg, Fe, Zn and Pb). This decreases the free ion concentration and causes a thermodynamic shift which favors further slag dissolution as predicted by Le Chatellier's principle.

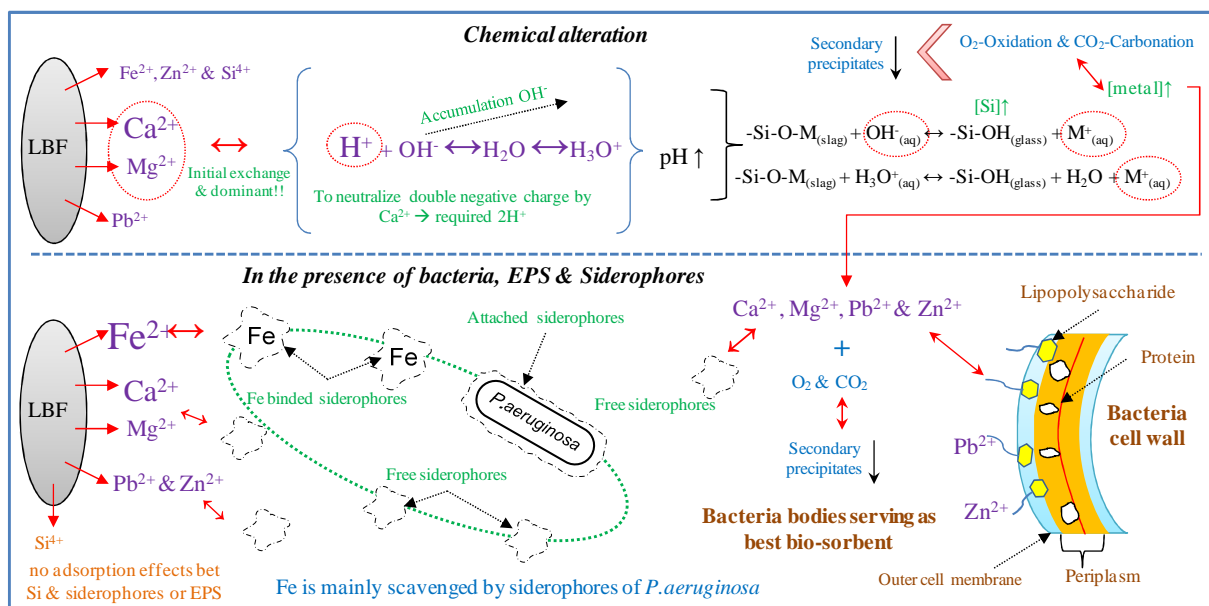


Figure 8.9. Alteration of LBF slags by the heterotrophic bacterium *Pseudomonas aeruginosa*.

8.5. Conclusions

Experiments to study the bio-alteration of lead blast furnace slags by *Pseudomonas aeruginosa* in a semi-flow through reactor were performed to simulate the release of potentially toxic elements from these slags. The results suggest that dissolution and bulk release of matrix elements (Ca, Si, Mg) as well as toxic elements (Zn and Pb) are equally governed by both chemical and biological processes, whereas Fe release can be solely driven by microbial activity via the production of soluble complexing molecules such as siderophores. Even though Pb is present as free droplets in the slag matrix, the bulk release is the lowest ($29.7 \mu\text{g g}^{-1}$) at the end of the experiment, where bio-alteration is thought to be at a minimum. Zn is significantly controlled by spinel mineral phases which are more resistant to weathering and alteration, but the amount released is significant ($260.4 \mu\text{g g}^{-1}$). The actively metabolizing heterotrophic bacteria can thus substantially increase elemental release rates

from slags compared to abiotic conditions. In addition, the bacteria are able to adsorb metal contaminants (Zn and Pb) and therefore might attenuate metal migration in soils. However, as bacteria can also migrate through soils, a better understanding of the combined effect of these two processes is required.

8.6. References

- Anderson, C.R., Pedersen, K., 2003. In situ growth of *Gallionella* biofilms and partitioning of lanthanides and actinides between biological material and ferric oxyhydroxides. *Geobiol*, 1: 169-178.
- Aouad, G., Geoffroy, V., Meyer, J.M., Crovisier, J.L., Damidot, D., Stille, P., 2005. Mise au point d'un milieu de culture pour l'étude de l'altération de silicates en présence de *Pseudomonas aeruginosa*. *Comptes Rendus Geoscience*, 337: 1340-1347.
- Aouad, G., Crovisier, J.L., Geoffroy, V.A., Meyer, J.M., Stille, P., 2006. Microbially-mediated glass dissolution and sorption of metals by *Pseudomonas aeruginosa* cells and biofilm. *J Hazard Mater*, 136: 889-895.
- Barna, R., Moszkowicz, P., Gervais, C., 2004. Leaching assessment of road materials containing primary lead and zinc slags. *Waste Manage*, 24: 945-955.
- Banerjee, N.R., Muehlenbachs, K., 2003. Tuff life: Bioalteration in volcanoclastic rocks from the Ontong Java Plateau. *Geochem Geophys Geosys*, 4: 1037-1059.
- Braud, A., Hoegy, F., Jezequel, K., Lebeau, T., Schalk, I.J., 2009. New insights into the metal specificity of the *Pseudomonas aeruginosa* pyoverdine-iron uptake pathway. *Environ Microbiol*, 11: 1079-1091.
- Chardon, E.S., Livens, F.R., Vaughan, D.J., 2006. Reactions of feldspar surfaces with aqueous solutions. *Earth Sci Rev*, 78: 1-26.
- Cheng, Y., Guo, Z., Liu, X., Yin, H., Qiu, G., Pan, F., Liu, H., 2009. The bioleaching feasibility for Pb/Zn smelting slag and community characteristics of indigenous moderate-thermophilic bacteria. *Bioresour Technol*, 100: 2737-2740.
- De Andrade Lima, L.R.P., Bernardez, L.A., 2011. Characterization of the lead smelter slag in Santo Amaro, Bahia, Brazil. *J Hazard Mater*, 189: 692-699.
- De Andrade Lima, L.R.P., Bernardez, L.A., 2012. Isotope Source Signatures for a Primary Lead Smelter Located Close to Todos os Santos Bay, Brazil. *Soil Sediment Contam: An Int J*, 20: 672-687.
- Deneele, D., 2002. Caractérisation, simulations expérimentales et thermodynamiques de l'altération de déchets vitreux: les scories de première fusion de plomb et de zinc. *PhD thesis manuscript*, Université Des Sciences et Technologies de Lille I and U.F.R. Des Sciences De La Terre, France, 1-242.

- Ettler, V., Legendre, O., Bodéan, F., Touray, J.C., 2001. Primary Phases and Natural Weathering of Old Lead–Zinc Pyrometallurgical Slag from PRÍbram, Czech Republic. *Can Mineral*, 39: 873-888.
- Ettler, V., Mihaljevic, M., Touray, J.C., Piantone, P., 2002. Leaching of polished sections: an integrated approach for studying the liberation of heavy metals from lead-zinc metallurgical slags. *Bulletin de la Société géologique de France*, 173: 161-169.
- Ettler, V., Piantone, P., Touray, J.C., 2003a. Mineralogical control on inorganic contaminant mobility in leachate from lead-zinc metallurgical slag: experimental approach and long-term assessment. *Mineral Mag*, 67: 1269-1283.
- Ettler, V., Komarkova, M., Jehlicka, J., Coufal, P., Hradil, D., Machovic, V., Delorme, F., 2004. Leaching of lead metallurgical slag in citric solutions-implications for disposal and weathering in soil environments. *Chemosphere*, 57: 567-77.
- Frugier, P., Gin, S., Minet, Y., Chave, T., Bonin, B., Godon, N., Lartigue, J.E., Jollivet, P., Ayral, A., De Windt, L., Santarini, G., 2008. SON68 nuclear glass dissolution kinetics: Current state of knowledge and basis of the new GRAAL model. *J Nucl Mat*, 380: 8-21.
- Gauthier, A., Le Coustumer, P., Motelica, M., Donard, O.F.X., 2000. Real time alteration of a nuclear waste glass and remobilization of lanthanide into an interphase. *Waste Manage*, 20: 731-739.
- Guibaud, G., van Hullebusch, E., Bordas, F., d'Abzac, P., Joussein, E., 2009. Sorption of Cd(II) and Pb(II) by exopolymeric substances (EPS) extracted from activated sludges and pure bacterial strains: modeling of the metal/ligand ratio effect and role of the mineral fraction. *Bioresour Technol*, 100: 2959-2568.
- Herisson, J., van Hullebusch, E.D., Moletta-Denat, M., Taquet, P., Chaussadent, T., 2013. Toward an accelerated biodeterioration test to understand the behavior of Portland and calcium aluminate cementitious materials in sewer networks. *Int Biodeterior Biodegrad*, 84: 236-243.
- Julien, C., Laurent, E., Legube, B., Thomassin, J.H., Mondamert, L., Labanowski, J., 2014. Investigation on the iron-uptake by natural biofilms. *Water Res*, 50: 212-220.
- Karimzadeh, L., Nair, S., Merkel, B.J., 2012. Effect of microbial siderophore DFOB on Pb, Zn, and Cd sorption onto zeolite. *Aqua Geochem*, 19: 25-37.
- Konhauser, K.O., 2007. Introduction to geomicrobiology. *Blackwell Publishing*.
- Liermann, L.J. et al., 2011. Extent and isotopic composition of Fe and Mo release from two Pennsylvania shales in the presence of organic ligands and bacteria. *Chem Geol*, 281: 167-180.
- Mahé-Le Carlier, C., Le Carlier de Veslud, C., Ploquin, A., Royer, J.J., 2000. Altération des scories de la métallurgie ancienne: un analogue de déchets vitrifiés. *Compt. Rend.Acad. Sci. (Paris), Série II. Sciences de la Terre et des planètes*, 330: 179-184.

- Moon, S.H., Park, C.-S., Kim, Y.-J., Park, Y.-I., 2006. Biosorption isotherms of Pb (II) and Zn (II) on Pestan, an extracellular polysaccharide, of *Pestalotiopsis sp. KCTC 8637P*. *Process Biochem*, 41: 312-316.
- Okabe, S., Odagiri, M., Ito, T., Satoh, H., 2007. Succession of sulfur-oxidizing bacteria in the microbial community on corroding concrete in sewer systems. *Appl Environ Microbiol*, 73: 971-980.
- Roberts, D., Nica, D., Zuo, G., Davis, J., 2002. Quantifying microbially induced deterioration of concrete: initial studies. *Int Biodeterior Biodegrad*, 49: 227-234.
- Seigneur, N., Bulteel, D., Damidot, D., Gauthier, A., Potdevin, J.L., 2006. Weathering of metallurgical slag heaps: multi-experimental approach of the chemical behaviours of lead and zinc. *Waste Manage Environ III*, 1: 31-40.
- Seigneur, N., Gauthier, A., Bulteel, D., Buatier, M., Recourt, P., Damidot, D., Potdevin, J.L., 2007. Effect of Pb-rich and Fe-rich entities during alteration of a partially vitrified metallurgical waste. *J Hazard Mater*, 149: 418-431.
- Seigneur, N., Gauthier, A., Bulteel, D., Damidot, D., Potdevin, J.L., 2008. Leaching of lead metallurgical slags and pollutant mobility far from equilibrium conditions. *Appl Geochem*, 23: 3699-3711.
- Sobanska, S., Ledésert, B., Deneele, D., Laboudigue, A., 2000. Alteration in soils of slag particles resulting from lead smelting. *Earth Planet Sci*, 331: 271-278.
- Uroz, S., Calvaruso, C., Turpault, M.P., Frey-Klett, P., 2009. Mineral weathering by bacteria: ecology, actors and mechanisms. *Trends Microbiol*, 17: 378-387.
- Verguts, P., 2005. Two dimensional mathematical simulation model for a non-ferrous blast furnace. *PhD thesis manuscript*, Katholieke Universiteit Leuven, Belgium: 1-168.
- Willscher, S., Pohle, C., Sitte, J., Werner, P., 2007. Solubilization of heavy metals from a fluvial AMD generating tailings sediment by heterotrophic microorganisms. *J Geochem Explor*, 92: 177-185.
- Wu, S.C., Luo, Y.M., Cheung, K.C., Wong, M.H., 2006. Influence of bacteria on Pb and Zn speciation, mobility and bioavailability in soil: A laboratory study. *Environ Pollut*, 144: 765-773.
- Yin, N.H., Sivry, Y., Avril, C., Borensztajn, S., Labanowski, J., Malavergne, V., Lens, P.N.L., Rossano, S., van Hullebusch, E.D., 2014. Bioweathering of lead blast furnace metallurgical slags by *Pseudomonas aeruginosa*. *Int Biodeterior Biodegrad*, 86: 372-381.

CHAPTER 9

Summary and Conclusions

Chapter 9

9.1. Introduction

Metallurgical activities can generate a huge amount of partially vitrified waste products which are either landfilled or recycled. Lead Blast Furnace (LBF) and Imperial Smelting Slags (ISF) slags are often disposed in the vicinity of metallurgical plants, and may be prone to weathering, releasing potentially toxic chemical components into the local environment. Thus, the aim of this research is to understand the chemical processes as well as the contribution of micro-organisms in weathering of metallurgical slags.

9.2. Chemical weathering of slags (Chapter 5 and 6)

9.2.1. Stability of primary mineral phases

The leachate chemistry was controlled by the dissolution of primary crystalline and glassy phases present in both LBF and ISF slags. In general, crystalline phases (either spinels or silicates) are well-known for being resistant while amorphous glassy phases are easily prone to weathering and releasing metals into the solution (Chapter 5). Partial dissolution of magnesiochromite (MgCr_2O_4) from LBF and gahnite (ZnAl_2O_4) from ISF slags can be expected at low pHs; 4 and 5.5. Spinel such as zincchromite (ZnCr_2O_4), magnetite ($\text{Fe}^{2+}\text{Fe}^{3+}_2\text{O}_4$), and franklinite (ZnFe_2O_4) can be resistant to weathering even at pH 4, whereas it is very likely that leachate chemistry can be influenced by partial dissolution of franklinite at pH 8.5 for LBF slag (Chapter 5, subsection 5.4.1.3). Likewise, the partial dissolution of hardystonite ($\text{Ca}_2\text{ZnSi}_2\text{O}_7$) and willemite (Zn_2SiO_4) can be expected at pH 10 for both slags. In comparison to spinels and silicates phases, the amorphous glassy phase of slags is prone to weathering and major contributor of metals into the solution at all pHs. Considering some of the spinels phases being prone to weathering at low pH as well as silicates phases at high pH, it is very likely that the dissolution of these phases are minimal at neutral pH, thus, the leachate chemistry at pH 7 are mainly governed by dissolution of glassy phase of the slags.

9.2.2. Zn isotopes signatures of primary mineral phases

As depicted in Figure 9.1, complete acid digestion of both LBF and ISF slags showed that bulk materials are enriched in heavier isotopes; with $\delta^{66}\text{Zn}_{\text{JMC}}$ $0.78 \pm 0.13\text{‰}$ and $0.13 \pm 0.06\text{‰}$ in ISF and LBF slags, respectively (Chapter 6). Rather lighter signatures can be observed in amorphous glassy phase of slags where the range of $\delta^{66}\text{Zn}$ lies between -0.42‰ for LBF and -0.35‰ for ISF with $\pm 0.08\text{‰}$ 2 sigma values. Meanwhile, heaviest signatures of overall crystalline phases can be extrapolated where $\delta^{66}\text{Zn}$ lies between 2.12‰ for LBF and 5.74‰ for ISF. The calculated Zn signatures of crystalline phases can be accounted for spinels: magnesiochromite (MgCr_2O_4), franklinite (ZnFe_2O_4), magnetite ($\text{Fe}^{2+}\text{Fe}^{3+}_2\text{O}_4$) in LBF; zincchromite (ZnCr_2O_4), gahnite (ZnAl_2O_4) in ISF; and for silicates phases; hardystonite ($\text{Ca}_2\text{ZnSi}_2\text{O}_7$) and willemite (Zn_2SiO_4) for both slags.

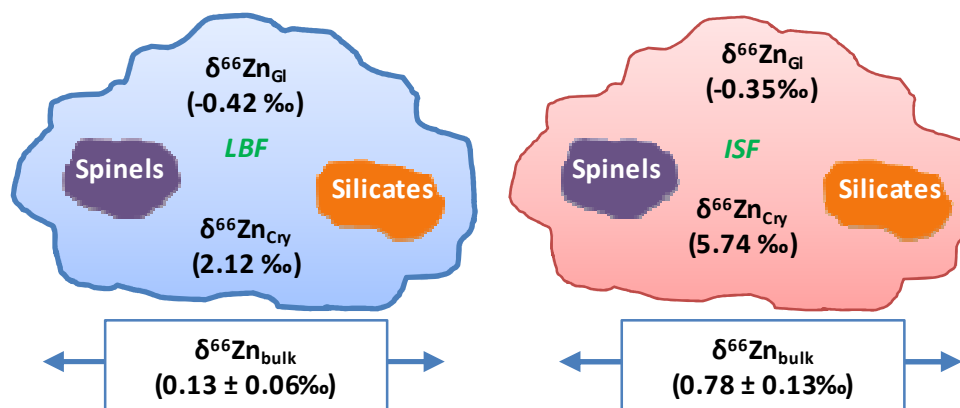


Figure 9.1. Zn isotopes signatures of bulk slags (measured), amorphous glassy part and crystalline phases (extrapolated).

9.2.3. Evolution of leachate chemistry

The concentration of Ca and Zn can be related to pH where the highest concentration at pH 4 and the lowest concentration at pH 10 can be observed under both atmospheres for both LBF and ISF slags (Chapter 5). The leachability of Fe was limited at pH 8.5 and 10 for LBF slag under both atmospheres, whereas that of Fe was possible even at high pHs under nitrogen atmosphere for ISF slag, compared to Fe is under detection limit under open-air atmosphere. In addition, the concentration of Si was higher at pH 4 and 10 for both slags, whereas the concentrations were much higher under nitrogen atmosphere compared to open-air atmosphere. Unlike other elements, the concentration of Pb from both slags was independent of pHs and atmospheres, with high fluctuations in concentrations due to its presence as metallic Pb droplets in the slags.

In addition, the faster log dissolution rates of Si were observed at pH 4 for LBF slags (-7.92 to $-8.03 \text{ mol.m}^{-2}.\text{s}^{-1}$) compared to (-8.03 to $-8.13 \text{ mol.m}^{-2}.\text{s}^{-1}$) for ISF slags, suggesting that LBF slags are prone to weathering at acidic conditions regardless of the atmospheres. Similarly, the slighter faster log dissolution rates of Si were observed under open-air atmospheres for both slags (-9.69 to $-9.79 \text{ mol.m}^{-2}.\text{s}^{-1}$), compared to that under nitrogen atmosphere (-10.05 to $-9.53 \text{ mol.m}^{-2}.\text{s}^{-1}$), suggesting that both slags are prone to higher weathering at alkaline condition under open-air atmosphere rather than under anoxic conditions.

9.2.4. Secondary precipitates

The duration of the slag-water interaction time as well as the effects of the atmospheres played a great role in the formation of new secondary phases (Chapter 5). The presence of oxygen and carbon dioxide led to the formation of oxide and carbonates phases under open-air atmospheres whereas mostly hydroxides were formed under nitrogen atmosphere. The secondary precipitates observed in this study are mainly oxides, carbonates and clay phases which are predicted by thermodynamic model Visual MINTEQ and further confirmed by SEM and TEM analysis as shown in Figure 9.2.

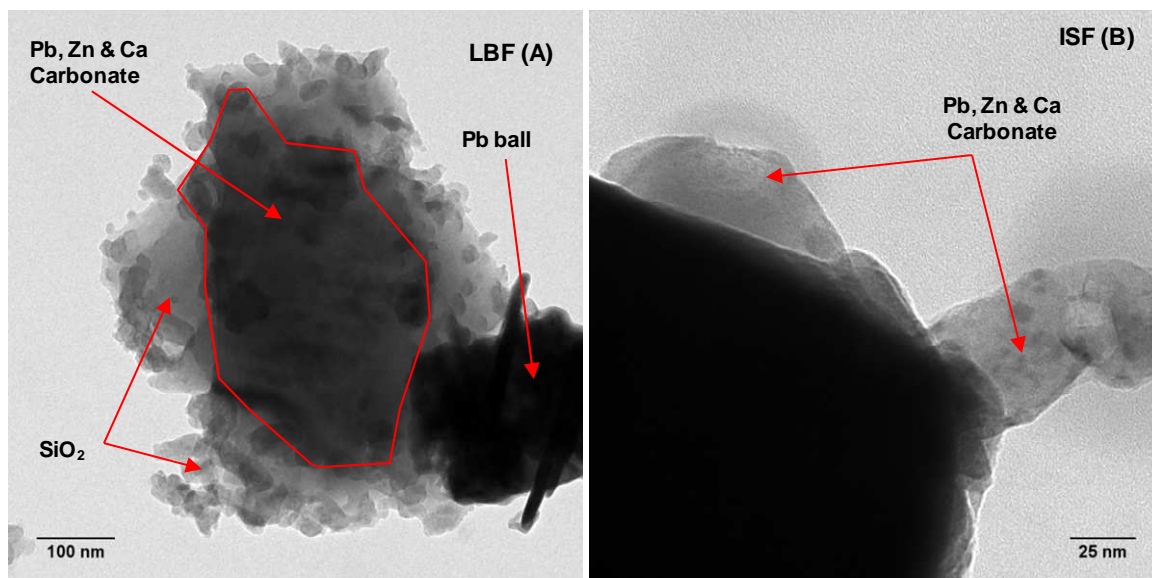


Figure 9.2. TEM observation on precipitation of Ca, Pb and Zn carbonates during weathering of (A) LBF slags and (B) ISF slags under open air atmosphere.

9.2.5. Zn isotopes fractionation induced by chemical processes

Zn dissolution was related to extremes zinc isotopic signatures in the leachate as a function of pHs, leaching time, and atmospheres (Chapter 6). For instance, heavier $\delta^{66}\text{Zn}$ values can be observed at low pH than at high pH for both slags; i.e. 0.03‰ and -1.25‰ for LBF, 0.89‰ and -1.16‰ for ISF after 6 h of leaching at pH 4 and 10, respectively under open-air atmosphere. In addition, the signatures of the leachate became enriched in heavier isotopes with time under nitrogen atmospheres for both slags; for instance, from -0.53‰ after 6 h to 0.85‰ after 216 h for ISF slag at pH 10. This may imply that the absence of secondary precipitates allows more congruent slag dissolution and, thus, weathered Zn reaches isotopic signature closer to the bulk slag.

On the other hand, the formation of new secondary phases induced massive Zn isotopes fractionation for both slags at pH 7, 8.5 and 10 where the fractionation can be identified by comparing the $\delta^{66}\text{Zn}$ signatures under both atmospheres (Figure 9.3). During weathering of LBF at pH 7, formation of ferrihydrite (FeOOH) with possible Zn adsorption onto it could induce $\Delta^{66}\text{Zn}$ of 0.70‰ after leaching for 24 h, whereas formation of FeOOH , PbCO_3 , and Zn-Al LDH phases induced higher fractionation with $\Delta^{66}\text{Zn}$ of 1.50‰ after leaching for 216 h. When the rapid precipitation of $\text{Zn}(\text{OH})_2$ alone occurred, the signatures of the leachate can be as light and stable as -2.10‰ to -2.35‰ during weathering of LBF at pH 8.5 under nitrogen atmosphere. On the other hand, the precipitation of $\text{Zn}(\text{OH})_2$ along with $\text{Fe}(\text{OH})_2$ induced $\Delta^{66}\text{Zn}$ of 0.2‰ during weathering of ISF at pH 8.5. In addition, the fractionation induced by co-precipitation of Ca and PbCO_3 where partial cooperation of Zn inside with a rather consistent $\Delta^{66}\text{Zn}$ values of 1.13‰ during weathering of both slags at pH 10. Thus, the fractionation of Zn was significantly induced during formation of different secondary phases

either as oxides, oxyhydroxides, hydroxides, clay minerals or carbonates, and the fractionation occurred via adsorption or co-precipitation processes.

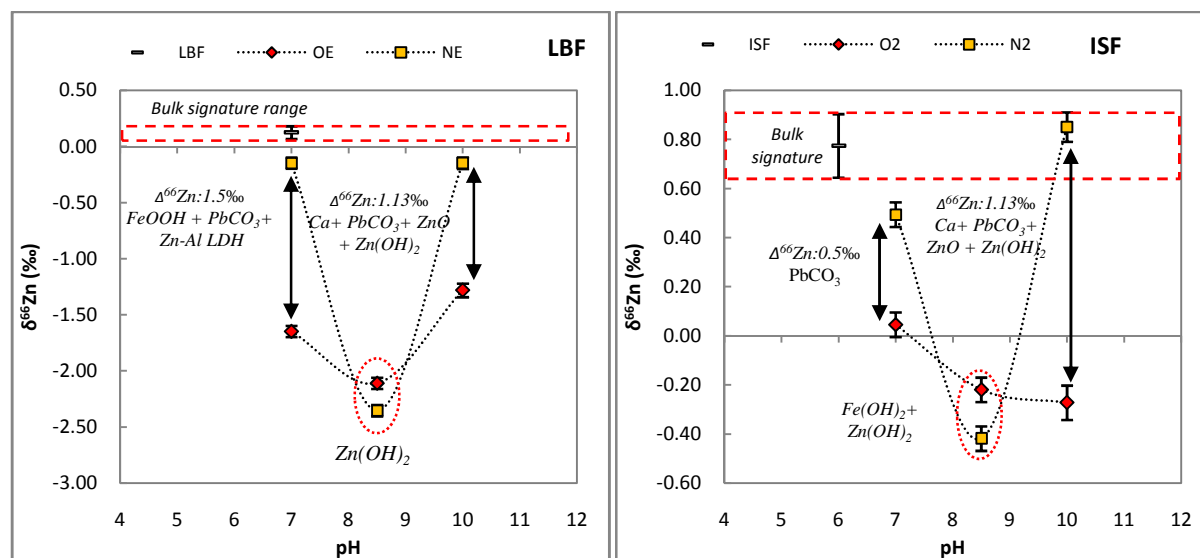


Figure 9.3. Fractionation of Zn isotopes induced by (co)precipitation and sorption processes after weathering of LBF and ISF slags for 216 h.

9.3. Biological weathering of slags (Chapter 7 and 8)

9.3.1. Slags as micro-nutrient substrate

The fastest growth of *Pseudomonas aeruginosa* was observed in the presence of slags, whereas no poor bacterial growth (absorbance of 0.01) was observed without the presence of slags (Chapter 7). Thus, this implies that microbial growth was not only possible, but was also enhanced in the presence of slags, serving as micro-nutrients (i.e. Fe, Ca, Mg,...) source for the growth.

9.3.2. Effect of abiotic factors

At first glance, the concentration of Zn and Pb are higher in ultrapure water medium (UPW) than in growth medium (GM), which can be related to solution pH (pH: 6.8 and 7.8 in UPW and GM experiments, respectively) where the enhancement of metal solubility in acidic pH is a well-known process. In UPW, the solubility of Pb was mainly controlled by carbonate and hydroxide phases, whereas Zn was not controlled by precipitates formation the solubility indices were under saturation. On the other hand, phosphate was the main species controlling the solubility of Ca, Zn and Pb in GM where the saturation indexes were ranging from 0.2 to 1.4. The formation of possible secondary precipitates of Zn ($Zn_3(PO_4)_2 \cdot 4H_2O_{(s)}$) and Pb ($PbHPO_4$, $Pb(CO_3)$ and $Pb(OH)_2$) was indicated by thermodynamic modeling and then confirmed by SEM. On the other hand, Mg showed a different behavior as its concentration

went even higher in GM than in UPW, which could be due to the presence of complexation agents like phosphates, or sulfate in GM.

9.3.3. Effect of *Pseudomonas aeruginosa*

Pseudomonas sp. needs Fe for its growth and is well-known for producing siderophores which are involved in Fe complexation and Fe metabolic acquisition (Chapter 7 and 8). This is very likely the main reason why the Fe concentration (i.e. solubility) is strongly enhanced in the experiments with the presence of bacteria. In addition to Fe, the dissolution of matrix elements (Ca, Si, Mg) as well as other elements (Zn and Pb) were enhanced in the presence of bacteria both in bioreactor operated in batch condition as well as in a semi-flow through reactor with intermittent leachate renewal conditions. The elevated concentrations of the elements can be related not only to the activities of bacteria, but also the presence of siderophores which may also enhance the dissolution (via a ligand promoted dissolution mechanism). In addition, the bacterial cells can be served as good sorbents for Fe, Pb and Zn as 0.08% out of 0.12% total Fe, 0.07% out of 0.10% of total Pb and 0.15% out of 0.31% total Zn are found as sorbed on to particulate parts.

9.3.4. Weathering mechanisms

One can assume that pure chemical reactions (i.e. solid-liquid interactions) are initiated first, prior to being enhanced by the presence of bacteria (Figure 9.4). During early stage of weathering, hydrolysis profoundly modified the silicate network by attacking bridging bonds (Si-O-M) which consequently led to the release of elements embedded in silica matrix. Such dissolution of cations into the solutions consequently led to the slag's surface being negatively charged. The negative charge in the silicon network is neutralized by H^+ from H_2O , resulting in a pH increase. In the presence of *Pseudomonas aeruginosa*, the preferential extraction of Fe by the bacteria has further weakened the bonding of the glass matrix. Simultaneously, as bacterial bodies are good sorbents for cations, where the sorption have decreased the free ion concentration and causes a thermodynamic shift which favors even further slag dissolution as predicted by Le Chatellier's principle.

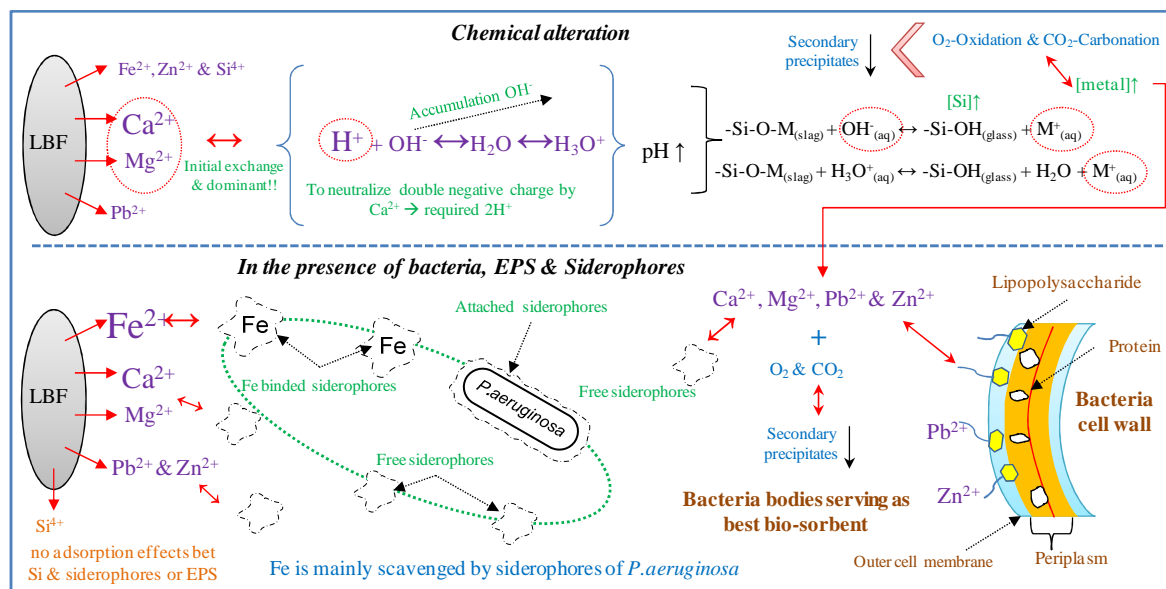


Figure 9.4. Weathering of slags by the heterotrophic bacterium *Pseudomonas aeruginosa*.

9.3.5. Slag alteration and secondary precipitates

The surface morphology of LBF had significantly changed after a long immersion time in the different media (UPW, GM and GM+B). The glass surface alteration layer in UPW medium was more porous whereas the zones closer to the edge were more altered in GM medium. In addition, the alteration was non-uniform and mostly found at the edge where there was a contact between the leaching medium and bacteria. Likewise, diffusion on the edge of the matrix and highly fractured glass surface can be observed in the presence of the bacteria. The dissolution of glassy phases is highly prone to weathering whereas spinels appeared to be very stable since they were protuberant objects at the weathered glass surface. Furthermore, the bacterial colonization and adhesion as a biofilm on the slag's surface can also be observed.

Lead carbonate is the dominant secondary phases found in UPW medium whereas formation of phosphate with Fe, Pb, Ca, and Zn was observed in GM and GM+B medium (Figure 9.5). Thus, the presence of *Pseudomonas aeruginosa* did not affect on the types of Zn and Pb secondary phases, indicating that this bacterium did not favor biomineralization or bioprecipitation, but rather enhanced Zn and Pb solubilities by sorption onto microbial cell wall and complexation with microbial by-products.

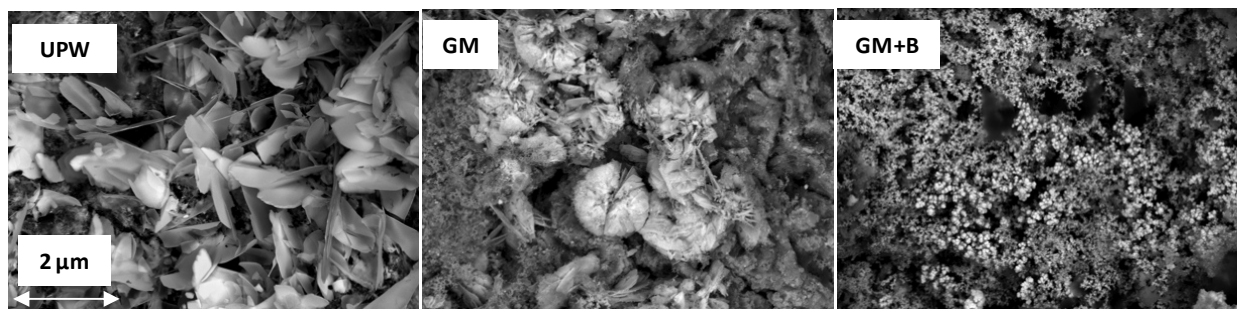


Figure 9.5. Precipitation of secondary phases on weathered slags in UPW, GM, and GM+B observed by SEM.

9.3.6. Cumulative metal release (comparison of weathering conditions)

Total bulk releases of Fe, Si, Pb and Zn from two bioweathering tests were compared after 150 days of alteration of slags in the presence of *Pseudomonas aeruginosa* shown in Figure 9.6. In the presence of *Pseudomonas aeruginosa*, higher bulk release of Fe, Zn and Si were observed under leachate renewal condition ($270 \mu\text{g g}^{-1}$, $260 \mu\text{g g}^{-1}$, $507 \mu\text{g g}^{-1}$ of Fe, Zn and Si) compared to those under leachate stagnant condition ($34 \mu\text{g g}^{-1}$, $45 \mu\text{g g}^{-1}$, $167 \mu\text{g g}^{-1}$ of Fe, Zn and Si). No effect of different leaching conditions was observed on bulk release of Pb: $30 \mu\text{g g}^{-1}$ for both conditions. In addition, the green bars are the indication of the effect of growth media alone (phosphate, sulfate and succinate salts) where the bulk release were significantly lower.

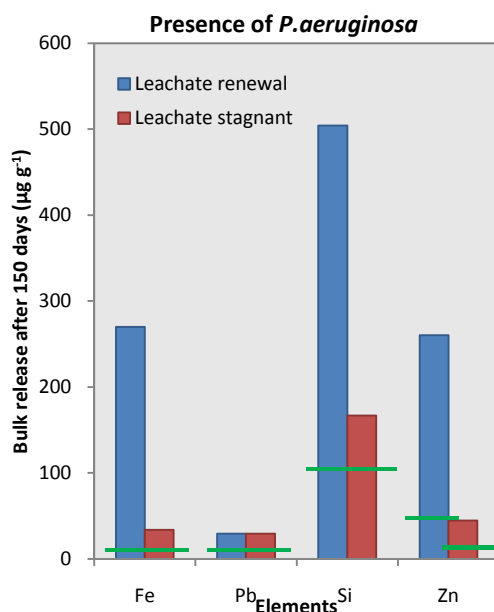


Figure 9.6. Bulk release of Fe, Pb, Si and Zn after 150 days of bioweathering in comparison between leachate renewal and leachate stagnant conditions.

9.4. Future perspectives

While conducting this research, the author came across a few obstacles and limitations which might possibly serve as the bridge for further development in future research directions. The limitation lies within the following context:

- Many questions are still remaining concerning field weathering conditions and to predict the long-term (i.e. tens to hundreds of years) reactivity of these metallurgical wastes or to relate laboratory test results with measured values in the field.
- There are still rooms to determine the alteration rates and kinetics of each individual crystalline or glassy phase present in metallurgical slags contributing to the overall alteration of slags even at the laboratory scale.
- Similarly, the real isotopic signatures of each individual phase present in the phase still a mystery as it is physically impossible to separate each phases for analysis. Thus, application of laser ablation coupled with MC-ICP-MS could be an interesting alternative.
- The adsorption studies of Zn onto inorganic mineral phases could be further extended to more mineral phases such as clay; and the application laboratory data on adsorption studies (with oxides and oxy-hydroxides) in real geological setting will be interesting.
- Zn isotopic data during its precipitation as ZnCO_3 , ZnO , predominant phases during oxidative environments, as well as co-precipitation of Zn together with other elements (Ca, Pb, Fe) either as oxides or carbonates will be a step further in understanding the mechanism.
- In many geological settings, it is well-known that soil can accommodate different species of micro-organisms and the influence of other microbial species or their consortia on the weathering of slags will be interesting. With such knowledge, heterotrophic leaching can be an alternative for bio-metal recovery from alkaline slags where improvement in the leaching performance can be achieved by manipulation of the leaching conditions.

